

DISTINCT PROPERTIES OF THE ATRIAL VOLTAGE-GATED SODIUM CHANNEL

By

Sian-Marie O'Brien

A thesis submitted to
The University of Birmingham
for the degree of
DOCTOR OF PHILOSOPHY

Institute of Cardiovascular Sciences
College of Medical and Dental Sciences
The University of Birmingham

July 2019

UNIVERSITY OF
BIRMINGHAM

University of Birmingham Research Archive

e-theses repository

This unpublished thesis/dissertation is copyright of the author and/or third parties. The intellectual property rights of the author or third parties in respect of this work are as defined by The Copyright Designs and Patents Act 1988 or as modified by any successor legislation.

Any use made of information contained in this thesis/dissertation must be in accordance with that legislation and must be properly acknowledged. Further distribution or reproduction in any format is prohibited without the permission of the copyright holder.

Abstract

Sodium handling properties of left atria (LA) were compared to those of left ventricle (LV), with the aim to understand the atria's susceptibility to arrhythmia and improve therapy. Mouse LA sodium channels displayed distinctive activation, inactivation and recovery kinetics compared to LV sodium channels. Distinctive voltage dependence of LA sodium channel inactivation was instrumental in reducing I_{Na} in LA compared to LV, when initiated from physiological holding potentials. Flecainide sodium channel inhibition was greater in LA than LV, likely also due to differences in kinetic properties of the sodium channels between chambers. Additionally, the greater inhibitory effect of flecainide at more positive membrane potentials could result in even greater LA sodium channel inhibition *in vivo*.

Activation and inactivation distinctions observed between LA and LV sodium channels were conserved between chambers in the $Plako^{+/-}$ mouse. However, there was no difference in physiological I_{Na} density, sodium channel recovery or flecainide inhibition between $Plako^{+/-}$ LA and LV chambers.

The novel Langendorff-free isolation method produced high yields of viable mouse cardiomyocytes comparable in morphology, signalling, calcium handling and sodium channel electrophysiology to cardiomyocytes isolated using the traditional Langendorff method. This maintained that injection isolation is a valuable method for obtaining cardiomyocytes for cardiac research.

Acknowledgements

I would like to take this opportunity to thank my lead supervisor Dr Davor Pavlovic, for his tutelage, guidance and encouragement. His enthusiasm for my work and belief in my ability has been instrumental to my studies. Many thanks to my additional supervisors, Professor Paulus Kirchhof and Dr Larissa Fabritz, for their valued help and advice. In addition, thank you to Dr Andrew Holmes, for being a great mentor and friend, I will always appreciate the expert knowledge you imparted.

Many thanks to the support from the whole of the Translational Research on Heart Failure and Arrhythmias group. Special thanks to the friends I made within the group, for the kindness, support, crosswords, shared chips and much more. Thank you to Clara Apicella and Claire Hepburn for keeping me company in the molecular biology lab and for just being your wonderful selves.

Outside of University I would like to thank my friends back home in Liverpool, for reminding me that it is also important to still have some fun. Thank you to David Kelly, for your encouragement and confidence in me.

Finally, the greatest thanks to my parents for their unconditional love and support. Without you I would have never been able to complete this academic journey.

Dedication

To my Granddad Terence, for all your love and shaping me into the person I am
today.

Contents

1. Introduction	1
1.1. Summative overview	1
1.2. Cardiac physiology	3
1.2.1. Basic anatomy and function of the heart	3
1.2.2. Cardiomyocytes	5
1.2.3. Cardiac conduction system	7
1.2.4. Cardiomyocyte resting membrane potential	9
1.2.5. Pacemaker action potential	11
1.2.6. Human ventricular action potential	14
1.2.7. Human atrial action potential	17
1.2.8. Effective refractory period	20
1.2.9. Cardiac excitation-contraction coupling	20
1.3. Sodium handling pathways	23
1.3.1. Voltage-gated sodium channel	24
1.3.1.1. Sodium channel α -subunit and gating	24
1.3.1.2. Sodium channel β -subunit	28

1.3.1.3. Late sodium current	30
1.3.2. Sodium-calcium exchanger	30
1.3.3. Sodium-potassium ATPase pump	32
1.3.4. Sodium-hydrogen exchanger	33
1.4. Cardiac arrhythmias	34
1.4.1. Atrial fibrillation	34
1.4.2. AF mechanisms.....	37
1.4.2.1. AF mechanisms underlying ectopic firing	38
1.4.2.2. Basic mechanisms underlying re-entry	39
1.4.2.3. Electrical determinants of AF	41
1.4.3. AF rate and rhythm control therapies	42
1.4.3.1. Flecainide pharmacology	46
1.5. Study Hypotheses	50
2. Materials and Methods	52
2.1. Ethical statement and study approval	52
2.2. Animal models.....	52
2.3. Western blotting methods	53
2.3.1. Western blot statistical analysis.....	53

2.3.2. Mouse heart excision.....	53
2.3.3. Mouse sample preparation.....	56
2.3.4. SDS-Polyacrylamide Gel (SDS-PAGE) for mouse samples.....	57
2.3.5. Semi-dry electrophoretic transfer	57
2.3.6. Human tissue collection.....	58
2.3.7. Human sample preparation	58
2.3.8. SDS-Polyacrylamide Gel (SDS-PAGE) for human samples	60
2.3.9. Isolated cardiomyocyte sample preparation	60
2.3.10. Membrane probing	61
2.3.11. Visualisation of membranes	64
2.3.12. Membrane stripping and re-probing	65
2.3.13. Image analysis.....	65
2.4. Whole-cell patch clamp electrophysiology	66
2.4.1 Langendorff-based mouse cardiomyocyte Isolation.....	66
2.4.2 Injection-based mouse cardiomyocyte Isolation.....	68
2.4.3. Calcium reintroduction.....	72
2.5. Whole-cell patch clamp electrophysiology	73
2.5.1. I_{Na} recordings.....	73

2.5.2. Patch clamp statistical analysis	75
2.6. Calcium, cell and sarcomere length measurements	79
2.6.1. Plating of isolated cardiomyocytes	79
2.6.2. Calcium handling and sarcomere length measurements	79
3. Sodium handling in the atria and ventricles	81
3.1. Chapter introduction and overview.....	81
3.2. Electrophysiology results	85
3.2.1. Mouse LA sodium channels activate at more negative holding potentials than LV sodium channels.....	85
3.2.2. LA peak I_{Na} is smaller than LV I_{Na} at physiologically relevant holding potentials	88
3.2.3. Mouse LA sodium channels inactivate at more negative holding potentials than LV sodium channels.....	91
3.2.4. Mouse LA sodium channels have slower time dependent recovery than LV sodium channels	93
3.2.5. Flecainide alters I/V curve morphology and activation potential of LA and LV sodium channels	94
3.2.6. Flecainide sodium channel inhibition increases at more positive holding potentials with a greater effect in the LA.....	98
3.2.7. Flecainide alters LA and LV sodium channel inactivation	101

3.2.8. Flecainide slows sodium channel recovery in the LA.....	103
3.3. Protein expression	105
3.3.1. Na _v 1.5 expression in WT mouse LA and LV	105
3.3.2. Na _v 1.5 β-subunit expression in WT mouse LA and LV	109
3.3.3. Na _v 1.5 β-subunit expression in human LA and LV.....	111
3.3.4. Expression of the genes that encode SCN5A, SCN2B and SCN4B in healthy human LA and LV	113
3.4. Chapter synopsis and discussion.....	115
3.4.1. Overview of main findings	115
3.4.2. Physiological I _{Na} density comparison between LA and LV	116
3.4.3. Voltage dependence of inactivation and the effect on peak LA and LV I _{Na}	119
3.4.4 Pathophysiological considerations due to differences in I _{Na} inactivation between LA and LV	122
3.4.5. Sodium channel activation differences between LA and LV.....	126
3.4.6. Sodium channel recovery differences between LA and LV	129
3.4.7. Flecainide sodium channel inhibition in the LA and LV	130
3.4.8. Varying Na _v 1.5 expression in WT mouse LA and LV	136
3.4.9. Na _v β2 and Na _v β4 expression is lower in WT mouse LA than LV ...	138

3.4.10. Na _v β2 expression is greater in human diseased LA than in healthy LA.....	142
4. Plakoglobin deficiency and sodium handling in the atria and ventricles	147
4.1. Chapter introduction and overview.....	147
4.2. Electrophysiology results	151
4.2.1. LA sodium channels activate at more negative holding potentials than LV sodium channels in the Plako ^{+/-} mouse.....	151
4.2.2. No difference in peak I _{Na} between LA and LV at physiologically relevant holding potentials in the Plako ^{+/-} mouse	154
4.2.3. LA sodium channels inactivate at more negative holding potentials than LV sodium channels in the Plako ^{+/-} mouse.....	156
4.2.4. No difference in time dependent recovery between LA and LV sodium channels in the Plako ^{+/-} mouse	158
4.2.5. No difference in flecainide inhibition between LA and LV sodium channels in the Plako ^{+/-} mouse.....	160
4.2.6. Flecainide alters LA and LV sodium channel inactivation in the Plako ^{+/-} mouse	165
4.2.7. Flecainide has no effect on recovery of LA or LV sodium channels in the Plako ^{+/-} mouse	168
4.3. Chapter synopsis and discussion.....	171

4.3.1. Overview of main findings	171
4.3.2. Physiological I_{Na} density and inactivation of LA and LV in the Plako ^{+/-} mouse.....	172
4.3.3. Sodium channel activation differences of the LA and LV in the Plako ^{+/-} mouse	176
4.3.4. No difference in sodium channel recovery between LA and LV in the Plako ^{+/-} mouse	177
4.3.5. Flecainide sodium channel inhibition of LA and LV in the Plako ^{+/-} mouse.....	178
5. Langendorff-free technique for mouse cardiomyocyte isolation	183
5.1. Chapter introduction and overview.....	183
5.2. Protocol optimisation.....	191
5.3. Functionality of injection-isolated cardiomyocytes	192
5.3.1. Cell and sarcomere length of injection isolated LV cardiomyocytes	193
5.3.2. Adrenergic response of injection-isolated LV cardiomyocytes	194
5.3.3. Injection-isolated LV cardiomyocyte sodium channel IV and activation	196
5.4. Comparison of function and signalling characteristic between injection-based and Langendorff-based isolation techniques.....	198

5.4.1. Comparison of injection and Langendorff isolated LV cardiomyocyte cell and sarcomere length	199
5.4.2. Pacing effect on injection and Langendorff isolated LV cardiomyocytes.....	200
5.4.3. Adrenergic response of injection and Langendorff isolated LV cardiomyocytes.....	203
5.4.4. Injection and Langendorff isolated LV cardiomyocyte I_{Na} IV and activation	204
5.4.5. Injection and Langendorff isolated LV cardiomyocyte sodium channel inactivation.....	207
5.4.6. Injection and Langendorff isolated LV cardiomyocyte signalling cascades	208
5.5. Chapter synopsis and discussion.....	210
5.5.1. Overview of main findings	210
5.5.2. Protocol optimisation	211
5.5.3. Comparable contractile and calcium handling properties of injection and Langendorff isolated LV cardiomyocytes.....	213
5.5.4. Comparable I_{Na} of injection and Langendorff isolated LV cardiomyocytes.....	215

5.5.5. Comparable signalling cascade effects of injection and Langendorff isolated LV cardiomyocytes.....	216
5.5.6. Potential injection-isolation method limitations	217
6. Overall discussion.....	219
6.1. General outcomes.....	219
6.2. Physiological relevance of I_{Na} distinctions between the LA and LV	220
6.3. Importance of LA I_{Na} distinctions as potential atrial-specific drug target	221
6.4. Significance of greater $Na_v\beta 2$ expression in diseased human LA	225
6.5. Importance of no difference in I_{Na} density between $Plako^{+/-}$ LA and LV.....	226
6.6. Flecainide has no differential inhibition between $Plako^{+/-}$ LA and LV	227
6.7. Impact of a simplified Langendorff-free isolation method that produces high yields of viable mouse cardiomyocytes	228
6.8. Study limitations	229
6.8.1. General limitations.....	229
6.8.2. Patch clamp limitations.....	230
6.8.3. Western blot limitations	231
6.9. Future experiments	232
6.9.1. Electrophysiology experiments.....	232

6.9.2. Molecular experiments	233
References	235

Figures

Figure 1.1. Structure and blood flow through the heart.....	5
Figure 1.2. SA node action potential.....	14
Figure 1.3. Ventricular action potential.	16
Figure 1.4. Morphology and ionic currents of human atrial and ventricular action potentials.	19
Figure 1.5. A ventricular Ca^{2+} transport schematic.....	22
Figure 1.6. A schematic representation of VGSC gating.....	27
Figure 1.7. A schematic representation of VGSC structure.....	27
Figure 1.8. Diagram comparing movement of electrical impulse between NSR and AF.....	37
Figure 1.9. Mechanistic concepts of re-entrant arrhythmia.....	41
Figure 2.1. Cannulation of ascending aorta.....	55
Figure 2.2. Diagram of whole cell patch clamp general set up and principle.....	75
Figure 3.1. LA and LV I_{Na} I/V relationship and sodium channel activation.	87
Figure 3.2. I_{Na} density at varying holding potentials.	90
Figure 3.3. LA and LV sodium channel inactivation.....	92
Figure 3.4. LA and LV time dependent sodium channel recovery.....	94

Figure 3.5. LA and LV I_{Na} I/V and sodium channel activation with the addition of flecainide.	97
Figure 3.6. Sodium channel flecainide inhibition in LA and LV at different holding potentials.....	100
Figure 3.7. LA and LV I_{Na} inactivation with the addition of flecainide.	102
Figure 3.8. Flecainide effect on LA and LV time dependent sodium channel recovery.....	104
Figure 4.1. $Na_v 1.5$ expression in mouse LA and LV.....	108
Figure 4.2. $Na_v \beta 2$ and $Na_v \beta 4$ expression in mouse LA and LV.....	110
Figure 4.3. $Na_v \beta 2$ and $Na_v \beta 4$ expression in diseased human LA and LV.	112
Figure 4.4. $Na_v \beta 2$ expression in diseased and healthy human LA.....	113
Figure 4.5. Expression of the mRNAs that encode $Na_v 1.5$ and the $Na_v \beta$ - subunits in healthy human LA and LV.	114
Figure 5.1. WT and Plako ^{+/-} LA and LV I_{Na} I/V relationship and sodium channel activation.	153
Figure 5.2. I_{Na} density in Plako ^{+/-} LA and LV at varying holding potentials.....	155
Figure 5.3. Plako ^{+/-} LA and LV sodium channel inactivation.....	157
Figure 5.4. WT and Plako ^{+/-} LA and LV time dependent sodium channel recovery.....	159

Figure 5.5. Plako ^{+/-} LA and LV I _{Na} I/V with the addition of flecainide.	162
Figure 5.6. Plako ^{+/-} LA and LV sodium channel activation with the addition of flecainide.	164
Figure 5.7. Plako ^{+/-} LA and LV I _{Na} inactivation with the addition of flecainide.....	167
Figure 5.8. Flecainide effect on Plako ^{+/-} LA and LV time dependent sodium channel recovery.	170
Figure 6.1. Schematic of a Langendorff apparatus.....	186
Figure 6.2. Injection-based isolation method.....	189
Figure 7.1. EDTA and pH optimisation.	192
Figure 7.2. Frequency response of LV injection-isolated cells.	194
Figure 7.3. Adrenergic response of LV injection-isolated cells.....	196
Figure 7.4. Injection isolated LV cardiomyocyte I/V relationship and sodium channel inactivation.	198
Figure 7.5. Diastolic cell length and sarcomere length of Langendorff and injection isolated cells.....	200
Figure 7.6. Pacing effect on Langendorff and injection isolated cells.....	202
Figure 7.7. Adrenergic responses of Langendorff and injection isolated cells.....	204
Figure 7.8. Langendorff and injection isolated LV cardiomyocyte I/V relationship and sodium channel activation.	206

Figure 7.9. Langendorff and injection isolated LV cardiomyocyte sodium channel inactivation.....	208
Figure 7.10. Stress signalling cascade associated protein expression in Langendorff and injection isolated LV cardiomyocytes.	210

Tables

Table 1.1: Primary antibodies used for mouse Western blot experiments.	62
Table 1.2: Secondary antibodies used for mouse Western blot experiments.....	63
Table 1.3: Primary antibodies used for human Western blot experiments.	63
Table 1.4: Secondary antibodies used for human Western blot experiments.	64
Table 1. 5: Voltage patch clamp protocols.....	77
Table 2.1: Individual molecular weight band data for Na _v 1.5 expression in mouse WT LA and LV.	109

List of abbreviations

4-AP	4-Aminopyridine
AAD	Antiarrhythmic drug
AF	Atrial fibrillation
ANOVA	Analysis of variance
AP	Action potential
APD	Action potential duration
ARVC	Arrhythmogenic right ventricular cardiomyopathy
AU	Arbitrary unit
AV node	Atrioventricular node
BDM	Butanedione monoxime
Ca ²⁺	Calcium ion
CAST	Cardiac Arrhythmia Suppression Trial
CV	Conduction velocity
DAD	Delayed afterdepolarisation
DMSO	Demiethyl sulfoxide
EAD	Early afterdepolarisation

ECC	Excitation-contraction coupling
ECG	Electrocardiogram
E_K	Equilibrium potential for K^+
E_{Na}	Equilibrium potential for Na^+
ERK	Extracellular signal-regulated kinase
ERP	Effective refractory period
Flec	Flecainide
HEK	Human embryonic kidney
HF	Heart failure
HRP	Horseradish peroxidase
I_{CaL}	Inward Ca^{2+} current (via L-type Ca^{2+} channels)
I_{CaT}	Inward Ca^{2+} current (via T-type Ca^{2+} channels)
I_f	Funny current
Ig	Immunoglobulin
I_K	K^+ current
I_{K1}	Inward rectifier K^+ current
I_{Kr}	Potassium rectifier current (rapid)
I_{Ks}	Potassium rectifier current (slow)

I_{Kur}	Ultra-rapid delayed rectifier K^+ current
I_{max}	Maximum current
I_{Na}	Na^+ current
I_{NaL}	Late Na^+ current
ISO	Isoproterenol
I_{to}	Transient outward potassium current
K^+	Potassium ion
$[K^+]_i$	Intracellular K^+ concentration
$[K^+]_o$	Extracellular K^+ concentration
LA	Left atria
L-type	Long-lasting Ca^{2+} channels
LV	Left ventricle
LVAD	Left ventricular assist device
mRNA	Messenger ribonucleic acid
mV	Millivolt
Na^+	Sodium ion
$Na_v1.1-9$	Sodium channel 1.1-9
NCX	Sodium-calcium exchanger

NHE	Sodium-hydrogen exchanger
NKA	Sodium-potassium ATPase
NSR	Normal sinus rhythm
OD	Optical density
pA	Picoamperere
PBS	Phosphate buffered saline
PBS-T	Phosphate buffered saline tween
PD	Pore domain
pF	Picofarad
PKA	Protein kinase A
PKC	Protein kinase C
Plako	Plakoglobin
PLM	Phospholemman
RA	Right atria
RV	Right ventricle
RyR2s	Ryanodine receptors
SA node	Sinoatrial node
SD	Standard deviation

SEM	Standard error of the men
SERCA	Sarco-endoplasmic reticulum calcium-ATPase
SL	Sarcomere length
SR	Sarcoplasmic reticulum
SUNDS	Chinese sudden unexplained nocturnal death syndrome
TN-C	Troponin-C
TN-I	Troponin-I
T-tubules	Transverse tubules
T-type	Transient Ca ²⁺ channels
VGSC	Voltage-gated sodium channels
V _m	Volts per metre
V _{max}	Maximum upstroke velocity
VSD	Voltage-sensing domain
WT	Wild-type

1. Introduction

1.1. Summative overview

Intracellular Na^+ concentration $[\text{Na}^+]_i$ is an essential modulator of action potential (AP) waveform, calcium cycling and impulse propagation throughout the myocardium (1). To enable cell excitability a Na^+ gradient across cardiomyocyte membranes must be maintained. Therefore, $[\text{Na}^+]_i$ is regulated by a balance between the influx and efflux of Na^+ via a number of transmembrane pumps, channels and transporters (2). Over the last few decades there has been increasing interest in the regulation of $[\text{Na}^+]_i$, as deregulation is associated with cardiac disease and may contribute to pathophysiology (3). The processes driving physiological regulation of $[\text{Na}^+]_i$ in health and disease are relatively well studied in the ventricles. However, the fundamental difficulties in studying the atria and atrial cardiomyocytes have resulted in few direct comparisons of the way Na^+ is handled between the ventricles and atria. As isolation of workable cardiomyocytes is a key issue for the study of the atria, this thesis outlines a new method for ventricular isolation that can be utilised for atrial isolation and describes the viability of cells compared to those that have been isolated using the more classical method.

Studying Na^+ handling specifically in the atria could aid in understanding the atria's susceptibility to arrhythmia and also potentially highlight atrial specific targets for treatment of atrial fibrillation (AF). Distinctions between atrial and

ventricular sodium channel kinetics have been identified in several mammalian species (4-6). However, it is essential that these findings be considered in physiological context. Consequently, results presented in this study aim to develop an understanding of the clinical relevance/importance of Na⁺ handling distinctions between cardiac chambers. A number of sodium channel inhibiting drugs have been used in the treatment of AF (7) and this thesis also aims to characterise inhibitor effects on sodium channels in the atria compared to the ventricles.

Additionally, it is essential to establish whether distinctions shown in this study and previous mammalian studies are representative of what would be observed between human atria and ventricles, in order to consider the clinical relevance of findings. Molecular experiments described within this thesis identify differences in the proteins associated with the sodium channels between human atrial and ventricular chambers and between healthy and diseased cardiac tissues. Therefore, a discussion into what the consequences of these molecular distinctions are, in terms of the effect of disease on Na⁺ handling within the different chambers of the heart, is contained within this thesis.

1.2. Cardiac physiology

1.2.1. Basic anatomy and function of the heart

The mammalian heart is a muscular organ that lies inside the thoracic cavity surrounded by a fluid filled sac called the pericardium, which serves as protection. The circulatory system is defined as the heart and the system of blood vessels that carry blood around the body. Circulation of blood with adequate perfusion of the organs and tissues is essential to sustain life, by delivering oxygen and nutrients, alongside carrying away waste products (8).

The wall of the heart consists of three layers of tissue. The epicardium is the outer layer and is primarily composed of connective tissue, including elastic fibers and adipose tissue. It acts as a protective layer and assists in the production of the pericardial fluid that fills the pericardial cavity and aids in reducing friction between pericardial membranes. The coronary blood vessels that supply the heart wall with blood are also found in this layer of heart. The myocardium is the middle and the thickest layer of the heart, consisting of the cardiac muscle fibers that enable contraction. The endocardium is the layer that lines the inner heart chambers, covers heart valves and is continuous with the endothelium of the large blood vessels, providing a smooth surface, enabling blood to flow freely (9).

The heart consists of four distinct hollow chambers. The two upper chambers are the right and left atrium and the two lower chambers are right and left ventricles (Figure 1.1). The septum is a muscular wall that separates the left chambers from the right chambers. The right atrium (RA) receives deoxygenated (carbon-dioxide enriched) blood via the inferior and superior vena cava from the systemic circulation. The RA contracts and the blood flows into the right ventricle (RV), which contracts to eject blood into the pulmonary artery, delivering it to the lungs. In the lungs the blood is oxygenated. The left atrium (LA) receives this oxygenated blood from the lungs via the pulmonary veins and contracts, filling the left ventricle (LV), which contracts to eject blood into the aorta and systemic arterial system of the body. There are four valves that insure the flow of blood is unidirectional by preventing backflow. The aortic valve is found between the LV and aorta, the mitral valve between the LA and LV, the pulmonary valve between the RV and pulmonary artery and tricuspid valve between the RA and RV (9).

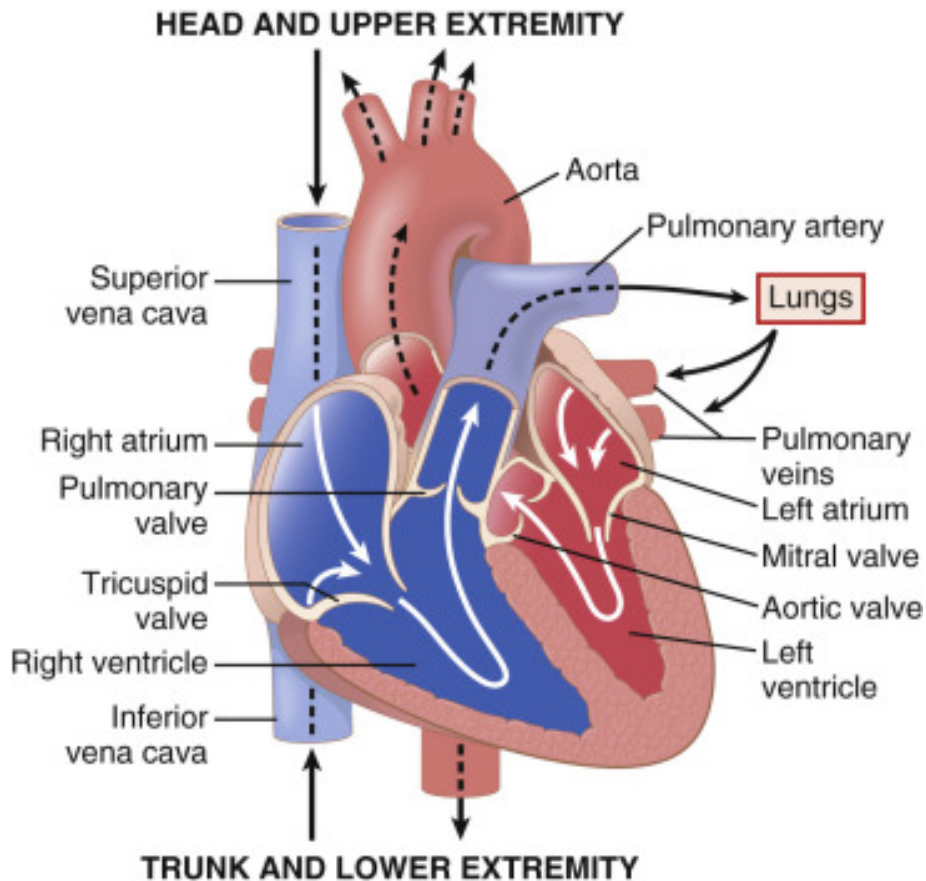


Figure 1.1. Structure and blood flow through the heart.

The arrows show the direction of blood flow. The blue denotes the circulation of deoxygenated blood and the red denotes the circulation of oxygenated blood. Image extracted from (10).

1.2.2. Cardiomyocytes

The myocardium is an organised tissue comprised of immune cells, smooth muscle cells, fibroblasts and cardiomyocytes (the fundamental contractile cells). Cardiomyocytes have a striated subcellular structure and are connected to neighbouring cardiomyocytes by intercalated discs consisting of desmosomes, providing structural attachment of myocytes and an electrical connection via gap junctions (11). Gap junctions are essential in conducting the electrical

impulse throughout the myocardium, by providing low resistance pathways between cardiomyocytes. As desmosomes link intracellularly to the intermediate filament cytoskeleton, it is the network of adhesive bonds they form that gives the heart its mechanical strength. Therefore, if cardiac desmosomal adhesion breaks down, as with particular autoimmune and genetic diseases, the heart cannot uphold mechanical stress and integrity of the myocardium can be lost (12). Desmosomes are also important for signalling, regulating the availability of signalling molecules, participating in cell proliferation, differentiation and morphogenesis (12).

Atrial and ventricular cardiomyocytes develop their distinctive, cell-specific characteristics at an early embryonic stage by regulated gene expression. Ventricular cardiomyocytes are elongated rectangular shaped cells with many myofibrils and mitochondria (for ATP production). Myofibrils are repeating units (sarcomeres) composed of thin actin filaments and anchored at the Z-disks at the end of the sarcomere and thick myosin filaments, which interlock and interact with the thin filaments. Atrial cardiomyocytes differ from ventricular cardiomyocytes, having a thinner smaller shape with fewer transverse tubules (T-tubules), which are 20-450nm extensions of the membrane that penetrate into the cell (13). Atrial cardiomyocytes have more caveolae, 50-100nm lipid raft invaginations of the plasma membrane. Unlike ventricular cardiomyocytes, which are multinucleated, atrial cardiomyocytes typically have only one central elongated nucleus (14, 15).

1.2.3. Cardiac conduction system

The contracting chambers of the heart are controlled by the cardiac conduction system. This system generates electrical impulses known as action potentials (APs) and conducts them throughout the myocardium, stimulating the heart to contract. APs are a result of transient changes in ion conductance across cardiomyocyte membranes. Ion channels and transporters are membrane-embedded proteins that selectively allow passage of ions, which is the primary cause of changes in conductance (8).

The normal cardiac conduction system pathway starts at the sinoatrial (SA) node, the dominant pacemaker that generates an impulse at the junction of the superior vena cava and RA. The cells within the SA node are characterised as having no true resting membrane potential, instead they produce regular, spontaneous APs. Although pacemaker activity is spontaneously generated by SA nodal cells, the rate of this activity can be changed considerably by external factors; including autonomic nerves, hormones, ion concentrations, medication and ischemia/hypoxia. From the SA node the electrical impulse spreads throughout the RA and LA via cell-to-cell conduction at a velocity of around 0.5m/sec. The wave of APs depolarises the atrial myocardium, initiating atrial muscular contraction and resultant filling of the ventricles (8).

The impulse is conducted via the atrial myocardium, towards the atrioventricular (AV) node, which is a specialised region of cells located in the inferior-posterior region of the interatrial septum. At the AV node, conduction is slowed considerably to around 0.05m/sec to allow sufficient time for complete atrial depolarisation and contraction before depolarisation progresses to the ventricles. The impulse then enters the apex of the ventricles and spreads throughout the ventricles via the specialised Bundle of His conduction system. The impulse then streams down the left and right bundle branches along the interventricular septum, at a rapid velocity of around 2m/sec. The bundle branches then divide into the extensive Purkinje fibers system that conduct the impulses throughout the ventricles at a velocity of around 4m/sec. This rapid spread of electrical impulse across the ventricles enables a coordinated depolarisation of the ventricular myocardium and uniform contraction (16).

A synchronised conduction system within the heart is essential to ensure the rapid and organised depolarisation of cardiomyocytes, required for efficient and accurate contraction. Electrical conduction across the heart is influenced by autonomic nerve activity. Autonomic control is most apparent at the AV node as sympathetic activation increases conduction velocity by increasing the rate of depolarisation, reducing the normal delay of conduction, therefore reducing the time between atrial and ventricular contraction. Conversely, parasympathetic activation decreases conduction velocity at the AV, increasing time between atrial and ventricular contraction (16).

1.2.4. Cardiomyocyte resting membrane potential

The intracellular voltage potential with respect to the extracellular voltage potential under resting conditions is known as the resting membrane potential (RMP). With stimulation, the normally negative voltage potential inside the cell (negative membrane potential), can temporarily become more positive, resulting in the generation of an AP. Membrane potentials are established by an asymmetric distribution of ions on each side of the cardiomyocyte membrane, selective permeability of the cell by specific ion channels and the activity of electrogenic pumps that maintain ion concentrations across the membrane (8).

Cardiomyocytes have distinctive concentrations of ions across their membrane, the most significant being K^+ , Na^+ , Cl^- and Ca^{2+} . Inside a cardiomyocyte the concentration of K^+ is high but low on the outside of the cell, resulting in a chemical gradient for K^+ to diffuse out of the cell. Whereas, Ca^{2+} and Na^+ concentrations are higher outside of the cell, favouring inward diffusion of those ions (17).

Cardiomyocytes have channels that allow K^+ to move across the cell membrane so that it diffuses down its chemical gradient out of the cell. The negative charge across the membrane that would be required to oppose the movement of K^+ out of the cells is termed the equilibrium potential for K^+ (E_K). In

electrochemistry, the Nernst equation is an equation that defines the relationship between the concentrations of an ion on either side of a perfectly selective membrane and so the potential difference (voltage) that would be measured across the membrane under equilibrium conditions. Therefore, the Nernst equation can provide a value for the voltage that must exist across the membrane in order to balance a chemical gradient (17). The E_K can be calculated using the Nernst equations as follows:

$$E_K = \frac{-RT}{zF} \ln \frac{[K^+]_o}{[K^+]_i} = -96mV$$

Where R= universal gas constant ($8.314 \text{ J.K}^{-1}.\text{mol}^{-1}$), T= temperature in Kelvin, z=1 as K^+ is monovalent, F= Faraday's constant ($96,485 \text{ C.mol}^{-1}$), $[K^+]_o$ (extracellular K^+ concentration) =4mM and $[K^+]_i$ (intracellular K^+ concentration) =150mM.

Contrasting to the pacemaker cells in the nodal tissue of the heart, non-pacemaker cells have a stable RMP that rarely depolarises spontaneously. The RMP for a ventricular myocyte is around -80 to -90mV, near to the equilibrium potential for K^+ , as cardiomyocytes are most permeable to K^+ compared to other ions. The key current that sets the RMP is the inward rectifier K^+ current (I_{K1}). As E_k is -96mV there is a net electrochemical outward driving force of around 6-16mV acting on K^+ . This small net outward driving force and finite permeability of cardiomyocytes to K^+ , results in a slow outward leak of K^+ from the cells. However, regardless of the leaking K^+ , the chemical gradient is

maintained due to Na^+/K^+ -ATPase pumps that actively transport K^+ back into cardiomyocytes. The Kir2.1 potassium channel is the major channel responsible for $I_{\text{K}1}$ and it has a lower expression in the atria compared to the ventricles. Therefore, atrial cardiomyocytes have lower density of $I_{\text{K}1}$ (around 5-6 fold less) than ventricular cardiomyocytes, and this explains their resulting depolarised RMP of at around -65 to -80mV(18-20).

1.2.5. Pacemaker action potential

An AP results from the rapid depolarisation of the myocyte membrane followed by repolarisation back to RMP of the cell. The AP in nodal cells differs to the AP generated in cardiomyocytes of the atria and ventricles. The SA node is the primary pacemaker site within the heart and characterised as having no true RMP, generating regular spontaneous APs. Distinctive to pacemaker cells, the AP depolarising current is caused by the relatively slow influx of Ca^{2+} , with no fast Na^+ currents. This causes the SA nodal cells to have relatively slower depolarisation and therefore slower APs. Therefore, APs in SA and AV pacemaker cells as known as “slow response” APs, as they have a slower rate of depolarisation than non-pacemaker cells. Non-pacemaker APs, inversely referred as “fast response” AP’s, due to more rapid depolarisation, are found throughout the myocardium (21). Although pacemaker activity is spontaneously generated by the SA nodal cells it can be modified by autonomic nerves, drugs, hormones, ischemia and hypoxia.

SA nodal cell APs has 3 phases. The ions responsible for change in membrane potential during the AP are predominantly Ca^{2+} and K^+ , and to a lesser extent Na^+ (Figure 1.2). When the membrane is repolarised, Na^+ channels open, conducting a slow inward Na^+ current called the “funny current” (I_f) (I_f is a mixed Na^+ - K^+ current, therefore it can also occur as a result of K^+ influx). The I_f results in the membrane potential depolarising, initiating phase 4 of the AP that consists of this spontaneous depolarisation. As the membrane potential reaches -50mV transient (T-type) calcium channels open, enabling inward Ca^{2+} current (I_{CaT}) down its electrochemical gradient, further depolarising the cell. When the membrane potential depolarises to approximately -40mV the long-lasting (L-type) calcium channels open with a resulting inward Ca^{2+} current (I_{CaL}). This further depolarises the cell until the AP threshold of -40 to 30mV is reached and phase 0 commences. Also, during phase 4 there is a slow decline in K^+ efflux (I_K) as the K^+ channels responsible for phase 3 close, contributing to the depolarising pacemaker potential.

Phase 0 is the AP depolarisation phase, caused by increased I_{CaL} . The I_f and I_{CaT} declines during this phase as their respective channels close. As Ca^{2+} influx is slow the rate of depolarisation is much slower than that of cardiac cells. This is followed by repolarisation in phase 3, as K^+ channels open, resulting in I_K and L-type calcium channel inactivation and closure. The subsequent hyperpolarised state is essential for pacemaker channels to activate. Therefore, once the nodal cell is repolarised to approximately -60mV in phase 3, the AP phase cycle is spontaneously repeated.

In SA nodal pacemaker cells during depolarisation the membrane potential moves towards the equilibrium potential for Ca^{2+} , about +134mV. During repolarisation Ca^{2+} conductance decreases and K^+ conductance increases, resulting in membrane potential becoming closer toward the equilibrium potential of K^+ , as stated above -96mV, according to the Nernst equation. AV nodal cell APs also have intrinsic pacemaker activity produced by the same ionic currents as the SA nodal cells, determined by changes in slow inward Ca^{2+} and K^+ current, with no fast Na^+ currents.

Spontaneously released Ca^{2+} from the SR (known as a Ca^{2+} spark) into the cytosol is involved in the “calcium clock” mechanism that also determines pacemaker potential. The rise in intracellular Ca^{2+} activates the NCX to extrude one Ca^{2+} out of the cell in exchange for three Na^+ into the cell, depolarising the membrane potential. The extruded Ca^{2+} is later pumped back into the cell via Ca^{2+} channels on the cell surface and SR membranes, allowing a flow of Ca^{2+} into the cell, continuously depolarising the membrane potential (22).

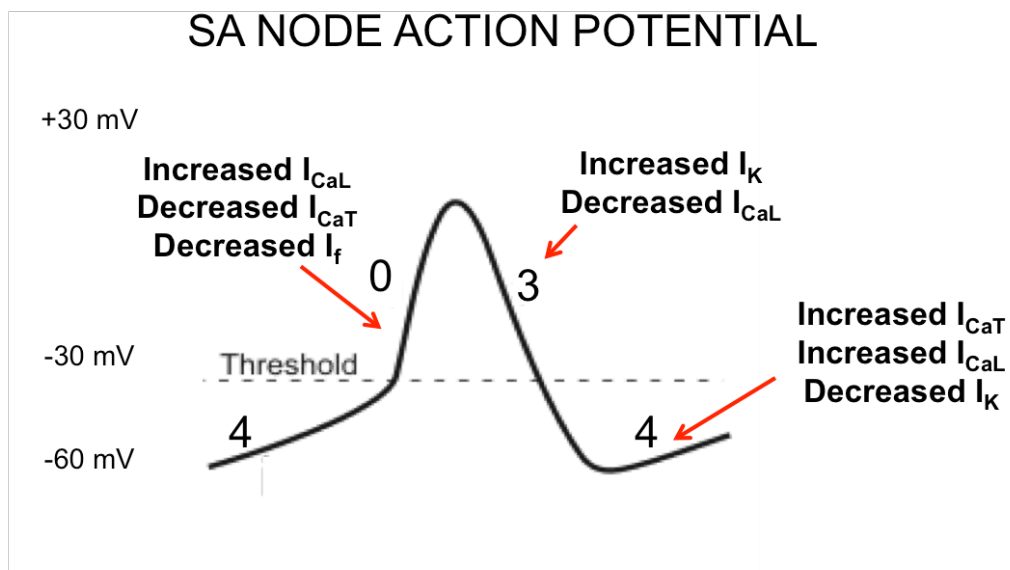


Figure 1.2. SA node action potential.

The numbers refer to the phase of the AP. The respective membrane potential is shown to the left of the AP. Figure adapted from (23).

1.2.6. Human ventricular action potential

Atrial and ventricular cardiomyocytes are examples of cells that generate non-pacemaker AP's. The type of ion channels responsible for determining the AP in ventricular and atrial cardiomyocytes are mostly the same (21). However, the expression and regulation differ in some of the ion channels and this is what results in the AP of a ventricular cardiomyocyte having different morphology to that of an atrial cardiomyocyte (24).

A normal human ventricular cardiomyocyte AP has five phases (Figure 1.3). Phase 4 is the RMP phase (-90mV for ventricular cardiomyocytes) and is associated with high K^+ currents (I_{K1}), in which K^+ ions are leaving the cell and

making the membrane potential negative. At the same time, fast sodium channels and L-type calcium channels are closed. Phase 0 occurs when cells are rapidly depolarised by an AP at a neighbouring cell, to a threshold voltage of around -70mV.

Phase 0 is classified by a rapid upstroke with a large and fast depolarisation of the cardiomyocyte membrane, due to the rapid influx of Na^+ ions along their electrochemical gradient, generating the “fast-response” AP. This inward Na^+ current (I_{Na}) generates the initiation and propagation of APs from cardiomyocyte to neighbouring cardiomyocyte throughout the myocardium, consequently assuming a central role in the excitability of the myocardial cells and accurate conduction of the electrical impulse across the heart (1). At the same time that sodium channels open, outward K^+ current diminishes as potassium channels close. This results in the membrane potential moving away from E_{K} and closer toward the equilibrium potential for Na^+ (E_{Na}), which is +52mV (if the same conditions are used as in the previously described Nernst equation) (17).

Phase 1 of the ventricular AP represents an initial repolarisation that is a result of the fast depolarisation activated, 4-AP (aminopyridine)-sensitive, Ca^{2+} independent transient outward K^+ current (I_{to}). However, due to the transient nature of I_{to} and also a simultaneous large increase in slow inward Ca^{2+} , repolarisation is delayed, described as phase 2. This inward calcium I_{CaL} is via L-type calcium channels that open when the membrane depolarises to around -

40mV. This plateau phase prolongs the AP duration (APD) and distinguishes the cardiac non-pacemaker APs from nerve and skeletal muscle APs. There are an additional two functionally distinct K^+ current in the myocardium, rapidly and slowly delayed rectifier potassium currents (I_{Kr} and I_{Ks} respectively), so named due to their voltage-dependent kinetics of recovery (25). The repolarisation of phase 3 occurs when potassium conductance increases and leads to the activation of I_{Kr} and I_{Ks} alongside the inactivation of Ca^{2+} channels (26, 27).

VENTRICULAR ACTION POTENTIAL

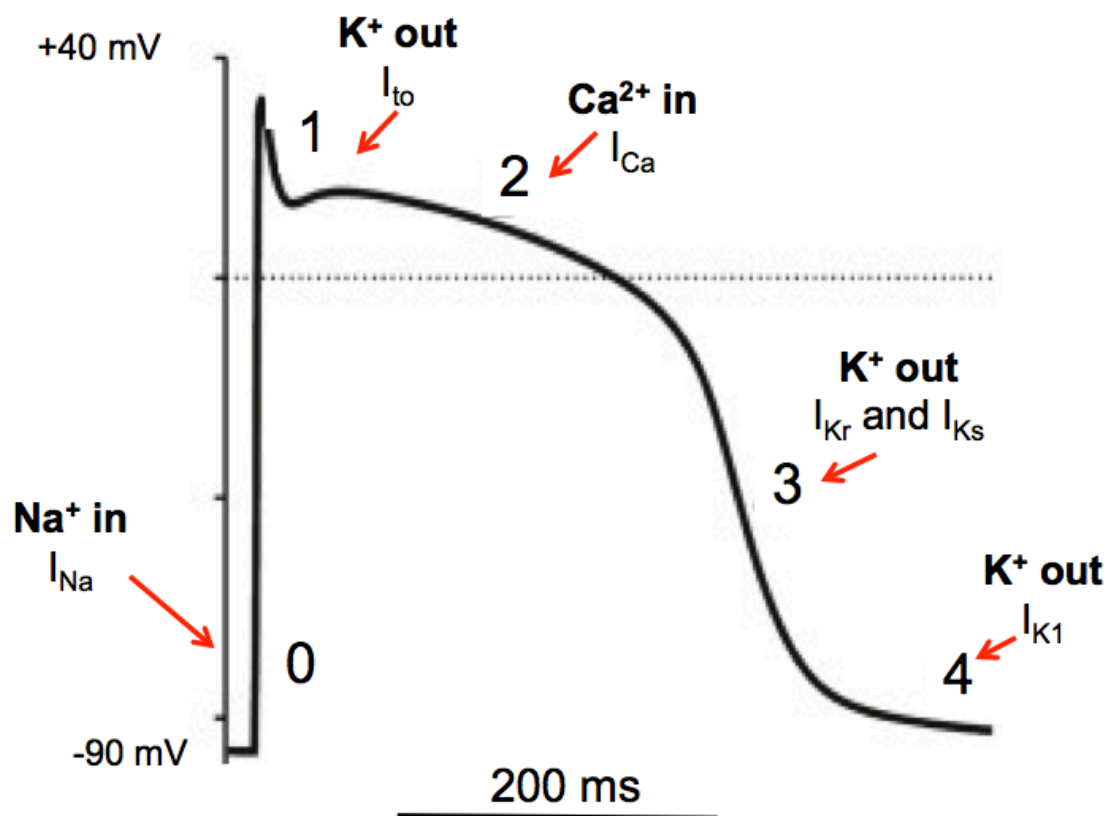


Figure 1.3. Ventricular action potential.

The numbers refer to the phase of the AP. The respective membrane potential is shown to the left of the AP. Figure adapted from (28).

1.2.7. Human atrial action potential

As previously stated, atrial APs differ from ventricular APs, aside of the difference in RMP (phase 4). The human atrial AP characteristically exhibits a more triangular morphology compared to that of the ventricular AP, which has a spike-and-dome shape with the prominent plateau phase (Figure 1.4). The characteristic difference in morphology of the human atrial AP compared to the ventricular AP is observed in most mammalian species, except for rats and mice, where both atrial and ventricular cardiomyocytes display short, triangular APs (29, 30).

Maximum upstroke velocities (V_{max}) of human atrial APs have been reported to be between 150-300V/s (19, 31, 32), notably less than the 300-400V/s reported for ventricular APs (33, 34). V_{max} has long been established as a measure of I_{Na} in cardiac myocytes (19, 31). The lower V_{max} of the atrium is possibly associated with the more depolarised RMP compared to that of the ventricles, as it would be expected that a more positive RMP would lead to reduced I_{Na} .

Additionally, as detailed previously, the atrial RMP is more depolarised due to a smaller I_{K1} , but this smaller density of I_{K1} is also partly accountable for the slower late phase of repolarisation in the atria. Human atrial cardiomyocytes exhibit a 2-fold greater density of the I_{Kr} current (generated predominantly by

the $K_v4.3$ channel) compared to that of the ventricles, which is responsible for the initial phase 1 repolarisation phase in the atria (Figure 1.4). Additionally, the slow component of the transient outward current I_{Ks} , generated from the $K_v1.4$ channel, is completely absent in the atria, but exists in the ventricles (Figure 1.4) (24). However, the atria do express three functional delayed rectifier K^+ currents that contribute to AP repolarisation. The ultra-rapid delayed rectifier K^+ current I_{Kur} (generated by the $K_v1.5$ channel) is exclusive to the atria and is active during the plateau phase of the AP (Figure 1.4). Its atrial specific nature has resulted in the I_{Kur} being an attractive target of antiarrhythmic drugs (AADs) for AF treatment (35).

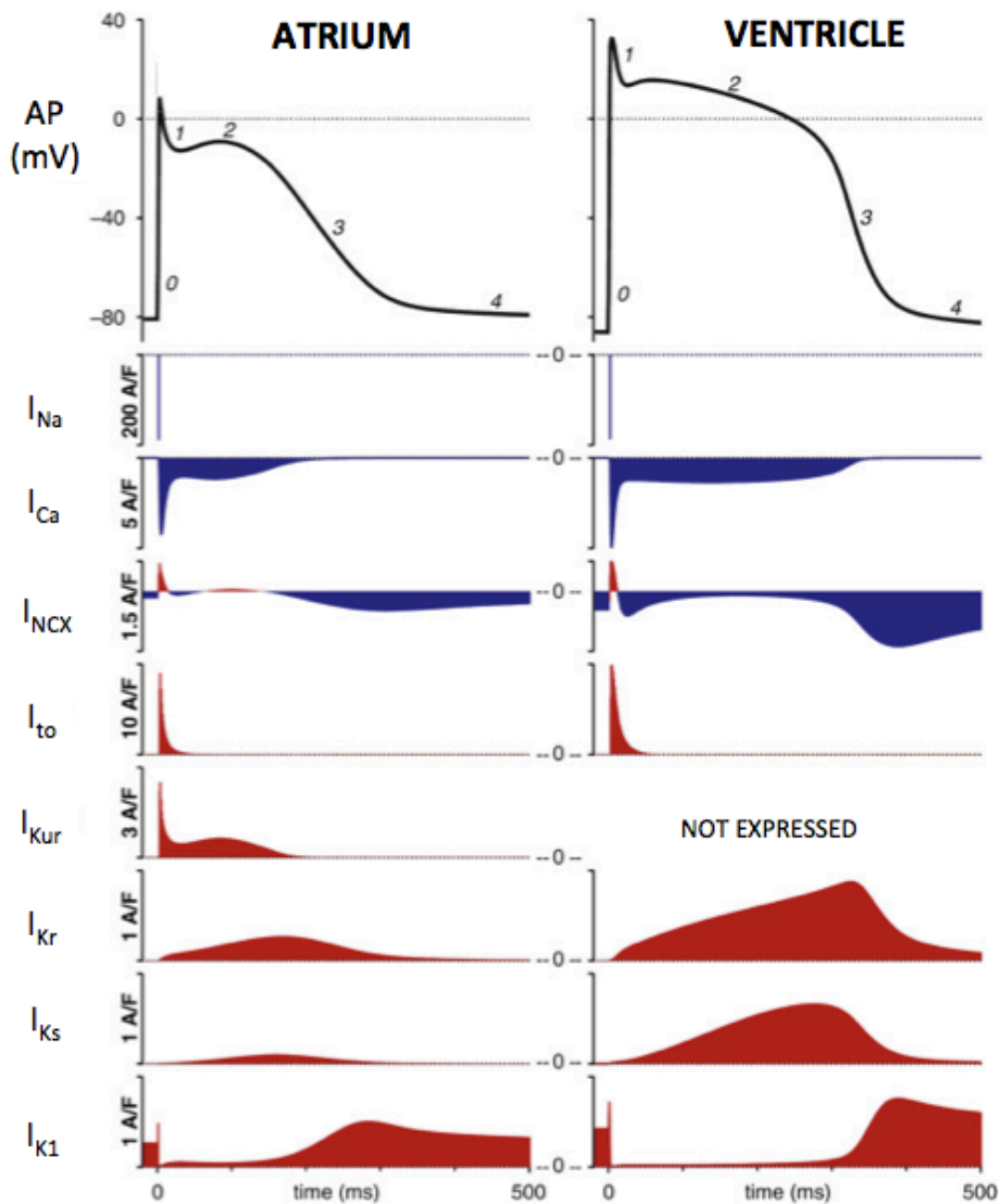


Figure 1.4. Morphology and ionic currents of human atrial and ventricular action potentials.

The AP morphology is shown by the top left and right hand side figures for the respective chamber. The numbers refer to the phase of the AP. For each current profile the thin horizontal line represents zero current. The blue inward currents fall below the line and red outward currents are above it. Figure adapted from (28).

1.2.8. Effective refractory period

After phase 0 and during phases 1,2 and part of 3 of the AP, another AP cannot be initiated as the voltage-gated sodium channels (VGSCs) are in the non-conducting closed state and must recover back to the closed resting state before they can reopen. This period is known as the effective refractory period (ERP). Consequently, the length of the ERP restricts the frequency of APs (and thus contractions) that the cardiac tissue can generate. Therefore, the ERP is protective as it inhibits multiple, compounded AP's from arising, that would render the heart unable to adequately fill with and eject blood (23).

1.2.9. Cardiac excitation-contraction coupling

The electrical activation of a cardiomyocyte triggers contraction followed by relaxation, known as excitation-contraction coupling (ECC). ECC includes the initial membrane depolarisation via the AP and activation of the Ca^{2+} transient, including the myofilament contractile response to the Ca^{2+} transient (Figure 1.5)(36).

In a ventricular cardiomyocyte an AP moves along the cell sarcolemma and down into the T-tubule system depolarising the cell membrane. Voltage-sensitive L-type calcium channels open and Ca^{2+} enters into the cell during phase 2 of the AP (Figure 1.4). The resulting I_{CaL} triggers a subsequent release of large amounts of Ca^{2+} from the sarcoplasmic reticulum (SR), via SR calcium

release channels called ryanodine receptors (RyR2s), causing intracellular Ca^{2+} ($[\text{Ca}^{2+}]_i$) to rise. As previously described, atrial cardiomyocytes have fewer T-tubules than ventricular cardiomyocytes, and the cells making up the SA node, AV node and Purkinje fibers have almost none. In the regions that lack T-tubules, I_{CaL} initiates SR Ca^{2+} release only at the surface membrane junctions (37).

The released free Ca^{2+} binds to troponin-C (TN-C), part of the regulatory complex attached to the thin filaments. This stimulates a conformational change in the regulatory complex that causes troponin-I (TN-I) to expose a site on the actin molecules, which can then bind to the myosin ATPase located on the myosin head. This binding instigates ATP hydrolysis, providing energy for a conformational change to transpire in the actin-myosin complex. The overall consequence of the conformational changes is the action of the actin and myosin filaments sliding past each other (a ratchet motion) shortening the length of the sarcomere. This ratchet motion cycle ensues when the cytosolic Ca^{2+} remains elevated (38).

Therefore, it is essential for the $[\text{Ca}^{2+}]_i$ to decline for cardiac relaxation and ventricular filling to occur. I_{CaL} slows at the end of phase 2 of the AP and the SR sequesters Ca^{2+} by an ATP-dependent Ca^{2+} pump, sarco-endoplasmic reticulum calcium-ATPase (SERCA). Additionally, Ca^{2+} is also transported out of the cell by the sodium-calcium exchanger (NCX) pump (39). The resultant

reduction of cytosolic Ca^{2+} concentration triggers removal of Ca^{2+} from TN-C. The unbinding of Ca^{2+} from TN-C causes a conformational change in the troponin complex, leading to the return of TN-I inhibition of the actin-binding site. A new ATP binds to the myosin head, displacing the ADP and the sarcomere length is restored, with subsequent muscle relaxation (38, 40). See Figure 1.5 for a schematic summarising this.

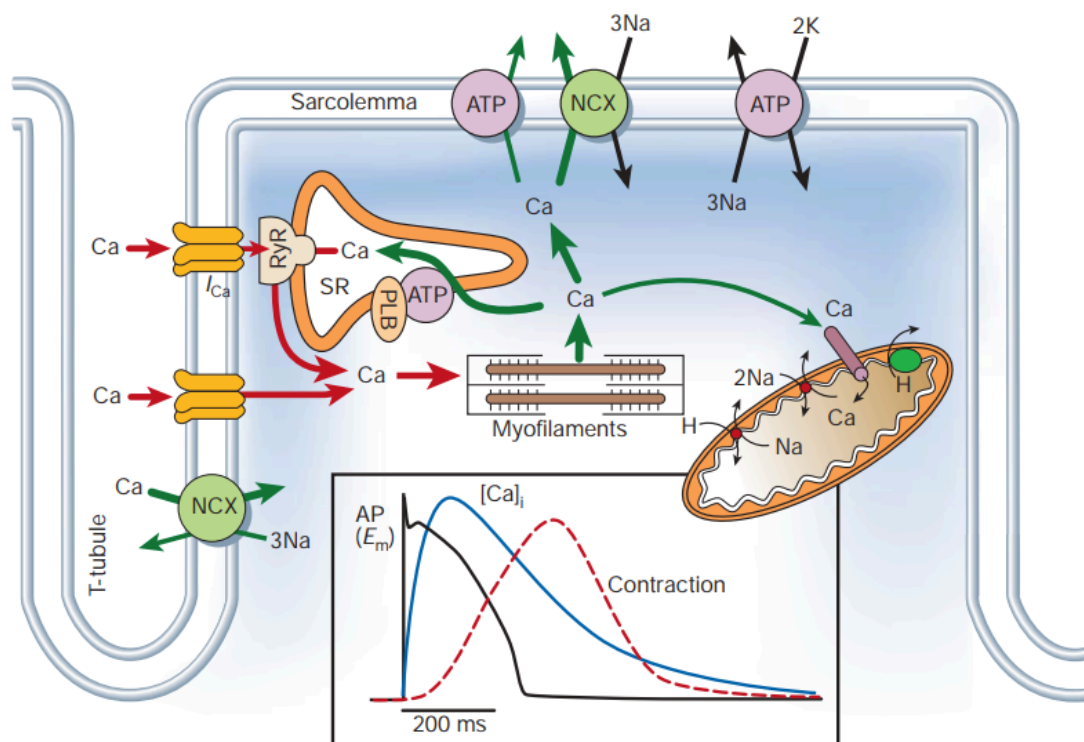


Figure 1.5. A ventricular Ca^{2+} transport schematic.

The different cardiomyocyte forms of Ca^{2+} transportation. A rabbit ventricular cardiomyocyte time AP, Ca^{2+} transient and contraction is shown inset. Figure extracted from (40).

1.3. Sodium handling pathways

In the heart $[\text{Na}^+]_i$ is involved in numerous vital cell functions, such as excitability as a key modulator of AP waveform, ECC, pH regulation, energy metabolism and cardiac development and growth. Na^+ homeostasis is complex, regulated in cardiac myocytes by a balance of Na^+ influx and efflux pathways. In a healthy cardiomyocyte there is a steady state electrochemical gradient favouring Na^+ influx. This potential energy is utilised by Na^+ specific channels and transporters that couple Na^+ influx to the co- or counter-transport of other ions and solutes (2).

Under typical conditions sodium channels and $\text{Na}^+/\text{Ca}^{2+}$ exchange are the primary Na^+ influx pathways. However, additional transport mechanisms, such as Na^+/H^+ exchange, can become greatly activated and potentially increasingly important during altered conditions, including acidosis (41). The Na^+ extrusion from cardiomyocytes occurs principally via the Na^+/K^+ -ATPase pump. $\text{Na}^+/\text{Ca}^{2+}$ antiporter and Na^+/H^+ exchange are also present in the mitochondria and are critical to mitochondrial function (42, 43). The paired fluxes of Na^+ with Ca^{2+} and H^+ make the detailed understanding of $[\text{Na}^+]_i$ regulation crucial to the understanding of cardiac ECC and pH regulation.

1.3.1. Voltage-gated sodium channel

VGSC's are a class of intrinsic transmembrane proteins that are responsible for the initiation and propagation of the AP in electrically excitable cells, activated by fluctuations in cardiomyocyte membrane potential. Mammalian VGSCs are formed of a pore-forming α -subunit (260kDa) that is associated with one or two β -subunits (30-40kDa) (44).

1.3.1.1. Sodium channel α -subunit and gating

The α -subunit (pore-forming subunit) is capable of forming a fully functional channel and can generate electrical impulses independent of the auxiliary β -subunits. The mammalian species express nine functional VGSC α -subunit isoforms, $\text{Na}_v1.1$ -1.9. The primary α -subunit isoform expressed in the heart is $\text{Na}_v1.5$, encoded by the *SCN5A* gene located on chromosome 3p21, forming the principal electrophysiological and pharmacological properties of the I_{Na} within the myocardium (45, 46). However, $\text{Na}_v1.5$ expression has also been detected in other tissues, including the brain and gastrointestinal smooth muscle (47). Similarly, expression of the $\text{Na}_v1.1$ (44, 48-50), $\text{Na}_v1.2$ (49), $\text{Na}_v1.3$ (50, 51), $\text{Na}_v1.4$ (52), $\text{Na}_v1.6$ (50, 51) and $\text{Na}_v1.8$ (49) isoforms have also been determined in the heart but contribute to a very small proportion of the total cardiac sodium current compared to $\text{Na}_v1.5$.

All eukaryotic VGSCs have shown to have similar overall folding patterns. The α -subunits are large, single-chain polypeptides that consist of approximately

2000 amino acid residues organised into four homologous transmembrane domains (DI-DIV), covalently or non-covalently linked to one or two β -subunits via the N and C termini (53). Figure 1.7 illustrates a schematic representation of a VGSC.

There are three distinct primary states for VGSCs (Figure 1.6): a closed resting state, an open conducting state, and a non-conducting inactivated state. The rapid depolarisations of the cardiomyocyte and conduction of the electrical impulse depend on $\text{Na}_v1.5$ availability and if channels are in a closed or open state (54). Each DI-DIV domain of the VGSC is composed of two sub-domains: a cytoplasmic sub-domain and a transmembrane sub-domain. The domains are linked by intracellular loops and each domain is comprised of six transmembrane segments (S1–S6). Segment S1-S4 from each domain form the structural component with the function of regulating the channel opening upon depolarisation of the membrane, known as the voltage-sensing domain (VSD) (Figure 1.7).

At RMP (-80 to -90mV in LV and -60 to -80mV in LA), $\text{Na}_v1.5$ is in the closed resting state and in this configuration the activation gate is closed and inactivation-gate is open. There are conformational changes of the channel gates in response to changes in voltage. The S4 segment is positively charged and involved in the voltage-dependent activation of the channel. The VSD is linked to the pore domain (PD) by an intracellular loop between the S4 and S5

segments. The PD physically conducts Na^+ into the cardiomyocyte and is lined by S6 segments, forming the intracellular cavity known as the activation-gate (55, 56). When the membrane depolarises the positively charged S4 segment moves towards the extracellular surface and this motion transfers to the PD via intracellular linkers, resulting in a conformational change, causing opening of the activation gate and so also the channel pore. This means that the channel is in the open conducting state and Na^+ enters the cardiomyocyte, driven by the electrochemical gradient (54). As described, this inward current causes the initiation and propagation of action potentials throughout the myocardium, subsequently playing a central role in the excitability of myocardial cells and accurate conduction of the electrical impulse throughout the heart (1).

The channel inactivation-gate is formed and stabilised by the C-terminal domain and the intracellular loop between DIII on S6 and DIV on S1 (57, 58). During membrane depolarisation this loop (inactivation-gate) acts as a hinged lid and folds toward the intracellular opening of the α -subunit pore, inactivating the channel. This conformational change renders the channel to be in the non-conducting inactivated state, as Na^+ can no longer enter the cardiomyocyte. When the membrane repolarises the VGSC recovers from inactivation and the S4 segments return to the closed resting state, available for a subsequent depolarisation and the inactivation-gate unfolds out of the α -subunit pore.

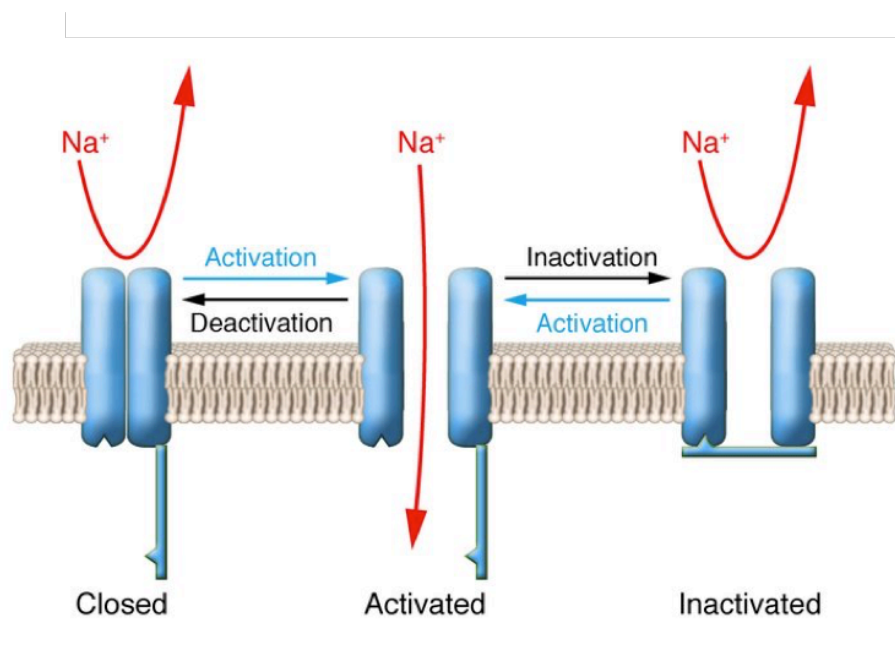


Figure 1.6. A schematic representation of VGSC gating. A representation of the three distinct primary gating states of a VGSC. Figure extracted from (59).

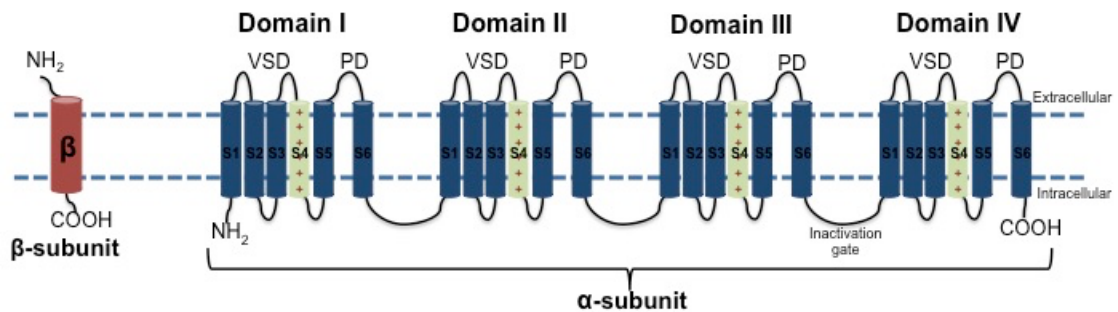


Figure 1.7. A schematic representation of VGSC structure. The four (I-IV) domains are labelled above the respective S1-S6 segments. The PD and VSD are labelled above the respective segments. The positively charged S4 segments are shown in green. The β -subunit isoform has not been specified. Figure adapted from (60).

1.3.1.2. Sodium channel β -subunit

Most VGSCs isolated from mammalian cells contain associated β -subunits and as detailed previously, VGSCs are composed of one α -subunit and one or two β -subunits. The VGSC β -subunits are type 1 intrinsic membrane proteins, members of the immunoglobulin (Ig) domain family of cell-adhesion molecules. The V-type Ig domain is connected to a single α -helical transmembrane domain and a carboxy-terminal intracellular region (Figure 1.7). There are 4 identified β -subunits of sodium channels, $\beta 1$ and $\beta 3$ that are non-covalently linked with the α -subunit (61, 62) and $\beta 2$ and $\beta 4$ that are inter-subunit disulfide-linked to the α -subunit (63, 64).

Studies in heterologous expression systems and in native cells have revealed that VGSC β -subunits regulate properties of the α -subunits, including level of plasma membrane expression, subcellular localisation, channel gating kinetics and voltage dependence (53, 65). Although there are some discrepancies in observations, it is generally agreed that co-expression of $\beta 1$ with $\text{Na}_v1.5$ in vitro promotes $\text{Na}_v1.5$ trafficking to the plasma membrane, resulting in increased peak I_{Na} (53, 66). However, it has been shown that the co-expression of $\beta 2$ and $\beta 4$ subunits with $\text{Na}_v1.5$ has little to no effect on I_{Na} density but experiments were conducted using hyperpolarised holding potentials, so may not be representative of I_{Na} effects in vivo (4, 67). Furthermore, studies of mutated $\beta 3$ have shown reduced I_{Na} density, supporting the notion that $\beta 3$ co-expression with $\text{Na}_v1.5$ increases I_{Na} density (68-70).

The β -subunits have also been shown to affect the gating kinetics of VGSCs. The expression of $\beta 1$ with $\text{Na}_v1.5$ has shown to result in a negative shift in steady-state inactivation of the channel (71). However, others have shown opposing results, observing a positive shift in steady-state inactivation (72). Similarly, the effect of $\beta 1$ co-expression on the activation of $\text{Na}_v1.5$ has been inconclusive, with some reporting no effect (44), others reporting a negative shift (73) and others reporting positive shifts (72). Additionally, $\beta 1$ co-expression was shown to reduce the persistent current, known as the late Na^+ current (I_{NaL}), (74).

Co-expression of $\beta 2$ and $\beta 4$ with $\text{Na}_v1.5$ shifted the steady-state inactivation kinetics positively and caused faster recovery of the channel (4). Others found a negative shift in activation with $\beta 4$ (64) but this is conflicting with no difference in activation voltage when $\text{Na}_v1.5$ is expressed with both the $\beta 2$ and $\beta 4$ subunits compared to $\text{Na}_v1.5$ expression alone (4). Additionally, silencing of the $\beta 2$ subunit in ventricular cardiomyocytes has resulted in an increase in I_{NaL} (75). Co-expression of $\beta 3$ with $\text{Na}_v1.5$ studies have also shown contradictory results, negative shifts (70) and positive shifts (69) in the steady-state inactivation of the channel.

1.3.1.3. Late sodium current

After opening briefly in phase 0 of the AP, $\text{Na}_v1.5$ ordinarily inactivates and remains in the non-conducting inactivated state until complete repolarisation. However, VGSCs that remain open after initial depolarisation create a small persistent current known as I_{NaL} , lasting throughout phase 2 of the AP. Although I_{NaL} peak is very small compared to the peak I_{Na} (approximately <1%) (76), it occurs throughout the low conductance phase of the AP and has proven to contribute to AP morphology, plateau potential and AP duration (APD) in human ventricular cardiomyocytes. As membrane resistance is great during the AP plateau, even a slight increase of inward current can cause APD prolongation (77). Although the magnitude of I_{NaL} is small, due to its persistence throughout the AP, the resultant Na^+ loaded into the cardiomyocytes is actually comparable to that of the I_{Na} (76).

1.3.2. Sodium-calcium exchanger

NCX is the dominant Ca^{2+} efflux mechanism in cardiomyocytes and is therefore an essential modulator of cardiomyocyte Ca^{2+} regulation, Ca^{2+} cycling and contractile function (2). There are three mammalian NCX isoforms that are expressed in a tissue-specific manner, NCX1-3 (78). NCX1 is the primary isoform expressed in the mammalian heart (79). NCX1 is a plasma membrane protein, consisting of 10 transmembrane segments with a molecular weight of 110kDa and appears to assemble as dimers. Studies have shown that NCX1 is distributed throughout the cardiomyocyte surface membrane, with some studies

suggesting there is a higher density within the t-tubules (80, 81). However, NCX1 localisation remains controversial (82).

NCX1 binds and transports one Ca^{2+} ion in exchange for three Na^+ ions across the cardiomyocyte plasma membrane, resulting in electrogenic transport that can be measured as an ionic current (83). On a beat-to-beat basis, NCX has the main function of extruding Ca^{2+} from cardiomyocytes during relaxation and diastole, balancing Ca^{2+} entry via L-type Ca^{2+} channels during cardiac excitation (84, 85). Therefore, small changes in NCX activity can significantly alter Ca^{2+} homeostasis. However, as NCX is driven by the trans-membrane Na^+ gradient, aside from extrusion of Ca^{2+} in exchange for Na^+ , the “forward mode”, the NCX can also act inversely in “reverse mode”, facilitating Ca^{2+} influx and Na^+ efflux. The direction of the NCX mode of activity is determined upon the physiological conditions of membrane potential and intracellular concentrations of Ca^{2+} and Na^+ (86).

Therefore, an increase in $[\text{Na}^+]_i$ can result in a decrease in NCX “forward mode”, subsequently leading to increased $[\text{Ca}^{2+}]_i$ and an increase in force of contraction. Equally, high $[\text{Na}^+]_i$ can lead to “reverse-mode” NCX activation and trigger Ca^{2+} overload. A significant rise in $[\text{Ca}^{2+}]_i$ controls the activity of a number of sarcolemmal ion channels and affects release of $[\text{Ca}^{2+}]_i$ from the SR, causing a subsequent arrhythmogenic increase (87). With a sufficiently large

Ca^{2+} release from the SR, the NCX can generate a depolarising current and even prematurely activate $\text{Na}_v1.5$ (3).

1.3.3. Sodium-potassium ATPase pump

The sodium-potassium ATPase (NKA) pump is an electrogenic transmembrane ATPase pump that utilises energy from ATP hydrolysis to extrude three Na^+ ions in exchange for two K^+ ions in, leading to net movement of charge. It consists of an α -subunit of approximately 110kDa and a β -subunit of 55kDa. Four isoforms of the α -subunit, $\alpha1-4$ and three β -isoforms, $\beta1-3$ have been detected in mammalian cells (88).

The NKA α -subunit contains the binding sites for ATP, Na^+ , K^+ and cardiac glycosides. It transports 3 Na^+ out in exchange for 2 K^+ in for each ATP hydrolyzed. The principal isoform responsible for bulk Na^+/K^+ regulation in the cardiomyocytes is $\alpha1$. However, $\alpha2$ is accountable for $\text{Na}^+/\text{K}^{2+}$ regulation in the t-tubules and consequently maintaining contractility (89). Association with the β -subunit is essential to stabilise the α -subunit in the endoplasmic reticulum and in directing the $\alpha\beta$ -complex to the plasma membrane (90). The $\beta1$ and $\beta2$ isoforms are the primary isoforms expressed in the human heart (91, 92).

Phospholemman (PLM) is a small transmembrane protein that associates with and inhibits NKA, principally by reducing its affinity for internal Na^+ (93). The

inhibition is relieved upon phosphorylation of PLM by protein kinase A (PKA) at site Serine68 or protein kinase C (PKC) at both sites Serine68 and Serine63 (94).

1.3.4. Sodium-hydrogen exchanger

The sodium-hydrogen exchanger (NHE) is a ubiquitously expressed integral membrane protein that regulates intracellular pH, volume and $[Na^+]_i$, by extrusion of one H^+ in exchange for one extracellular Na^+ . There are nine known isoforms of mammalian NHE's, categorised NHE1-9. The first discovered isoform, NHE1, is the best characterised and is the primary cardiomyocyte isoform (95). The efflux of Na^+ via the NKA pump provides a constant driving force for H^+ extrusion and Na^+ influx via the NHE.

NHE1 is a protein of 815 amino acid residues with a molecular mass of 85kDa. It consists of two domains: an N-terminal membrane domain that transports ions and a C-terminal cytoplasmic regulatory domain that controls activity and facilitates cytoskeletal interactions (96). NHE1 is constitutively phosphorylated and further phosphorylation increases its activity and although it does not use ATP directly, ATP depletion decreases its activity significantly (97).

1.4. Cardiac arrhythmias

As described previously, ionic currents in cardiomyocytes generate a propagating wave of electrical potential, triggering a co-ordinated and directed contraction in order to pump blood around the body effectively. This sequence of processes is known as Normal Sinus Rhythm (NSR). Cardiac arrhythmia is a disturbance of NSR resulting from abnormalities in the electrophysical properties of the heart and it is a widespread and growing problem. Several pathological conditions can cause electrophysiological disturbances that are proarrhythmic, including acute ischemia, structural and/or biochemical abnormalities such as heart failure, cardiac fibrosis, cardiac hypertrophy, or genetically determined arrhythmia syndromes, electrolyte or hormonal imbalances and medication usage that alter ion fluxes and/or the effects of the autonomic nervous system of the heart (98).

Electrical disturbances can lead to arrhythmia in the upper and lower chambers of the heart. Atrial fibrillation (AF) is the most common sustained cardiac arrhythmia in clinical practice and is recognised as an increasing health-care burden (99).

1.4.1. Atrial fibrillation

AF affects around 2% of the UK population and is becoming progressively more prevalent (99). Over the last few decades, hospital admissions for AF have

increased by two thirds, likely owed to an aging population, more frequent diagnosis as a result of improved monitoring, a rising prevalence of chronic heart disease and improved survival from disorders such as acute myocardial infarction (100).

AF is characterised by a loss of the ordinarily close synchrony of the excitation and resting phases between atrial cardiomyocytes, triggering cells in different regions of the atria to depolarise, repolarise and become excited again in an uncoordinated fashion (101, 102) (Figure 1.8). The irregular pattern of excitation renders the affected atria incapable of coordinated contraction (103). Additionally, in AF the ventricular rate is often irregular as impulses enter the AV node from the atria at irregular times (104). However, as atrial contraction typically plays a minor role in ventricular filling, most individuals can tolerate AF if ventricular rate is adequate to maintain cardiac output, so AF is not immediately life threatening (105).

Nonetheless, AF is a major cause of morbidity and mortality, as a result of stroke and thromboembolism, congestive heart failure, sudden death and impaired quality of life (106, 107). Due to increase in AF incidence it is anticipated that cardiovascular morbidity and economic costs will rise substantially (108). Evidenced by AF prevalence, the atria appear more susceptible to arrhythmia generation than the ventricles but the reason for this is yet to be clearly identified.

AF is characterised by progression over time and classified into three forms, paroxysmal, persistent and permanent. Paroxysmal AF is defined as short, self-terminating episodes that convert to NSR within 7 days. Persistent AF is defined as recurrent episodes requiring intervention for restoration of sinus rhythm. Permanent AF is defined when AF is accepted and no attempts are made to restore sinus rhythm. It is thought that AF evolves from paroxysmal to persistent and then permanent as a result of atrial remodelling due to AF, although there are exceptions to this rule (109). This auto-reinforcing property has been replicated in animals models and termed as “AF begetting AF” (110). Paroxysmal, persistent and permanent forms of AF necessitate personalised approaches to management (111), calling for a more individualised understanding of the drivers of AF (112). Though AF has been acknowledged and studied greatly since the early twentieth century, and despite the progress made in stroke prevention by anticoagulation, management is inadequate and a greater understanding of AF mechanisms is crucial to understand the atria’s susceptibility and improve therapy.

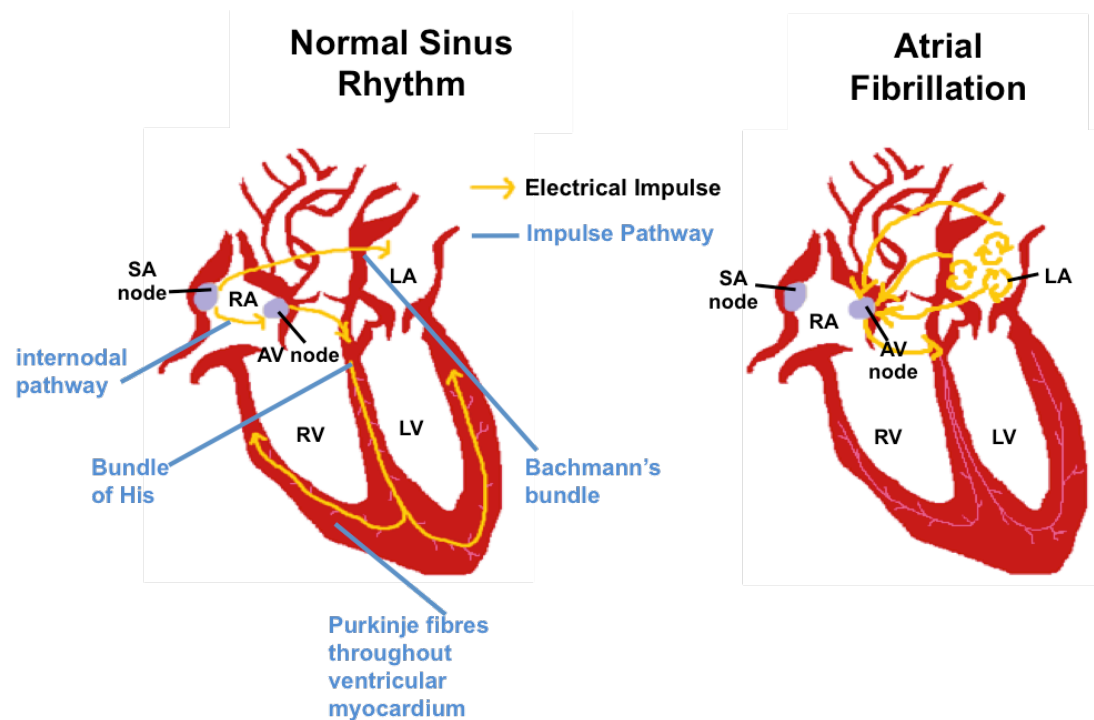


Figure 1.8. Diagram comparing movement of electrical impulse between NSR and AF.

In the NSR heart the impulse is initiated by the SA node in the RA and travels to the AV node via the internodal pathways and to the LA via the Bachmann's bundle pathway. Via the AV node the impulse travels to the Bundle of His and is divided between the RV and LV bundle branches. The impulse reaches the Purkinje fibres and spreads throughout the ventricular myocardium. In the atrial fibrillation heart the typical electrical impulse pathways are not followed and the impulse is spread in a disordered abnormal manner. This image was created by the author of this thesis.

1.4.2. AF mechanisms

The mechanism that sustains AF is referred to as the "driver". The irregularity of atrial electrical impulses in AF can be due to an irregular response to a rapid regularly discharging driver as a result of random ectopic firing, a localised re-entry circuit or multiple re-entry circuits that vary in time and space (111).

1.4.2.1. AF mechanisms underlying ectopic firing

Normal cardiomyocyte APs remain at resting potential after repolarisation, maintained by the high K^+ permeability and resulting inward I_{K1} . However, atrial cardiomyocytes also have a pacemaker current (I_f) that is much smaller than I_{K1} . When there is a change in the balance with decreased I_{K1} and/or increased I_f , enhanced automaticity can occur. This results in diastolic membrane depolarisation that enables abnormal AP initiation and therefore AF generation (113).

Early afterdepolarisations (EADs) comprise of irregular secondary membrane depolarisation during AP phase 3 repolarisation. The primary causing factor of EADs is APD prolongation, enabling L-type Ca^{2+} channels to recover with resulting inward I_{CaL} depolarising the membrane triggering an irregular AP (114). Additionally, abnormal diastolic release of Ca^{2+} from the SR causes delayed afterdepolarisations (DADs) (115). As previously described, the SR Ca^{2+} stores are regulated by a balance between Ca^{2+} release from the SR into the cytosol via RyRs channels and Ca^{2+} uptake into the SR via SERCA (39). Although this system is adaptive to increase of acute stress-related conditions, sustained Ca^{2+} loading or functionally defective RyRs can cause abnormal diastolic RyRs Ca^{2+} release. The released Ca^{2+} is extruded via the NCX, with a net depolarising inward positive Na^+ current underlying DADs during phase 4 of the AP and abnormal AP generation (115).

1.4.2.2. Basic mechanisms underlying re-entry

Re-entry sustains AF by generating a rapidly firing driver with fibrillatory propagation or by producing multiple irregular re-entry circuits. The basic concept of re-entry was described over 100 years ago in experimental models (102). Re-entry is modelled as either the leading-circle or spiral-wave model. In both models the preservation of continuous activity relies on atrial properties, with a balance between a shortened ERP and slowed excitability of the cardiomyocytes (116).

In the leading-circle model (Figure 1.9), re-entry circuits are established spontaneously in a 'circuit' length (the wavelength [WL]), quantified by the distance the impulse travels in 1 ERP. This can be calculated by the following equation: $WL = ERP \times CV$ (conduction velocity) (117). It has been shown that the shorter the WL the greater number of simultaneous re-entry circuits the atria can sustain. Likewise, the longer the WL, the fewer re-entry circuits can be housed by the atria. Consequently, reduction in ERP and/or CV can promote re-entrant AF and increasing either (i.e. with drugs) can suppress AF (118).

The main difference between the leading-circle and spiral-wave models is the predicted responses to VGSC blockade. The leading circle model supports the understanding of the promotion of AF with CV reduction that is observed with Na⁺ channel mutations (119). However, the efficacy of Na⁺ channel blockers for

AF treatment contradicts the leading-circle, as you would expect the resulting reduction in CV would in fact promote AF (116, 120).

Although scientists have shown appreciation for the leading-circle model, the spiral-wave theory has been more recently developed with modern theoretical analysis (Figure 1.9) (121). The spiral-wave model is related to the leading-circle but is somewhat different. The activity induced by a spiral-wave follows the inside to outside of the excitable medium, keeping its shape and rotating around a core of constant size, shape and velocity. For a convex spiral-wave, electrical impulses radiate outward and each cardiomyocyte on the wavefront activates more than one cardiomyocyte downstream, reducing CV as the ratio of excited cells to resting is less. For a concave spiral-wave electrical impulse radiates inwards, each cardiomyocyte on the wave front activates less than one cardiomyocyte, increasing CV, as the ratio of excited cells to resting cells is greater (116).

Therefore, the excited to resting cell ratio mismatch, limits the current that depolarises each cell ahead of the wave front. Decreasing current results in slower rate of voltage rise ahead of the wave front and a longer period before VGSCs are activated. This results in slowing the propagation of abnormal APs, by decreasing the stimulating power of the activation front. Theoretically, reduced ERP can also promote spiral-wave re-entry by increasing and

stabilising spiral-wave rotors. Therefore, both models explain AF occurrence with APD shortening (116).

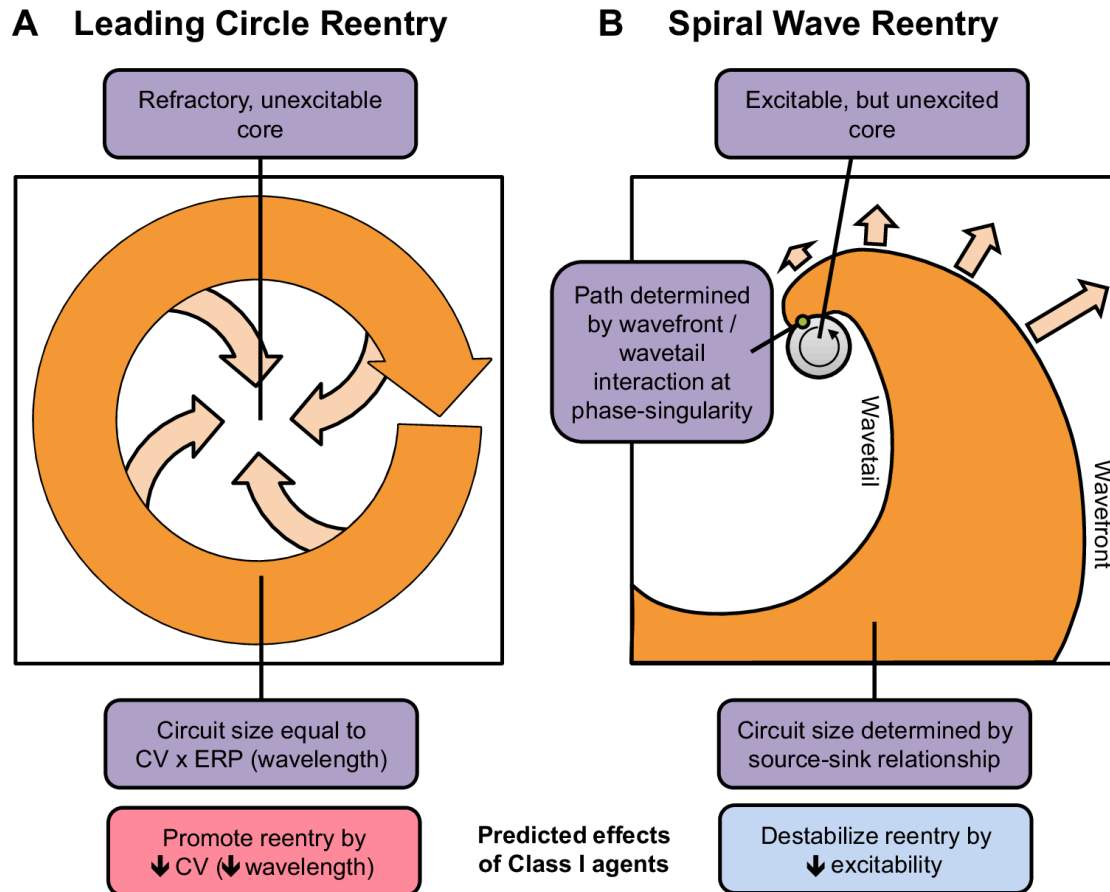


Figure 1.9. Mechanistic concepts of re-entrant arrhythmia.

A) A depiction of the leading circle concept based on re-entrant excitation travelling around an unexcitable core. The circuit size is determined by wavelength (distance travelled by the electrical impulse in one ERP). B) A depiction of the spiral wave concept based on re-entry occurring around an excitable but continuously unexcited core. Re-entry relies on the balance of current-source/tissue excitability (favouring propagation) and current-sink (impairing propagation). Figure extracted from (122).

1.4.2.3. Electrical determinants of AF

The movement of ions via membrane channels and transporters controls the electrical properties of a cardiomyocyte and can be a determinant of AF

generation and/or maintenance. Increase in inward Ca^{2+} and Na^+ prolong APD and escalate the likelihood of EAD generation. Conversely, a decrease in inward Ca^{2+} shortens APD, as does an increase in outward K^+ , due to resultant repolarisation of the cardiomyocyte. As previously described with the leading-circle model, APD shortening promotes re-entrant AF as the circuit ERP is reduced and repolarisation is accelerated (123).

Changes seen in Na^+ handling have proven to be a factor in AF generation and maintenance (124). AP initiation and spread depends on inward I_{Na} during phase 0, making it a determinant of CV. Therefore, loss of function mutations of SCN5A with reduced I_{Na} have shown to slow conduction and in turn promote AF. Additionally, gain of function mutations of SCN5A have shown to induce AF due to increased APD and excitability leading to EADs (54, 125). Likewise, it has been demonstrated that I_{NaL} is upregulated in some pathophysiological settings, potentially disrupting the repolarisation (phase 3) of the AP with APD prolongation, also leading to development of EADs (126, 127).

1.4.3. AF rate and rhythm control therapies

The typical aims of AF treatment in order of importance are: prevention of thromboemboli, control of ventricular response, restoration of NSR, and maintenance of NSR by preventing recurrence. For AF treatment patients age, degree of symptoms and presence of underlying heart disease are considered (128). In order to reduce the risk of thromboembolic events anticoagulants are

used, as AF can result in blood stasis in the atria (129, 130). Current treatment therapies for AF involve the use of rate and rhythm control approaches as well as surgical interventions. There are also upstream therapies, targeting pathophysiological processes underlying the structural changes associated with AF, aiming to prevent occurrence or recurrence by slowing the progression of remodelling (131).

Rate control strategies regulate ventricular rate by targeting the AV node as it transmits electrical signals from the atria, in order to minimise the common AF symptom of excessive ventricular rate and in turn prevent tachycardia-associated cardiomyopathy (132). Rate control therapies include the use of negatively chronotropic drugs (such as β -blockers or digoxin) or electrophysiological/surgical intervention (133). However, with rate control the atria continue to fibrillate so additional medication is required to reduce the risk of thromboembolic events (133). Additionally, there are risks associated with rate control drugs, the ventricular rate can be slowed too much and result in complications, such as sinus bradycardia and heart block. Therefore, patients prone to these symptoms, notably the elderly, may need AV node ablation and permanent pacemaker implantation (133).

Commonly, patients with AF have substantial symptoms despite rate control and require restoration of NSR. Non-invasive rhythm control strategies convert the heart to NSR with AADs, directly altering electrical currents (134). Rhythm

control treatment is decided based upon patient symptoms, the classification of AF (paroxysmal, persistent or permanent), comorbidities, health and anticoagulation status. Rhythm control is considered most beneficial in patients <65 years old, with recent AF onset and limited underlying heart disease (7).

AADs that have been used for AF rhythm control are sodium and potassium channel blockers (135). The most common sodium channel blockers used clinically inhibit the VGSC, including propafenone and flecainide (136). They cannot be used in patients with structural heart disease, as they have shown to increase risk of ventricular arrhythmias and atrial flutter in patients with severe heart failure (134, 137). Other antiarrhythmic drugs inhibit various potassium channels (7), including sotalol, ibutilide, dofetilide and amiodarone (136). Although they can be used more freely, particularly amiodarone, they have extra cardiac side effects and have some proarrhythmic risk to ventricular arrhythmias with greater toxicity (128, 134, 135).

AADs work by blocking K^+ , Ca^{2+} and Na^+ channels and/or adrenergic receptors (138). However, the mechanisms of drugs differ greatly based on the ion channels targeted. Class IC work largely by blocking the VGSC in order to reduce the V_{max} , in turn reducing the excitation of cardiac tissue. On the other hand, IIIc drugs largely work by blocking K^+ channels and therefore prolonging the APD and refractoriness, delaying conduction (7). Nonetheless, despite these AAD categorisations, it has been shown that many rhythm control drugs

impact AF by targeting ion channels and adrenergic receptors outside of the defined class specifications (7, 135).

One of the newest areas of study is the development of atrial selective drugs; that work by targeting ion channels only within the atria. Atrial selective drugs could limit toxicity and reduce the increased risk of ventricular pro-arrhythmia associated with AADs (138). Drugs targeting K⁺ channels primarily expressed in the atria are in the early stages of development (139, 140) and atrial selective VGSC blockade has also been suggested as a possibility (4, 141, 142).

Overall, clinical trials have revealed that when comparing rate and rhythm control therapies there is no difference in mortality (143-146). However, findings were limited as age of the patient populations was restricted (60-80 years), patients with excessive stroke risk were taken off anticoagulant therapy and AADs with proven high toxicity were included (7, 136). A large on-going clinical trial (EAST – AFNET 4) currently examines whether an early rhythm control therapy with antiarrhythmic drugs or AF ablation can improve outcomes in patients with AF (107). Furthermore, if atrial selective drugs were established, the mortality risks associated with rhythm control would be greatly neutralised and the potential over rate control for safer AF treatment could be immense. However, in order to determine VGSC blocking atrial selective drugs, a greater understanding of atrial sodium handling is required.

1.4.3.1. Flecainide pharmacology

Class I AADs work by binding to and blocking VGSCs (7). Blocking VGSCs decreases the slope of phase 0, leading to a decrease in AP amplitude. The primary effect of reducing the rate and magnitude of depolarisation is to decrease conduction velocity to depress abnormal conduction. Different sodium channel blockers inhibit the fast upstroke of the AP, driven by the opening of VSGCs, to different extents, explaining their differential effects on cardiac conduction (147). Drug induced VGSC block accumulates with tachyarrhythmia increased firing frequencies, slowing the rate of AP generation in cardiomyocytes and reducing cardiac excitability (148, 149). This can explain why flecainide is effective in terminating AF (150).

Sodium channel blockers may also alter APD and ERP. Effects on ERP are not directly related to sodium channel blockade but also the related drug actions on potassium channels involved in repolarisation. Altering the ERP can either increase or decrease arrhythmogenesis, depending on the cause of the arrhythmia. For example, re-entry tachycardia can be interrupted by increasing ERP, as tissue is unexcitable for longer so is less likely to be re-excited by re-entrant currents. However, increasing APD can also result in the generation of EADs (as described earlier).

Flecainide acetate was first synthesised in 1972 (151). The clinical efficacy of flecainide as a potent inhibitor of the VGSC ($\text{Na}_v1.5$) in humans was confirmed

by several clinical trials and was first approved for oral use in 1984 (152-154). Flecainide has proven to convert AF into NSR in both animal and human trials, with a high affinity for open-state $\text{Na}_v1.5$ channels with slow unbinding kinetics from the channel during diastole. Therefore, flecainide slows recovery of $\text{Na}_v1.5$ during diastole, prolonging ERP, in a rate dependent manner (155). Additionally, due to increased atrial activation, AF causes increased $[\text{Na}^+]_i$ via VGSCs and in turn promotes Ca^{2+} entry via NCX as excessive Na^+ is being extruded. The resulting accumulation of $[\text{Ca}^{2+}]_i$ promotes ischemia and cellular dysfunction (156). However, flecainide attenuates $[\text{Ca}^{2+}]_i$ accumulation by blocking the VGSCs, reducing the oxidative stress processes and further atrial remodelling that would otherwise occur as a result of increased $[\text{Ca}^{2+}]_i$ (157).

However, it has been demonstrated that flecainide use was associated with increased proarrhythmic events in patients with severe cardiac disease (158). Following the publication of the 1989 Cardiac Arrhythmia Suppression Trial (CAST) there was a major revision of the role of AADs. The trial was designed to investigate the efficacy of Class I AADs in patients post myocardial infarction with reduced ejection fraction and recurrent ventricular ectopic beats. Flecainide was shown to suppress ventricular ectopy but also had a threefold increase in arrhythmic death compared to the placebo (159). Nevertheless, due to its efficacy at blocking $\text{Na}_v1.5$, flecainide became recommended as a first line therapy for patients with AF, as long as there was no evidence of structural heart disease (160). Furthermore, recent data has reinforced the safety of using flecainide in patients without structural heart disease (161).

Flecainide was also shown to inhibit the opening of K^+ channels in atrial and ventricular cardiomyocytes, particularly effecting I_{Kr} , resulting in prolonged APD (162). However, Kvam et al., demonstrated that flecainide shortens APD in the Purkinje fibers, due to VGSC blockade (163). Additionally, recent studies have found that flecainide reduces SR Ca^{2+} release by blocking RyR2s, potentially preventing DADs and triggered activity (164). Flecainide has also demonstrated the proarrhythmic effect of converting AF into atrial flutter and potentially resulting in rapid tachycardia. However, the reported rate of this proarrhythmic effect is only 3-5% and has been associated with high adrenergic conditions (165). Therefore, drugs such as β -blockers, diltiazem and verapamil, that have AV blockade properties, can be administered concomitantly with flecainide to reduce risk (156). Additionally, flecainide exerts a negative inotropic effect and can significantly reduce stroke volume index and LV ejection fraction and increase RA and pulmonary capillary wedge pressures, in patients with coronary artery disease, congestive heart failure and already reduced ejection fraction. These outcomes are related to the reduction of inward Na^+ and Ca^{2+} into cardiomyocytes (156).

The efficacy of oral and intravenous flecainide in hindering recent onset AF has been compared to other AADs in several clinical trials. One trial found that intravenous flecainide was shown to cause earlier reversion of recent onset AF to NSR compared to intravenous amiodarone (166). Additionally, another trial

showed that a higher proportion of patients reverted to NSR when treated with intravenous flecainide compared to intravenous amiodarone and propafenone (167). Conversely, a different study found that oral flecainide had a similar conversion rate to NSR as oral propafenone (168). However, it should be recognised that the findings from the different clinical trials are affected by distinctions in the study design characteristics, methodological limitations and the time intervals from drug initiation to assessment of reversion to NSR.

The long-term efficacy and safety of flecainide treatment for AF prevention compared to other AADs or placebo has been extensively studied. In the prevention of AF recurrence, it has been established that oral flecainide is superior to placebo (169) but similar to propafenone (170, 171), quinidine (172) and sotalol (169). Flecainide has shown to be better tolerated than quinidine and had a lower rate of adverse events compared to propafenone (170, 171). Overall, a meta-analysis of 60 trials concluded that 2/3 of patients responded to short-term flecainide treatments and 1/2 to long-term treatment (173).

When selecting the right AAD for AF treatment many considerations need to be made in order for treatment to be tailored to each patient. Flecainide has been used for AF treatment extensively for over 30 years and its ability to reduce AF symptoms and provide long-term restoration of NSR has been well established (174). In younger patients without co-existing structural heart disease, the breadth of knowledge accumulated over the last few decades supports

flecainide as a safe and effective option to achieve and maintain NSR (156). However, an increased understanding of VGSC blockade properties of flecainide in the atria compared to ventricles would give a greater insight into its true value as an AF medication.

1.5. Study Hypotheses

As it has been described previously, β -subunits regulate the biophysical properties of the $\text{Na}_v1.5$ α -subunit, with alterations in the gating of VGSCs dependent on co-expression of $\beta1-4$ subunits (4, 64, 69-74). Furthermore, atrial and ventricular differences in expression of $\beta2$ and $\beta4$ were shown by Chen et al., in human and rat myocardium (4). Therefore, it is hypothesised in this thesis that there will also be distinctive expression of the $\beta2$ and $\beta4$ subunits between the atria and ventricles in the mouse model and these distinctions will lead to differences in the sodium channel gating kinetics between the chambers. Differences in VGSC gating kinetics may also lead to chamber distinctions in inhibition with a sodium channel blocking AAD.

Additionally, loss-of-function mutations in desmosomal proteins (desmoplakin, plakophilin or plakoglobin) were shown to cause changes in morphological structure and be a primary cause of an inherited cardiomyopathy (175-177). Knockdown of the gene that encodes plakophilin 2 in mice has proven to decrease I_{Na} density and alter channel gating kinetics in rat ventricular

cardiomyocytes, with a significant arrhythmogenic decrease in CV (178). As heart samples from ARVC patients with reduced plakoglobin expression revealed reduction in ventricular $\text{Na}_v1.5$ at the intercalated disks (179, 180) it is postulated in this thesis that I_{Na} density and channel gating kinetics may also be altered in plakoglobin deficient mice.

High quality cardiomyocytes are essential for experimental investigation of VGSC kinetics. The simple Langendorff-free isolation technique we developed is able to provide high yields of healthy cardiomyocytes to enable electrophysiological data to be collected more efficiently.

2. Materials and Methods

2.1. Ethical statement and study approval

All animal surgical procedures/experiments were conducted according to the rules and regulations of the Animals (Scientific Procedures) Act, 1986, approved by the Home Office (PFDAAF77F), the institutional review board at the University of Birmingham and the local authorities.

Prof. Giuseppe Faggian at the University of Verona provided all human tissue samples. Human surgical procedures/sample donations were conducted under the consent of the donors and according to the rules and regulations of the Human Tissue Act 2006.

2.2. Animal models

Experiments were conducted on male and female adult mice (12-20 weeks old), bred on the 129/sv background. Some experiments in the Langendorff-free technique for mouse cardiomyocyte isolation chapter were conducted on C57/BL6J male and female (8-12 weeks old) mice, this is specified with the relevant data. Mice were housed in individually ventilated cages, with sex-matched littermates (2-7 mice/cage), under standard conditions (12 hour light/dark cycle, 22°C and 55% humidity). Food and water were available *ad*

libitum. The visible health status of all mice (body weight, grooming, bearing) was monitored daily.

Experiments were performed on wild type and heterozygous Plakoglobin deficient mice (Plako^{+/-}) (181).

2.3. Western blotting methods

2.3.1. Western blot statistical analysis

Data were expressed as mean \pm standard error, unless otherwise stated. Statistical analysis was performed using one way Analysis of Variance (ANOVA) with Tukey's's post hoc analysis where appropriate, when comparing three or more groups. Unpaired Student t-tests were used when comparing tissue from two different chambers. Significance was taken as $P < 0.05$ (GraphPad Prism 7.0b).

2.3.2. Mouse heart excision

Mice were weighed. For heart excision under deep terminal anaesthesia, each mouse was placed inside the anaesthesia chamber with 4% isoflurane in O₂, 1.5L/min with active scavenging of surplus gas, using the Fluovac system for mice with table-top anaesthesia system and small induction box (Harvard Apparatus U.K. #726425), until breathing rate significantly slowed and the

righting reflex was absent. The mouse was removed from the induction box and the pedal reflex was checked (by a firm toe pinch) as a measure of deep pain recognition, to ensure that the mouse was under deep anaesthesia before any incisions were made. Mice were placed in a supine position on a polystyrene block with the limbs taped down and sacrificed through death by exsanguination. Thoracotomy was performed using scissors, to expose the heart under continuing deep terminal isoflurane anaesthesia via a face mask with active scavenging of surplus gas (4% isoflurane in O₂, 1.5L/min). The heart was extracted using curved scissors to excise vessels (avoiding laceration of the aorta).

Hearts were then placed in polystyrene standard weighing boats with 40ml of ice cold Krebs buffer (0.118 mol/L NaCl, 0.02488 mol/L NaHCO₃, 0.00118 mol/L KH₂PO₄, 0.011 mol/L Glucose, 0.00083 mol/L MgSO₄.7H₂O, 0.00352 mol/L KCl, 0.0018 mol/L CaCl₂ adjusted to pH 7.3) with 50uL of heparin (LEO Laboratories, Ltd, UK) to reduce risk of thrombus formation. Krebs buffer was ice cold to encourage cardioplegia (temporary cessation of cardiac activity) to aid cannulation.

The heart was transferred to a 50ml glass petri dish, containing 40ml of ice cold Krebs buffer on a stand that housed a 2ml syringe with attached cannula of outer diameter 1mm, as seen in Figure 2.1. The aorta was cannulated and secured with a suture in less than 3 minutes in the 50ml glass petri dish to limit

any tissue damage, as shown in Figure 2.1. The syringe attached to the cannula was used to flush the heart with 2ml of Krebs via retrograde perfusion. Pressure from retrograde perfusion caused the aortic valve to close, forcing the buffer flowing in via the cannula into the coronary circulation. It was essential to ensure the cannula and syringe were free of air bubbles to avoid the introduction of air into the isolated heart.

The chambers and septum of the heart were separated, placed into 1.5mL Eppendorf tubes (Thermo Scientific; #3451) and snap frozen in liquid nitrogen. Samples were stored at -80°C until required for Western blotting experiments.

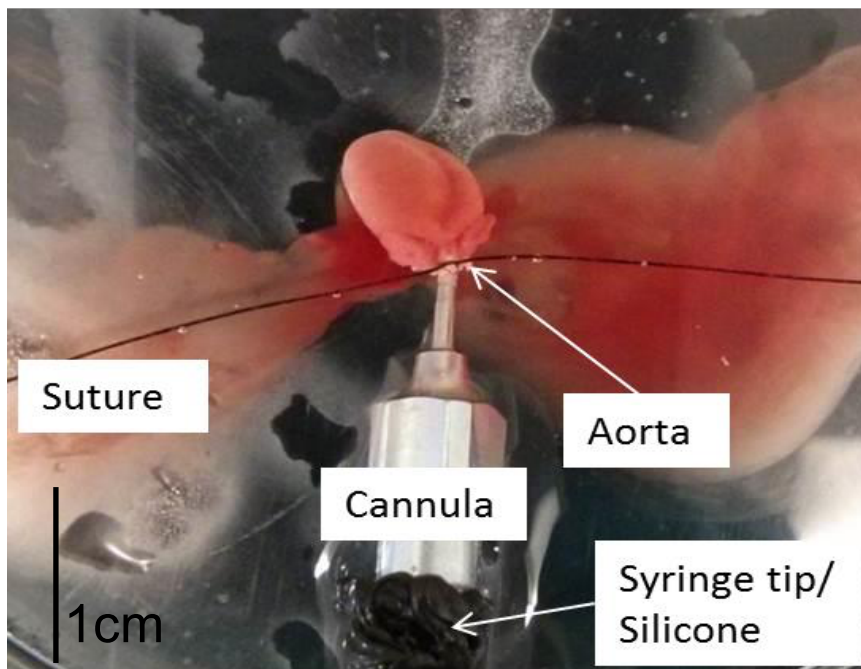


Figure 2.1. Cannulation of ascending aorta.

Photograph of a mouse heart cannulated via the aorta submerged in cold Krebs buffer solution in 50ml petri dish. The dish was held into place using blue tack on a custom stand that also holds the buffer filled syringe with attached cannula. The cannula is secured by fine suture, which is seen as the black string above the cannula across the image. The cannula is attached to a 2ml

syringe and secured with black silicone. When the heart was flushed with buffer from the syringe the blood was expelled, as seen by the red clouded regions in the image (182).

2.3.3. Mouse sample preparation

Weights of the heart chambers were recorded. Atria were put into 0.5mL homogenising CK14 Precellys tubes (KTO3961-1-203.0.5) and ventricles into 2mL homogenising CK14 Precellys tubes (KT03961-1-003.2). Samples were homogenised in homogenisation buffer (Tris adjusted to pH 7.3, 1 protease cocktail inhibitor tablet (Roche Diagnostics; complete ULTRA Tablets, Mini, EASYpack; 05892970001) diluted in 10mL buffer, with phosphatase cocktail inhibitor 2 (Sigma; #p5726) and 3 (Sigma; #P0044)) added (both 1:100 concentration). The homogenisation buffer was added to the tubes containing the tissue in a ratio of 1mg of tissue: 10uL of buffer. The tubes were loaded onto the Precellys24 Homogeniser set to 5000rpm for 2x 15seconds. Homogenates were transferred into 2.0mL Eppendorf tubes (Thermo Scientific; #3434) and diluted 2 times in SDS sample buffer (i.e. 1mg of tissue: 20uL of buffer) (100mM Tris, 20% w/v glycerol, 5% w/v β -mercaptoethanol, 4% w/v SDS and 0.2% bromophenol blue, pH 6.8). This resulted in samples with a protein concentration of \approx 1.5ug of protein/1ul of sample solution, tested using Qubit protein assay kit (Life Technologies; #Q33211).

2.3.4. SDS-Polyacrylamide Gel (SDS-PAGE) for mouse samples

Samples were centrifuged using the Hettick® MIKRO 220R centrifuge for 10 minutes 14000RPM at 2°C so that sediment was separated and could be avoided during loading. Then 10uL of sample (≈15ug of protein) was loaded onto, 4-15% gradient Mini-PROTEAN® TGX™ gels (Bio-Rad; #4561084) immersed in running buffer (0.025M Tris base, 0.19M glycine and 0.1% w/v sodium dodecyl sulphate). 8uL Precision Plus™ Protein Dual-Colour Standard (Bio-Rad; #1610374) was ran alongside samples for molecular weight estimation. 90-140V was applied to the gels using a PowerPac™ Basic power supply (Bio-Rad; #1645050) until the visible sample buffer line reached the bottom of the gels.

2.3.5. Semi-dry electrophoretic transfer

Proteins were transferred from Mini-PROTEAN® TGX™ gels onto methanol (VWR chemicals; 20847.307) activated TransBlot® Turbo™ mini-size polyvinylidene difluoride membranes (Bio-Rad, #170-4156) using a Trans-Blot® Turbo™ semi-dry electrophoretic transfer system (Bio-Rad; #170-4155). Single Trans-Blot® Turbo™ Mini-size Transfer Stacks (Bio-Rad; #1703966) were placed in the semi-dry transfer sandwiching the membrane. Bio-Rad 1.3A, 25V and 30M transfer protocol was ran for 10 minutes.

2.3.6. Human tissue collection

Tissue samples were collected during heart transplant, left ventricular assist device (LVAD) fitting, aortic valve replacement, coronary artery bypass, mitral valve repair, subaortic membrane removal surgeries or from deceased organ donors.

The operating surgeon separated the samples and they were snap frozen in liquid nitrogen, then stored at -80°C in 1.5mL Eppendorf tubes (Thermo Scientific; #3451) until required for Western blotting experiments.

2.3.7. Human sample preparation

The excised frozen tissue was crushed with a cryogenic tissue pulveriser (Cellcrusher; Ballina) in a pestle and mortar manner. The pulveriser was cooled in liquid nitrogen and the frozen sample was placed in the chamber and was pulverised by hitting the pestle portion with a mallet. The pulverised samples were then removed from the chamber using an ice-cooled spatula and put in a 1.5mL Eppendorf tubes (Thermo Scientific; #3451) and stored at -80°C . After each sample was removed from the pulveriser it was cleaned in warm water and then wiped down with ethanol then cooled again in liquid nitrogen.

A portion of each of the pulverised tissue samples (approximately relative to the size of a mouse left ventricular sample) was put into 2.0mL Eppendorf tubes

(Thermo Scientific; #3434). Samples were homogenised in 150uL of homogenisation buffer (Tris adjusted to pH 7.3, 1 protease cocktail inhibitor tablet (Roche Diagnostics; complete ULTRA Tablets, Mini, EASYpack; 05892970001) diluted in 10mL buffer, with phosphatase cocktail inhibitor 2 (Sigma; #p5726) and 3 (Sigma; #P0044)) added (both 1:100 concentration). The homogenisation buffer was added to the tubes containing the tissue and the samples were homogenised using a mechanical handheld homogeniser on setting 6 (Power Gen 125, Fisher Scientific) over dry ice to keep the sample cool. The handheld homogeniser was cleaned using distilled water between each sample homogenisation. Homogenates were centrifuged using the Hettick® MIKRO 220R centrifuge for 10 minutes 14000RPM at 2°C. A volume of the centrifuged samples was transferred into 2.0mL Eppendorf tubes (Thermo Scientific; #3434), without disturbing the visible lipid deposit on the surface and unhomogenised detritus at the bottom of the tube.

The Qubit protein assay kit (Life Technologies; #Q33211) was used to quantify the amount of protein in each sample. Sample buffer was added each sample (100mM Tris, 20% w/v glycerol, 5% w/v β -mercaptoethanol, 4% w/v SDS and 0.2% bromophenol blue, pH 6.8) with the volume calculated using the results of the protein assay in order to achieve a concentration of 1.5ug of protein/1ul of solution. For human samples it was essential that the final volume of the sample solution was $\geq 50\%$ sample buffer (homogenisation buffer: sample buffer, 1: \geq 1) to ensure adequate volume of sample buffer for denaturing of

proteins and breakage of disulphide bonds. Samples were then vortexed for uniformity.

2.3.8. SDS-Polyacrylamide Gel (SDS-PAGE) for human samples

Samples were heated to 90°C for 8 minutes before loading when probing for Na_vβ2 and Na_vβ4 but left unheated when probing for Na_v1.5. 12uL of sample (18ug of protein) was loaded onto, 4-15% gradient Mini-PROTEAN® TGX™ gels (Bio-Rad; #4561084) immersed in running buffer (0.025M Tris base, 0.19M glycine and 0.1% w/v sodium dodecyl sulphate). 8uL Precision Plus™ Protein Dual-Colour Standard (Bio-Rad; #1610374) was ran alongside samples for molecular weight estimation. 90-140V was applied to the gels using a PowerPac™ Basic power supply (Bio-Rad; #1645050) until the visible sample buffer line reached the bottom of the gels.

2.3.9. Isolated cardiomyocyte sample preparation

For Western blot experiments comparing protein expression in injection-isolated and Langendorff-isolate cardiomyocytes cells were pipetted onto laminin-coated coverslips (10mm diameter) in the absence of 1,2-butanedione monoxime (BDM) and kept in culture for media for 4 hours. Plates were then placed on ice, cells were washed with ice cold phosphate buffered saline (PBS), and lysed by addition of a ureabased lysis buffer (235 mmol/l Tris pH 6.8, 18.75% glycerol, 5.6% sodium dodecyl sulfate, 6 mol/l urea, 1 mmol/l dithiothreitol), containing

Halt™ protease and phosphatase inhibitor cocktail (Thermo Scientific). Total cell lysates were prepared by scraping of wells and transfer to 1.5 ml tubes on ice, passage through a 27 G needle x 5, and incubation at 4°C for 30 min with nutation. SDS-page was carried out as described in mouse sample preparation above.

2.3.10. Membrane probing

Membranes were each submerged in 15mL of dissolved, non-fat, dried powdered milk (AppliChem; 04021011) diluted to 5% in PBS (Sigma-Aldrich; P4417-50TAB; 0.01mol/L phosphate buffer; 0.0027 mol/L KCl; 0.1037 mol/L NaCl; pH 7.3) with 0.1% TWEEN® 20 (PBS-T) (Sigma Aldrich; 9005-64-5) and incubated over night at 4°C. The membranes were incubated for 1 hour with primary IgG antibodies diluted in non-fat, dried powdered milk diluted to 1% in PBS-T at room temperature (see Table 1.1 and 1.3 for primary antibody details).

Membranes were then washed for 1 hour with 6 changes (every 10 minutes) in PBS-T to remove unbound antibody. The membranes were then incubated for 1 hour at room temperature with the appropriate horseradish peroxidase linked-conjugated (HRP) secondary IgG antibodies diluted in non-fat, dried powdered milk diluted to 1% in PBS-T at room temperature (see Table 1.2 and 1.4 for secondary antibody details). The membranes were then washed for one hour with 6 changes in PBS-T to remove unbound antibody.

Table 1.1: Primary antibodies used for mouse Western blot experiments.

Target of antibody	Concentration used	Animal Source	Company and catalogue number
Na _v 1.5	1:200	Rabbit, polyclonal	Alomone, ASC-005
Na _v β2	1:400	Rabbit, polyclonal	Alomone, ASC-007
Na _v β4	1:800	Rabbit, polyclonal	Alomone, ASC-044
NHE ₁	1:200	Mouse, monoclonal	Santa Cruz Biotechnology, sc-58635
NCX	1:1000	Mouse, monoclonal	Swant, R3F1
NKA α1	1:1000	Mouse, monoclonal	Santa Cruz Biotechnology, sc-28800
PLM pSer63	1:1000	Sheep, polyclonal	Badrilla, A010-110
GAPDH	1:4000	Mouse, monoclonal	ThermoFisher Scientific, AM4300
Total-ERK1/2	1:1000	Rabbit, polyclonal	New England Biolabs, 9102
Phospho-	1:1000	Rabbit, polyclonal	New England

ERK1/2			Biolabs, 9101
Total- PKC- α 1	1:1000	Mouse, monoclonal	Santa Cruz, sc-8393
Total PLM	1:500	Rabbit, polyclonal	Abcam, ab75597
Ser-63 PLM	1:2000	Sheep, polyclonal	Badrilla, A010-110

Table 1.2: Secondary antibodies used for mouse Western blot experiments.

Target of antibody	Concentration used	Source animal	Company and catalogue number
Rabbit	1:7500	Donkey	GE Healthcare, NA934V
Rabbit	1:4000	Goat	Merck, AP307P
Mouse	1:4000	Sheep	GE Healthcare, NA931V
Sheep	1:1000	Donkey	R&D Systems, HAF016

Table 1.3: Primary antibodies used for human Western blot experiments.

Target of	Concentration	Animal Source	Company and

antibody	used		catalogue number
Na _v 1.5	1:200	Rabbit, polyclonal	Alomone, ASC-005
Na _v β2	1:200	Rabbit, polyclonal	Alomone, ASC-007
Na _v β4	1:400	Rabbit, polyclonal	Alomone, ASC-044
GAPDH	1:4000	Mouse, monoclonal	ThermoFisher Scientific, AM4300
α-Actinin	1:2500	Mouse, monoclonal	Sigma-Aldrich, A7811

Table 1.4: Secondary antibodies used for human Western blot experiments.

Target of antibody	Concentration used	Source animal	Company and catalogue number
Rabbit	1:4000	Goat	Merck, AP307P
Mouse	1:4000	Sheep	GE Healthcare, NA931V

2.3.11. Visualisation of membranes

The membranes were submerged in 5ml of detection reagent (GE Healthcare, ECL Western Blotting Detection Reagents, Amersham, RPN2106) and placed

between 2 sheets of transparency film. Densitometry was performed to quantify the levels of chemiluminescence using the Odessey Fc Imaging System. The optical density readings (OD) acquired from the densitometry recordings were taken to proportionally monitor the level of protein expression.

2.3.12. Membrane stripping and re-probing

Calnexin or GAPDH was used as a loading control for Western Blots. The expression of calnexin/GAPDH was measured once the membranes had been stripped of primary and secondary antibody. Membranes were washed in PBS-T for 10 minutes, submerged in stripping buffer (Restore™ PLUS Western Blotting) for 15 minutes and re-washed in PBST for a further 10 minutes. The membranes were then blocked in 5% milk dissolved in PBS-T over night at 4°C. Membranes were then re-probed using the previously described antibody incubation methods.

2.3.13. Image analysis

The raw densitometry values obtained for the proteins were normalised by their corresponding densitometry value for calnexin or GAPDH to correct the data for possible variations in protein concentration between samples or loading errors of the samples onto the gels. In order to combine data (when severable blots were used to achieve larger sample sets) the calnexin/GAPDH normalised values were again normalised to the mean of LV values within each blot.

2.4. Whole-cell patch clamp electrophysiology

2.4.1 Langendorff-based mouse cardiomyocyte Isolation

Hearts of 129/sv background (15-20W) were isolated under isoflurane anaesthesia, as described previously (2.3.2 Mouse Heart Excision).

Solutions were perfused at 4mL/min, 36-37°C in the Langendorff set up. The cannulated heart was transferred to the Langendorff apparatus and perfused with Krebs buffer (0.118 mol/L NaCl, 0.02488 mol/L NaHCO₃, 0.00118 mol/L KH₂PO₄, 0.011 mol/L Glucose, 0, 0.00083 mol/L MgSO₄·7H₂O, 0.00352 mol/L KCl, 0.0018 mol/L CaCl₂, pH 7.3) for 4-5 minutes. Krebs solution (minus CaCl₂) was perfused through the Langendorff system for 5 minutes to clear out Ca²⁺ from the heart, causing the heart to consequently cease contracting. The heart was digested using the enzyme solution (0.118 mol/L NaCl, 0.02488 mol/L NaHCO₃, 0.00118 mol/L KH₂PO₄, 0.011 mol/L Glucose, 0, 0.00083 mol/L MgSO₄·7H₂O, 0.00352 mol/L KCl, 0.02 mol/L Taurine, 0.03 CaCl₂, Liberase TM Research Grade (Roche, Indianapolis, IN), 0.1% Bovine Serum Albumin, 20mM taurin and 3µmol CaCl₂, pH 7.3), until the heart was judged to be sufficiently soft (digestion time judged on appearance of heart tissue). If the heart was being digested well it would enlarge and go pale (salmon pink) within 1-2 minutes of the Liberase reaching the cannula. Enzyme digestion varied between different hearts but would generally fall between 15-25 minutes.

The heart and cannula were then removed from the Langendorff apparatus and placed into a petri 10ml dish filled with "STOP solution" (0.025 mol/L KCl, 0.01 mol/L KH_2PO_4 , 0.005 mol/L HEPES, 0.002 mol/L $\text{MgSO}_4 \cdot 7\text{H}_2\text{O}$, 0.02 mol/L Glucose, 0.01 mol/L DL aspartic acid potassium salt, 0.1% Bovine Serum Albumin, 0.1 mol/L L-Glutamic acid potassium salt, 0.02 mol/L Taurine, 0.0005 mol/L EGTA, 0.005 mol/L Creatine, pH 7.2). Then 5mL of the "STOP solution" was perfused through the heart using a 5mL syringe to inhibit the enzyme digestion activity any further.

The LA and LV chambers were dissected from the digested heart and placed into separate small 10ml petri dishes containing 1mL/2ml respectively of the "STOP solution". The chambers were then gently teased apart with forceps and triturated gently to release the cells using glass pipettes with increasing resistance (smallest diameter \approx 0.3-0.5mm). The cells were then checked under the microscope to see if they were well triturated. Further 2mL/4ml respectively (LA/LV) of Krebs solution (no CaCl_2) was added to each petri dish. The LA cell suspension was transferred into a 15mL falcon tube using a Pasteur pipette, without creating bubbles. The LV cell suspension was pipetted over 200um nylon gauze into a 50mL falcon tube. The LV cells were left to settle down to form a pellet for 15 minutes and 4mL of supernatant was then removed without disturbing the pellet.

All data within this Thesis that utilised isolated cardiomyocytes relied on this method of isolation, aside of the data specified as using the injection-based isolation method in the Langendorff-free technique for mouse cardiomyocyte isolation chapter.

2.4.2 Injection-based mouse cardiomyocyte Isolation

Mice were initially weighed before any surgical procedure. Each mouse was placed inside the anaesthesia chamber with 4% isoflurane in O₂, 1.5L/min with active scavenging of surplus gas, using the Fluovac system for mice with table-top anaesthesia system and small induction box (Harvard Apparatus U.K. #726425), until breathing rate significantly slowed and the righting reflex was absent. The mouse was removed from the induction box and the pedal reflex was checked (by a firm toe pinch) as a measure of deep pain recognition, to ensure that the mouse was under deep anaesthesia before any incisions were made. Mice were placed in a supine position on a polystyrene block with the limbs taped down. Thoracotomy was performed using scissors, to expose the heart under continuing deep terminal isoflurane anaesthesia via a face mask with active scavenging of surplus gas (4% isoflurane in O₂, 1.5L/min).

With round-end forceps the left lung was moved aside to expose the descending aorta and inferior vena cava. Both were cut using scissors and the heart was gently held using curved forceps. Using 10ml sterile syringe with attached 27 G hypodermic needle (ensuring there are no bubbles inside) 7ml of

4°C EDTA buffer (0.13 mol/L NaCl, 0.005 mol/L KCl, 0.0005 mol/L NaH₂PO₄, 0.01 mol/L HEPES, 0.01 mol/L Glucose, 0.01 mol/L BDM, 0.01 mol/L Taurine, 0.005 mol/L EDTA, adjusted to pH 7.8 and sterilised using 0.2µm filter) was injected steadily over a 1 minute period into the base of the RV, with the needle penetrating no more than 2mm into the RV wall. This caused contractions to quickly cease and blood to be flushed out of the heart.

The ascending aorta was then clamped with a curved-end haemostatic clamp, avoiding clamping the atrial appendages. The clamped heart was then removed by incision around the outside of the forceps and transferred into a 65ml glass petri dish, containing 40ml of 4°C EDTA buffer (0.13 mol/L NaCl, 0.005 mol/L KCl, 0.0005 mol/L NaH₂PO₄, 0.01 mol/L HEPES, 0.01 mol/L Glucose, 0.01 mol/L BDM, 0.01 mol/L Taurine, 0.005 mol/L EDTA, adjusted to pH 7.8 and sterilised using 0.2µm filter), ensuring the heart was submerged.

Using 10ml sterile syringe with attached 27 G hypodermic needle (ensuring there are no bubbles inside) 10ml of the same 4°C EDTA buffer was injected into the LV of the heart, 2-3mm above the apical point, with the needle penetrating no more than 2mm into the LV wall. During this injection very little pressure was used, with a flow rate of 1ml per 2-3 minutes in order to avoid perforation of the LA appendage. With this any remaining blood was cleared out of the coronary circulation and the heart became pale in colour.

After 6 minutes or injection of all 10ml of buffer (whatever was first) the needle was removed from the LV and the heart was transferred to another 50ml glass petri dish, containing 30ml of 4°C perfusion buffer (0.13 mol/L NaCl, 0.005 mol/L KCl, 0.0005 mol/L NaH₂PO₄, 0.01 mol/L HEPES, 0.01 mol/L Glucose, 0.01 mol/L BDM, 0.01 mol/L Taurine, 0.001 mol/L MgCl₂, adjusted to pH 7.8 and sterilised using 0.2µm filter). To clear remaining EDTA within the heart, 3ml of the same perfusion buffer was injected into the LV via the perforation made during the first injection, with the needle penetrating no more than 2mm into the LV wall. During this injection very little pressure was again used, with a flow rate of 1ml per 1-2 minutes. After 2 minutes or injection of all 3ml of buffer (whatever was first) the needle was removed from the LV and the heart was transferred to a 50ml petri dish, containing 10ml of 37°C (warmed in a water bath) collagenase buffer (0.13 mol/L NaCl, 0.005 mol/L KCl, 0.0005 mol/L NaH₂PO₄, 0.01 mol/L HEPES, 0.01 mol/L Glucose, 0.01 mol/L BDM, 0.01 mol/L Taurine, 0.001 mol/L MgCl₂, with 0.5mg/ml of collagenase 2 and 0.5mg/ml of collagenase 4, adjusted to pH 7.8 and sterilised using 0.2µm filter).

The same pre-heated to 37°C 10ml (4-7 syringes) collagenase buffer was injected into the LV via the perforation made during the first injection, with the needle penetrating no more than 2mm into the LV wall. The injection rate was sufficient to keep the heart inflated, typically 2ml/minute, but increased as the procedure progressed. Following injection of collagenase with each syringe 10ml of buffer was removed from the petri dish with an empty syringe to prevent overflow. The volume, and therefore number of syringes, of collagenase puffer

required varied between hearts, depending on the age, size and health of the heart. Complete digestion was determined when there was reduction in resistance to injection pressure, when the heart lost its shape and rigidity, when holes began appearing and when it turned pale and fluffy at the surface. Additionally, ejection of cardiomyocytes into the effluent buffer was also visible to the naked eye.

Once complete digestion was confirmed the clamp was removed from the aorta and the chambers and septum of the heart were separated and placed into separate small 10ml petri dishes containing 3ml respectively of the collagenase solution. The chambers were then gently teased apart with forceps and triturated gently to release the cells using glass pipettes with increasing resistance (smallest diameter \approx 0.3-0.5mm). Then 5ml of "STOP solution" (0.025 mol/L KCl, 0.01 mol/L KH_2PO_4 , 0.005 mol/L HEPES, 0.002 mol/L $\text{MgSO}_4 \cdot 7\text{H}_2\text{O}$, 0.02 mol/L Glucose, 0.01 mol/L DL aspartic acid potassium salt, 0.1% Bovine Serum Albumin, 0.1 mol/L L-Glutamic acid potassium salt, 0.02 mol/L Taurine, 0.0005 mol/L EGTA, 0.005 mol/L Creatine, pH 7.2) was added to each petri dish and each suspension was gently pipetted for a further 2 minutes.

The cells were then checked under the microscope to see if they were well triturated. The LA cell suspension was then transferred into a 15mL falcon tube using a Pasteur pipette, without creating bubbles. The LV cell suspension was

pipetted over 200um nylon gauze into a 50mL falcon tube. The LV cells were left to settle down to form a pellet for 20 minutes and 4mL of supernatant was then removed without disturbing the pellet. Supernatant was removed so that atrial cells were suspended in 3ml and ventricular cells were suspended in 6ml of buffer.

2.4.3. Calcium reintroduction

KB Buffer with Ca^{2+} (0.025 mol/L KCl, 0.01 mol/L KH_2PO_4 , 0.005 mol/L HEPES, 0.002 mol/L $\text{MgSO}_4 \cdot 7\text{H}_2\text{O}$, 0.02 mol/L Glucose, 0.01 mol/L DL aspartic acid potassium salt, 0.1% Bovine Serum Albumin, 0.1 mol/L L-Glutamic acid potassium salt, 0.02 mol/L Taurine, 0.0005 mol/L EGTA, 0.005 mol/L Creatine, 0.018 mol/L CaCl_2) was added to the suspension of cells in the falcon tube to a final Ca^{2+} concentration of 1.8mM over a 1.5 hour period. The KB buffer was added to the LA/LV cell suspensions in the following increments: firstly 100/200ul, 15 minutes later 100/200ul, 15 minutes later 400/800ul, 30 minutes later 600/1200ul then finally another 600/1200ul 30 minutes later (respectively LA/LV as LV suspension was x2 the volume of LA suspension at beginning of calcium reintroduction). Cells were then left in this suspension for at least 20 minutes at room temperature before use. Experiments were performed within 5 hours of isolation.

2.5. Whole-cell patch clamp electrophysiology

2.5.1. I_{Na} recordings

150 μ L of dissociated LA and LV cells were pipetted onto laminin-coated coverslips (10mm diameter) and allowed to adhere for 15-20 minutes. The coverslips were then transferred to a dry bath recording chamber under a microscope (Axiovert 25, Zeiss). The silver electrode wire used was chlorinated in a solution of 20mM NaCl. Cells were perfused with extracellular patch clamp solution (0.01 mol/L NaCl, 0.13 mol/L $C_5H_{14}ClNO$, 0.01 mol/L HEPES, 0.0012 mol/L $MgCl_2$, 0.0018 mol/L $CaCl_2$, 0.01 mol/L Glucose, 0.002 mol/L NiCl, 0.0045 mol/L KCl) adjusted to pH 7.4 with CsOH, at a rate of 2mL/minute.

Whole cell patch clamp recordings were obtained in voltage clamp mode using pipettes were pulled from borosilicate glass capillaries (Model P-97, Intracel) using a microprocessor-controlled puller (30-0057, Harvard Apparatus). They were automatically heat polished and had an input resistance of 2.2-3 M Ω . The glass pipette microelectrodes were filled using a 2mL syringe with attached micro-loader tip with internal solution (0.15 mol/L CsCl, 0.01 mol/L HEPES, 0.01 mol/L EGTA, 0.005 mol/L MgATP, 0.0005 mol/L $MgCl_2$, 0.02 mol/L TEA) adjusted to pH 7.2 with CsOH. The microelectrode was then placed into the pipette holder and positive pressure was applied using a 5ml syringe, displacing about 0.5mL of air through the pressure control system and pressure held in the pipette by closing the three-way valve. Experiments were performed at $22 \pm 0.5^\circ C$.

The microelectrode was homed into the bath that held the cell suspension coverslip using a micromanipulator (Scientifica) and the amplifier (AXOPATCH-1D, Axon Instruments, CA) was set to voltage-clamp mode. The pipette offset was corrected, so the currents measured at that point were considered as 0 pA. The seal test protocol was applied through the electrode (see Table 1.5). The cell of interest was then approached by the microelectrode (avoiding nuclei), until the tip touched the cell (enough to create a very small dimple in the cell) and the positive pressure was released in order to form a seal between the microelectrode and the cell and the voltage clamp was changed to -80mv. Once a minimum of a 1G Ω seal occurred (maybe requiring some suction by mouth) the cell was broken into using continuous light suction until the membrane broke and if a 1G Ω minimum access resistance was achieved the test protocols were run immediately (see Table 1.5). As the membrane of the cells acts as a capacitor, when the microelectrode breaks into the intracellular space, the current response to the seal tests should show exponential decay.

For current comparison of +/- sodium channel blocker, the baseline recordings were performed followed by recordings with flecainide 1 μ mol/L in the extracellular patch clamp solution after it had been ran through the system for 5 minutes, to ensure the flecainide free solution had been cleared from the bath recording chamber. All experiments were performed at room temperature.

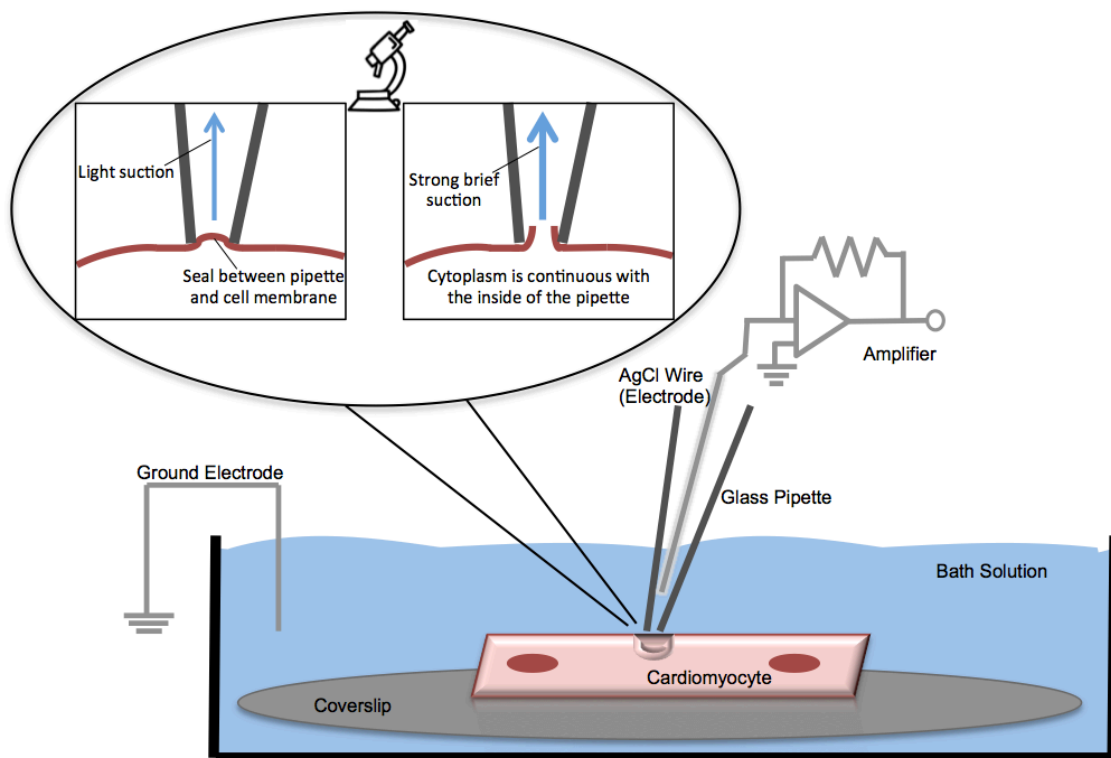


Figure 2.2. Diagram of whole cell patch clamp general set up and principle.

Shown are cells adhered to coverslips and submerged in bath solution, glass pipette containing the internal electrolyte solution, with positive pressure, causes a visible dimple on the surface of the cardiomyocyte when near to the cell. The glass pipette is sealed to membrane of the cell by removing positive air pressure. The electrode inside the glass pipette is connected to a highly sensitive amplifier, recording currents flowing through the channels in the cell membrane. This image was created by the author of this thesis.

2.5.2. Patch clamp statistical analysis

All experiments were performed and analysed in blinded fashion to genotype in littermate pairs (control vs. heterozygous Plakoglobin deficient mice ($Plako^{+/-}$) (181). However, blinding was not possible when performing experiments comparing cardiomyocytes from different chambers as atrial and ventricular cardiomyocytes have different morphologies so could be identified. Data were

expressed as mean \pm standard error, unless otherwise stated. Statistical analysis was performed using unpaired Student t-tests when comparing cardiomyocytes from different chambers/hearts and paired parametric Student t-tests were used when comparing the same cardiomyocytes under two different conditions (i.e. measurements before and after perfusion of flecainide). two-way ANOVA with Tukey's post-hoc analysis was used when two variables were being tested. Significance was taken as $P < 0.05$ (GraphPad Prism 7.0b).

Data was analysed using Signal 6.0 (Axon Instruments). I/V curves were fitted using the modified Boltzmann equation:

$$I_{Na} = G_{max}(V_m - V_{rev}) / (1 + \text{Exp}[(V_{0.5} - V_m)/k]) \text{ (equation 1).}$$

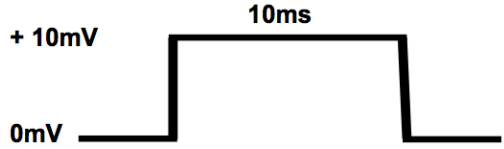
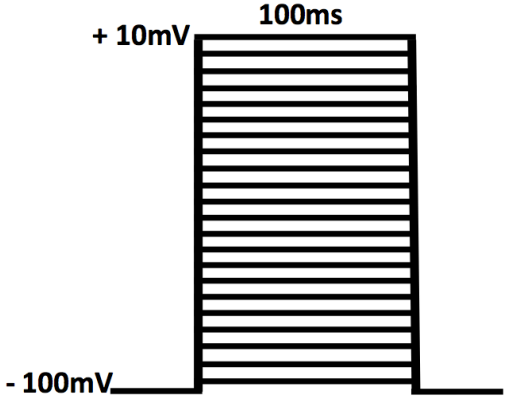
Where I_{Na} is current density at a given test potential (V_m), G_{max} is the peak conductance, V_{rev} is the reverse potential, $V_{0.5}$ is the membrane potential at 50% current activation and k is the slope constant that describes the steepness of the current activation.

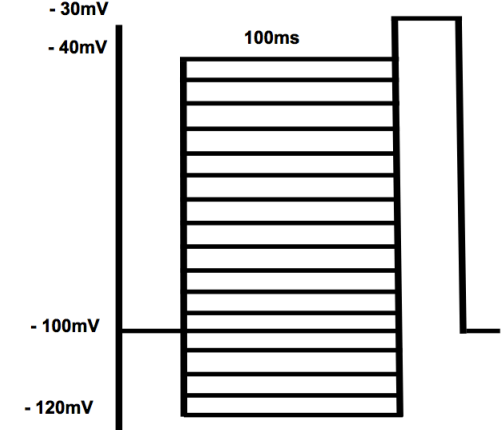
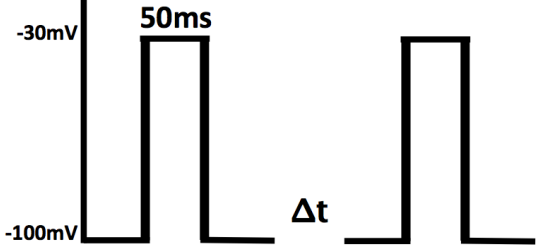
I_{Na} inactivation curves were fitted using the equation:

$$\text{Normalised } I_{Na} = 1 - (1 / (1 + \text{Exp}[(V_{0.5} - V_m)/k])) \text{ (equation 2).}$$

Where V_m is the pre-pulse potential, $V_{0.5}$ is the pre-pulse potential at which I_{Na} is half maximally inactivated and k is the slope constant that describes the steepness of the inactivation curve (183).

Table 1. 5: Voltage patch clamp protocols.

<p>Seal Test Protocol</p>	<p>A 10mV test pulse at 10ms. The oscilloscope shows the square current response to the seal test. The amplitude of the response is relative to the resistance of the pipette (larger the amplitude: greater the resistance).</p>	
<p>I/V Relationship Protocol</p>	<p>Sodium currents were evoked by voltage steps from a holding potential of -100 to +10mV in 5mV increments from a holding potential of -100mV.</p>	

<p>Steady State-Inactivation Protocol</p>	<p>Currents were activated by stepping the voltage to the potential at which the peak current is achieved (-100 to -30mV) but are preceded by stepping pre-pulse potentials at which the membrane is maintained for 100ms from -120 to -40mV in 5mV increments. The current amplitudes after the pre-pulse potential are normalised to the peak current recorded (pre-pulse current).</p>	
<p>Na⁺ Channel Recovery Protocol</p>	<p>Currents were activated by stepping the voltage to the potential at which the peak current is achieved (-100 to -30mV) and again after different time intervals. The current amplitudes at each time interval after the pre-pulse are normalised to the largest current (the current with the greatest time lapse from the pre-pulse). Time intervals after initial current: 1ms, 5ms, 7ms, 10ms, 20ms, 30ms, 50ms, 100ms, 300ms and 900ms</p>	

2.6. Calcium, cell and sarcomere length measurements

2.6.1. Plating of isolated cardiomyocytes

Tissue culture surfaces were coated with 5 µg/ml laminin in PBS for 1 hour at 37°C or 4°C overnight. Laminin solution was drawn off and well surface was washed 1x with PBS before isolated cardiomyocytes were plated.

2.6.2. Calcium handling and sarcomere length measurements

Measurement of intracellular Ca^{2+} and sarcomere length was performed in freshly isolated left ventricular cardiomyocytes using an integrated contractility/photometry system (IonOptix Corporation, US). Isolated cardiomyocytes were loaded with 1 µmol/L of Fura-2-AM (Invitrogen, US) for 30 min, allowed to de-esterify for 20 min and then perfused with standard Tyrode's solution: NaCl 130 mmol/L, KCl 5.4 mmol/L, HEPES 10 mmol/L, MgCl_2 0.5 mmol/L, CaCl_2 1.8 mmol/L, and glucose 10 mmol/L (pH 7.4) in an open-perfusion chamber mounted on the stage of an upright microscope (Olympus).

Myocytes were stimulated (1-3 Hz) using an external stimulator (Grass Technologies, US). Dual excitation (at 360 and 380 nm; F1 and F0) was delivered using OptoLED light sources (Cairn Research, UK) and emission light was collected at 510 nm (sampling rate 1 kHz). Simultaneous changes in calcium transients and sarcomere length were recorded using IonOptix

software. Parameters measured include calcium amplitude, diastolic and systolic (peak) calcium levels, calcium transient decay (t) and % sarcomere length (SL) shortening. All measurements were performed at room temperature (183).

3. Sodium handling in the atria and ventricles

3.1. Chapter introduction and overview

$[Na^+]_i$ is an essential modulator of a range of physiological functions within the heart. I_{Na} governs the initiation and propagation of the AP, thus controlling cardiac excitability and CV of electrical stimuli across the heart (1). Blocking sodium channels decreases the rate of depolarisation, also leading to decrease in AP amplitude and CV (98). Therefore, inhibiting sodium channels with AADs can assist in maintaining NSR by suppressing arrhythmias, which are a result of abnormal conduction (184). Subsequently, a variety of sodium channel modulating drugs are used as treatment of AF.

Pharmacological rhythm control therapy is often associated with modification of otherwise normal and therefore healthy ventricular electrophysiology, possibly resulting in the adverse effect of developing lethal ventricular arrhythmias (147). This lead to an emphasis on the development of atrial-selective medications, in order to avoid altering ventricular electrophysiology of AF patients and improve efficacy and safety of AADs. This has stemmed increasing interest in comparing potential differences in the way sodium channels function between ventricles and atria, as chamber distinctions may provide targets for atrial-selective sodium channel blockade. Greater knowledge of sodium channel properties in the atria, compared to the ventricles, may enable understanding of the mechanisms that lead to drug selectivity of atrial sodium channels (4, 5, 184)

and potentially lead to development of novel atrial selective AADs.

Although it has been shown that several mammalian species display different biophysical properties between LA and LV sodium channels (4, 5, 142, 185, 186), these studies have not yet been conducted in mice. Furthermore, the molecular causes explaining differences in I_{Na} between chambers have not been fully established. A considerable amount of cardiac research and drug development relies on the use of mouse whole tissue and isolated cardiomyocytes, partly due to the wide availability of genetically modified murine models. Hence we characterised sodium channel function in mouse atrial and ventricular cardiomyocytes. Additionally, it is also imperative to explore the physiological relevance of the differences observed in sodium channel properties in the LA and LV, in order to develop a better understanding of what distinctions may exist between the chambers under the biological conditions expected *in vivo*. Physiologically relevant information may enhance understanding of what differences exist in sodium channel function in the upper and lower chambers of the heart. These mechanistic insights may potentially lead to improvements in treatment options and development of new AP therapeutics.

It has been shown previously that β -subunits regulate the biophysical properties of the $Na_v1.5$ α -subunit (53, 65). As detailed in the introduction of this thesis, studies have shown negative and/or positive shifts in steady-state inactivation

of the channel when $\text{Na}_v1.5$ is co-expressed with $\beta1-4$ subunits (4, 69-72). Similarly, experiments co-expressing the $\beta1$ subunit found negative and positive shifts in activation of the sodium channel (72, 73). Co-expression of the $\beta4$ subunit has displayed a negative shift in activation (64) but experiments co-expressing both $\beta2$ and $\beta4$ together showed no difference in activation kinetics. Furthermore, co-expression of $\beta2$ and $\beta4$ with $\text{Na}_v1.5$ has also shown to cause faster recovery of the channel. Therefore, we investigated the concentration of β -subunits in LA and LV.

Chen et al., found that human and rat myocardium expressed less $\beta2$ and $\beta4$ in the LA compared to the LV (4). They consequently suggested that distinctive expression of the $\beta2$ and $\beta4$ subunits between the atria and ventricles leads to differences in the sodium channel gating kinetics between the chambers. In their experiments, using isolated rat atrial and ventricular cardiomyocytes, they showed that atrial cardiomyocytes displayed distinct sodium channel inactivation and recovery properties compared to the sodium channels of ventricular cardiomyocytes. Independent experiments conducted in HEK 293 cells expressing $\text{Na}_v1.5$ demonstrated that inactivation and recovery of sodium channels is altered following co-expression of $\beta2$ and $\beta4$ subunits. Chen et al., therefore proposed that the differences in biophysical properties between the atrial and ventricular rat cardiomyocytes are driven by alterations in expression of $\beta2$ and $\beta4$ subunits (4). However, whether the same differences in $\beta2$ and $\beta4$ expression exist between mouse LA and LV is not known.

Investigation of β -subunit expression in healthy and diseased human LA and LV chambers could help to establish whether β -subunit expression is linked to cardiac disease susceptibility and/or progression. Furthermore, examination of how sodium is handled in the upper and lower chambers of the heart could offer insight into the mechanisms driving sodium handling in different chambers of the heart in health and disease (2).

The aims of this investigation are summarised below:

- To assess sodium channel biophysical properties in isolated mouse LA and LV cardiomyocytes and interpret the significance of potential chamber distinctions under physiological circumstances.
- To examine the effects of flecainide on the sodium channels in isolated mouse LA and LV cardiomyocytes.
- To examine the differences in expression of sodium channels between LA and LV chambers.
- To examine β -subunit expression in diseased human myocardium samples.

3.2. Electrophysiology results

3.2.1. Mouse LA sodium channels activate at more negative holding potentials than LV sodium channels

Experiments were performed on isolated WT mouse LA and LV cardiomyocytes to compare the sodium channel I/V relationship, using the relevant I/V patch clamp protocol described in the materials and methods (Table 1.5). This protocol enabled assessment of the voltage/current relationship and sodium channel activation.

Figure 3.1A shows raw representative traces of the I_{Na} from LA and LV cardiomyocytes, with greater peak I_{Na} in LV cardiomyocytes before normalising to cell capacitance. Individual ventricular cardiomyocytes have a larger membrane surface area than atrial cardiomyocytes, shown by the difference in capacitance values (Figure 3.1B), as capacitance is relative to membrane surface area (187). Therefore, individual LV cells will have more sodium channels across the greater membrane surface (188). It is essential for I_{Na} to be normalised against cell size (capacitance), in order to understand the physiology of the individual sodium channels and sodium channels over a set comparative area in both LA and LV cardiomyocytes. The patch clamp protocol is also shown in Figure 3.1A. The current-voltage relationship of the sodium channels (Figure 3.1C) shows that from a holding potential of -100mV, LA (n=42/13 cells/mice) and LV (n=28/13 cells/mice) sodium channels have a peak

current potential of -30mV, at which I_{Na} amplitude was comparable in both chambers (Figure 3.1D).

The I/V curve data was fitted to a Boltzmann function to obtain the voltage dependence of the conductance activation of sodium channels using the initial downward slope of the curve (as described in the material and methods). This allows comparison of the voltage potential at which half of the sodium channels were activated (V_{50}) in the LA and LV. It is evident that atrial sodium channels activated at significantly more negative potentials than ventricular sodium channels (Figure 3.1E).

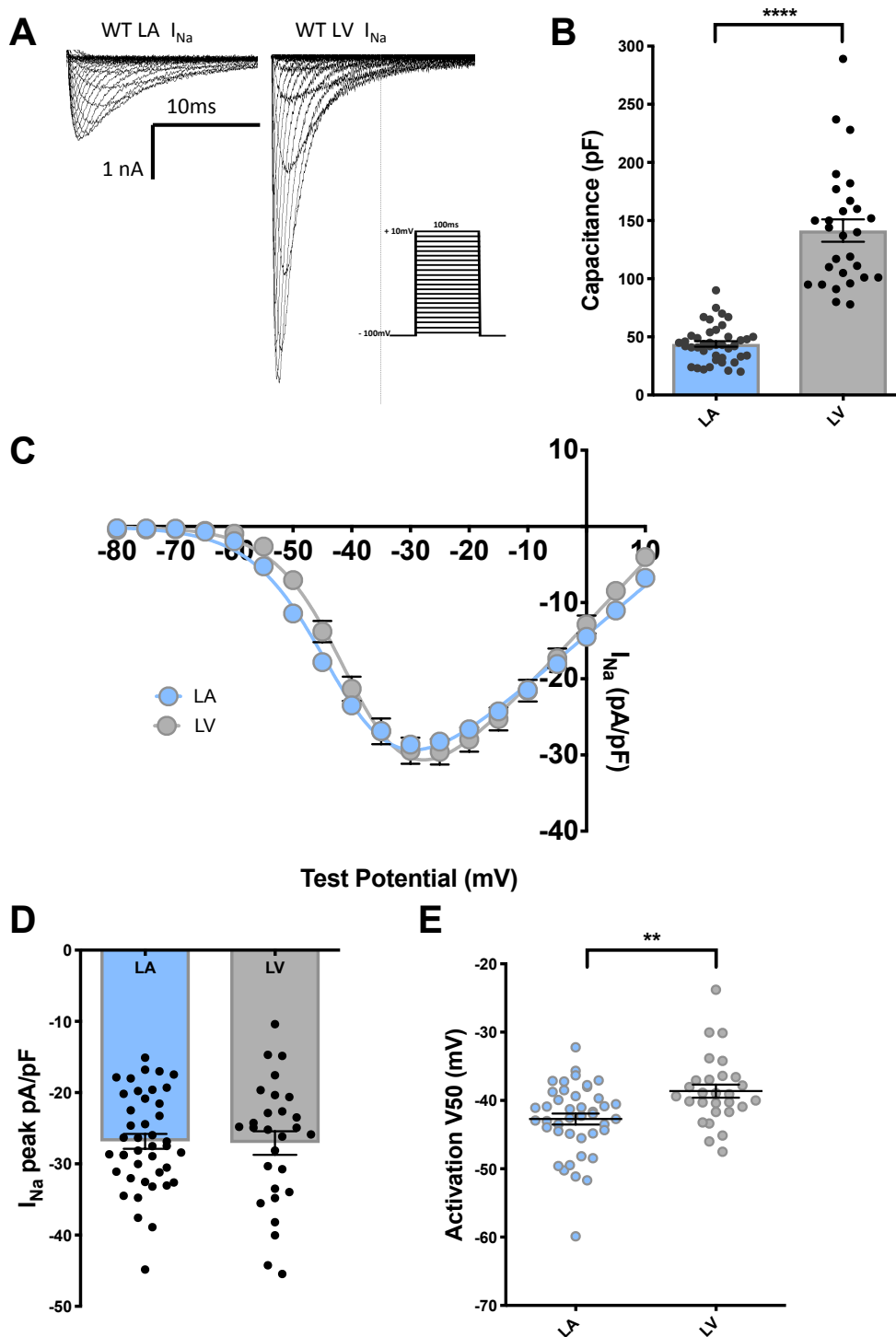


Figure 3.1. LA and LV I_{Na} I/V relationship and sodium channel activation. I_{Na} I/V curve and channel activation in LA and LV cardiomyocytes from WT mouse hearts. A) LA and LV representative raw I_{Na} traces with patch clamp protocol on the right. B) LA and LV cell capacitance (LA= 43.98 ± 2.412 pF; n=42/13 cells/mice; LV= 141.4 ± 9.592 pF; n=28/13 cells/mice) ****p<0.0001. C) Current-voltage relationship of I_{Na} density in LA (n=42/13 cells/mice) and LV (n=28/13 cells/mice). D) I_{Na} peak density at a step from -100mV to -30mV in LA

(-26.84 ± 1.651 pA/pF; n=42/13 cells/mice) and LV (-26.84 ± 1.037 pA/pF; n=28/13 cells/mice). E V₅₀ of activation fitted to the Boltzmann distribution in LA (-42.71 ± 0.8017 mV; n=42/13 cells/mice) and LV (-38.63 ± 0.9488 mV; n=28/13 cells/mice) **P<0.01. Error bars indicate \pm S.E.M. significance taken as *P<0.05 with unpaired Student t-test.

3.2.2. LA peak I_{Na} is smaller than LV I_{Na} at physiologically relevant holding potentials

Experiments were performed on isolated WT mouse LA and LV cardiomyocytes to measure the peak I_{Na} at varying holding potentials using the steady state inactivation patch clamp protocol described in the material and methods chapter (Table 1.5). The protocol enables the evaluation of the relationship between the holding potential (pre-pulse potential) of the cell and the current amplitude upon stimulation, and in turn how many sodium channels are available for activation at the different holding potentials. Data was analysed from the -120 to -75mV holding potential range of the pre-pulse, as current amplitudes were negligible at the more positive holding potentials, so could not be measured/compared.

I_{Na} amplitude against holding potential relationship differs between the LA and LV. I_{Na} is greater in LA cardiomyocytes at more negative holding potentials of -120 to -105mV compared to LV I_{Na} current density. At the -100mV holding potential, I_{Na} is comparable in both LA and LV cardiomyocytes and at holding potentials more positive than -100mV, I_{Na} current density is greater in LV cardiomyocytes (LA=40/13 and LV=28/13 cells/mice). The red box highlights the hyperpolarised holding potential commonly used in patch clamp protocols to

measure sodium current properties. The green box highlights the physiological holding potential range of cardiomyocytes (Figure 3.2A). In Figure 3.2B I_{Na} is greater in LA than LV at -120mV holding potential. Conversely, the reverse is seen in Figure 3.2C, at the -75mV holding potential, where I_{Na} is significantly smaller in LA than LV.

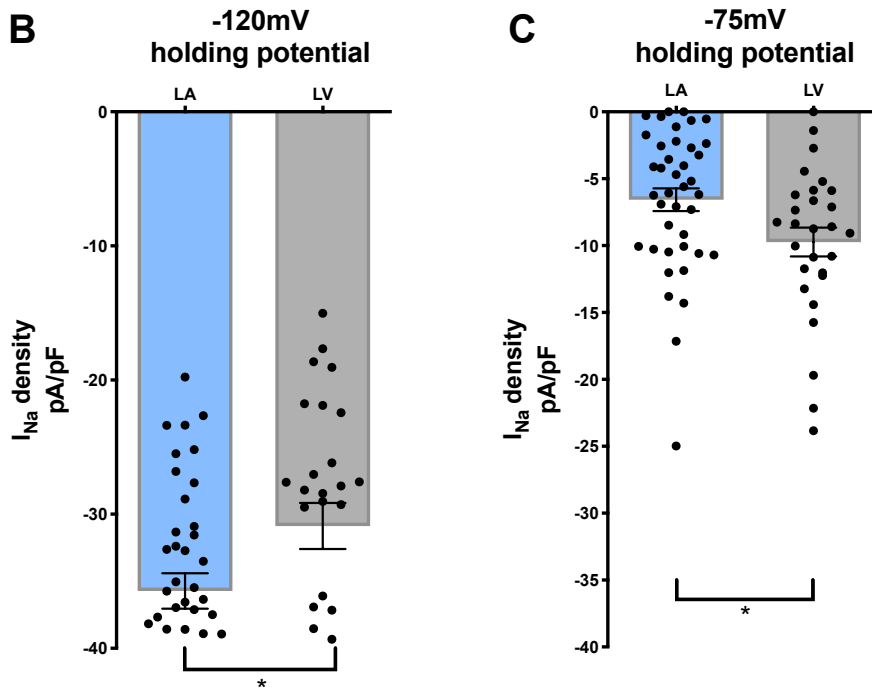
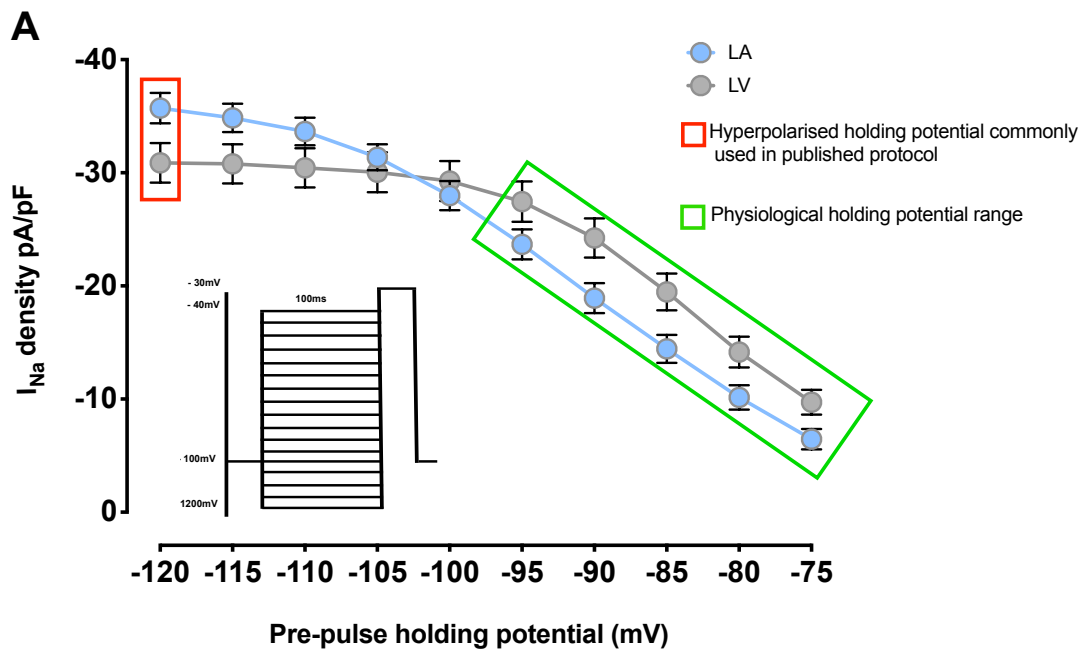


Figure 3.2. I_{Na} density at varying holding potentials.

I_{Na} in LA and LV cardiomyocytes from WT mouse hearts at varying holding potentials. A) I_{Na} mean density/holding potential relationship from with protocol shown inset, LA (n=40/13 cells/mice) and LV (n=28/13 cells/mice), denote holding potentials of interest. B) I_{Na} density at -120mV holding potential in LA (-35.72 ± 1.718 pA/pF; n=40/13 cells/mice) and in LV (-30.89 ± 1.322 pA/pF; n=28/13 cells/mice) * $p < 0.05$. C) I_{Na} density at -75mV holding potential in LA (-6.569 ± 0.8474 pA/pF; n=40/13 cells/mice) and LV (-9.735 ± 1.075 pA/pF;

n=28/13 cells/mice) *p<0.05. Error bars indicate \pm S.E.M. significance taken as *P<0.05 with unpaired Student t-test.

3.2.3. Mouse LA sodium channels inactivate at more negative holding potentials than LV sodium channels

Experiments were performed on isolated WT mouse LA and LV cardiomyocytes to compare the potential at which the sodium channels inactivate (are no longer available), using the relevant steady-state inactivation patch clamp protocol described in the materials and methods chapter (Table 1.5). The voltage dependence of steady-state inactivation (channel availability, I/I_{max}) was determined from this protocol, as shown in Figure 3.3A and fitted to the Boltzmann function.

The LA sodium channel inactivation potential is negatively shifted compared to the LV sodium channel inactivation potential (LA=41/13 and LV=27/13, cells/mice) (Figure 3.3A). This is confirmed in Figure 3.3B V50 for inactivation. The percentage of channel inactivation increases at more positive holding pre pulse potentials and Figure 3.3C uses the data from Figure 3.3A to illustrate the percentage of channel inactivation at varying pre pulse holding potentials. At -120mV (the holding potential commonly used in other patch clamp studies of the sodium channel) there is no difference in inactivation, however at -100mV, inactivation is greater in LA sodium channels. Additionally, at -75mV (within the

physiologically holding potential range of LA membranes), inactivation is greater in LA sodium channels.

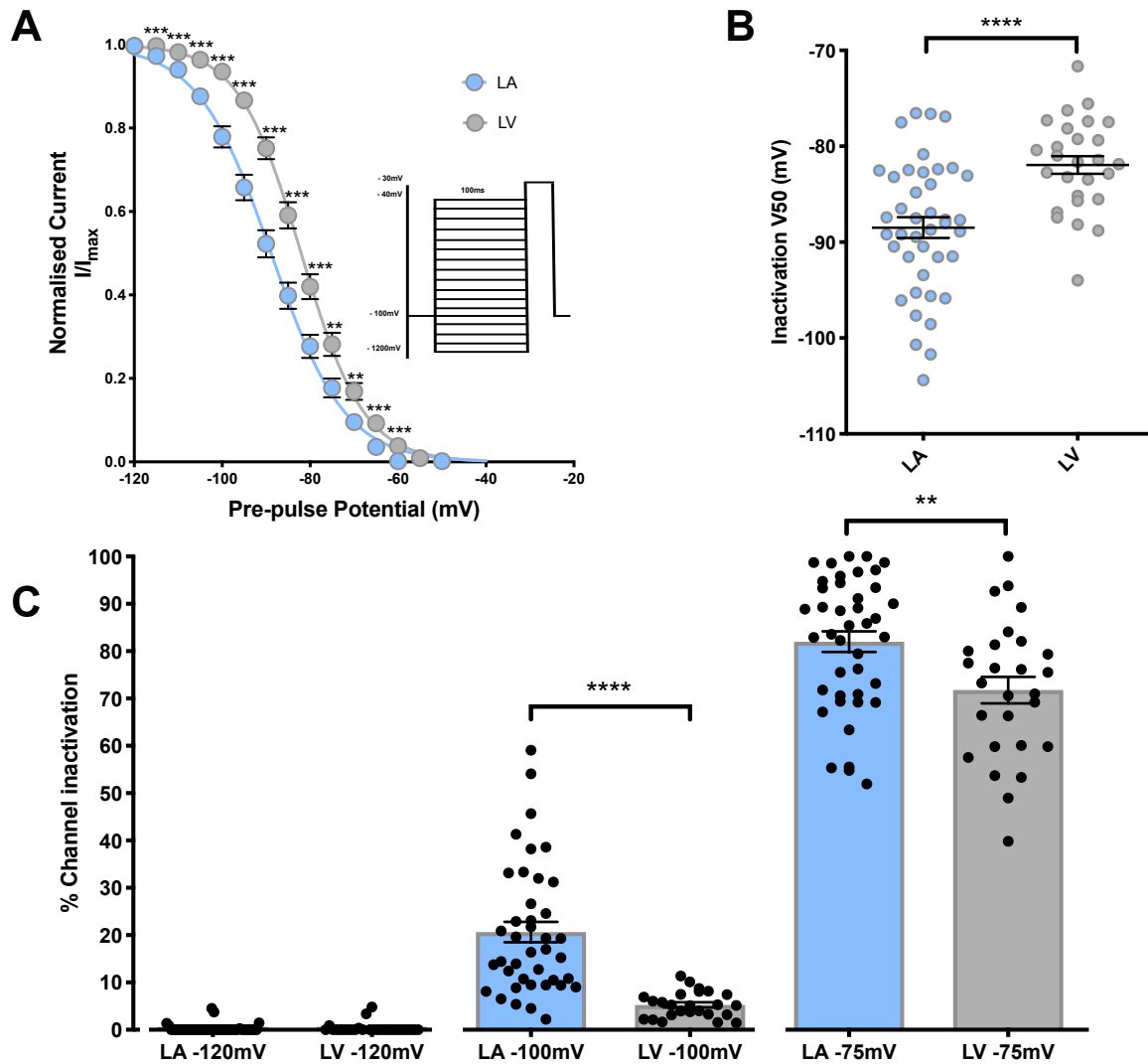


Figure 3.3. LA and LV sodium channel inactivation.

Channel steady-state inactivation in LA and LV cardiomyocytes from WT mouse hearts. A) Curve of normalised I_{Na} inactivation (I/I_{max}) fitted to the Boltzmann function in LA (n=41/13 cells/mice) and LV (27/13 cells/mice). B) V_{50} of inactivation fitted to the Boltzmann distribution in LA (-88.48 ± 1.08 mV; n=41/13 cells/mice) and LV (-81.95 ± 0.923 mV; n=27/13 cells/mice) **** $P < 0.0001$. C) Percentage of channel inactivation at different holding potentials; -120mV (LA= $0.296 \pm 0.147\%$; n=41/13 cells/mice; LV= $0.2143 \pm 0.923\%$; n=27/13 cells/mice), -100mV (LA= $20.644 \pm 2.172\%$; n=41/13 cells/mice; LV= $5.256 \pm 0.59\%$; n=27/13 cells/mice) **** $P < 0.0001$, -75mV (LA= $82 \pm 2.172\%$; n=41/13 cells/mice; LV= $71.78 \pm 2.795\%$; n=27/13 cells/mice) ** $P < 0.01$. Error bars

indicate \pm S.E.M. significance taken as $*P < 0.05$ with unpaired Student t-test between LA and LV in all data sets (N.B. in C only LA and LV data within each holding potential group were compared against each other, not between different holding potentials).

3.2.4. Mouse LA sodium channels have slower time dependent recovery than LV sodium channels

Experiments were performed on isolated WT mouse LA and LV cardiomyocytes to study the time dependent kinetics of recovery after inactivation, using the relevant channel recovery protocol described in the materials and methods (Table 1.5). Normalised peak current amplitudes were plotted and fitted to a one-phase association exponential function and the time when half of the channels were recovered and available for re-activation (P50) was determined in the LA and LV cardiomyocytes.

The LA sodium channel recovery time is shifted to the right, slower compared to the LV sodium channel recovery (LA=38/13 and LV=28/13 cells/mice) (Figure 3.4A), demonstrated clearly by the P50 for recovery.

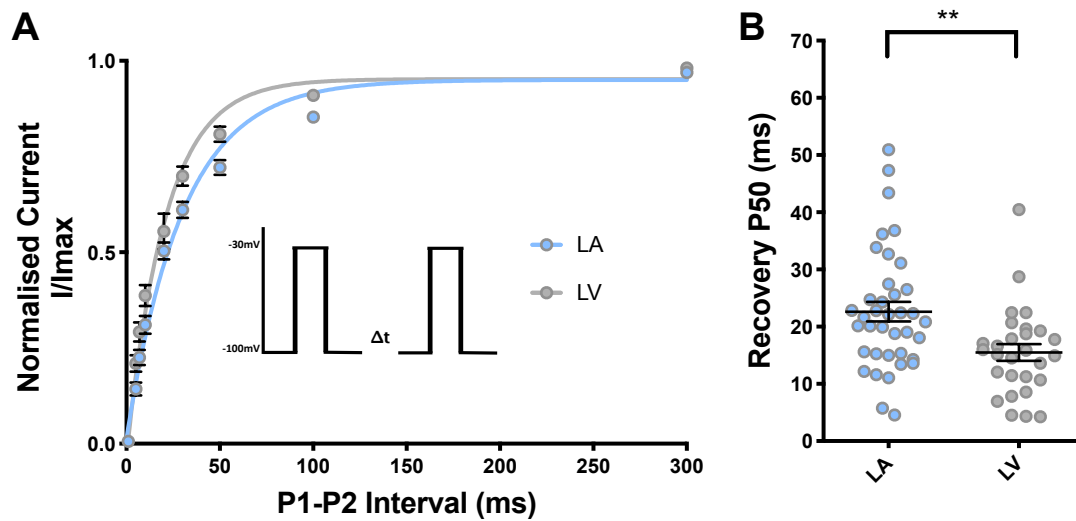


Figure 3.4. LA and LV time dependent sodium channel recovery. Channel recovery in LA and LV cardiomyocytes from WT mouse hearts. A) Curve of normalised sodium channel recovery (I/I_{max}) fitted to one-phase association with protocol shown inset in LA ($n=38/13$ cells/mice) and LV ($28/13$ cells/mice). B) P50 of recovery in LA (22.62 ± 1.703 ms; $n=38/13$ cells/mice) and LV (15.49 ± 1.456 ms; $n=28/13$ cells/mice) $**P<0.01$. Error bars indicate \pm S.E.M. significance taken as $*P<0.05$ with unpaired Student t-test.

3.2.5. Flecainide alters I/V curve morphology and activation potential of LA and LV sodium channels

Experiments were performed on isolated WT mouse LA and LV cardiomyocytes in the absence or presence of $1\mu\text{mol}$ flecainide, to compare peak I_{Na} inhibition between the chambers, using the I/V patch clamp protocol described in the materials and methods chapter (Table 1.5). This protocol enabled assessment of the effect of flecainide addition on voltage/current relationship and sodium channel activation. Sodium channel inhibition was measured by calculating the difference between the control currents and the currents after flecainide exposure as a percentage.

The raw LA and LV sodium currents $\pm 1\mu\text{mol}$ flecainide are shown in Figure 3.5A, with the patch clamp protocol shown on the right. The flecainide currents are visibly smaller than the control currents recorded in the absence of flecainide. The current-voltage relationships of the sodium channels in control LA against LA $+1\mu\text{mol}$ flecainide are shown in Figure 3.5B (LA control $n=11/6$ cells/mice; LA plus flecainide $n=11/6$ cells/mice) and in control LV against LV $+1\mu\text{mol}$ flecainide in Figure 3.5C (LV control $n=14/4$ cells/mice; LV plus flecainide $n=14/4$ cells/mice). The addition of flecainide clearly alters the curve morphology in both LA and LV. The peak of both curves is significantly reduced with the addition of flecainide compared to the control curves, shown in figure 3.5D and 3.5E, with peak current data from the -100mV to -30mV step. However, the inhibition of peak I_{Na} amplitudes is significantly greater in the LA than in LV (Figure 3.5F).

The I/V curve data was fitted to a Boltzmann function to obtain the voltage dependence of the conductance activation of sodium channels using the initial downward slope of the curve. This allows comparison of the voltage potential at which half of the sodium channels were activated (V_{50}) between LA control and LA $+1\mu\text{mol}$ flecainide (Figure 3.5G) and between LV control and LV $+1\mu\text{mol}$ flecainide (Figure 3.5H). The addition of flecainide results in sodium channel activation at significantly more negative potentials in both LA and LV cardiomyocytes (Figure 3.6G and Figure 3.5H). The negative shift effect on the activation potential of the sodium channels with flecainide addition appears to

be greater in LA than LV sodium channels (Figure 3.5I), but this is not significant.

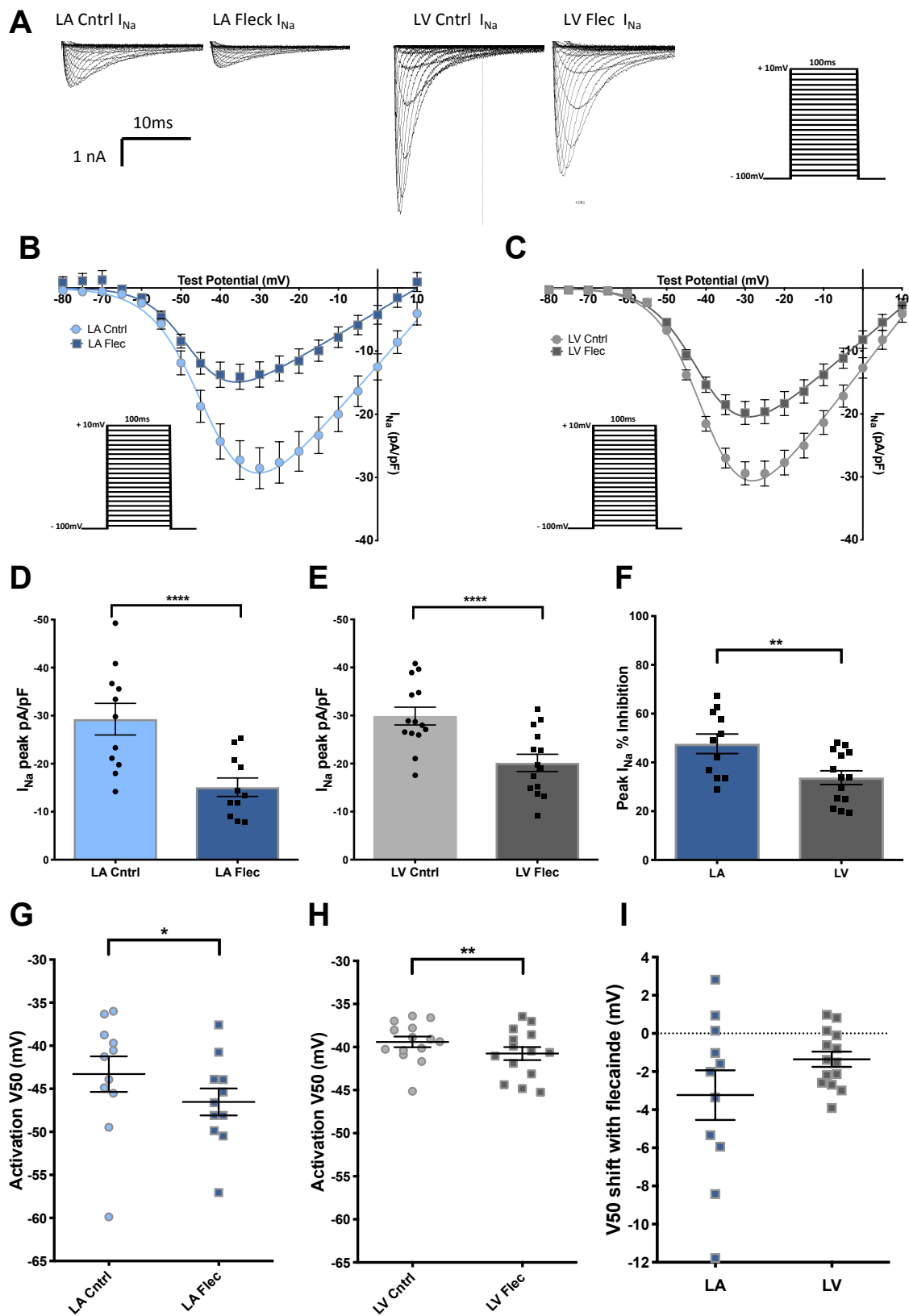


Figure 3.5. LA and LV I_{Na} I/V and sodium channel activation with the addition of flecainide.

I_{Na} I/V curve and channel activation +/- flecainide in LA and LV cardiomyocytes from WT mouse hearts. A) LA and LV representative raw I_{Na} traces +/- 1 μ mol flecainide, with patch clamp protocol on the right. B) Current-voltage relationship of I_{Na} density in LA (n=11/6 cells/mice) C) Current-voltage relationship of I_{Na} density in LV (n=14/4 cells/mice). D) LA I_{Na} peak density at a step from -100mV to -30mV (LA control= -29.27 ± 3.291 pA/pF; n=11/6 cells/mice; LA plus flecainide= -15.09 ± 1.923 pA/pF; n=11/6 cells/mice) ****p<0.0001 E) LV I_{Na} peak density at a step from -100mV to -30mV (LV control= -29.89 ± 1.851 pA/pF; n=14/4 cells/mice; LV plus flecainide= -20.15 ± 1.797 pA/pF; n=14/4 cells/mice) ****p<0.0001. F) Peak I_{Na} percentage inhibition (LA= $47.64\% \pm 4.029$; n=11/6 cells/mice; LV= $33.77\% \pm 2.824$; n=14/4 cells/mice) **p<0.01). G) LA V50 of activation fitted to the Boltzmann distribution (LA control= -43.29 ± 2.063 mV; n=11/6 cells/mice; LA plus flecainide= -46.52 ± 1.589 mV; n=11/6 cells/mice) *p<0.05 H) LV V50 of activation fitted to the Boltzmann distribution (LV control= -39.4 ± 0.621 mV; n=14/4 cells/mice; LV plus flecainide= -40.75 ± 0.983 mV; n=14/4 cells/mice) **p<0.01. I) Shift in V50 activation after the addition of flecainide (LA = -3.232 ± 1.302 mV; n=11/6 cells/mice; LV= -1.352 ± 0.397 mV; n=14/4 cells/mice). Error bars indicate \pm S.E.M. Significance taken as *P<0.05 with paired Student t-test for C-F and unpaired Student t-test for G.

3.2.6. Flecainide sodium channel inhibition increases at more positive holding potentials with a greater effect in the LA

To compare the effect of different holding potentials on I_{Na} inhibition between the chambers the currents were measured using the steady state inactivation patch clamp protocol described in the material and methods chapter (Table 1.5). The protocol enables the evaluation of the relationship between the holding potential (pre-pulse potential) of the cell and the current amplitude upon stimulation, and in turn can be representative of the magnitude of sodium channels inhibited by 1 μ mol flecainide at the different holding potentials. Data was analysed from the -120 to -75mV holding potential range of the pre-pulse, as current amplitudes reached 0pA/pF at the more positive holding potentials, so they could not be measured/compared.

Figure 3.6A shows there is a positive correlation between percentage inhibition of I_{Na} and holding potential in both LA (n=12/6 cells/mice) and LV (n=14/4 cells/mice). At more positive holding potentials flecainide is more effective at inhibiting sodium channels. This is confirmed, as at the most negative holding potential, of -120mV, sodium currents were inhibited less than at the most positive holding potential analysed, in LA cardiomyocytes and in LV cardiomyocytes (Figure 3.6B and 3.6C).

Moreover, Figure 3.6A shows that percentage inhibition of I_{Na} in the presence of 1 μ mol flecainide is greater in LA than in LV at all of the holding potentials recorded from. At -120mV and at the -70mV holding potential inhibition of I_{Na} was significantly greater in LA than in LV (Figure 3.6D and Figure 3.6E).

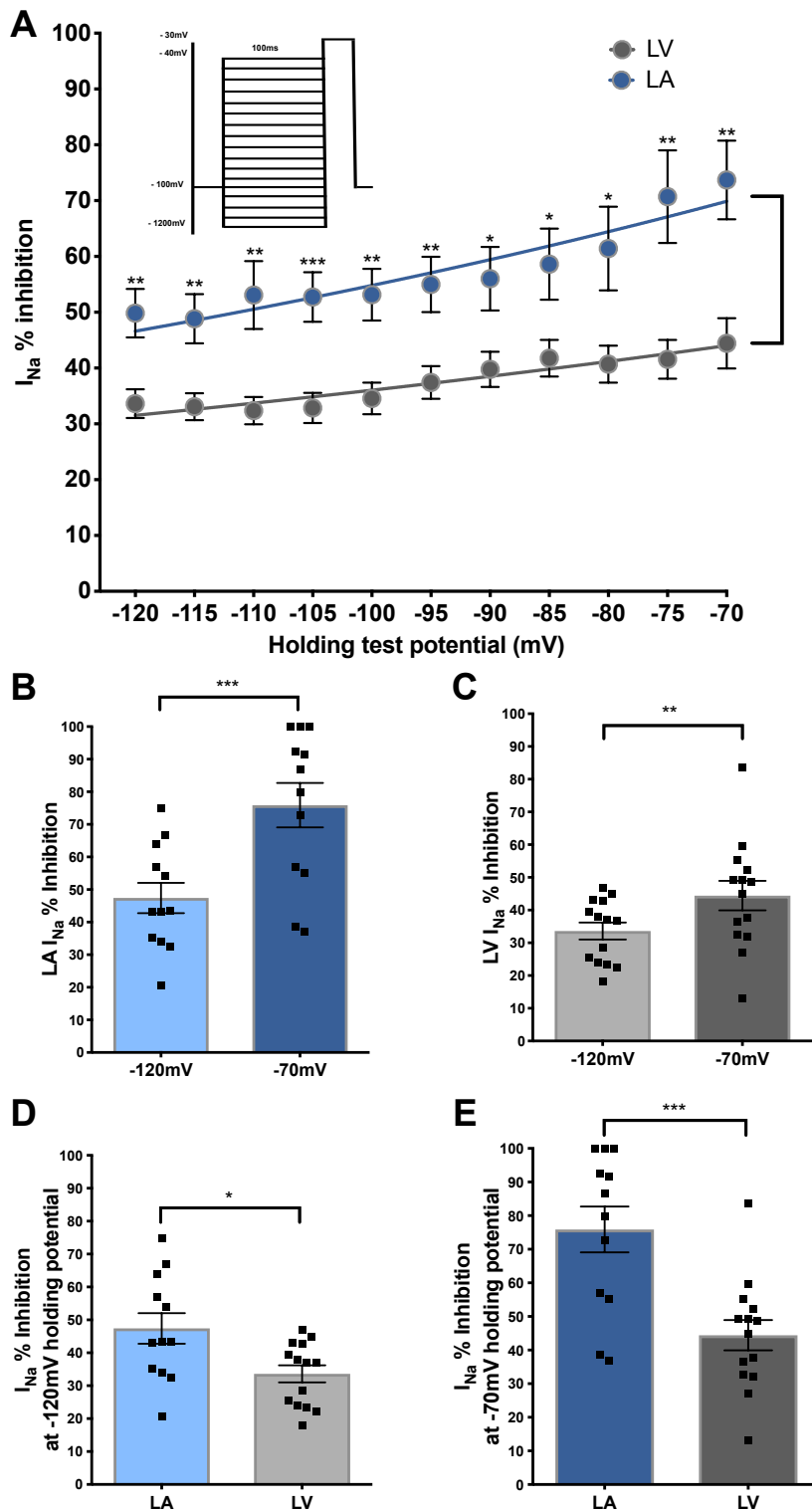


Figure 3.6. Sodium channel flecainide inhibition in LA and LV at different holding potentials.

Percentage of I_{Na} inhibition in LA and LV cardiomyocytes. A) I_{Na} percentage inhibition at varying holding potentials in LA (n=12/6 cells/mice) and LV cardiomyocytes (12/6 cells/mice). B) LA I_{Na} percentage inhibition at -120 and -

70mV (-120mV=47.41% \pm 4.642; n=12/6 cells/mice; -70mV=75.89% \pm 6.801; n=12/6 cells/mice) ***p<0.001. C) LV I_{Na} percentage inhibition at -120 and -70mV (-120mV=33.61% \pm 2.58; n=14/4 cells/mice; -70mV=44.43% \pm 4.508; n=14/4 cells/mice) **p<0.01. D) LA and LV I_{Na} percentage inhibition at -120 (LA=47.41% \pm 4.642; n=12/6 cells/mice; LV=33.61% \pm 2.580; n=14/4 cells/mice) *p<0.05. E) LA and LV I_{Na} percentage inhibition at -70 (LA=75.89% \pm 6.801; n=12/6 cells/mice; LV=44.43% \pm 4.508; n=14/4 cells/mice) ***p<0.001. Error bars indicate \pm S.E.M. significance taken as *P<0.05; paired Student t-test in B and C and unpaired Student t-test in D and E.

3.2.7. Flecainide alters LA and LV sodium channel inactivation

Experiments were performed on isolated WT mouse LA and LV cardiomyocytes to compare the potential at which the sodium channels inactivate (are no longer available) in the presence and absence of flecainide, using the relevant steady-state inactivation patch clamp protocol described in the materials and methods (Table 1.5). The voltage dependence of inactivation (channel availability, I/I_{max}) was determined from this protocol, as shown inset in Figure 3.7A and 3.7C and fitted to the Boltzmann function.

There is a shift in the inactivation potential of the sodium channels between the control and +1 μ mol flecainide in both the LA (n=12/6 cells/mice) and LV (n=14/4 cells/mice), demonstrated by the V50 for inactivation (Figure 3.7B and Figure 3.7D). Nevertheless, the shift in the inactivation potential of the sodium channels between the control LA and +1 μ mol flecainide LA is greater than the shift seen in the LV, demonstrated by the V50 voltage shifts (Figure 3.7E) but this is not significant, likely due to a larger standard deviation of the LA dataset.

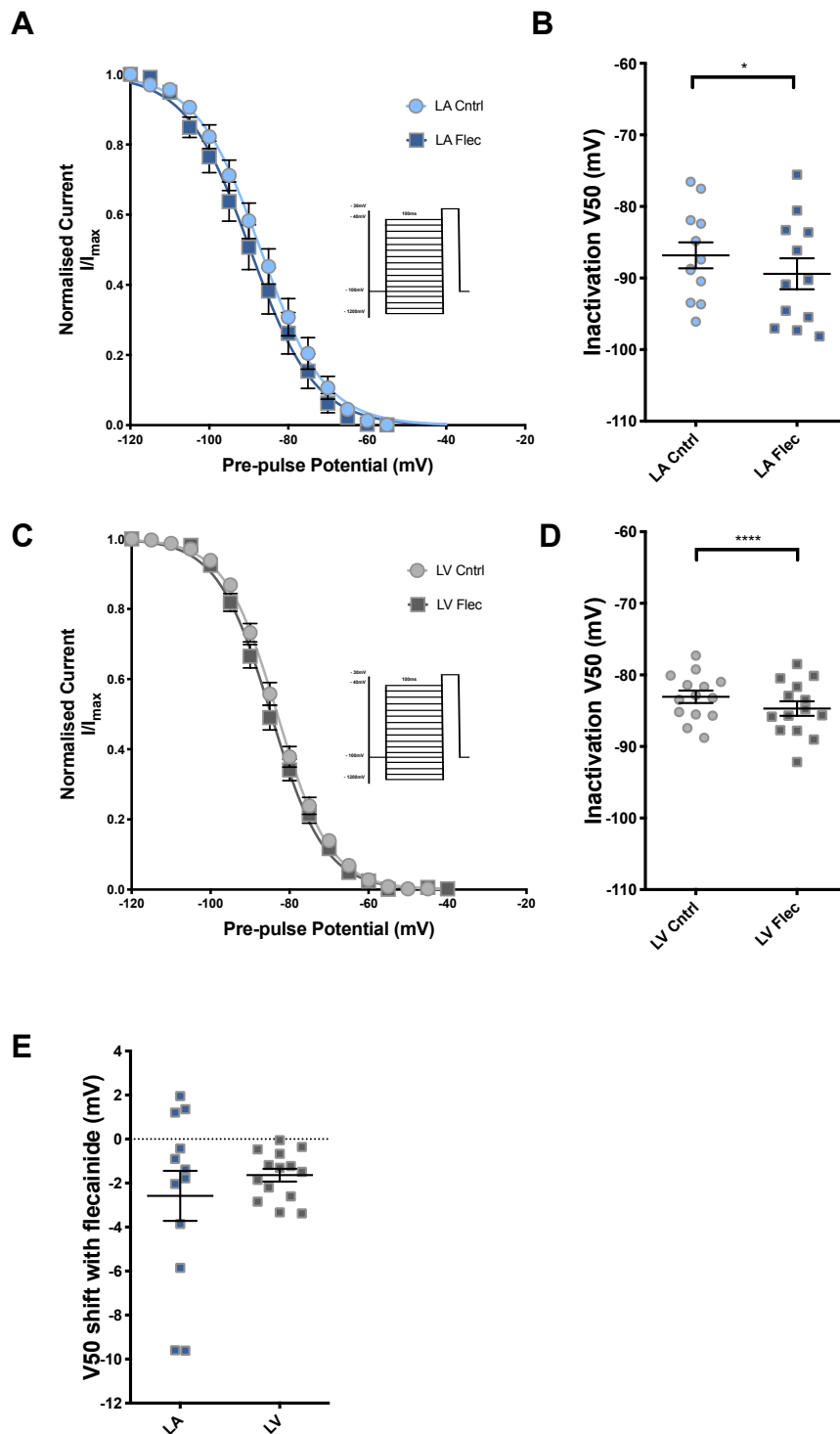


Figure 3.7. LA and LV I_{Na} inactivation with the addition of flecainide.

Channel inactivation +/- flecainide in LA and LV cardiomyocytes from WT mouse hearts. A) LA curve of normalised I_{Na} inactivation (I/I_{max}) fitted to the Boltzmann function ($n=12/6$ cells/mice). B) LA V50 of inactivation fitted to the Boltzmann distribution (LA control= -86.82 ± 1.821 mV; $n=12/6$ cells/mice; LA plus flecainide= -89.4 ± 2.156 mV; $n=12/6$ cells/mice) $*p<0.05$. C) LV curve of normalised I_{Na} inactivation (I/I_{max}) fitted to the Boltzmann function ($n=14/4$

cells/mice). D) LV V50 of inactivation fitted to the Boltzmann distribution (LV control= $-83.06 \pm 0.8622\text{mV}$; n=14/4 cells/mice; LV plus flecainide= $-84.7 \pm 1.016\text{mV}$; n=14/4 cells/mice) **** $p < 0.0001$ E) V50 inactivation shift with flecainide (LA= $-2.78 \pm 1.139\text{mV}$; n=12/6 cells/mice; LV= $-1.639 \pm 0.2927\text{mV}$; n=14/4 cells/mice).

3.2.8. Flecainide slows sodium channel recovery in the LA

Experiments were performed on isolated WT mouse LA and LV cardiomyocytes to study the time dependent kinetics of recovery after inactivation in the presence and absence of flecainide, using the relevant channel recovery protocol described in the materials and methods (Table 1.5). Normalised peak current amplitudes were plotted and fitted to a one-phase association exponential function and the time when half of the channels were recovered (P50) was determined in the LA and LV cardiomyocytes.

In the LA (n=12/6 cells/mice) there was a clear right shift in the sodium channel recovery time in the presence of $1\mu\text{mol}$ flecainide (Figure 3.8), demonstrating that channel recovery was significantly slower after flecainide was added, confirmed by the P50 in Figure 3.8B. However, in the LV (n=14/4 cells/mice) the sodium channel recovery time was not altered by the addition of flecainide (Figure 3.8C), confirmed by the sodium channel P50 for recovery (Figure 3.8D).

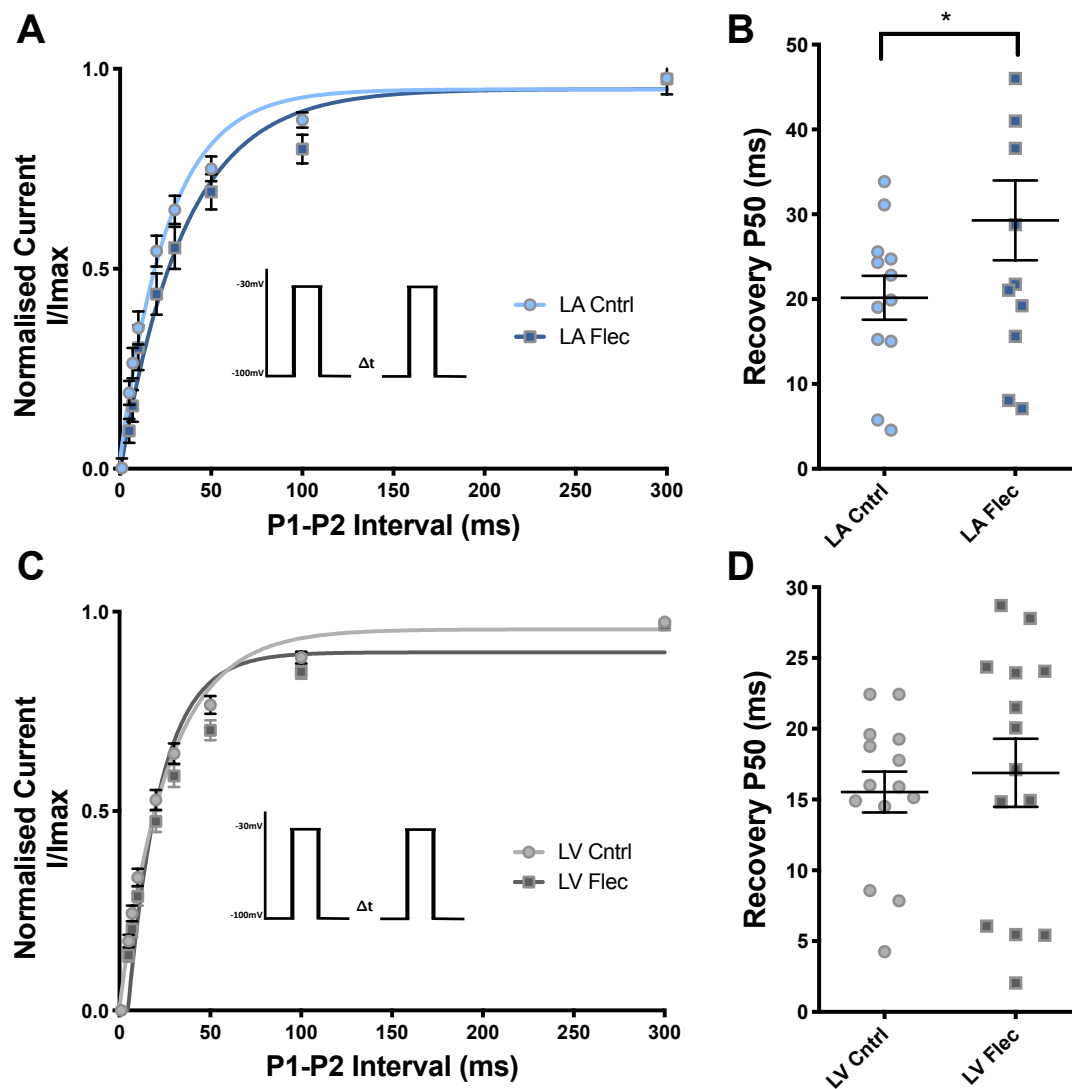


Figure 3.8. Flecainide effect on LA and LV time dependent sodium channel recovery.

Channel recovery in control/flecainide LA and LV cardiomyocytes from WT mouse hearts. A) LA curve of normalised sodium channel recovery (I/I_{max}) fitted to one-phase association with protocol shown inset ($n=12/6$ cells/mice). B) LA P50 of recovery (LA control= 20.16 ± 2.589 ms; $n=12/6$ cells/mice; LA plus flecainide= 29.29 ± 4.709 ms; $n=12/6$ cells/mice) $*p<0.05$. C) LV curve of normalised sodium channel recovery (I/I_{max}) fitted to one-phase association with protocol shown inset ($n=14/4$ cells/mice). D) LV P50 of recovery (LV control= 15.53 ± 1.441 ms; $n=14/4$ cells/mice; LV plus flecainide= 16.88 ± 2.408 ms; $n=14/4$ cells/mice). Error bars indicate \pm S.E.M. significance taken as $*P<0.05$ with paired Student t-test.

3.3. Protein expression

3.3.1. Na_v1.5 expression in WT mouse LA and LV

Western blot experiments were performed on WT mouse LA and LV tissue homogenates, in order to assess whether the protein expression of Na_v1.5 (the major cardiac sodium channel isoform) varies between the atrial and ventricular chambers. The only antibody that worked (Alomone, ASC-005) consistently displayed multiple bands on the blots; the expected 250kDa and 75kDa bands (shown on the data sheet attached to the antibody) and an additional band of 25kDa. Lower molecular weight bands can arise from degradation of the sample during processing steps. However, samples were immediately snap frozen after collection, stored at -80°C and always kept on ice during the homogenisation process so degradation was avoided. Additionally, protease inhibitors were also included in the homogenisation buffer to prevent protease activity and protein splicing during sample preparation.

In order to determine whether the additional bands are due to the Na_v1.5 protein or were due to technical artifacts, several optimisation steps were used. To determine whether multiple bands seen on the blot were a result of non-specific binding of the secondary antibody, separate experiments were conducted in the absence of the primary antibody. This resulted in a blank image (data not shown), as expected, and verified that the additional bands were not due to non-specific binding of the secondary antibody. Although the Na_v1.5 protein was expected to be abundant in the samples non-specific

binding to proteins of greater abundance may have been likely. To avoid this type of non-specific binding an increase in the duration of washes was done, doubling washing time, with no effect on the additional bands appearance. Experiments were also done with the primary antibody pre-incubated with the blocking peptide provided with the antibody and all three bands were no longer present, proving that the bands observed are indeed $\text{Na}_v1.5$. Lower concentrations of primary and secondary antibody were also tested, but this resulted in blank blots (data not shown).

Therefore, the data for the $\text{Na}_v1.5$ protein expression in mouse LA and LV samples has been analysed and presented using the densities of the individual molecular weight bands alone as well as averaging the densities of all three bands. Other groups that have used this antibody have either only analysed data using the largest band (189) or not stated what the molecular weight of the analysed band was (190, 191).

Figure 4.1A is a copy of the rat brain tissue Western blot example provided, on the Alomone data sheet for the $\text{Na}_v1.5$ antibody, clearly showing two expected bands at around 250kDa and 75kDa. Figure 4.1B is an example of a whole Western blot generated in this study, showing three distinct bands with the $\text{Na}_v1.5$ antibody at 250kDa, 75kDa and 25kDa. Figure 4.1B also shows a representative GAPDH Western blot band at 37kDa molecular weight, used for normalisation.

Figure 4.1C shows $\text{Na}_v1.5$ protein expression using only the largest 250kDa band. Using the 250kDa band, expression of the $\text{Na}_v1.5$ protein is shown to be greater in the LA than LV (LA n=13; LV n=13). Figure 4.1D shows data from the 250kDa and 75kDa bands combined (Figure 4.1A). When 250kDa and 75kDa band are combined, expression of the $\text{Na}_v1.5$ protein is greater in the LV than LA (LA n=13; LV n=13). Figure 4.1E is a combination of all three bands that were visible on the Western blot (seen in Figure 4.1B) and also shows greater expression of the $\text{Na}_v1.5$ protein in the LV than LA (LA n=13; LV n=13). Table 2.1 shows data obtained from all of the bands individually. The difference in the expression on $\text{Na}_v1.5$ between LA and LV varies, dependent on which Western blot bands were analysed.

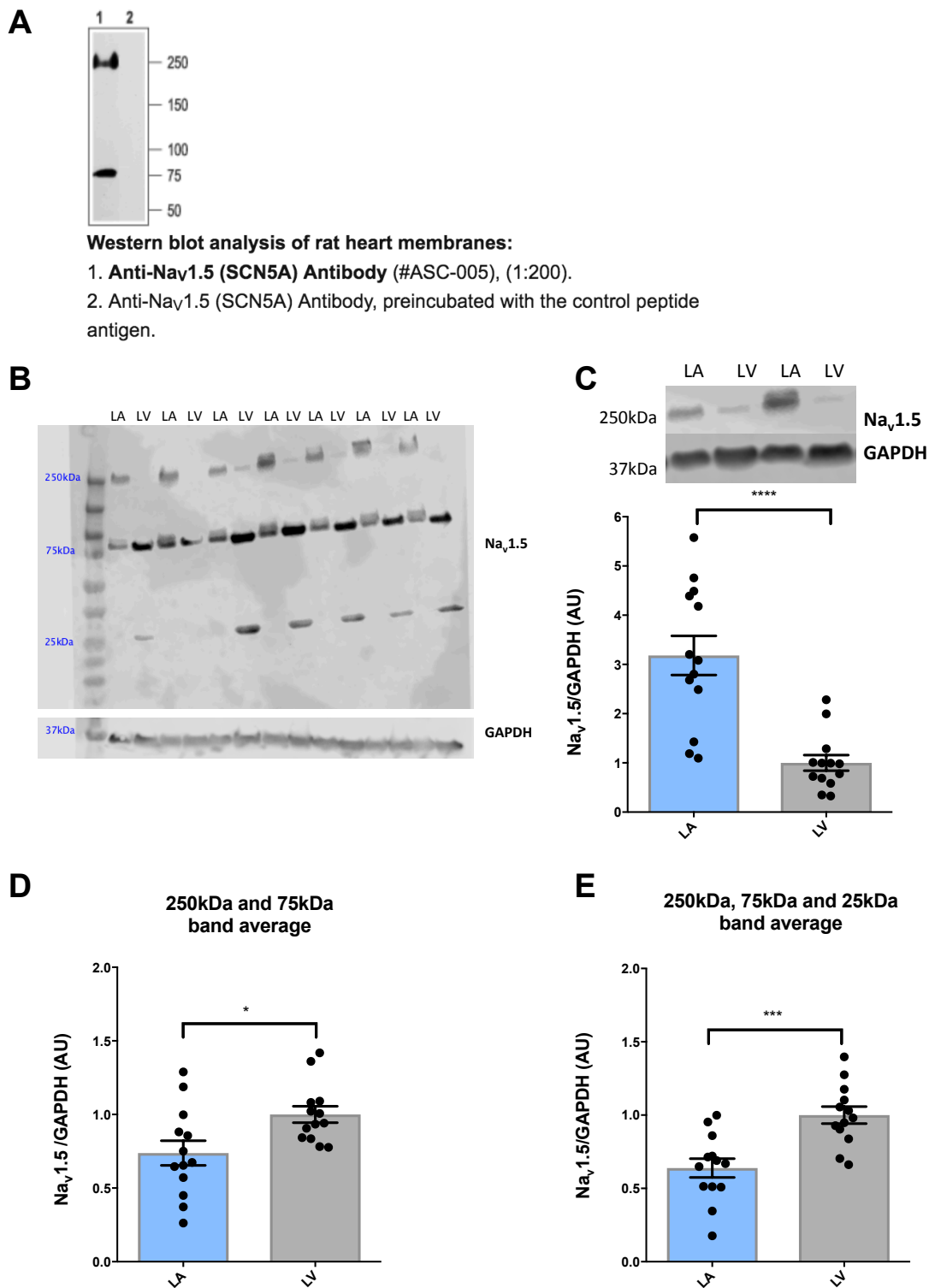


Figure 4.1. Na_v1.5 expression in mouse LA and LV.

Expression of Na_v1.5 protein in LA and LV tissue from WT mouse hearts. A) The Western blot example provided on the Alomone data sheet for the Na_v1.5 antibody (192). B) Top: image of the whole Na_v1.5 Western blot obtained, showing three distinct bands with the Na_v1.5 antibody at 250kDa, 75kDa and 25kDa, bottom: representative GAPDH Western blot band. C) Analysis of the

250kDa band alone (LA=3.182 ± 0.3977AU; n=13; LV=1.00 ± 0.1598AU; n=13) ****p<0.0001. D) Analysis of the 250kDa and 75kDa band combination (LA=0.7381 ± 0.08387AU; n=13; LV=1.00 ± 0.005585AU; n=13) *p<0.05. E) Analysis of the 250kDa, 75kDa and 25kDa band combination (LA=0.6392 ± 0.06412AU; n=13; LV=1.00 ± 0.05798AU; n=13) ***p<0.001. Error bars indicate ± S.E.M. significance taken as *P<0.05 with unpaired Student t-test.

Table 2.1: Individual molecular weight band data for Na_v1.5 expression in mouse WT LA and LV.

Molecular weight of Na _v 1.5 antibody band	Normalised protein expression in LA (AU)	Normalised protein expression in LA (AU)	Unpaired Student t-test significance
250kDa	3.182 ± 0.3977	1.00 ± 0.1598	****p<0.0001
75kDa	0.3818 ± 0.04430	1.00 ± 0.04894	****p<0.0001
25kDa	0.4835 ± 0.05624	1.00 ± 0.07739	****p<0.0001

3.3.2. Na_v1.5 β-subunit expression in WT mouse LA and LV

A lower expression of Na_vβ2 and Na_vβ4 was observed in LA rat myocardial tissue compared to the LV rat myocardial tissue (4). The same study also found that currents of Na_v1.5 co-expressed with Na_vβ2 and Na_vβ4 subunits in HEK 293 cells had a more positive activation potential, more positive inactivation and faster recovery of the sodium channels, compared to HEK 293 cells expressing Na_v1.5 alone (4). Therefore, the I_{Na} in the HEK 293 cell expressing Na_v1.5 with Na_vβ2 and Na_vβ4 subunits could be likened to the I_{Na} in LV cardiomyocytes and likewise the I_{Na} in HEK 293 cell expressing Na_v1.5 alone could be compared to

LA cardiomyocyte I_{Na} . In this study we investigated whether the described differences in expression of the β -subunits was conserved in mouse and human tissue.

Western blot experiments were performed on WT mouse LA and LV tissue homogenates, in order to assess whether the protein expression of the $Na_v\beta_2$ and $Na_v\beta_4$ subunits varies between the atrial and ventricular chambers. Figure 4.2A shows the Western blot for $Na_v\beta_2$ with a 15kDa band and GAPDH that was used for normalisation with a 37kDa molecular weight. The expression of the β_2 is lower in the LA than in the LV (LA n=6; LV n=6). Figure 4.2B shows the Western blot for $Na_v\beta_4$ with a 25kDa band and a 37kDa GAPDH that was used for normalisation. The expression of the β_4 is lower in the LA than in the LV (LA n=6; LV n=6).

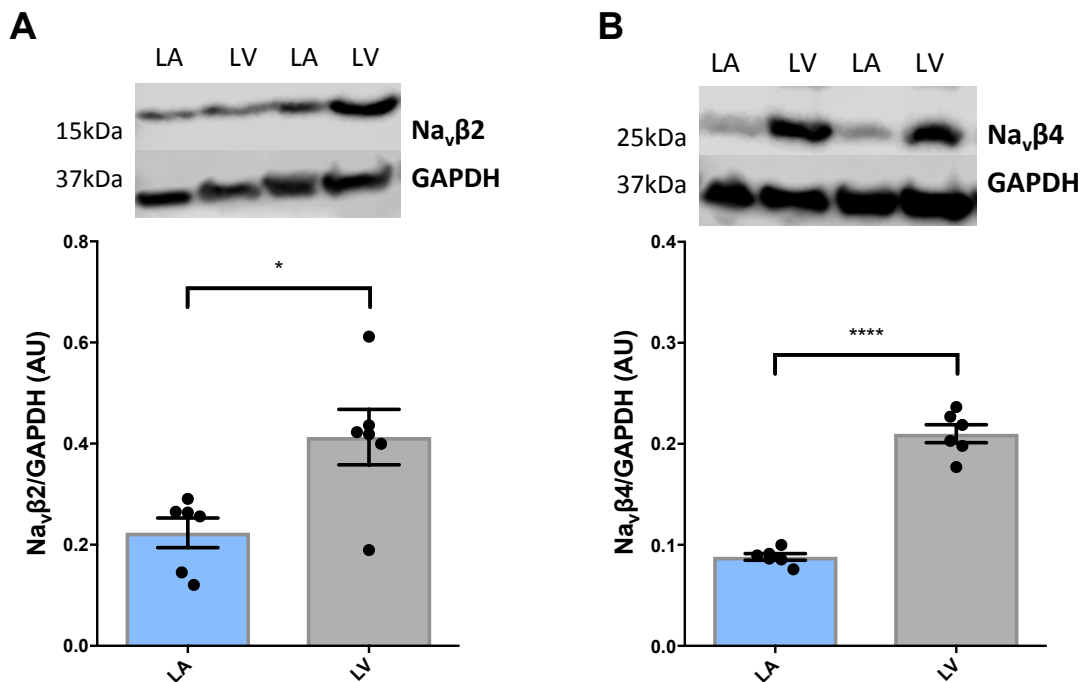


Figure 4.2. $Na_v\beta_2$ and $Na_v\beta_4$ expression in mouse LA and LV.

Expression of Na_vβ2 and Na_vβ4 protein in LA and LV tissue from WT mouse hearts. A) Raw example blot of GAPDH and Na_vβ2 Western blots. Analysis of the Na_vβ2 protein band normalised with GAPDH (LA=0.2237 ± 0.02926AU; n=6; LV=0.4131 ± 0.05483AU; n=6) *p<0.05. B) Raw example blot of GAPDH and Na_vβ4 Western blots. Analysis of the Na_vβ4 protein band normalised with GAPDH (LA=0.0881 ± 0.003234AU; n=6; LV=0.21 ± 0.008832AU; n=6) ****p<0.0001. Error bars indicate ± S.E.M. significance taken as *P<0.05 with unpaired Student t-test.

3.3.3. Na_v1.5 β-subunit expression in human LA and LV

Western blot experiments were performed on diseased and healthy human LA and LV tissue homogenates, in order to assess the protein expression of the Na_vβ2 and Na_vβ4 subunits. As Na_vβ2 and Na_vβ4 subunits are greater in mouse LA than LV, it is interesting to examine whether the same difference is seen between diseased human LA and LV. Hearts are classified as diseased due to a reduced ejection fraction below 50%.

Figure 4.3A shows the Western blot for Na_vβ2, with a 50kDa band and associated GAPDH that was used for normalisation with a 37kDa molecular weight. The expression of the β2 is higher in the LA than in the LV (LA n=6; LV n=6), contrary to the findings in healthy mouse tissue (Figure 4.2A). Figure 4.3B shows the Western blot for Na_vβ4 with a 25kDa band and associated GAPDH that was used for normalisation with a 37kDa molecular weight. There is a pattern of much lower expression of the β4 in the LA compared to the LV, matching findings in the healthy mouse tissue (see Figure 4.2B), but likely due to the small n numbers and data variability this is not significant (LA n=6; LV n=6).

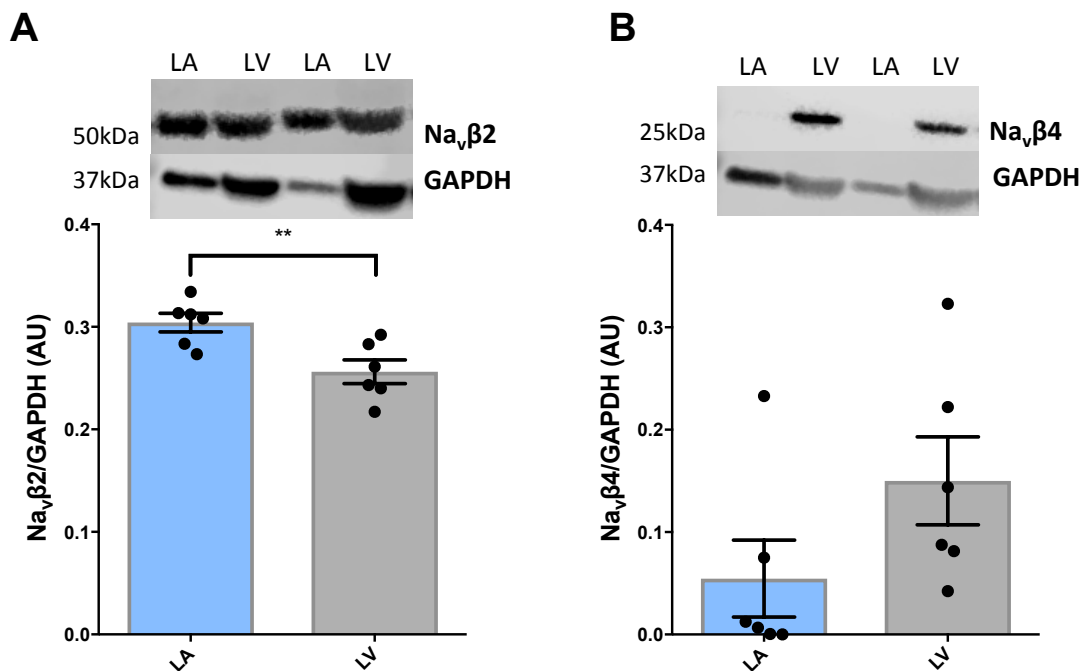


Figure 4.3. Na_vβ2 and Na_vβ4 expression in diseased human LA and LV. Expression of Na_vβ2 and Na_vβ4 protein in LA and LV tissue from diseased human hearts. A) Raw example blot of GAPDH and Na_vβ2 Western blots. Analysis of the Na_vβ2 protein band normalised with GAPDH (LA=0.3041 ± 0.00902AU; n=6; LV=0.2562 ± 0.01155AU; n=6) **p<0.01. B) Raw example blot of GAPDH and Na_vβ4 Western blots. Analysis of the Na_vβ4 protein band normalised with GAPDH (LA=0.0546 ± 0.03751AU; n=6; LV=0.15 ± 0.04394AU; n=6). Error bars indicate ± S.E.M. significance taken as *P<0.05 with unpaired Student t-test.

Western blot experiments were performed on human healthy LA and diseased LA tissue homogenates, in order to assess whether the protein expression of Na_vβ2 varies. Healthy tissue was collected from donor hearts that were not used for transplantation.

Figure 4.4A shows the Western blot for Na_vβ2 with a 50kDa band and associated GAPDH that was used for normalisation with a 37kDa molecular

weight. The expression of the $\beta 2$ is higher in the diseased LA than in the healthy LA (LA n=4; LV n=4).

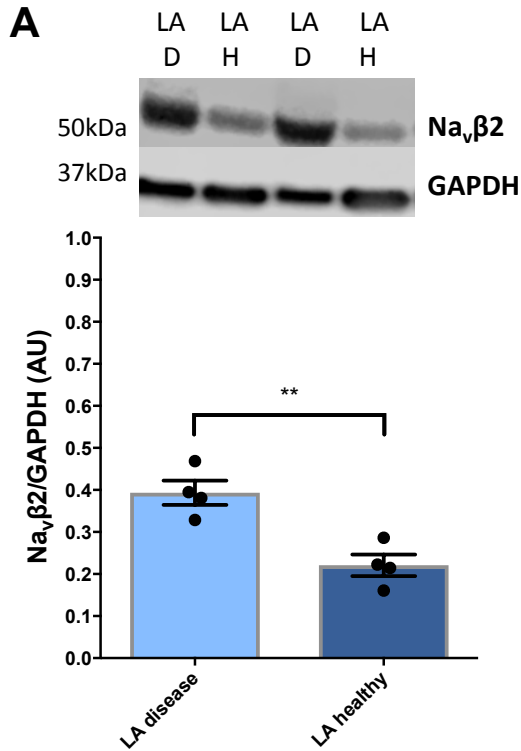


Figure 4.4. $\text{Na}_v\beta 2$ expression in diseased and healthy human LA.

Expression of $\text{Na}_v\beta 2$ protein in LA and LV tissue from diseased human hearts. Raw example blot of GAPDH and $\text{Na}_v\beta 2$ Western blots. Analysis of the $\text{Na}_v\beta 2$ protein band normalised with GAPDH (LA=0.3934 ± 0.02893AU n=4; LV=0.2209 ± 0.0257AU n=4) **p<0.01. Error bars indicate ± S.E.M. significance taken as *P<0.05 with unpaired Student t-test.

3.3.4. Expression of the genes that encode SCN5A, SCN2B and SCN4B in healthy human LA and LV

This work was performed by Dr Nathan Tucker.

RNA-sequencing was done on paired LA and LV samples from 4 donor hearts and the mRNA expression of SCN5A (the gene that encodes Na_v1.5), SCN2B and SCN4B (the genes that encode the Na_vβ2 and Na_vβ4 respectively).

There is no difference in SCN5A mRNA between the human LA and LV (LA n=4; LV n=4). However, there is a trend of lower mRNA expression of SCN2B in the human LA compared to the LV but this is not significant, likely due to variability and small data set (LA n=4; LV n=4). SCN4B is significantly lower in the human LA than LV (LA n=4; LV n=4) (Figure 4.5).

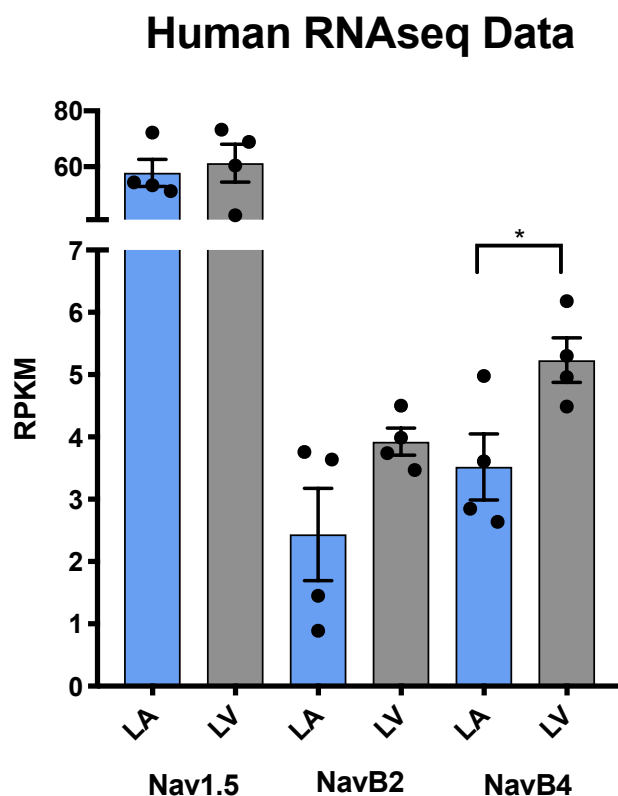


Figure 4.5. Expression of the mRNAs that encode Na_v1.5 and the Na_vβ-subunits in healthy human LA and LV.

The mRNA of SCN5A, SCN1B, SCN2B, SCN3B and SCN4B in healthy human LA and LV. Expression of SCN5A (LA=57.83 ± 4.857 RPKM n=4; LV=42.61 ± 6.780 RPKM; n=4). The mRNA expression of SCN2B (LA=2.435 ± 0.789 RPKM n=4; LV=3.925 ± 0.2191 RPKM; n=4). The mRNA expression of SCN4B

(LA=3.52 ± 0.5294 RPKM n=4; LV=5.233 ± 0.3568 RPKM; n=4) *p<0.05. Error bars indicate ± S.E.M. significance taken as *P<0.05 with unpaired Student t-test.

3.4. Chapter synopsis and discussion

3.4.1. Overview of main findings

The key findings of the chapter are described as follows:

- Mouse LA I_{Na} density is smaller than LV I_{Na} density at physiological RMP (-75mV). Density of LA I_{Na} is only greater than LV I_{Na} when the holding potential of the cells is hyperpolarised in comparison to normal physiological RMP.
- The biophysical properties of mouse LA and LV sodium channels differ. LA sodium channels activate and inactivate at more negative potentials and have slower time dependent recovery than LV sodium channels.
- Flecainide displays a more potent inhibition of LA sodium channels than LV sodium channels across the full range of holding potentials tested (-120 to -70mV).
- Expression of $Na_v1.5$ protein is greater in mouse LA than LV (when analysed using the standard 250kDa band) but the expression of $Na_v\beta2$ and $Na_v\beta4$ protein is reduced in mouse LA compared to LV. Conversely,

expression of $\text{Na}_v\beta 2$ protein is greater in human diseased LA than diseased LV.

3.4.2. Physiological I_{Na} density comparison between LA and LV

There have been several studies comparing the biophysical properties of mammalian atrial and ventricular sodium channels, that have resulted in multiple publications stating chamber distinctions in the sodium channel physiology. Different activation, inactivation and recovery kinetics of VGSCs in LA and LV cardiomyocytes of guinea pig, canine, rat and rabbit (4, 5, 142, 185, 186) have been shown. One of the conclusions from these studies is that the LA cardiomyocytes display greater peak I_{Na} than LV cardiomyocytes (4, 5, 142, 185, 186).

However, this does not correlate with what is understood about the physiology of the heart. Maximum rate of rise of the AP upstroke (V_{max}), has long been established as a measure of I_{Na} in cardiomyocytes (19, 31) and the V_{max} of atrial APs has been experimentally described as being between $\cong 150\text{-}300$ V/s (31, 32), compared to higher values of $300\text{-}400$ V/s for human ventricular cells (33, 34), with similar differences also shown in smaller mammals (193, 194). This contrasts with the published exclamation of atrial I_{Na} density being greater than ventricular, as in fact the opposite would be expected, considering that the atrial V_{max} is smaller than ventricular V_{max} .

However, there is no difference seen in mouse peak LA and LV I_{Na} in Figure 3.1D, with the -100mV holding potential that currents were initiated from, in order to obtain I/V data. No difference in I_{Na} density, at a -100mV holding potential, conflicts with what has been shown in other mammals in the previously stated publications. Consequently, further analysis was required into the effect of the holding potential on peak I_{Na} , as this was the only clear difference between this study and published data, which used a -120mV (or more negative) holding potential when obtaining I/V data (4, 5, 142, 185, 186).

In the data published in guinea pig, canine, rat and rabbit, that showed atrial peak I_{Na} was greater than ventricular peak I_{Na} (4, 5, 142, 185, 186), the -120mV holding potential used in these studies is much more negative than normal RMP of mammalian atrial and ventricular cardiomyocytes (19, 20). Protocols use hyperpolarised holding potential to ensure that all sodium channels are available for activation, so that currents recorded are representative of all of the sodium channels within the cells. This is demonstrated in Figure 3.3A, where minimal inactivation occurs (and therefore greatest current density) when sodium currents are initiated from at -120mV holding potential.

However, physiologically, in an *in vivo* setting, not all sodium channels would be available at normal mammalian RMP. This is evident in Figure 3.2; I_{Na} density is clearly much greater in both LA and LV chambers when currents are initiated from more negative potentials (-120mV Figure 3.2B), compared to when

currents are initiated from more physiological potentials (Figure 3.2C). Consequently, previously published data demonstrating greater LA I_{Na} compared to LV I_{Na} , is not physiologically relevant, due to protocols relying on the hyperpolarised holding potentials and not accounting for the effect of holding potential on current density between the chambers.

In order to gain understanding of physiologically relevant I_{Na} differences between chambers, it would be beneficial for cardiomyocytes to be examined under more physiological conditions. Therefore, patch clamp experiments could be performed at holding potentials of -65 to -80mV (20) for LA cardiomyocytes and -80 to -90mV (19) for LV cardiomyocytes. Figure 3.2A shows that I_{Na} density in LA at the holding potential of -75mV is -6.459pA/pF and LV I_{Na} at the -85mV holding potential is -19.479pA/pF. Hence, *in vivo* LA I_{Na} would be approximately a third that of LV I_{Na} , fitting more with what is understood about atrial and ventricular V_{max} (31-34, 193, 194). In Figure 3.2A, there is no difference between LA and LV I_{Na} density at -100mV holding potential. This clarifies why no difference is seen in peak I_{Na} in Figure 3.1D, as the -100mV holding potential was used to collect peak current data.

3.4.3. Voltage dependence of inactivation and the effect on peak LA and

LV I_{Na}

Sodium channel inactivation positively correlates with depolarisation of holding potential voltage in both the LA and LV (Figure 3.3A). The difference in sodium channel inactivation kinetics between the atrial and ventricular sodium channels results in a greater impact of change in holding potential on LA I_{Na} density. Figure 3.3A shows a negative shift in LA sodium channel inactivation compared to LV sodium channel inactivation. This is supported by the significant V_{50} data in Figure 3.3B, 50% of the LA sodium channels are inactivated at -88.481mV , compared to the more positive -81.952mV for LV sodium channels.

$\text{Na}_v1.5$ sodium channels adopt one of three structurally distinct states: open, closed and inactivated. As described in the introduction of this thesis, sodium channels activate (open) when the membrane potential depolarises and reaches the threshold for the activation gate to open, followed by a rapid influx of Na^+ . This state is brief due to the rapid closure of the inactivation gate; this is referred to as the inactivated (closed) state (195, 196). Therefore, negative regulation of sodium channel conductance occurs via this inactivation as influx of Na^+ is halted. Recovery from this inactivation occurs upon further repolarisation, the channel recovers from the inactivated (closed) state (inactivation gate opens) and deactivates to the original closed available state (activation gate is closed), this is known as the deactivated (closed) state. The functional difference between the inactivated (closed) and deactivated (closed)

state is that channels inactivate when the cell depolarises, rendering it unavailable to open and conduct Na^+ , whereas the deactivated state occurs during hyperpolarisation and channels are available to open when the cell depolarises. Consequently, in order for channels to be available for activation they must return to the deactivated (closed) state. The period of the inactivated (closed) state is important, as the influx of Na^+ and therefore the upstroke of the AP rely on the sodium channels being available to open (197).

Therefore, the negative shift in LA sodium channel inactivation results in a greater proportion of channels remaining in the inactivated (closed) state than the LV sodium channels at holding potentials more positive than -120mV (Figure 3.3A), so fewer are available for activation. To measure whether reduction in peak I_{Na} is a result of the negative shift in voltage dependence of inactivation, peak I_{Na} can be compared to currents initiated from more positive holding potentials. When initiated from a holding potential of -120mV , the LA I_{Na} density is -35.721pA/pF (Figure 3.2A). When this current density is reduced by the percentage of channel inactivation at -100mV (20.644%) (Figure 3.3C), the value is -28.347pA/pF , which is comparable to the LA I_{Na} density observed when the current is initiated from -100mV holding potential, of -26.84pA/pF (Figure 3.2A). The same is seen when this calculation is also done with the LV I_{Na} data. When initiated from a holding potential of -120mV , the I_{Na} density is -30.89pA/pF in the LV (Figure 3.2A). When this current density is reduced by the percentage of channel inhibition at -100mV (5.256%) (Figure 3.3C), the value is -29.27 , which is comparable to the LV I_{Na} density when the current is initiated

from a -100mV holding potential, of -27.08pA/pF (Figure 3.2A). Therefore, taking into account channel inactivation percentage at the different holding potentials and reducing the maximal current achieved (the current initiated from -120mV) by that percentage equates to the I_{Na} density value at the different holding potentials.

As previously described, sodium channel inactivation is negatively shifted in the LA compared to the LV (Figure 3.3A), with a resulting reduction in LA I_{Na} at physiological holding potentials. The sodium channel inactivation gate is usually described as open during the RMP phase of the AP (198), this clearly is not always accurate. At the RMP expected *in vivo* (-65 to -90mV), larger proportions of LA sodium channels remain in an inactivated closed state. Sodium channels do not need to open before they inactivate (199) and the hyperpolarised membrane potentials required for the sodium channels to enter the deactivated closed state would not occur naturally *in vivo*. Therefore, some sodium channels, more in the LA than LV because of the more negative inactivation and the more positive membrane potential *in vivo*, are in a perpetual inactivated closed state and can be rendered dormant physiologically.

3.4.4 Pathophysiological considerations due to differences in I_{Na} inactivation between LA and LV

As demonstrated in Figure 3.3A, the negative shift in inactivation of LA sodium channels means that *in vivo*, LA I_{Na} density is less than LV I_{Na} density. This is important as smaller I_{Na} would lead to reduced CV, which as previously described can be proarrhythmic and may suggest a possible cause of the atria's susceptibility to arrhythmia (1). Therefore, sodium channel blocking drugs, such as flecainide, could further contribute to arrhythmia generation, as conduction slows (200).

In large mammals, such as dogs and humans, the $I_{Na,late}$ has been shown to modulate APD by providing a sustained influx of Na^+ , disrupting the balance of inward Ca^{2+} and outward K^+ during the AP plateau (201). APD prolongation, as a result of more positive sodium channel inactivation and more positive sodium channel activation and subsequent $I_{Na,late}$, is linked to arrhythmogenesis. Enhanced $I_{Na,late}$ can instigate repolarisation failure and result in EAD's, causing a regenerative L-type Ca^{2+} channel re-activation or providing sufficient time for sodium channels to recover and reactivate (127). Additionally, DAD's can follow full repolarisation via Ca^{2+} overload in sodium-calcium overload conditions (202). As described in the data here, LA sodium channels may be less likely to reactivate prematurely as hyperpolarisation is required for sodium channels to convert from the inactivated state and be available for activation. Therefore,

atria may display negligible or smaller $I_{Na,late}$ compared to the ventricles and this may be considered as cardioprotective.

Conversely, LA sodium channels may remain open during the plateau phase of the AP due to the shift in inactivation potential and could in fact have a greater $I_{Na,late}$ compared to the ventricles. Luo et al., demonstrated this by showing greater $I_{Na,late}$ density in rabbit atrial cardiomyocytes compared to ventricular cardiomyocytes (203). This is also supported by additional studies that have demonstrated ranolazine, an $I_{Na,late}$ blocker, as an effective AF treatment (204-207). However, ranolazine inhibition of potassium channels also needs to be considered, as K_r block has the antiarrhythmic effect of prolonging APD (208, 209).

However, direct voltage clamp measurements comparing $I_{Na,late}$ from rabbit atrial and ventricular cardiomyocytes found no difference in $I_{Na,late}$ density when currents were measured from a -80mV holding potential (210). Nevertheless, it must be considered that these experiments utilised additional agents to prolong the sodium channel open time and facilitate reopening to increase $I_{Na,late}$, in order for it to be possible to measure such small currents. Therefore, the normal gating kinetics of the sodium channels in these studies may have been altered, and perhaps not be representative of what would occur *in vivo*. Furthermore, other studies have shown that accurate direct voltage clamp measurements comparing $I_{Na,late}$ from healthy WT atrial and ventricular cardiomyocytes under

physiological conditions is extremely difficult, as the currents are so small or appear non-existent (211).

Depolarisation of the RMP can occur as a result of medication, ischemia or hypoxia. For example, acute myocardial ischemia causes a series of complex biochemical alterations in the myocardium, including acidosis with a rapid rise in local extracellular K^+ . As predicted in the Nernst equation, increases in extracellular K^+ results in depolarisation (17). A rise in extracellular K^+ occurs due to a fall in ATP in the absence of blood flow, which results in the opening of ATP-modulated K^+ channels, that are normally inhibited with physiological levels of intracellular ATP and inhibition of the ATP-dependent NKA pump. As the RMP depolarises there is expected to be an increase in sodium channel inactivation and therefore I_{Na} amplitude decrease, resulting in slower CV (212). Given the accepted determinants of re-entry, slower conduction decreases the size of the re-entrant circuit and increases the number of circuits, increasing the likelihood of AF occurrence (213). Therefore, the negatively shifted inactivation of LA sodium channels suggests that the LA are likely to experience greater slowing in conduction, under conditions that may depolarise the RMP, potentially leading to arrhythmia generation. This is a feasible mechanism for the atria's increased susceptibility to arrhythmia compared to the ventricles if the RMP becomes depolarised.

Acidosis can result in depolarisation of the RMP (214). The arrhythmic effect of a shift in inactivation with acidosis has been shown in patients with the R1512W mutation in SCN5A, that was identified as the first cause of Chinese sudden unexplained nocturnal death syndrome (SUNDS) (215) but showed no obvious loss of function of the cardiac sodium channel *in vitro* (216). Patch clamp experiments measuring I_{Na} on *Xenopus* oocytes expressing sodium channels with the R1512W mutation have revealed a 4-5mV negative shift in the steady-state inactivation curves compared to their WT counterparts (216), this shift is comparable to the differences observed between LA and LV sodium channel inactivation (Fig 3.3A). It was shown that slight acidosis conditions resulted in significant loss of function of the mutant sodium channel in cells with the R1512W mutation, compared to cells expressing WT $Na_v1.5$ (216). This suggested that nocturnal sleep disorders-associated with slight acidosis could trigger the lethal arrhythmia underlying the sudden death of people with this genetic defect. This again endorses that the more negative inactivation of LA sodium channels could result in a greater susceptibility to arrhythmia compared to the LV, under conditions that shift RMP positively, such as acidosis.

Antiarrhythmic drugs, Class I: fast sodium channel blockers, Class II: beta blockers and Class IV: calcium channel blockers, can have the adverse effect of decreasing CV and so can be proarrhythmic (165). Therefore, factors that affect the RMP, such as electrolyte abnormalities, fibrosis, ischemia and inflammation are important to consider when treating AF. The sensitivity of atrial sodium channel inactivation to depolarisation of the RMP could result in conduction

slowing, with antiarrhythmic drugs contributing to this. Indeed, proarrhythmic risk of flecainide treatment in patients with structural heart disease is well documented, as they would likely have fibrosis and/or inflammation and/or ischemia (159). Consequently, in patients with conditions that result in depolarised RMP, the development of atrial specific drugs that shift the inactivation of sodium channels to more positive potentials or repolarise the RMP could be protective against AF.

3.4.5. Sodium channel activation differences between LA and LV

Activation of sodium channels depends upon voltage sensing, whereby alterations in membrane potential promote change to the channel conformation. The sodium channels are closed under resting conditions and those that are in the deactivated (closed) state are available for activation (opening), when the membrane potential depolarises and reaches the threshold for the channel activation gate to open, followed by a rapid influx of Na^+ . The influx of Na^+ into the cardiomyocyte results in a positive feedback loop, with more sodium channels activating in response to the depolarising membrane potential, driving the AP upstroke until there is inactivation (closure) of the channels (217, 218).

The LA -4.08mV shift in the V_{50} activation potential detected in this study reveals that the voltage at which half of the sodium channels are available for activation is more negative compared to that of the LV sodium channels (Fig 3.1E). This difference in V_{50} activation potential is also supported by previously

published findings in rabbit LA and LV cardiomyocytes (5). It would be expected, that a negative shift of the voltage dependence of LA sodium channel activation would decrease the voltage difference between the RMP and the activation threshold, leading to increased I_{Na} . However, this is counteracted by the greater negative shift in the voltage dependence of LA sodium channel inactivation (Fig 3.3A), resulting in a decrease in channel availability, leading to a decreased LA I_{Na} compared to LV I_{Na} , when initiated from physiological holding potentials (Fig 3.2C).

This negative shift in V_{50} activation potential of the LA sodium channels suggests an enhancement of excitability of LA cardiomyocytes compared to LV cardiomyocytes. Negative shifts in the voltage dependence of sodium channel activation permits channel activation with smaller depolarisations. This can result in premature initiation of the sodium channels with minor depolarisation and therefore could instigate DAD generation via Ca^{2+} oscillations in sodium-calcium overload conditions. Although it has been shown here that there are a smaller proportion of LA sodium channels available for activation at physiologically relevant holding potentials, those that are available are more sensitive to an untimely depolarisation of membrane potential and may be more susceptible to premature activation, offering a foundation to the atria's greater susceptibility to arrhythmia. Consequently, identifying the molecular determinants driving enhanced atrial sodium channel activation at hyperpolarised potentials may reveal novel drug targets for treatment of AF in patients.

The R1512W mutation in SCN5A, that was identified as the first cause of Chinese SUNDS described above, has also shown to cause a -5.1mV negative shift in activation in *Xenopus* oocytes (216), comparable with the shift observed between LA and LV sodium channels (Figure 3.1E). Rook et al., also suggest that this shift in activation to more negative potentials could lead to enhanced excitability of cardiomyocytes and also be a mechanism for the arrhythmogenesis observed in patients that have the R1512W mutation (216).

However, as previously discussed, the greater difference in V₅₀ inactivation of the sodium channels at physiological potentials in both the LA and LV, overrides the activation differences at physiologically relevant potentials, as shown by the fact that the LA peak I_{Na} is smaller than the LV I_{Na} (Fig 3.2C). Altering the activation kinetics of the LA sodium channel in order to inhibit AF may not only suppress premature activation but would also result in a reduction in I_{Na} , which in itself may be proarrhythmic due to reductions in CV. Additionally, inactivation derives much of its voltage dependence from coupling to activation, so the rate of inactivation increases as a result of conformational changes in the sodium channel activation domain (219, 220). Therefore, altering the activation region/kinetics could also alter inactivation kinetics and lead to undetermined and potentially unsafe further modifications in I_{Na} .

3.4.6. Sodium channel recovery differences between LA and LV

After sodium channels activate and open, inactivation closes the sodium channel, preventing it from reopening until there is adequate time for recovery. Subsequently channels undergo deactivation, after which re-excitation is permitted. The extent of sodium channel inactivation and time dependence of recovery from inactivation controls the ERP, where AP initiation cannot occur (221). The recovery process occurs on a millisecond timescale, with exponential kinetics that are accelerated with hyperpolarisation (222).

Studies on sodium channels with the I1768V mutation on SCN5A, underlying LQT-3 syndrome, results in channel reopening during repolarisation due to faster recovery by 28.9ms compared to WT counterparts. This causes increased $I_{Na,late}$, due to channel reopening, producing severe prolongation of the AP plateau, with the resultant arrhythmic triggers described previously because of this late current (223, 224). Therefore, the faster recovery of the LV sodium channels could be considered to be proarrhythmic. However, the LA sodium channel P50 for recovery time is only 6.83ms slower than LV sodium channel recovery (Figure 3.4B), a substantially smaller difference than what is described between the I1768V mutation on SCN5A and the WT.

Unlike the LQT-3 syndrome mutations that are linked with faster recovery of the sodium channels, the p.I848fs SCN5A mutation, associated with Brugada syndrome, has been shown to slow recovery time of the sodium channels (224).

The slowing in recovery results in a decrease in I_{Na} as channels do not recover quickly enough to be available for reactivation when another AP is generated, leading to decrease in AP amplitude and CV (98). As described previously, a reduction in CV is associated with arrhythmia generation, so a slower recovery time of the sodium channels may also be considered proarrhythmic. As recovery is accelerated with hyperpolarisation (222) and *in vivo* LV have more negative RMP than the LA, differences in recovery could be amplified.

Overall, it is difficult to determine the effect of a slower recovery of sodium channels in the atria compared to ventricles, or whether the time difference in recovery is substantial enough to make one chamber more susceptible to conduction disturbances than the other. Further studies, examining the effects of these biophysical characteristics under physiological (increased heart rate) and pathophysiological stressors (ischemia, fibrosis) are required to gain a greater understanding of the impact of modulation of recovery kinetics on heart function and arrhythmia predisposition in the different chambers of the heart.

3.4.7. Flecainide sodium channel inhibition in the LA and LV

The LA sodium channels are clearly distinctive to the LV sodium channels, with more negative V_{50} inactivation, more negative V_{50} activation, slower recovery and smaller peak I_{Na} at physiological holding potentials. It is clear that the negative shift in V_{50} for inactivation is responsible for reduced LA I_{Na} at physiological potentials, but whether or not the differences in kinetics are

responsible for the atria's susceptibility to arrhythmias requires further examination.

The difference in LA and LV sodium channel kinetics can alter the susceptibility to sodium channel blocking drugs and therefore drug efficacy in different chambers of the heart. If AADs block LA sodium channels more effectively due to these kinetic distinctions, there may be potential atrial specific AF drugs that work without altering electrophysiology of otherwise normally functioning ventricles. Existing studies with several AADs suggest that sodium channels in atrial cardiomyocytes/tissue are more sensitive to their blockade than ventricular sodium channels; ranolazine in canines (142), amiodarone in canines (185), dronedarone in rats (4) and ranolazine in rabbits (5). The greater sensitivity of LA sodium channels to these drugs may be as a result of the differences in channel gating kinetics.

As previously described, flecainide is a Class IC AAD and its efficacy has been confirmed by several clinical trials (152, 153). Flecainide has a high affinity for open-state sodium channels with slow unbinding kinetics from the channels during diastole, owing to a slowing of recovery during diastole and prolongation of refractoriness (225). Flecainide also inhibits the opening of potassium channels, prolonging APD in the ventricles and atria (163). However, it has been demonstrated that flecainide use was associated with increased proarrhythmic events in patients with severe cardiac disease, as described

previously (158). Nevertheless, flecainide is still recommended as one of the first line therapies for pharmacological conversion and maintenance of NSR in patients with AF (226).

Open and inactivated channels are more susceptible to block from Class I AADs than resting deactivated closed state channels (7). As shown in Figure 3.3, a larger proportion of LA sodium channels, compared to LV sodium channels, are inactivated at physiological membrane potentials and they activate (open) at more negative potentials (Figure 3.1), with slower recovery to the deactivated closed state (Figure 3.4). This suggests that Class I drugs can target the LA sodium channels more than the LV sodium channels at physiological membrane potentials, as a greater proportion of the LA sodium channels will be in the open and inactivated states (227). Figure 3.5A clearly shows that flecainide inhibits both LA and LV I_{Na} , as currents are visibly smaller with the addition of 1 μ mol flecainide and the peak of both I/V curves are significantly reduced (Figure 3.5D and 3.5E). However, the percentage inhibition of peak I_{Na} is considerably greater in the LA than the LV, by 18.87% (Figure 3.5F). This is likely due to the LA channels being more available for inhibition because of the differences in channel gating kinetics (227). Therefore, this provides evidence that flecainide is more selective to atrial sodium channels.

Furthermore, as demonstrated in Figure 3.6 and previously described by others (228), there is a positive correlation between percentage inhibition of I_{Na} and holding potential in both LA and LV cardiomyocytes. As holding potential depolarises, the inhibition of sodium channels with 1 μ mol flecainide increases. However, percentage inhibition with flecainide is significantly greater in LA sodium channels than in LV sodium channels at all of the holding potentials recorded. This is particularly important, as the RMP of the atria is more positive than that of the ventricles *in vivo*, so the two mechanisms contributing to its greater effectiveness are: 1. greater inhibition due to the difference in RMP, and 2. greater inhibition of LA I_{Na} regardless of holding potential. Therefore, in order to get a true representation of flecainide inhibition between the chambers, the percentage inhibition can be compared from the data at each of the chambers respective to approximate RMP *in vivo*. Using Figure 3.6A, at -75mV LA I_{Na} inhibition is 70.71% and at -85mV LV I_{Na} inhibition is 41.78%, suggesting that flecainide would be approximately 28.93% more effective at inhibiting atrial sodium channels at physiological holding potentials *in vivo*.

There is also a significant negative shift in the inactivation potential of the sodium channels in both the LA and LV post flecainide addition (Figure 3.7). The LA shift in the inactivation potential of the sodium channels is -1.141mV greater than the shift observed in the LV (Figure 3.7E), but this is not significant, possibly due to the spread of data and small data set. However, the trend of greater shift in LA sodium channel inactivation is probably partly accountable for the greater inhibition of LA sodium channels with flecainide. More sodium

channels would therefore be inhibited at the physiological RMP of the atria so would not be available for activation and I_{Na} density would be reduced.

LV sodium channel recovery was not affected by the addition of flecainide but LA sodium channel recovery time was increased when flecainide was added to the cells (Figure 3.7B). The increase in recovery time would reduce $I_{Na,late}$, safeguarding from prolongation of the AP plateau and the resultant arrhythmic triggers described previously because of this late current (223, 224). Additionally, with increase in channel recovery time the LA ERP would increase (221) and this could be protective against re-entrant AF (118).

Similarly, in canines and rabbits ranolazine has proven to have greater inhibition of LA sodium channels than LV sodium channels. This is likely due to it being an inactivated-state sodium channel blocker, as a greater proportion of atrial sodium channels are in the inactivated state (5, 142). It is also claimed that ranolazine has no known proarrhythmic effects, unlike flecainide, so may be more suitable for patients with pre-existing heart conditions (229). Likewise, with similar ion channel block profile and kinetics to ranolazine, amiodarone has also proven to have greater affinity for the LA sodium channels. In canine tissue amiodarone has been shown to reduce V_{max} of the atria significantly, but like flecainide does still have some effect on the LV, also reducing LV V_{max} but to a lesser extent (185). Dronedarone inhibition of rat cardiomyocyte sodium channels has also proven to be greater in the LA than LV. Dronedarone

negatively shifts LA and LV sodium channel inactivation, with a greater shift in the LA and slows recovery in both chambers but with a greater effect in the LV (4). Dronedarone appears to act very similarly to flecainide but predominantly blocks potassium channels to prolong repolarisation, not target sodium channels primarily. Additionally, dronedarone potency decreases as the heart rate increases, so is unlikely to be as useful in fast-firing, fibrillating atria, unlike flecainide (230).

Therapeutic effectiveness of flecainide is mediated by reduction in I_{Na} , decreasing the rate and magnitude of depolarisation and subsequent decrease in CV, thereby depressing abnormal conduction in AF patients. From the data provided here it is evident that flecainide is more effective in the LA than LV. Greater percentage inhibition and also the effects on inactivation and recovery time that would reduce CV demonstrate this. Additionally, flecainide is a use-dependent drug, meaning its inhibition increases as rate of contraction increases (231). Therefore in AF patients, flecainide is likely to have a greater effect on atrial sodium channels as atrial tissue would be firing at a faster rate than ventricular tissue.

Overall, comparisons of atrial selectiveness of flecainide to the other AADs is difficult, as the other studies do not provide direct percentage inhibition data of the sodium channels at physiological holding potential ranges. Furthermore, the effects on the other ion channels, aside of the sodium channels, needs to be

considered when assessing the effectiveness for AF treatment. Also, none of the AADs previously tested by others have proven to specifically target only LA sodium channels, so electrophysiological effects on normally functioning ventricles may still occur.

3.4.8. Varying Na_v1.5 expression in WT mouse LA and LV

As demonstrated in Figure 3.2A, at physiological holding potentials LA I_{Na} density is less than LV I_{Na} density. However, LA I_{Na} density is greater than that of the LV at the -120mV holding potential, when all sodium channels are available for activation. This is in agreement with previously published studies using hyperpolarised holding potentials to measure I_{Na} density (4, 5, 142, 185, 186). Therefore, data presented here and by others (4, 5, 142, 185, 186) suggests that the LA have a greater density of sodium channels, even though many are dormant under physiological conditions. Na_v1.5 protein expression data shown in Fig 4.1C analysing the band at the expected/standard molecular weight, shows greater expression in LA compared to LV. This explains greater I_{Na} in LA cardiomyocytes at the -120mV holding potential (Figure 3.2A). Na_v1.5 protein expression was also greater in rat LA compared to LV myocardium but this was not significant, as demonstrated by Chen et al., with n=4 (4). Nevertheless, considering that a greater proportion of the LA sodium channels are inactive at physiological RMPs, if Na_v1.5 expression was greater in the LA it would not be evident when measuring currents *in vivo*.

Antibody specificity and selectivity are unclear and indeed several bands at varying molecular weights were observed. When the additional bands were analysed individually (Table 2.1), aside of the primary 250kDa band expected and analysed by others (4, 189), there was opposing results to those shown in Figure 4.1C, as shown in Figure 4.1D and Figure 4.1E. Analysis using a combination of the data from the other bands shows that expression of Na_v1.5 is greater in LV compared to LA, contradicting Figure 4.1C. This also opposes the findings of Chen et al. in rat atrial and ventricular cardiomyocytes that showed no difference in SCN5A gene expression. The mRNA data in Figure 4.4 corresponds with the findings of Chen et al., in that no difference is observed in SCN5A expression between the healthy human LA and LV, though these are based on a limited number of samples (n=4). Clearly, more analysis in larger tissue sample sets is needed to be able to detect differences in SCN5A expression between chambers in the human heart, as illustrated by the large variability even in the controlled mouse setting here (Figure 4.1).

Although the data of Chen et al., showed a trend for greater Na_v1.5 protein expression in the mouse LA, there was no significant difference. However, that study used a 260kDa band for the protein expression analysis and provided no description on whether bands of any other molecular weight were visible on the Western blots (4). Also, Chen et al., provided no Na_v1.5 expression data between the human LA and LV, which is unexpected, considering they measured the expression of all the Na_vβ-subunit proteins (4). This may be due

to poor reactivity of the antibody with human samples, as observed in this study.

Therefore, no conclusive report can be provided on whether $\text{Na}_v1.5$ expression is greater in the LA or LV as the data is varied depending on how it is analysed and there is contradiction with previously published data (4). Moreover, no other antibodies tried in this study were successful or demonstrated improved signals. Another limitation of the work presented here is that the Western blotting measured $\text{Na}_v1.5$ protein expression within the whole tissue, and did not discriminate between sodium channels in cardiomyocytes alone, nor does it discriminate between the functional channels at the membrane surface and those in the secretome (188).

3.4.9. $\text{Na}_v\beta2$ and $\text{Na}_v\beta4$ expression is lower in WT mouse LA than LV

A reduction of $\text{Na}_v\beta2$ and $\text{Na}_v\beta4$ expression in mouse LA compared to LV myocardium is clearly demonstrated (Figure 4.2). This is comparable to protein expression findings reported in rat myocardial tissue and in healthy human tissue (4). Figure 4.4 also corresponds with this, as significantly less SCN4B (the gene that encodes $\text{Na}_v\beta4$) is expressed in the healthy human LA compared to the LV. In Figure 4.4 there is also a trend for less SCN2B (the gene that encodes $\text{Na}_v\beta2$) expression in the LA, although this is not significant likely due to the variability in data and small data set.

The lower expression of Na_vβ2 and Na_vβ4 subunits in atrial cardiomyocytes may be responsible for the negative shift in activation, negative shift in inactivation and slower recovery of the LA sodium channels. This is supported by voltage clamp experiments that measured I_{Na} in HEK 293 cells co-expressing Na_v1.5 with and without Na_vβ2 and Na_vβ4 subunits together. Chen et al., showed that kinetic properties of sodium channels co-expressing Na_v1.5 with Na_vβ2 and Na_vβ4 subunits were similar to those of the ventricular sodium channels, with more positive activation potential, more positive inactivation and faster recovery of the sodium channels. Equally, kinetic properties of sodium channels expressing Na_v1.5 alone were similar to those of the atrial sodium channels (4). However, it is difficult to determine whether it is the co-expression of Na_vβ2 or Na_vβ4 individually, or a combination of the two that causes the change in kinetic properties of the sodium channel, as experiments were only done on HEK 293 cells co-expressing both subunits together.

These findings are supported by further published data that established the voltage dependence of activation and inactivation was positively shifted in HEK 293 cells with the co-expression of Na_v1.2 (232) and Na_v1.8 (233) with Na_vβ2. Neuronal sodium currents measured in β2^{-/-} mice also had a negative shift in inactivation and resultant decrease in I_{Na} density compared to their WT counterparts (234).

However, it has also been reported that $\text{Na}_v\beta 2$ co-expression with $\text{Na}_v1.3$ in Chinese hamster ovary cells (235) and most relevant to this study $\text{Na}_v1.5$ in HEK 293 cells (64), had no effect on the channel gating kinetics. Similarly opposing the above stated finding, $\text{Na}_v\beta 4$ co-expression has been shown to cause negative shifts in activation and negative shift in inactivation, or no effect on inactivation with $\text{Na}_v1.1$, $\text{Na}_v1.2$ and $\text{Na}_v1.4$ in HEK 293 cells and had no effect on the channel gating kinetics when co-expressed with $\text{Na}_v1.5$ (64, 236). Also, I_{Na} that was measured in mutant mice with genetically lower levels of $\text{Na}_v\beta 4$ showed a positively shifted activation compared to I_{Na} measured in mice with higher $\text{Na}_v\beta 4$ expression (237).

Although it would be expected that the I_{Na} in cells with $\text{Na}_v\beta 2$ loss of function mutation would be more comparable to LA cells, as they have lower $\text{Na}_v\beta 2$ expression, this was not demonstrated in Chinese hamster ovary cells co-expressing $\text{Na}_v1.5$ with $\text{Na}_v\beta 2$ loss of function mutation. Current activation and inactivation was positively shifted compared to $\text{Na}_v1.5$ co-expressed with WT $\text{Na}_v\beta 2$ (238). This opposes the suggestion that it is the lower $\text{Na}_v\beta 2$ expression in the LA that negatively shifts sodium channel activation and inactivation.

The same group found that $\text{Na}_v\beta 2$ loss of function mutations reduced I_{Na} density when currents were initiated at hyperpolarised potentials (238). At first this seems confusing, as you would expect a positive shift in inactivation to cause increase I_{Na} . However, under the experimental conditions used it is

understandable, as the difference in inactivation compared to cells expressing WT $\text{Na}_v\beta 2$ is negligible at the hyperpolarised potentials that were used to measure peak I_{Na} . Conversely, the positive shift in activation in the cells co-expressing the mutated $\text{Na}_v\beta 2$ means that more of the sodium channels would not have activated and opened, compared to those co-expressing the WT $\text{Na}_v\beta 2$.

Nevertheless, the $\text{Na}_v\beta 2$ loss of function mutation was identified in patients with AF and associated with a distinctive ECG phenotype. This supports the notion that the lower expression of $\text{Na}_v\beta 2$ within the atria and the resulting effects on the sodium channel gating kinetics may be accountable for the atria's susceptibility to arrhythmia (238). Watanabe et al., suggested that the AF susceptibility of those patients was due to the reduced I_{Na} resulting in slowed conduction and as previously described, this is a substrate for re-entrant arrhythmias (239).

Overall, there is a lot of inconsistency in the published data on the effect of $\text{Na}_v\beta 2$ and $\text{Na}_v\beta 4$ expression, with opposing information on whether the subunits affect sodium channel gating kinetics and how. Also, it has been well documented that the co-expression of the other Na_v β -subunits alongside $\text{Na}_v\beta 2$ and $\text{Na}_v\beta 4$ can cause further changes in channel gating kinetics (236, 238, 240, 241). Therefore, the effects of $\text{Na}_v\beta 1$ and $\text{Na}_v\beta 3$ expression on sodium channel function, and how all of the β -subunits interact with each other should be

considered. Nonetheless, Figure 4.2 clearly demonstrates lower expression of $\text{Na}_v\beta 2$ and $\text{Na}_v\beta 4$ and with the findings described by Chen et al., it is conceivable that the distinction in β -subunit expression is responsible for differences in the LA and LV sodium channel gating kinetics.

3.4.10. $\text{Na}_v\beta 2$ expression is greater in human diseased LA than in healthy

LA

Chen et al., compared the expression of the $\text{Na}_v\beta 2$ and $\text{Na}_v\beta 4$ subunits between human LA and LV tissue. The human tissue they used was from donor hearts that had failed to be used in transplantation surgery (234) so it can be assumed that the tissue was from healthy hearts. They found that the protein expression of both $\text{Na}_v\beta 2$ and $\text{Na}_v\beta 4$ was significantly less in the LA than in the LV, corresponding with their findings in rat tissue, findings in Figure 4.2 in mouse tissue and findings in Figure 4.4 healthy human tissue. Also, Figure 4.3B indicates that $\text{Na}_v\beta 4$ expression is much lower in the LA, comparable with the findings in rat tissue, healthy human tissue (4), mouse tissue in Figure 4.2 and findings in Figure 4.4 healthy human tissue. However, the difference in $\text{Na}_v\beta 4$ expression between the chambers is not significant, likely because of the small data set as human tissue is limited and there was some variability.

Conversely, Figure 4.3A reveals that the expression of $\text{Na}_v\beta 2$ is greater in the LA than the LV in the diseased human heart. This indicates that people most

susceptible to disease may already have different ratios of $\text{Na}_v\beta_2$ compared to what was seen in the healthy human tissue by Chen et al., where the LA had lower $\text{Na}_v\beta_2$. Conversely, it could be considered that disease progression affects the expression of the $\text{Na}_v\beta_2$, increasing it in the LA and/or reducing it in the LV. However, as the expression of $\text{Na}_v\beta_2$ is greater in the diseased LA compared to the healthy LA in Figure 4.4, it indicates that it is expression within the LA that is altered in diseased tissue, not expression in the LV. Although experiments measuring the expression of $\text{Na}_v\beta_2$ in diseased LV compared to healthy LV would be required, in order to determine whether changes in expression occur only in the LA or both chambers with disease. Therefore, the lack of LV healthy vs. disease data is a limitation within this study.

According to the sodium channel gating data here and published by Chen et al., an increase in $\text{Na}_v\beta_2$ in the diseased atria could result in the diseased atrial I_{Na} presenting more like the ventricular I_{Na} . Therefore, in disease the atrial sodium channels may activate at more positive potentials. This could result in a reduction in the excitability of diseased LA cardiomyocytes and could be cardioprotective against premature initiation of sodium channels with minor depolarisation, inhibiting arrhythmia generation. Interestingly, of all the diseased samples, one pair of LA and LV tissue samples came from a patient that presented with AF. The samples from this patient showed almost identical expression of $\text{Na}_v\beta_2$ between the chambers and were the only pair that did not show greater expression of $\text{Na}_v\beta_2$ in the LA compared to its LV counterpart.

Therefore, this patient may have been more susceptible to AF because there was no/less upregulation of $\text{Na}_v\beta_2$ in the LA.

However, a positive shift in activation could also lead to reduced I_{Na} as the threshold potential for activation is increased. This could lead to a reduction in CV, which as previously described can be proarrhythmic and may increase the atria's susceptibility to arrhythmia in diseased hearts (1). Therefore, in diseased patients, sodium channel blocking drugs, such as flecainide, could exasperate arrhythmia generation, as conduction could be slowed too much. However, there may also be a positive shift in inactivation counteracting the effects of a positive shift in activation if the diseased LA present with a more LV phenotype. This could result in an increased I_{Na} density *in vivo*, increasing CV and reducing the likelihood of arrhythmia generation (1). Therefore, sodium channel blocking drugs, such as flecainide, that reduce CV may be safe to use, although this is not supported by previous findings on the efficacy of flecainide in patients with cardiac disease (147).

Nevertheless, diseased atria may also display greater $I_{\text{Na,late}}$ compared to healthy atria, as the sodium channels in the atria could be more likely to inactivate and then activate prematurely if increased $\text{Na}_v\beta_2$ expression does alter gating kinetics. This has been shown in the ventricles of a dog heart failure (HF) model, where increased $I_{\text{Na,late}}$ was observed when compared with dogs without HF (242). Likewise, the ventricles of rat hearts post myocardial

infarction present with increased LV $I_{Na,late}$ (243). However, studies measuring atrial $I_{Na,late}$ in disease models are limited, most likely due to the difficulty of measuring such a small current.

As described previously, an enhanced $I_{Na,late}$ can instigate repolarisation failure and result in EAD's causing a regenerative L-type Ca^{2+} channel re-activation or providing sufficient time for sodium channels to recover and reactivate (127). Additionally, DAD's can follow full repolarisation via Ca^{2+} overload in sodium-calcium overload conditions (202). Furthermore, in diseased atria if greater $Na_v\beta_2$ expression causes the LA to follow the LV phenotype, sodium channel recovery would be quicker, potentially amplifying $I_{Na,late}$. This could cause severe prolongation of the AP plateau, with the resultant arrhythmic triggers described previously (223, 224). Therefore, inhibition of $I_{Na,late}$ that has been established as an effective arrhythmia treatment in the ventricles (77, 244, 245) may be more effective at treating AF in patients with severe cardiac disease than it is in patients without cardiac disease. This has been confirmed by the more potent suppression of AF by ranolazine, a drug that inhibits $I_{Na,late}$, in dogs with HF than in non-failing dog hearts (206).

However, due to inconsistency in the published data, it has not been conclusively confirmed that increased $Na_v\beta_2$ expression does cause the described changes in sodium channel gating kinetics or whether the co-expression of other Na_v β -subunits *in vivo* can cause further changes (236, 238,

240, 241). Therefore, additional research is required to compare I_{Na} when $Na_v1.5$ is expressed with/without all of the Na_v β -subunits individually and in different combinations together under physiological conditions. Further research would be essential in order to better clarify effects on gating kinetics in the diseased LA and how electrophysiology is altered.

4. Plakoglobin deficiency and sodium handling in the atria and ventricles

4.1. Chapter introduction and overview

Arrhythmogenic right ventricular cardiomyopathy (ARVC) is one of the most common inherited cardiomyopathies, characterised by fibrofatty replacement of cardiomyocytes. Prevalence of ARVC is approximately 1:2000-5000, with a greater proportion of men affected than women (246, 247). The primary clinical observations associated with ARVC are sudden death, ventricular arrhythmias, and heart failure (248, 249). The RV is predominantly affected (as specified in the name) and during the later stages of ARVC the RV dilates, reducing cardiac contractility and ejection fraction (250). Additionally, LV involvement may also occur with disease progression and can be the chamber of dominant disease presentation (251, 252).

Pharmacological options for ARVC treatment include antiarrhythmic agents, β -blockers and heart failure drug therapy (253). AAD treatment in ARCV patients aims to improve quality of life by inhibiting symptomatic ventricular arrhythmias. However, the efficacy of AAD therapy in ARVC patients has proven problematic to assess, as patients usually have multiple arrhythmic events over time and drugs are frequently changed (254). Therefore, due to a lack of ARVC case control studies, retrospective analyses and clinical registries, choice of a suitable AAD treatment is based on the experimental approach of clinicians,

resulting from personal experience, consensus, individual opinion and extrapolation from other diseases (253).

In 30-50% of cases ARVC is familial, classically inherited in an autosomal dominant fashion but recessive forms are also known. Loss-of-function mutations in desmosomal proteins (desmoplakin, plakophilin or plakoglobin) were shown to cause changes in morphological structure and be a primary cause of ARVC (175-177). Furthermore, reduced plakoglobin concentrations have been observed in many patients with ARVC, whether the primary mutation was in the plakoglobin gene or in another gene (255). Therefore, ARVC is considered a disease of the desmosome (181). Desmosomes are intracellular junctions that attach intermediate filaments to cell surfaces and provide cell-to-cell adhesion at the intercalated disks, as described previously (12). Mechanical stress weakens cell-to-cell adhesion and it has been established that environmental factors, such as endurance training, can exacerbate the ARVC phenotype in those with these desmosomal mutations. This explains ARVCs infamous association with the sudden death of young athletes (246).

It has been confirmed that plakoglobin deficiency in mice provokes the ARVC phenotype and endurance training aggravates RV arrhythmias (181). Plakoglobin, also known as γ -catenin, is a ≈ 82 kDa protein encoded by the JUP gene in humans. It is a key constituent of the desmosomes and responsible for adhesion between cardiomyocytes. Therefore, dysfunction of plakoglobin

diminishes mechanical adhesion of cardiomyocytes. This can result in RV dysfunction, as a result of the increased sensitivity to mechanical instability of the thinner RV wall (256, 257).

It has been challenging for scientists to identify a direct link between desmosomal proteins and cardiac electrophysiology. Studies have described a molecular crosstalk between desmosomes and both VGSCs and gap junction proteins at the intercalated discs. Knockdown of the gene that encodes plakophilin 2 in mice has proven to decrease I_{Na} density, negatively shift inactivation and prolong channel recovery in rat ventricular cardiomyocytes, with a significant decrease in conduction velocity and propensity for arrhythmia generation (178). Furthermore, heart samples from ARVC patients with reduced plakoglobin expression, revealed reduction in ventricular $Na_v1.5$ expression at the intercalated disks (179, 180). This could help develop an understanding of the mechanism underlying ARVC arrhythmogenesis in those with plakoglobin deficiency, if reduced $Na_v1.5$ expression results in reduced I_{Na} , as with the reduced plakophilin 2 expression described above. Alterations in $Na_v1.5$ function therefore may be partly accountable for the increased arrhythmia vulnerability in ARVC patients due to slowed conduction (180). However, whether desmosomal proteins and VGSCs interact directly, or via other molecular partners is yet to be established (180). Nevertheless, if I_{Na} is reduced in patients with desmosomal mutations it may provide a target for ARVC therapy. Conversely, AADs that further reduce I_{Na} may be proarrhythmic in ARVC patients due to additional conduction slowing.

Endurance training has been associated with increased AF risk (258). Further to the increase in ventricular arrhythmias, endurance training has also been associated with increased atrial arrhythmia generation with plakoglobin deficiency in mice in unpublished studies (259, 260). Therefore, functional experiments comparing $\text{Na}_v1.5$ biophysical properties between control and plakoglobin deficient hearts would provide further insight into the electrophysiological effects of desmosomal dysfunction. Additionally, patients with plakoglobin deficiency experiencing atrial arrhythmia would require treatment that also targets AF. Comparison of the effect of a VGSC blocking AAD, such as flecainide, in plakoglobin deficient hearts compared to WT hearts may offer insight into whether I_{Na} block is suitable for AF treatment and whether flecainide could also be used to treat ventricular arrhythmias in ARVC patients. As described above, I_{Na} may be reduced as a result of plakoglobin deficiency and this must be established in order to uncover whether flecainide treatment may in fact be proarrhythmic.

The aims of this investigation are summarised below:

1. To assess sodium channel biophysical properties in isolated plakoglobin deficient mouse LA and LV cardiomyocytes
2. To examine the effects of flecainide on the sodium channels in isolated plakoglobin deficient mouse LA and LV cardiomyocytes.

4.2. Electrophysiology results

4.2.1. LA sodium channels activate at more negative holding potentials than LV sodium channels in the Plako^{+/-} mouse

Experiments were performed on isolated Plako^{+/-} and WT mouse LA and LV cardiomyocytes to compare the sodium channel I/V relationships, using the relevant I/V patch clamp protocol described in the materials and methods (Table 1.5). This protocol enabled assessment of the voltage/current relationship and voltage dependency of sodium channel activation.

Figure 5.1A shows raw representative traces of the I_{Na} from Plako^{+/-} LA and LV cardiomyocytes, with greater peak I_{Na} in LV cardiomyocytes before normalising to cell capacitance. This is comparable to the WT counterpart raw currents in Figure 3.1A. The current-voltage relationship of the Plako^{+/-} LA and LV sodium channels (Figure 5.1B) shows that from a holding potential of -100mV, Plako^{+/-} LA (n=24/7 cells/mice) and Plako^{+/-} LV (n=41/10 cells/mice), sodium channels have a peak current potential at the -30mV step, comparable with WT.

Additionally, as in the WT, I_{Na} amplitude was comparable between Plako^{+/-} LA and LV (Figure 5.1E). No difference was observed in I_{Na} amplitude between the WT LV (n=28/13 cells/mice) and Plako^{+/-} LV (n=41/10 cells/mice). Similarly, I_{Na} amplitude is comparable between the Plako^{+/-} LA (n=24/7 cells/mice) and WT LA (n=42/13 cells/mice) (Figure 5.1E).

The I/V curve data was fitted to a Boltzmann function to obtain the voltage dependence of the conductance activation of sodium channels using the initial downward slope of the curve (as described in the material and methods). This allows comparison of the voltage potential at which half of the sodium channels were activated (V50) in WT and Plako^{+/-} LA and LV (Figure 5.1F). As exhibited in Figure 3.1E in Chapter 3 of this thesis, WT LA sodium channels activated at significantly more negative potentials than WT LV sodium channels. However, there is no difference between Plako^{+/-} LA and LV V50 activation (Figure 5.1F).

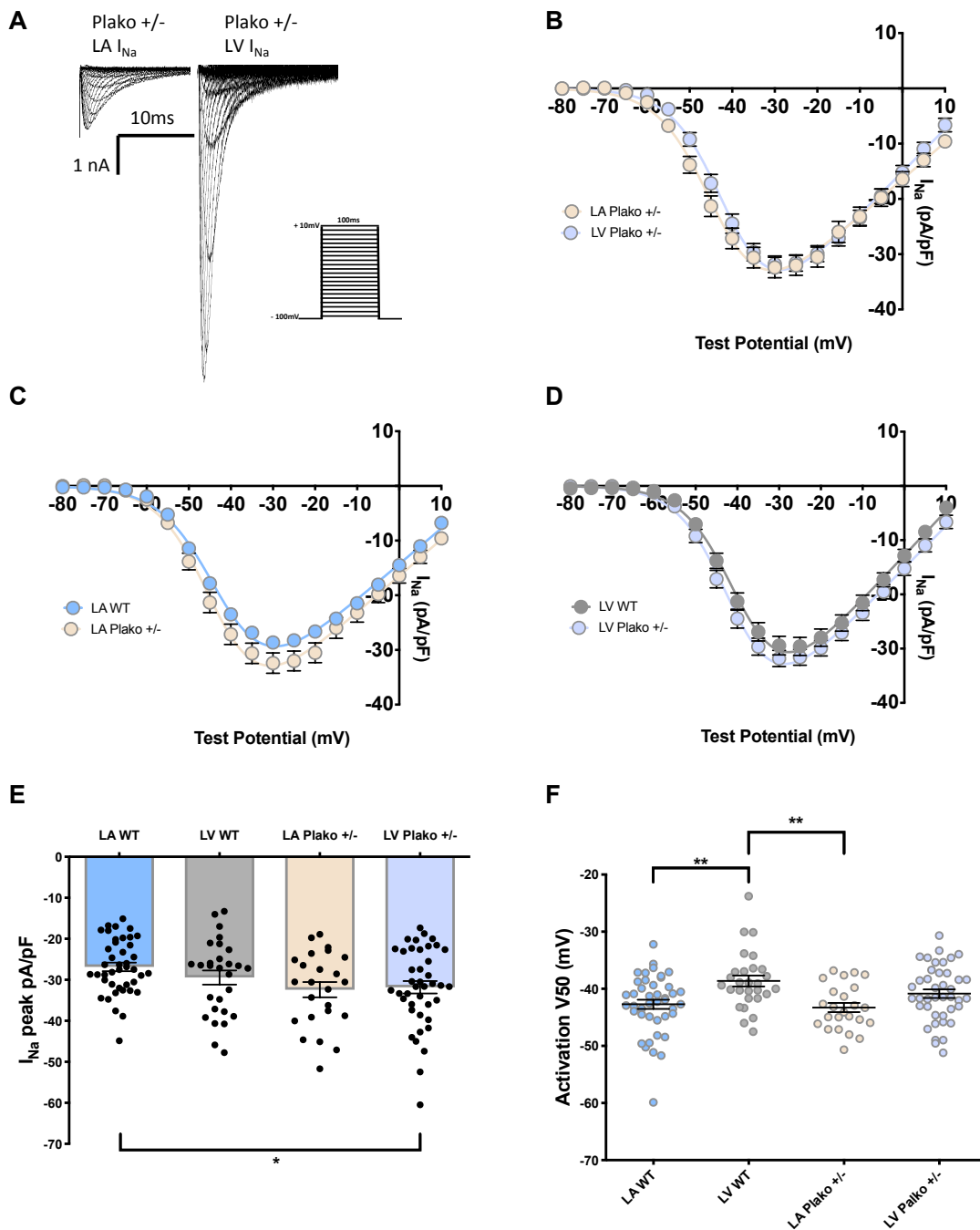


Figure 5.1. WT and Plako^{+/-} LA and LV I_{Na} I/V relationship and sodium channel activation.

I_{Na} I/V curve and channel activation in LA and LV cardiomyocytes from WT and Plako^{+/-} mouse hearts. A) Plako^{+/-} LA and LV representative raw I_{Na} traces in LA with patch clamp protocol on the right. B) Current-voltage relationship of I_{Na} density in Plako^{+/-} LA (n=24/7 cells/mice) and Plako^{+/-} LV (n=41/10 cells/mice). C) Current-voltage relationship of I_{Na} density in WT LA (n=42/13 cells/mice) and Plako^{+/-} LA (n=24/7 cells/mice). D) Current-voltage relationship of I_{Na} density in WT LV (n=28/13 cells/mice) and Plako^{+/-} LV (n=41/10 cells/mice). E) I_{Na} peak density at a step from -100mV to -30mV in WT LA (-26.84 ± 1.651pA/pF;

n=42/13 cells/mice), WT LV (-26.84 ± 1.037 pA/pF; n=28/13 cells/mice), Plako^{+/-} LA (-32.4 ± 1.858 pA/pF; n=24/7 cells/mice) and Plako^{+/-} LV (-31.82 ± 1.511 pA/pF; n=41/10 cells/mice). F) V₅₀ of activation fitted to the Boltzmann distribution in WT LA (-42.71 ± 0.8017 mV; n=42/13 cells/mice), WT LV (-38.63 ± 0.9488 mV; n=28/13 cells/mice), Plako^{+/-} LA (43.29 ± 0.8069 mV; n=24/7 cells/mice) and Plako^{+/-} LV (-40.85 ± 0.7612 mV; n=41/10 cells/mice). Error bars indicate \pm S.E.M. significance taken as *P<0.05 with two-way ANOVA followed by post-hoc multiple comparisons (Tukey's) test.

4.2.2. No difference in peak I_{Na} between LA and LV at physiologically relevant holding potentials in the Plako^{+/-} mouse

Experiments were performed on isolated Plako^{+/-} mouse LA and LV cardiomyocytes to measure the peak I_{Na} at varying holding potentials using the steady state inactivation patch clamp protocol described in the material and methods chapter (Table 1.5). The protocol enables the evaluation of the relationship between the holding potential (pre-pulse potential) of the cell and the current amplitude upon stimulation, and in turn how many sodium channels are available for activation at the different holding potentials. Data was analysed from the -120 to -75mV holding potential range of the pre-pulse, as current amplitudes were negligible at the more positive holding potentials, so could not be measured/compared.

Although the I_{Na} amplitude against holding potential relationship appears to differ between the Plako^{+/-} LA (n=24/7 cells/mice) and LV (n=38/10 cells/mice) (Figure 5.2A), similar to the WT counterparts (Figure 3.2A), differences between the Plako^{+/-} chambers are smaller and not significant. Although there is a trend

of greater I_{Na} in the $Plako^{+/-}$ LA at the $-120mV$ holding potential, the spread of data is pronounced and there is no significance (Figure 5.2B). Similarly, there is no difference in I_{Na} in the $Plako^{+/-}$ LA and LV at the $-75mV$ holding potential (Figure 5.2C).

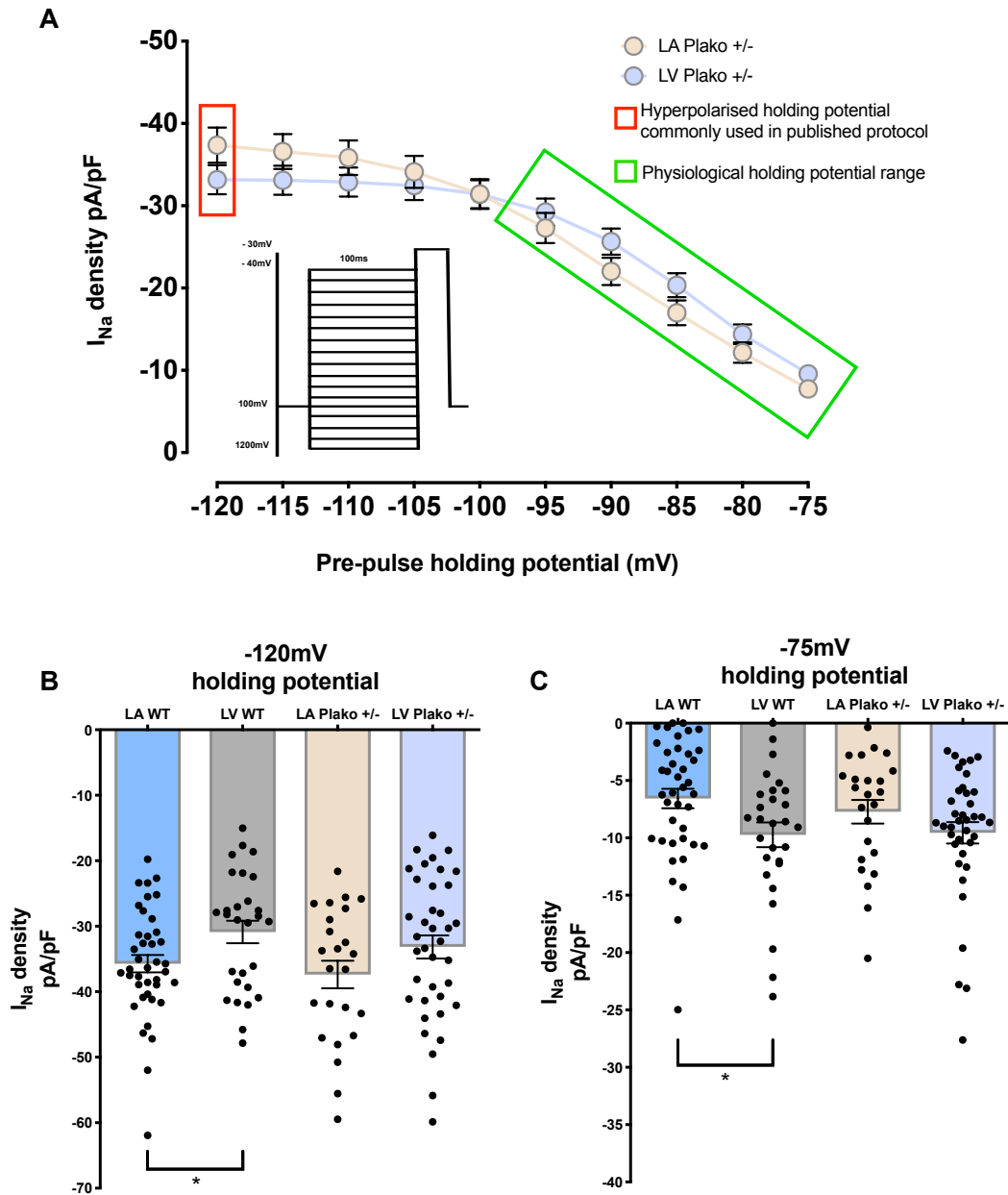


Figure 5.2. I_{Na} density in $Plako^{+/-}$ LA and LV at varying holding potentials. I_{Na} in LA and LV cardiomyocytes from $Plako^{+/-}$ mouse hearts at varying holding potentials. A) I_{Na} mean density/holding potential relationship from with protocol shown inset, $Plako^{+/-}$ LA (n=24/7 cells/mice) and $Plako^{+/-}$ LV (n=38/10

cells/mice), denote holding potentials of interest. B) I_{Na} density at -120mV holding potential in WT LA (-35.72 ± 1.718 pA/pF; n=40/13 cells/mice), WT LV (-30.89 ± 1.322 pA/pF; n=28/13 cells/mice), Plako^{+/-} LA (37.37 ± 2.098 pA/pF; n=24/7 cells/mice) and in Plako^{+/-} LV (-33.16 ± 1.761 pA/pF; n=38/10 cells/mice) C) I_{Na} density at -75mV holding potential in WT LA (-6.569 ± 0.8474 pA/pF; n=40/13 cells/mice), WT LV (-9.735 ± 1.075 pA/pF; n=28/13 cells/mice), Plako^{+/-} LA (-7.728 ± 1.028 pA/pF; n=24/7 cells/mice) and Plako^{+/-} LV (-9.56 ± 0.9292 pA/pF; n=38/10 cells/mice). Error bars indicate \pm S.E.M. significance taken as *P<0.05 with two-way ANOVA followed by post-hoc multiple comparisons (Tukey's) test.

4.2.3. LA sodium channels inactivate at more negative holding potentials than LV sodium channels in the Plako^{+/-} mouse

Experiments were performed on isolated WT and Plako^{+/-} mouse LA and LV cardiomyocytes to compare the potential at which the sodium channels inactivate (are no longer available), using the relevant steady-state inactivation patch clamp protocol described in the materials and methods chapter (Table 1.5). The voltage dependence of steady-state inactivation (channel availability, I/I_{max}) was determined from this protocol, as shown in Figure 5.3 A-C and fitted to the Boltzmann function.

The Plako^{+/-} LA (n=24/7 cells/mice) sodium channel inactivation potential is negatively shifted compared to the Plako^{+/-} LV (n=43/10 cells/mice) sodium channel inactivation potential (Figure 5.3A), confirmed by the V50 for inactivation (Figure 5.3D). There is no difference in sodium channel inactivation between Plako^{+/-} LA or LV and the respective WT counterparts (Figure 5.3B-C).

This is confirmed in Figure 5.3D V50 for inactivation (WT LA n=41/13 cells/mice; WT LV n=27/13 cells/mice).

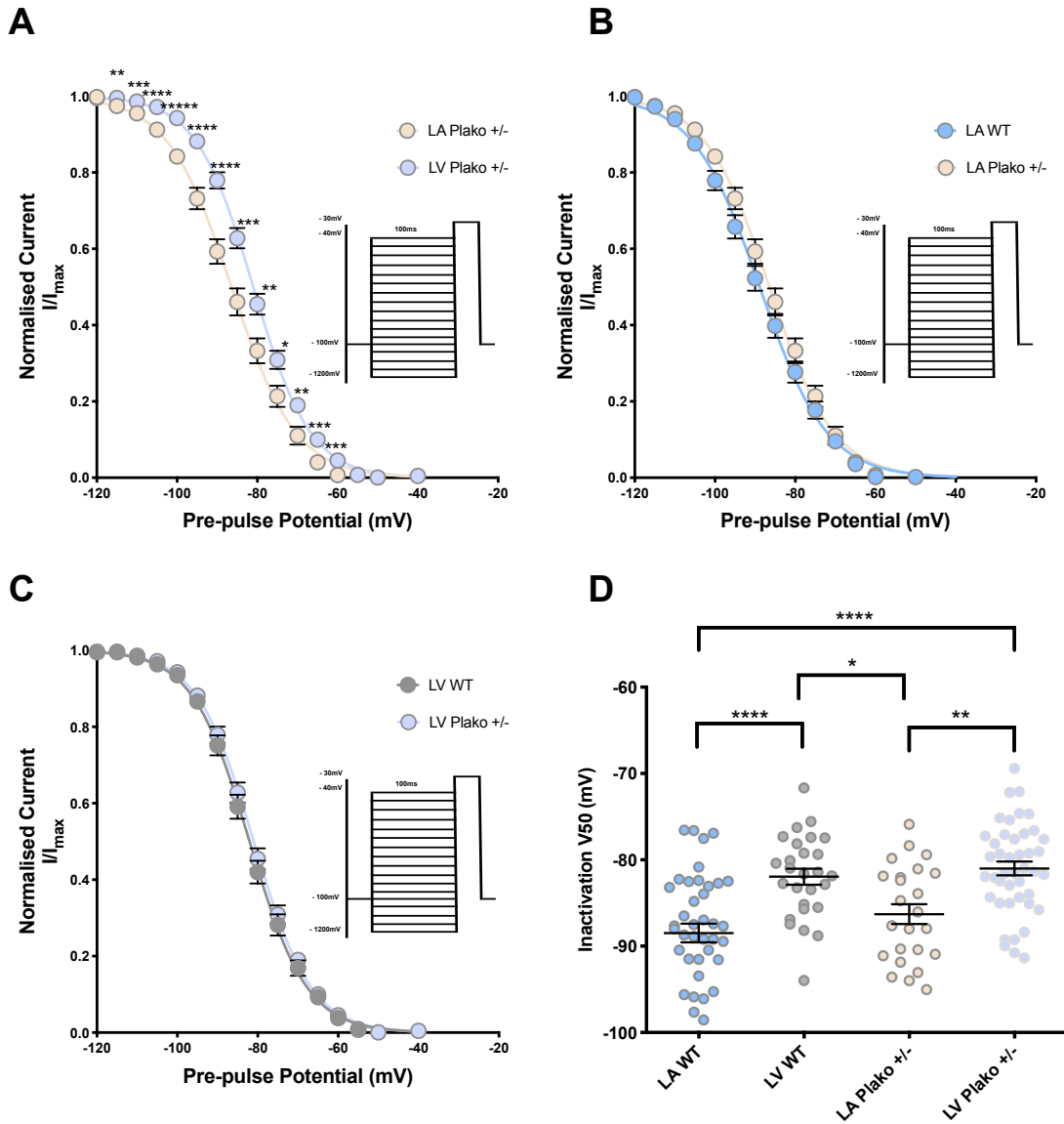


Figure 5.3. Plako^{+/-} LA and LV sodium channel inactivation.

Channel steady-state inactivation LA and LV cardiomyocytes from WT and Plako^{+/-} mouse hearts. A) Curve of normalised I_{Na} inactivation (I/I_{max}) fitted to the Boltzmann function in Plako^{+/-} LA (n=24/7 cells/mice) and Plako^{+/-} LV (43/10 cells/mice). B) Curve of normalised I_{Na} inactivation (I/I_{max}) fitted to the Boltzmann function in WT LA (n=41/13 cells/mice) and Plako^{+/-} LA (24/7 cells/mice). C) Curve of normalised I_{Na} inactivation (I/I_{max}) fitted to the Boltzmann function in WT LV (27/13 cells/mice) and Plako^{+/-} LV (43/10 cells/mice). D) V50 of inactivation fitted to the Boltzmann distribution in WT LA (-88.48 ± 1.08mV; n=41/13 cells/mice), WT LV (-81.95 ± 0.923mV; n=27/13

cells/mice), Plako^{+/-} LA (-86.29 ± 1.144mV; n=24/7 cells/mice) and Plako^{+/-} LV (-81.0 ± 0.7932mV; n=43/10cells/mice). Error bars indicate ± S.E.M. significance taken as *P<0.05 with two-way ANOVA followed by post-hoc multiple comparisons (Tukey's) test.

4.2.4. No difference in time dependent recovery between LA and LV sodium channels in the Plako^{+/-} mouse

Experiments were performed on isolated WT and Plako^{+/-} mouse LA and LV cardiomyocytes to study the time dependent kinetics of recovery after inactivation, using the relevant channel recovery protocol described in the materials and methods (Table 1.5). Normalised peak current amplitudes were plotted and fitted to a one-phase association exponential function and the time when half of the channels were recovered and available for re-activation (P50) was determined in the WT and Plako^{+/-} LA and LV cardiomyocytes.

Unlike with WT LA and LV, the Plako^{+/-} LA and LV sodium channel recovery curves overlap (Figure 5.4A) (Plako^{+/-} LA=23/7 and Plako^{+/-} LV=44/10 cells/mice) (Figure 5.4A). This is confirmed clearly by the P50 for recovery (Figure 5.4 D). This is due to the Plako^{+/-} LA sodium channel recovery being faster than WT LA sodium channel recovery (WT LA=38/13 and Plako^{+/-} LA=23/7 cells/mice) (Figure 5.4B), demonstrated by the P50 for recovery (Figure 5.4D), but not significant. However, there is no difference in recovery kinetics between WT LV and Plako^{+/-} LV as sodium channel recovery curves

overlap (WT LV=28/13 and Plako^{+/-} LV=44/10 cells/mice) (Figure 5.4C), demonstrated by the P50 for recovery (Figure 5.4D).

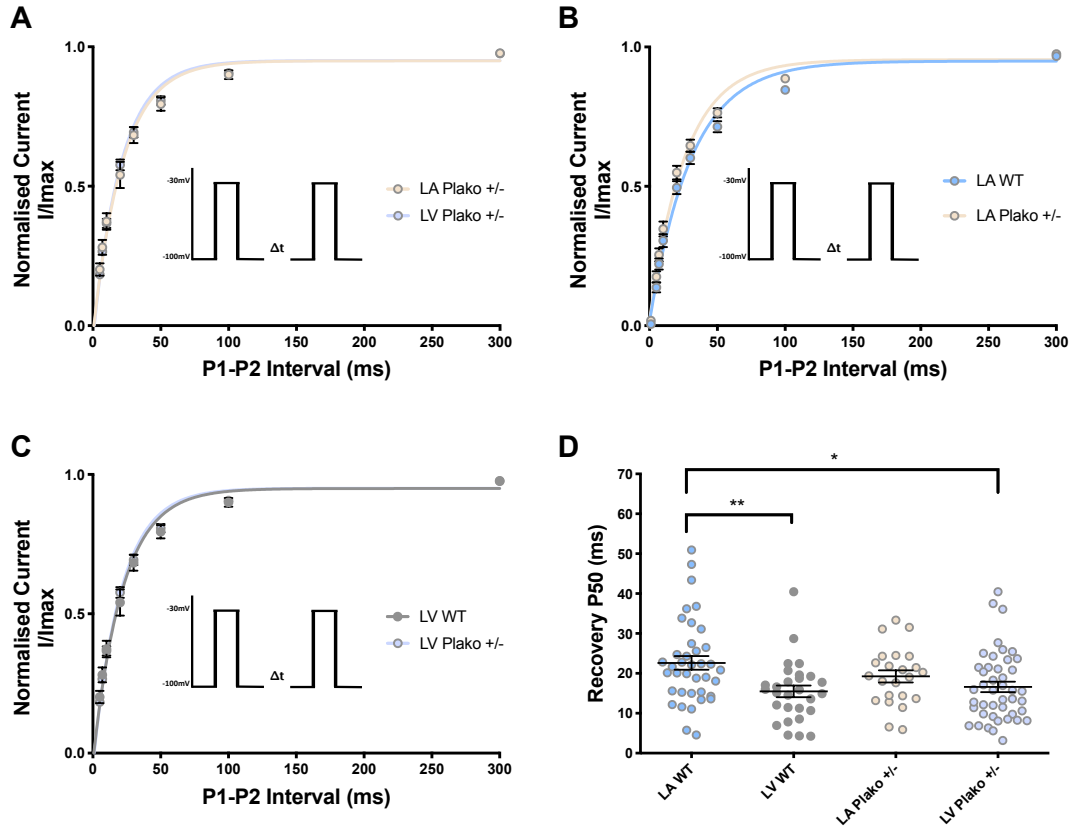


Figure 5.4. WT and Plako^{+/-} LA and LV time dependent sodium channel recovery.

Channel recovery in LA and LV cardiomyocytes from WT and Plako^{+/-} mouse hearts. A) Curve of normalised sodium channel recovery (I/I_{max}) fitted to one-phase association with protocol shown in inset Plako^{+/-} LA (n=23/7 cells/mice) and Plako^{+/-} LV (44/10 cells/mice). B) Curve of normalised sodium channel recovery (I/I_{max}) fitted to one-phase association with protocol shown in inset WT LA (n=38/13 cells/mice) and Plako^{+/-} LA (23/7 cells/mice). C) Curve of normalised sodium channel recovery (I/I_{max}) fitted to one-phase association with protocol shown in inset WT LV (n=28/13 cells/mice) and Plako^{+/-} LV (44/10 cells/mice). D) P50 of recovery in WT LA (22.62 ± 1.703ms; n=38/13 cells/mice), WT LV (15.49 ± 1.456ms; n=28/13 cells/mice), Plako^{+/-} LA (19.25 ± 1.512ms; n=23/7 cells/mice) and Plako^{+/-} LV (16.6 ± 1.303ms; n=44/10 cells/mice). Error bars indicate ± S.E.M. significance taken as *P<0.05 with two-way ANOVA followed by post-hoc multiple comparisons (Tukey's) test.

4.2.5. No difference in flecainide inhibition between LA and LV sodium channels in the Plako^{+/-} mouse

Experiments were performed on isolated WT and Plako^{+/-} mouse LA and LV cardiomyocytes in the absence or presence of 1 μ mol flecainide, to compare peak I_{Na} inhibition between the chambers, using the I/V patch clamp protocol described in the materials and methods chapter (Table 1.5). This protocol enabled assessment of the current relationship of ion channel activation and voltage-dependence of inactivation, to characterise the biophysical properties of the sodium channels with the addition of flecainide. Sodium channel inhibition was measured by calculating the difference between the control currents and the currents after flecainide exposure as a percentage.

The raw Plako^{+/-} LA and LV sodium currents +/-1 μ mol flecainide are shown in Figure 5.5A, with the patch clamp protocol shown on the right. The flecainide currents are visibly smaller than the control currents recorded in the absence of flecainide, confirming the occurrence of current inhibition. The current-voltage relationships of the sodium channels in control Plako^{+/-} LA against Plako^{+/-} LA +1 μ mol flecainide are shown in Figure 5.5B and in control Plako^{+/-} LV against Plako^{+/-} LV +1 μ mol flecainide in Figure 5.5C.

The addition of flecainide alters the curve morphology in both Plako^{+/-} LA (n=7/3 cells/mice) and LV (n=7/3 cells/mice). The peak of both curves is

significantly reduced with the addition of flecainide compared to the control curves, shown in Figure 5.5D-E.

As demonstrated in Figure 3.5F in Chapter 3 and here, inhibition of peak I_{Na} amplitudes is greater in the WT LA than in WT LV (Figure 5.5F). However, inhibition of peak I_{Na} amplitudes is no different between the $Plako^{+/-}$ LA and LV (Figure 5.5F). This is due to sodium channel % inhibition being greater in the $Plako^{+/-}$ LV than in the WT LV, although this is not significant (Figure 5.5F).

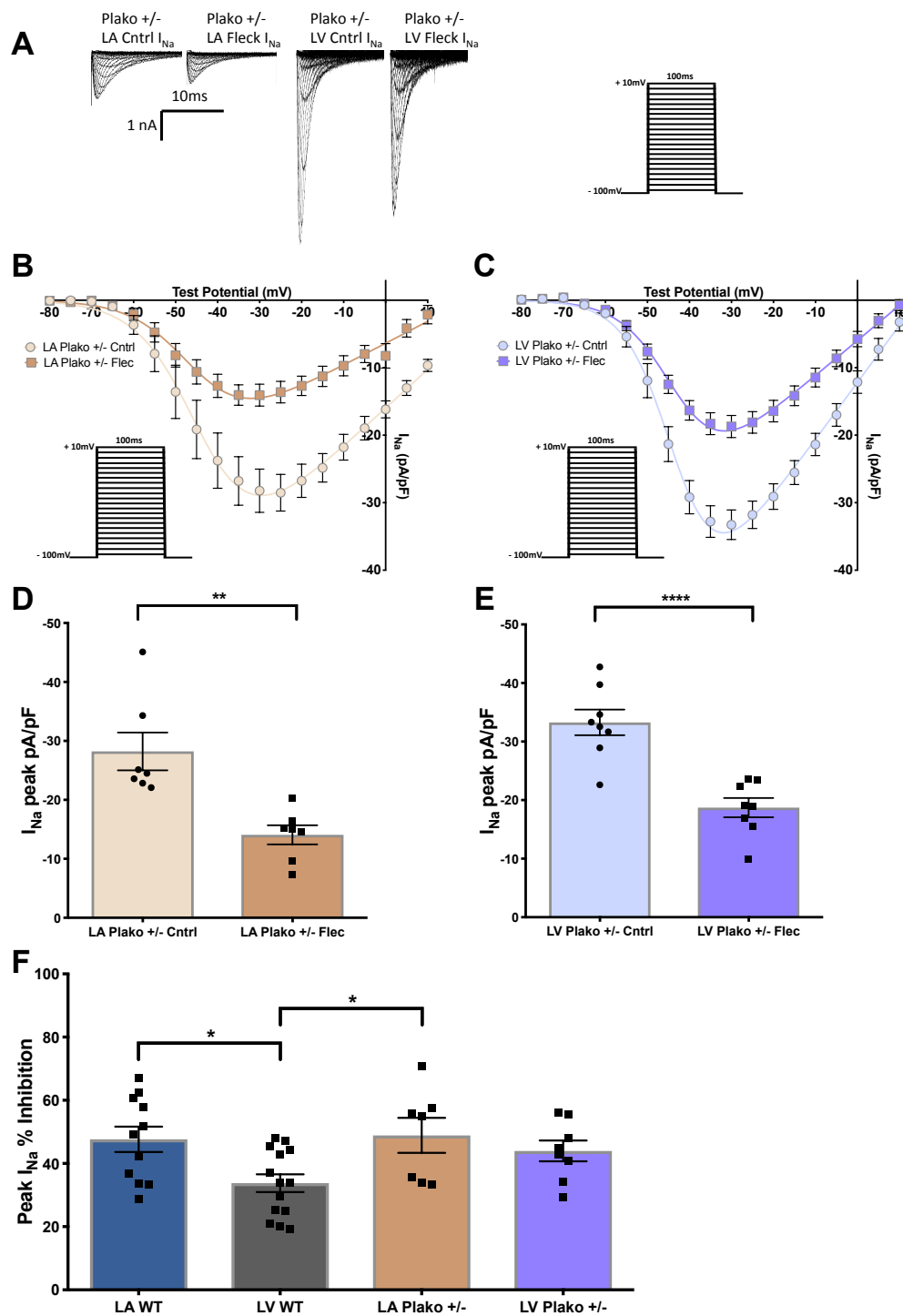


Figure 5.5. Plako^{+/-} LA and LV I_{Na} I/V with the addition of flecainide.

I_{Na} I/V curve and channel activation +/- flecainide in LA and LV cardiomyocytes from Plako^{+/-} mouse hearts. A) Plako^{+/-} LA and LV representative raw I_{Na} traces +/- 1 μ mol flecainide, with patch clamp protocol on the right. B) Current-voltage relationship of I_{Na} density in Plako^{+/-} LA (n=7/3 cells/mice) C) Current-voltage relationship of I_{Na} density in Plako^{+/-} LV (n=8/4 cells/mice). D) Plako^{+/-} LA I_{Na} peak density at a step from -100mV to -30mV (Plako^{+/-} LA control=-28.22 \pm 3.213pA/pF; n=7/3 cells/mice; Plako^{+/-} LA plus flecainide=-14.07 \pm 1.622pA/pF;

n=7/3 cells/mice) **p<0001. E) Plako^{+/-} LV I_{Na} peak density at a step from -100mV to -30mV (Plako^{+/-} LV control=-33.27 ± 2.190pA/pF; n=8/4 cells/mice; Plako^{+/-} LV plus flecainide=-18.72 ± 1.645pA/pF; n=8/4 cells/mice) ****p<0.0001.F) Peak I_{Na} percentage inhibition (WT LA=47.64% ± 4.029; n=11/6 cells/mice; WT LV=33.77% ± 2.824; n=14/4 cells/mice, Plako^{+/-} LA=48.9% ± 5.528; n=7/3 cells/mice and Plako^{+/-} LV=43.98% ± 3.306; n=8/4 cells/mice). Error bars indicate ± S.E.M. Significance taken as *P<0.05 with paired Student t-test for (D and E) and two-way ANOVA followed by post-hoc multiple comparisons (Tukey's) test (F).

The I/V curve data was fitted to a Boltzmann function to obtain the voltage dependence of the conductance activation of sodium channels using the initial downward slope of the curve. This allows comparison of the voltage potential at which half of the sodium channels were activated (V₅₀) between Plako^{+/-} LA control and Plako^{+/-} LA +1μmol flecainide (Figure 5.6G) and between Plako^{+/-} LV control and Plako^{+/-} LV +1μmol flecainide (Figure 5.6H). The addition of flecainide results in sodium channel activation at significantly more negative potentials in the Plako^{+/-} LA (n=7/3 cells/mice) (Figure 3.6G), but not in the Plako^{+/-} LV (n=8/4 cells/mice) (Figure 5.6H). The negative shift effect is shown in Figure 5.6I.

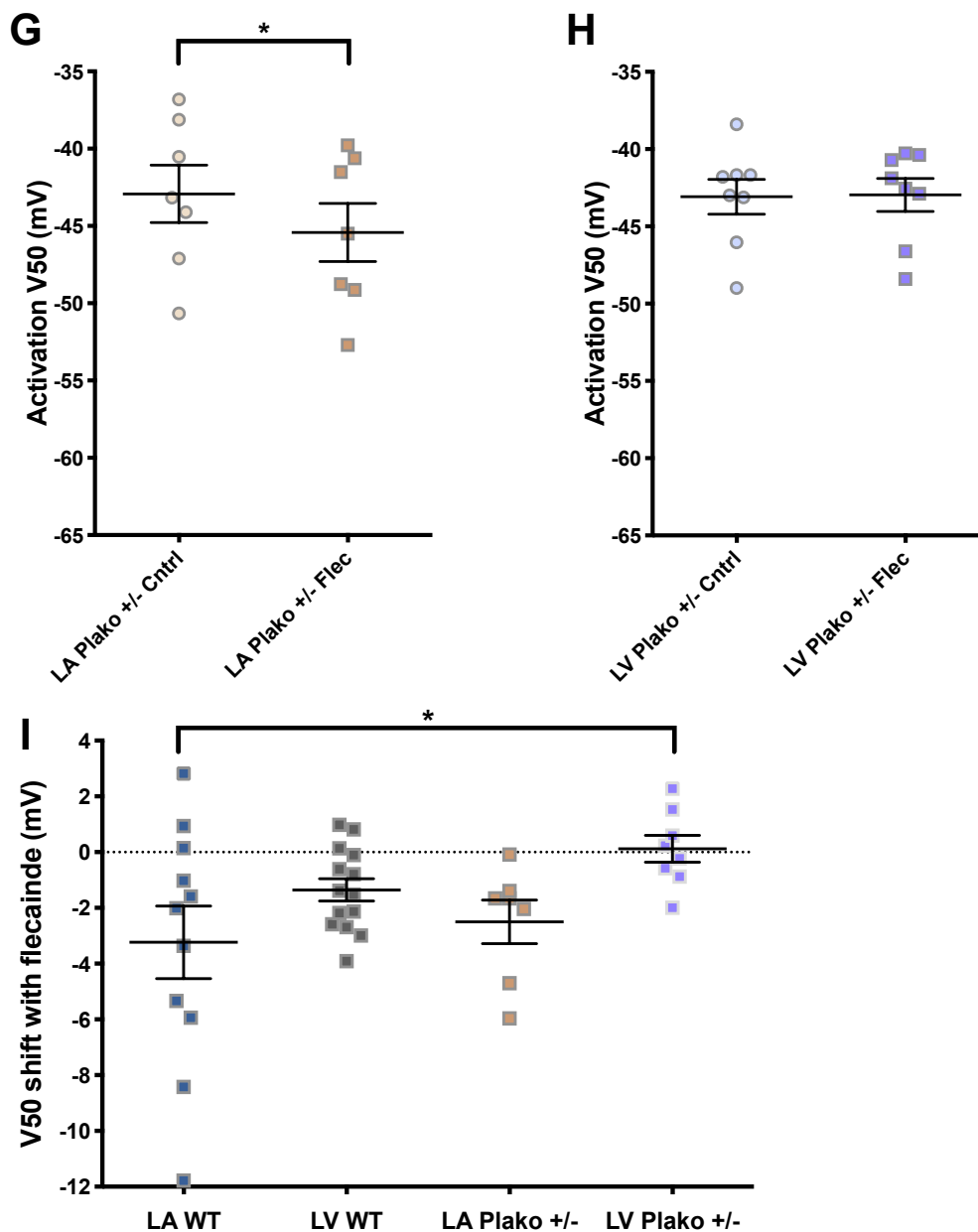


Figure 5.6. Plako^{+/-} LA and LV sodium channel activation with the addition of flecainide.

Sodium channel activation +/- flecainide in LA and LV cardiomyocytes from Plako^{+/-} mouse hearts. G) Plako^{+/-} LA V50 of activation fitted to the Boltzmann distribution (Plako^{+/-} LA control = -42.93 ± 1.858 mV; n=7/3 cells/mice; Plako^{+/-} LA plus flecainide = -45.43 ± 1.878 mV; n=7/3 cells/mice) *p<0.05. H) Plako^{+/-} LV V50 of activation fitted to the Boltzmann distribution (Plako^{+/-} LV control = -43.08 ± 1.128 mV; n=8/4 cells/mice; Plako^{+/-} LV plus flecainide = -42.96 ± 1.062 mV; n=8/4 cells/mice). I) Shift in V50 activation after the addition of flecainide (WT LA = -3.232 ± 1.302 mV; n=11/6 cells/mice; WT LV = -1.352 ± 0.397 mV; n=14/4 cells/mice, Plako^{+/-} LA = -2.5 ± 0.7788 mV; n=7/3 cells/mice and Plako^{+/-} LV = 0.12 ± 0.4808 mV; n=8/4 cells/mice. Error bars indicate \pm S.E.M. Significance taken

as $*P < 0.05$ with paired Student t-test for (G and H) and two-way ANOVA followed by post-hoc multiple comparisons (Tukey's) test (I).

4.2.6. Flecainide alters LA and LV sodium channel inactivation in the Plako^{+/-} mouse

Experiments were performed on isolated WT mouse LA and LV cardiomyocytes to compare the potential at which the sodium channels inactivate (are no longer available) in the presence and absence of flecainide, using the relevant steady-state inactivation patch clamp protocol described in the materials and methods (Table 1.5). The voltage dependence of inactivation (channel availability, I/I_{max}) was determined from this protocol, as shown in inset Figure 5.7A and 5.7C and fitted to the Boltzmann function.

There is a shift in the inactivation potential of the sodium channels between the control and 1 μ mol flecainide in both the Plako^{+/-} LA (n=6/3 cells/mice) and LV (n=10/4 cells/mice). This is confirmed by the significant negative shift in the V50 inactivation data (Figure 5.7B and 5.7D).

As demonstrated in Figure 3.7E Chapter 3, the shift in the inactivation potential of the sodium channels between the control WT LA and 1 μ mol flecainide LA is greater than the shift seen in the WT LV. This is demonstrated by the V50 voltage shifts but is not significant, likely due to a larger standard deviation of the LA dataset (LA n=12/6 cells/mice; LV n=14/4 cells/mice). Similarly, the shift

in the inactivation potential of the sodium channels between the control Plako^{+/-} LA and 1 μ mol flecainide Plako^{+/-} LA is greater than the shift seen in the Plako^{+/-} LV, demonstrated by the V50 voltage shifts (Figure 5.7E) but this is not significant, again likely due to a larger standard deviation of the LA dataset.

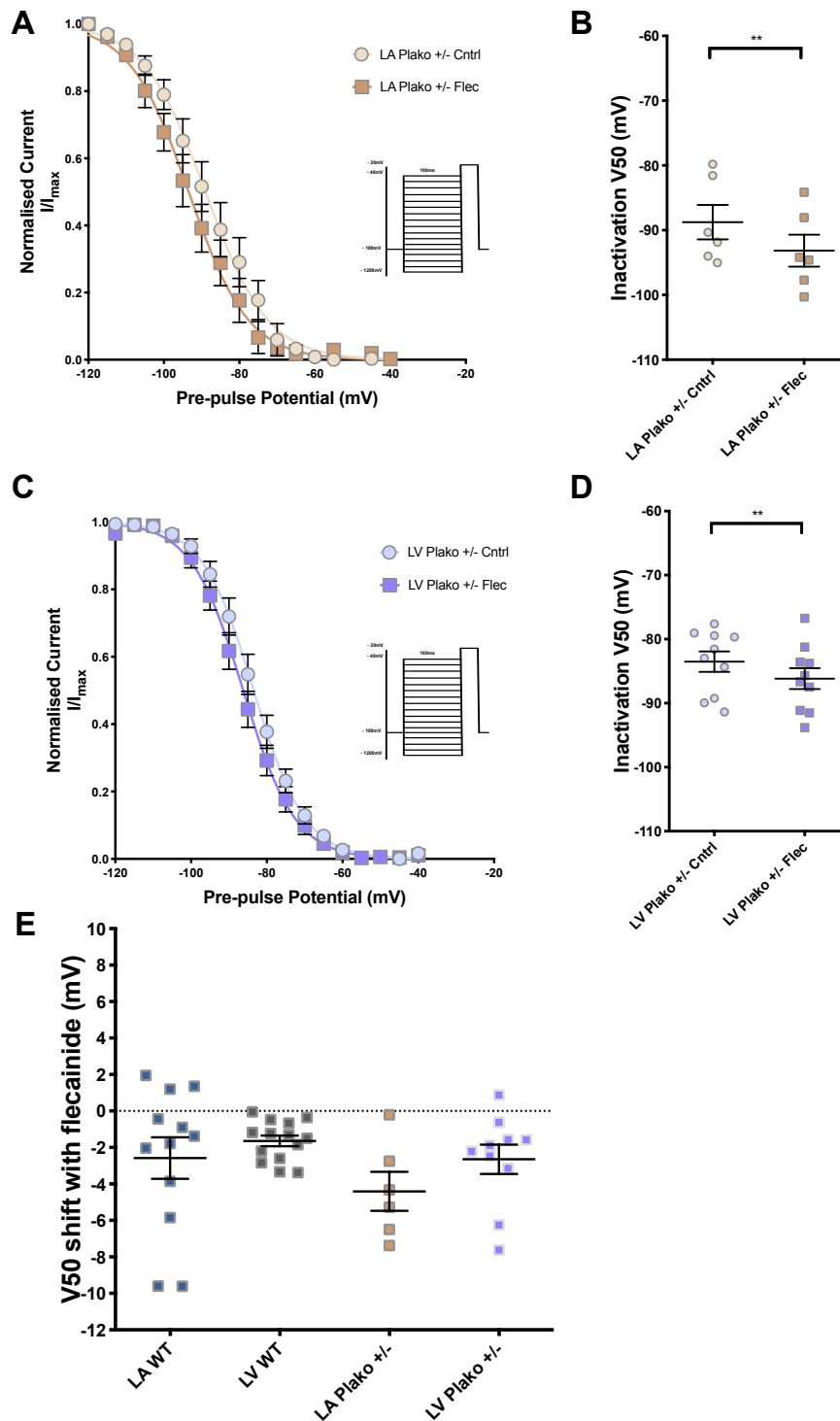


Figure 5.7. Plako^{+/-} LA and LV I_{Na} inactivation with the addition of flecainide.

Channel inactivation +/- flecainide in LA and LV cardiomyocytes from Plako^{+/-} mouse hearts. A) Plako^{+/-} LA curve of normalised I_{Na} inactivation (I/I_{max}) fitted to the Boltzmann function (n=6/3 cells/mice). B) Plako^{+/-} LA V50 of inactivation fitted to the Boltzmann distribution (Plako^{+/-} LA control=-88.76 ± 2.65mV; n=6/3 cells/mice; Plako^{+/-} LA plus flecainide=-93.17 ± 2.465mV; n=6/3 cells/mice)

**p<0.01. C) Plako^{+/-} LV curve of normalised I_{Na} inactivation (I/I_{max}) fitted to the Boltzmann function (n=10/4 cells/mice). D) Plako^{+/-} LV V₅₀ of inactivation fitted to the Boltzmann distribution (Plako^{+/-} LV control=-83.52 ± 1.588mV; n=10/4 cells/mice; Plako^{+/-} LV plus flecainide=-86.16 ± 1.631mV; n=10/4 cells/mice) **p<0.01. E) V₅₀ inactivation shift with flecainide (WT LA=-2.78 ± 1.139mV; n=12/6 cells/mice; WT LV=-1.639 ± 0.2927mV; n=14/4 cells/mice; Plako^{+/-} LA=-4.405 ± 1.07mV; n=6/3 cells/mice and Plako^{+/-} LV=0.689 ± 1.106mV; n=10/4 cells/mice). Error bars indicate ± S.E.M. Significance taken as *P<0.05 with paired Student t-test for (B and D) and two-way ANOVA followed by post-hoc multiple comparisons (Tukey's) test (E).

4.2.7. Flecainide has no effect on recovery of LA or LV sodium channels in the Plako^{+/-} mouse

Experiments were performed on isolated WT and Plako^{+/-} mouse LA and LV cardiomyocytes to study the time dependent kinetics of recovery after inactivation in the presence and absence of flecainide, using the relevant channel recovery protocol described in the materials and methods (Table 1.5). Normalised peak current amplitudes were plotted and fitted to a one-phase association exponential function and the time when half of the channels were recovered (P₅₀) was determined in the Plako^{+/-} LA and LV cardiomyocytes.

In the Plako^{+/-} LA (n=6/3 cells/mice) there was a clear right shift in the sodium channel recovery time in the presence of 1µmol flecainide (Figure 5.8A), suggesting that channel recovery was slower after flecainide was added. However, the P₅₀ in Figure 5.8B shows that the difference in recovery time is not significant, likely due to the large standard deviations of the flecainide data set. In the Plako^{+/-} LV (n=10/4 cells/mice) there was also a slight right shift in the

sodium channel recovery time in the presence of 1 μ mol flecainide (Figure 5.8C), suggesting that channel recovery was slightly slower after flecainide was added. However, the P50 in Figure 5.8D shows that there is no difference in recovery time. Figure 5.8E shows that the shift in recovery between the LA and LV after flecainide is significantly greater in the WT. However, there is no significant difference in the shift in recovery between the Plako^{+/-} LA and LV, although the Plako^{+/-} LA has a much greater shift, likely due to the large standard deviations of the data set.

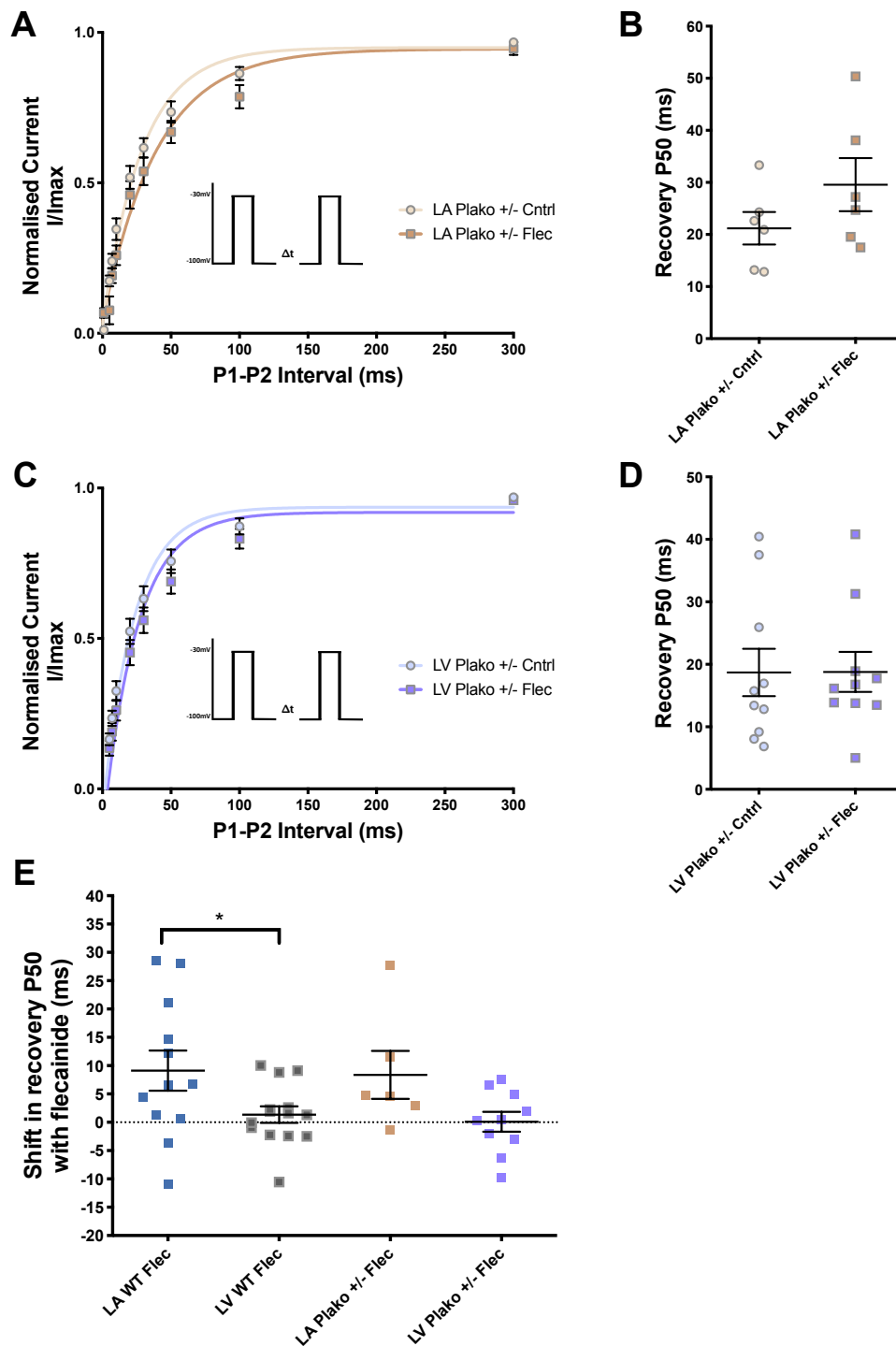


Figure 5.8. Flecainide effect on Plako^{+/-} LA and LV time dependent sodium channel recovery.

Channel recovery in control/flecainide LA and LV cardiomyocytes from Plako^{+/-} mouse hearts. A) Plako^{+/-} LA curve of normalised sodium channel recovery (I/I_{max}) fitted to one-phase association with protocol shown inset ($n=6/3$

cells/mice). B) Plako^{+/-} LA P50 of recovery (Plako^{+/-} LA control=21.2 ± 3.126ms; n=6/3 cells/mice; Plako^{+/-} LA plus flecainide=29.57 ± 5.097ms; n=6/3 cells/mice). C) Plako^{+/-} LV curve of normalised sodium channel recovery (I/I_{max}) fitted to one-phase association with protocol shown inset (n=10/4 cells/mice). D) Plako^{+/-} LV P50 of recovery (Plako^{+/-} LV control=18.7 ± 3.797ms; n=10/4 cells/mice; Plako^{+/-} LV plus flecainide=18.79 ± 3.196ms; n=10/4 cells/mice). E) Shift in recovery after flecainide addition (WT LA=9.124 ± 3.543ms; n=12/6 cells/mice; WT LV=1.354 ± 1.543ms; n=12/6 cells/mice; Plako^{+/-} LA=8.367 ± 4.226ms; n=6/3 cells/mice and Plako^{+/-} LV=0.09 ± 1.759ms; n=10/4 cells/mice). Error bars indicate ± S.E.M. Significance taken as *P<0.05 with paired Student t-test for (B and D) and two-way ANOVA followed by post-hoc multiple comparisons (Tukey's) test (E).

4.3. Chapter synopsis and discussion

4.3.1. Overview of main findings

The key findings of the chapter are described as follows:

- There is no difference in mouse Plako^{+/-} LA and LV I_{Na} density at any holding potential.
- The activation and inactivation of mouse Plako^{+/-} LA and LV sodium channels differ, but differences are not as pronounced as between WT LA and LV. Also, unlike between WT chambers, there is no difference in sodium channel recovery time.
- Flecainide inhibition does not differ between Plako^{+/-} LA and LV sodium channels, as inhibition is greater in Plako^{+/-} LV compared to WT LV sodium channels.

4.3.2. Physiological I_{Na} density and inactivation of LA and LV in the Plako^{+/-} mouse

As described in Chapter 3, there have been several studies comparing the biophysical properties of mammalian atrial and ventricular sodium channels, resulting in multiple publications stating chamber distinctions in the sodium channel physiology. Different activation, inactivation and recovery kinetics of the I_{Na} in LA and LV cardiomyocytes of guinea pig, canine, rat and rabbit (4, 5, 142, 185, 186) have been shown. One of the conclusions from these studies is that the LA cardiomyocytes display greater peak I_{Na} than LV cardiomyocytes when generated from hyperpolarised holding potentials (4, 5, 142, 185, 186).

Upon further analysis into the effect of the holding potential in WT LA and LV cardiomyocytes (Figure 3.2) I_{Na} density showed to be greatly affected by holding potential. In WT LA and LV chambers I_{Na} is greater when initiated from more negative potentials, compared to currents initiated from more physiological potentials, due to increased availability of the sodium channels. At -120mV holding potential WT LA I_{Na} is greater than WT LV I_{Na} (Figure 3.2B), in agreement with findings from other mammalian studies (4, 5, 142, 185, 186). However, at the -75mV holding potential WT LA I_{Na} is smaller than WT LV I_{Na} (Figure 3.2C). As discussed in Chapter 3, these findings are likely a consequence of differences in the inactivation kinetics between the WT LA and LV sodium channels (Figure 3.3). WT LA sodium channels inactivate at more negative voltages than WT LV sodium channels, so are less available at more

physiological positive holding potentials (Figure 3.3A). However, Plako^{+/-} LA and LV I_{Na} distinctions at different holding potentials do not coincide with the WT counterparts. There is no significant difference in the I_{Na} density of the Plako^{+/-} LA or LV at the -120mV holding potential or the -75mV holding potential (Figure 5.2).

The lack of difference in peak I_{Na} between the WT and Plako^{+/-} LV at the -100mV (Figure 5.1E), -120mV (Figure 5.2B) and -75mV (Figure 5.2C) holding potentials opposes the observed increased I_{Na} at -120mV holding potential in plakophilin 2 deficient rat ventricles compared to their WT counterparts (178). This suggests that the effects of plakophilin deficiency cannot be interpreted directly to be the effects of plakoglobin deficiency and that the desmosomal proteins may interact with VGSCs differently.

Likewise, it was suggested that there would be a proarrhythmic reduction in I_{Na} in the plakoglobin deficient ventricles, as heart samples from ARVC patients with reduced plakoglobin also had reduced LV and RV Na_v1.5 expression at the intercalated disks (179, 180). However, Figure 5.BC reveals that there is no difference in I_{Na} density between WT LV and Plako^{+/-} LV I_{Na} at -120mV holding potential, when all sodium channels would be available for activation. Therefore, this disputes the suggestion that a reduced ventricular I_{Na} may be responsible for the increased arrhythmia vulnerability in ARVC patients due to slowed conduction (179, 180).

There may be upregulation of other sodium channel isoforms contributing to the I_{Na} in plakoglobin deficient hearts, as current density is not altered. If so, decreased I_{Na} density would not be a mechanism underlying ARVC arrhythmogenesis in plakoglobin deficient patients. Nevertheless, it must also be assessed whether the observed reduction in LV and RV $Na_v1.5$ expression at the intercalated disks in ARVC plakoglobin deficient patients is conserved in the mouse model. If $Na_v1.5$ expression is also reduced in the ventricles of the plakoglobin deficient mouse, measurement of the expression of other sodium channel isoforms would be necessary in order to explain absence of change in peak I_{Na} .

There is a significant negative shift in the inactivation of $Plako^{+/-}$ LA sodium channels compared to those of the $Plako^{+/-}$ LV (Figure 5.3A), but the difference is visibly less than that seen between the WT counterparts (Figure 5.3D). Although the WT LV and $Plako^{+/-}$ LV inactivation curves overlap, suggesting no difference in inactivation kinetics (Figure 5.3C), the $Plako^{+/-}$ LA inactivation curve is shifted slightly positive to that of the WT LA inactivation curve (Figure 5.3B), although there is no significant difference in the inactivation V_{50} , this shift is clearly visible (figure 5.3D).

Therefore, this slight positive shift in $Plako^{+/-}$ LA sodium channel inactivation could account for the greater I_{Na} density at -75mV compared to the WT LA,

although this is not significant, likely due to data variability (Figure 5.2C). However, it could be expected that that Plako^{+/-} LA display greater I_{Na} *in vivo*. Therefore, amplified I_{Na} could be a causal factor of the increased atrial arrhythmia generation in endurance trained mice with plakoglobin deficiency (259, 260) as there could be increased atrial AP duration of Plako^{+/-} LA cardiomyocytes compared to WT LA cardiomyocytes.

Biophysical studies of a gain-of-function Na_v1.5 mutation in tsA201 cells has shown that AF generation is enhanced as a result of increased cellular excitability due to a 5.13mV positive shift in inactivation (261). However, the difference in inactivation between Plako^{+/-} LA and WT LA is only 2.19mV, and not significant (Figure 5.3D). Nevertheless, a slight positive shift in channel inactivation could result in enhanced I_{Na}, leading to calcium overload conditions (262) and exercise increases cyclic adenosine monophosphate levels, thus leading to intracellular calcium overload (263). Therefore, endurance trained Plako^{+/-} hearts could be particularly susceptible to calcium overload and the resulting DADs (202). This could lead to increased vulnerability to stress-induced triggered activity and contribute to AF development in plakoglobin deficient athletes undergoing endurance training.

As there is no difference in the inactivation kinetics between WT and Plako^{+/-} LV (Figure 5.3C) this conflicts with published findings that describe a plakophilin 2-dependent negative shift in inactivation in ventricular sodium channels,

compared to the WT counterparts (178). This again supports the notion that the effect of plakoglobin deficiency on sodium channels differs to the effect of plakophilin deficiency and that the desmosomal proteins may interact with VGSCs differentially.

4.3.3. Sodium channel activation differences of the LA and LV in the Plako^{+/-} mouse

Figure 3.1E and 5.1F show the -3.77mV shift in the V50 activation of the WT LA sodium channels compared to that of the WT LV sodium channels, supporting findings in rabbit LA and LV cardiomyocytes (5). This negative shift in V50 activation potential of the LA sodium channels suggests an enhancement of excitability and therefore arrhythmia generation in WT LA cardiomyocytes compared to WT LV cardiomyocytes, as described in Chapter 3.

However, in the Plako^{+/-} counterparts, the -2.44mV shift in the V50 activation of the Plako^{+/-} LA sodium channels compared to that of the Plako^{+/-} LV sodium channels is not significant (Figure 5.1F). The Plako^{+/-} LA V50 activation is significantly negatively shifted compared to that of the WT LV. Therefore, it can be presumed that the potential enhancement of excitability and therefore arrhythmia generation in Plako^{+/-} LA cardiomyocytes compared to WT LV cardiomyocytes is still possible, detailed greatly in Chapter 3 (241). The lack of difference between the Plako^{+/-} chambers is due to the -2.22mV negatively

shifted LV Plako^{+/-} activation V50 compared to that of WT LV, however, this not significant. Nevertheless, the shift in LV Plako^{+/-} activation V50 could suggest an enhancement of excitability and therefore arrhythmia generation, but also an enhanced sensitivity to sodium channel inhibition by flecainide (264), compared to WT LV. This would offer further explanation for the enhanced ventricular arrhythmia occurrence in ARVC patients with plakoglobin deficiency (251, 252).

4.3.4. No difference in sodium channel recovery between LA and LV in the Plako^{+/-} mouse

In Chapter 3, WT LA sodium channel P50 for recovery time is 6.83ms slower than WT LV sodium channel recovery (Figure 3.4B). This could suggest that the WT LV are more susceptible to channel reopening during repolarisation due to faster recovery, with the resultant arrhythmic triggers described previously. On the other hand, the slower recovery of WT LA sodium channels could result in decreased I_{Na} , leading to decrease in AP amplitude and conduction velocity (98). A reduction in conduction velocity is also associated with arrhythmia generation, so a slower recovery time of the sodium channels may also be considered proarrhythmic.

Figure 5.4A reveals that there is no difference in recovery kinetics between Plako^{+/-} LA and LV, suggesting that neither Plako^{+/-} chamber is more susceptible to arrhythmia than other due to distinctions in recovery kinetics.

Figure 5.4B shows that Plako^{+/-} LA recovery curve is left shifted compared to that of WT LA, suggesting that Plako^{+/-} LA sodium channels recovery quicker. This establishes why no difference is observed between the Plako^{+/-} LA and LV recovery. However, the P50 recovery in Figure 5.4D reveals that the 3.37ms difference in recovery time is not significant between WT and Plako^{+/-} LA. Although the difference is not significant it is evident that recovery is only different between the WT and Plako^{+/-} counterparts in the LA, emphasizing that plakoglobin deficiency has a greater effect on LA sodium channel recovery kinetics than those of the LV.

The effect of a slower recovery of sodium channels in the atria compared to ventricles in WT or the Plako^{+/-} hearts cannot be clearly determined. Further studies, examining the effects of these biophysical characteristics under physiological (increased heart rate) and pathophysiological stressors (ischemia, fibrosis) are required to gain a greater understanding of the impact of modulation of recovery kinetics on heart function and arrhythmia predisposition in the different chambers of the heart.

4.3.5. Flecainide sodium channel inhibition of LA and LV in the Plako^{+/-} mouse

No significant difference in peak I_{Na} (Figure 5.1E), activation (Figure 5.1F), inactivation (Figure 5.3D) and recovery (Figure 5.4D) was found between

Plako^{+/-} LA and LV chambers compared to their WT counterparts. As there was no reduction in I_{Na} peak at physiological holding potentials in the Plako^{+/-} LA and LV compared to WT counterparts (Figure 5.2C) it suggests that reduced I_{Na} is not causative of the arrhythmia susceptibility of plakoglobin deficient patients. Therefore, conduction is unlikely to be slowed in plakoglobin deficient hearts and sodium channel blocking drugs, such as flecainide, may not be any more proarrhythmic in plakoglobin deficient hearts than 'normal hearts'. Although there is no difference in sodium channel recovery kinetics between LA and LV Plako^{+/-} sodium channels, there are differences in voltage dependence of inactivation and possibly activation that mirror the WT counterpart distinctions. Therefore, the differences in Plako^{+/-} LA and LV sodium channel activation and inactivation kinetics may alter the susceptibility to flecainide, such as in the WT LA and LV (Figure 3.6).

As with the WT LA compared to WT LV, Plako^{+/-} LA sodium channels inactivate at more negative potentials compared to Plako^{+/-} LV sodium channels (Figure 5.3D). Open and inactivated channels are more susceptible to block from flecainide than deactivated closed state channels (227). Therefore, distinctions in sodium channel gating kinetics suggest that Plako^{+/-} LA sodium channels would be inhibited more than Plako^{+/-} LV sodium channels. However, sodium channels in both Plako^{+/-} LA and LV are clearly inhibited by flecainide (Figure 5.5D and 5.5E), with no detectable difference in % inhibition between the chambers (Figure 5.5F). This is due to the 10.21% greater inhibition of Plako^{+/-} LV sodium channels compared to WT LV sodium channels (Figure 5.5F). This

suggests that flecainide may be suitable for also treating the ventricular arrhythmias that occur in ARVC patients with plakoglobin deficiency and would not be selective for atrial sodium channels. This supports findings that demonstrate that the addition of flecainide alone (265) or in combination with other drugs (sotalol/metoprolol) (266, 267) can be an effective treatment for ventricular arrhythmias in ARVC patients.

Unlike in WT LV sodium channels, the addition of flecainide does not alter activation gating kinetics in Plako^{+/-} LV sodium channels. Flecainide negatively shifts WT LV sodium channel activation (Figure 3.5H) whereas Plako^{+/-} activation (Figure 5.6H) is unchanged. In the WT LV a negative shift in activation would result in more sodium channels being in an open state at physiological voltages and therefore more channels would be susceptible to further flecainide inhibition (227). In the Plako^{+/-} LV, a lack of activation shift would mean that more sodium channels remain in the closed state at physiological voltages and are therefore less susceptible to flecainide inhibition but are also less likely to activate prematurely.

However, as with WT LA and LV (Figure 3.7), flecainide addition results in a negative shift in inactivation of the Plako^{+/-} LA and LV sodium channels (Figure 5.8). The shifts in inactivation are comparable between the corresponding chambers in the WT (Figure 5.7E). The shift in Plako^{+/-} LA sodium channel

inactivation is -1.625mV greater than the Plako^{+/-} LV sodium channel activation but this is not significant, likely due to variation within both data sets.

As shown in Chapter 3, WT LA sodium channel recovery time was increased when flecainide was added to the cells (Figure 3.7B). This could potentially reduce $I_{Na,late}$, meaning that flecainide safeguards the WT LA from prolongation of the AP plateau and the resultant arrhythmic triggers described previously because of this late current (223, 224). Additionally, with increase in channel recovery time the WT LA ERP would increase (221) and this could be protective against re-entrant AF (118). Conversely, neither Plako^{+/-} LA or LV recovery time was significantly altered with flecainide addition. Therefore, the proposed cardioprotective mechanism that occurs as a result of slowed channel recovery would not occur with flecainide addition in Plako^{+/-} hearts (Figure 5.8). However, the shift in Plako^{+/-} LA recovery was comparable to the shift in WT LA recovery (Figure 5.8E) and may not have been significant due to pronounced data variability.

Overall, flecainide does not appear to be atrial selective in the Plako^{+/-} mouse, unlike in the WT mouse. Therefore, flecainide would not be an AF targeting drug for those with plakoglobin deficiency, as % inhibition of Plako^{+/-} LV I_{Na} was significantly greater than % inhibition of WT LV I_{Na} and ventricular electrophysiology could be altered. This is likely primarily due the differences in channel gating kinetics of both the Plako^{+/-} LA and LV compared to their WT

counterparts. Furthermore, as described in Chapter 3, the effects on the other ion channels, aside of the sodium channels, needs to be considered when assessing the effectiveness for AF treatment. However, ARVC patients predominantly present with ventricular arrhythmias over atrial arrhythmias (251, 252). Therefore, the ventricular electrophysiology in ARVC patients would be abnormal and the greater inhibition of Plako^{+/-} LV I_{Na} than WT LV I_{Na} with flecainide could be useful for suppressing ventricular arrhythmias as well as atrial arrhythmias.

5. Langendorff-free technique for mouse cardiomyocyte isolation

5.1. Chapter introduction and overview

The development of new clinical therapeutic approaches for treating cardiovascular disease is crucial. Therefore, model systems are essential to advance scientific understanding of the mechanisms, pathogenesis and progression of cardiovascular disease, alongside the testing of therapeutic approaches to restore cardiac function. The ideal model system is simply manipulated, reproducible, inexpensive, physiologically representative of the human model and ethically suitable (268).

Mice models have the distinctive properties that make them valued and indispensable in cardiac research. Mice have relatively low maintenance cost, short gestation time and are often easier to handle than larger mammal models (269). Although there are obvious significant differences between mice and humans, 99% of human genes have direct murine orthologs (270) and genetically modified mice can be selected within a reasonably short time due to their high breeding rate (271). Additionally, mouse and human hearts share many similarities and both express proteins with comparable functions and roles (272). Therefore, the use of mouse models provides a wealth of valuable insight into human cardiac physiology and over the past decade the mouse

model has become the most popular model choice to study human cardiovascular disease (269).

Animal models were initially only utilised for studying surgical and pharmacological interventions within the intact heart. Over time, advances in research lead to intact muscle preparations being used for experimental manipulation of the cardiac muscle (273). However, due to the large size of the intact muscle, in-depth electrophysiological examination proved difficult, as adequate control of membrane potential for voltage clamp experiments could not be achieved. These difficulties and the requirement for more in-depth electrophysiological data to progress cardiac research lead to the development of single cell isolation techniques.

Research using isolated cardiomyocytes can provide crucial understanding of cellular and sub-cellular physiology. Isolated mouse cardiomyocytes are extensively used for the study of cardiac function, as demonstrated within this Thesis. However, high quality cardiomyocytes are essential to successful experimentation. Nevertheless, after almost 50 years of cardiomyocyte isolation (274-276), there is no simple universally used method that guarantees high yields of viable cells. Researchers often face problems isolating high quality healthy cardiomyocytes and difficulties in isolation can unpredictably occur, even in laboratories that routinely isolate cardiomyocytes.

Some research groups have isolated cardiomyocytes by mechanical homogenisation (275, 276) and mechanical agitation with enzymatic digestion of tissue in a petri dish (277, 278). Though, when cardiomyocyte viability was reported upon, these early examples of mechanical digestion often exhibited low yields of intact cells. Today most research groups rely on the Langendorff-isolation method of retrograde perfusion via the aorta with enzymes (273). The Langendorff method was established in 1898 by Oscar Langendorff (279), mostly isolating cardiomyocytes from cat, dog and rabbit hearts. The general principle of this method is retrograde perfusion of the heart via a cannulated aorta (see Figure 6.1). This results in closure of the aortic valve and filling of the coronary arterial vasculature with perfusion buffer so that it passes through the vascular bed (280).

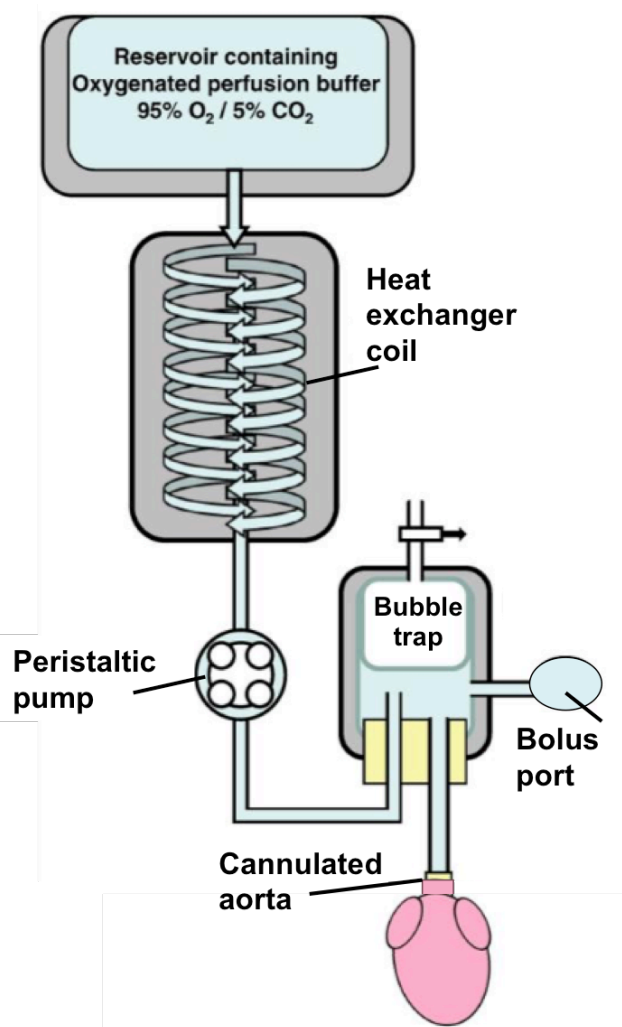


Figure 6.1. Schematic of a Langendorff apparatus.

Basic schematic of the Langendorff system. The heart is retrogradely perfused with buffer solution via the cannulated aorta. The buffer solution is driven from the reservoir to the heat exchanger coil by the peristaltic pump. Drugs etc. can be administered via the bolus port. The solution is kept at 37°C. Image adapted from (280).

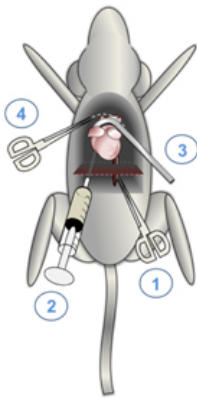
The original Langendorff isolation method has been modified and has evolved over time to deliver cardiomyocytes with increased potential for research. O'Connell et al., adapted the method, so that a two-fold increased yield (1-1.5 x10⁶) of rod-shaped cardiomyocytes from a mouse heart was achieved, compared to previously published reports (281). Importantly, adaptations also

provided calcium tolerant cardiomyocytes that could be isolated for measuring contractile function and Ca^{2+} transients (281). MacDougall et al., also modified the traditional Langendorff method so that cardiomyocytes could be isolated from the rat heart and myocardium could be processed/stored from the same heart. This modification resulted in the ethically, logistically and economically beneficial reduction of the number of animals required for research (282).

Nevertheless, even after many evolutions, research progress has been hindered by difficulties concerning the isolation of high-quality cardiomyocytes. The Langendorff cardiomyocyte isolation method demands specific commercial or custom-made equipment (as seen in Figure 6.1) with extensive training for the delicate and challenging technique. Additionally, Langendorff isolations face issues of sterility and often require anticoagulant pre-injection into animals, potentially affecting data outcomes (283, 284). These issues often cause significant financial, technical and logistical barriers to cardiac research.

Together with our colleagues in Singapore, we have developed a novel, recently published, Langendorff-free alternative approach to mouse cardiomyocytes isolation, as described in the Material and Methods 2.4.2 of this Thesis. A schematic overview of the injection-based isolation method is shown in Figure 6.2 (183). This method works by injection of digestion buffers directly into the ventricles of an adult mouse heart *ex vivo* and can conveniently produce high yields of functionally healthy cardiomyocytes, without expensive

equipment. Additionally, this isolation method can be performed in sterile conditions for culturing purposes and does not require heparin injection.



Chest cavity of anaesthetised mouse is opened to below diaphragm (red) to fully expose heart.

- (1) Descending aorta and inferior vena cava are cut.
- (2) 7 ml EDTA buffer is injected into apex of right ventricle.
- (3) Lahey forceps reach behind heart to clamp aorta.
- (4) Heart is removed by cutting behind clamp.



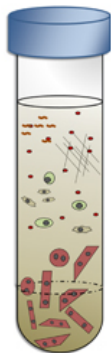
Clamped heart is submerged in 60 mm dish of EDTA buffer. 10 ml EDTA buffer is injected into apex of left ventricle (LV).

Heart is transferred to dish of perfusion buffer. 3 ml perfusion buffer is injected into apex of LV.

Heart is transferred to dish of collagenase buffer. 30-40 ml collagenase buffer injected into apex of LV, until digestion is apparent.



Clamp is removed. Heart may be separated into respective chambers as desired. Tissue is then pulled gently into $\sim 1\text{mm}^3$ pieces using forceps, and dissociated by gentle pipetting.



Stop buffer is added. Cell suspension is passed through 100 μm strainer and myocytes gravity settle for 20 min.

Supernatant containing non-myocyte cells, debris and extracellular matrix is collected. Myocytes then undergo two further rounds of gravity settling to achieve a pure population that may be harvested, applied in acute studies, or plated for in vitro culture.

Similarly, supernatant fractions are combined and centrifuged to isolate non-myocyte populations.

Figure 6.2. Injection-based isolation method.

A summary of the injection-based cardiomyocyte isolation method as described in the text of this thesis. Figure extracted from (183).

The reproducible yields of ≤ 1 million $81 \pm 6\%$ viable isolated cardiomyocytes per LV with the injection method are comparable to those of successful Langendorff isolations (183, 281). Since this injection-based cardiomyocyte isolation method was published, a vast amount of positive feedback has been received and several research groups have adopted this protocol with extensive number of citations (285-301). In order to establish the suitability of injection isolated cardiomyocytes for research, the functionality and morphology of the cells must be demonstrated and compared to published findings and cardiomyocytes isolated via the traditional Langendorff-based method.

The aims of this investigation are summarised below:

1. To compare the functionality of the injection isolated cardiomyocytes to published findings and directly to cardiomyocytes isolated using the Langendorff method. This will be done by assessing the contractile properties, calcium handling, sodium channel gating kinetics and adrenergic responses.
2. To assess calcium handling, stress-dependent hypertrophic signalling cascades and sodium channel gating kinetics of the injection isolated cardiomyocytes compared to those isolated using the Langendorff method.

5.2. Protocol optimisation

This work was performed and published by Ackers et al., (183). These experiments were conducted on C57/BL6 mice aged 8-12 weeks.

For optimisation experiments crude digestion product was monitored with percentage of viable rod-shaped cardiomyocytes quantified using a hemocytometer.

In the injection-isolation protocol, mouse hearts are perfused with divalent cation chelating EDTA in the buffers. Preclearance of the heart in vivo, with EDTA (injected into the right ventricle) inhibits contraction, prevents coagulation and weakens extracellular connections (274, 302-304) (see materials and methods chapter for details). In three independent experiments peak rod-shaped cardiomyocyte yields were tested in the presence of different pH. Peak rod-shaped cardiomyocyte yields were achieved with the dissociation buffer at pH 7.8 (Figure 7.1A) and 5mmol/L EDTA buffer concentration (Figure 7.1B). Under these conditions the injection method provided reproducible yields of ≤ 1 million $81 \pm 6\%$ cardiomyocytes (183), comparable to yields from Langendorff-isolation (281, 305, 306).

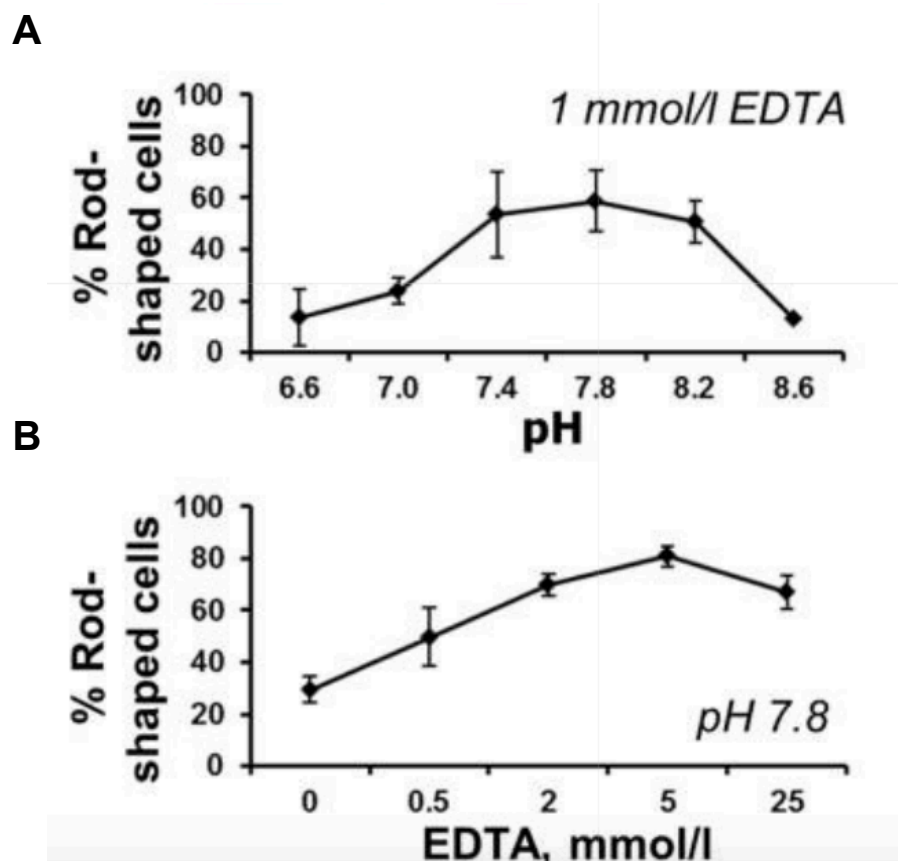


Figure 7.1. EDTA and pH optimisation.

A) Optimisation of dissociation buffer pH. B) Optimisation of EDTA concentration. Data shows mean \pm S.D, n=3 independent experiments.

5.3. Functionality of injection-isolated cardiomyocytes

During isolation of cardiomyocytes there is a risk of cellular damage and/or activation of stress response pathways, potentially altering *in vivo* or downstream transcriptional profiles. Therefore, experiments were performed to assess the functional characteristics of the injection-isolated cells.

5.3.1. Cell and sarcomere length of injection isolated LV cardiomyocytes

Sian-Marie O'Brien isolated the cardiomyocytes and Dr Davor Pavlovic performed the calcium and cell/sarcomere length experiments. These experiments were conducted on C57/BL6 mice aged 8-12 weeks.

Frequency response was measured in injection-isolated cardiomyocytes. Representative traces of electrically paced injection isolated LV cardiomyocytes exhibit characteristic (307-311) frequency-dependent changes in calcium transients (Figure 7.2A) and sarcomere length (SL) (Figure 7.2B). This is demonstrated in Figure 7.2C, diastolic Ca^{2+} transient amplitude increases in a frequency-dependent manner and is significantly greater at 4Hz frequency than at 1Hz. Figure 7.2D shows that Ca^{2+} transient decay (τ) is significantly less at the 3Hz frequency than at 1Hz. This is in accordance with other mouse data that is contrary to data from other mammals (312, 313). SL shortening is significantly reduced at 3Hz and 4Hz frequency than at 1Hz.

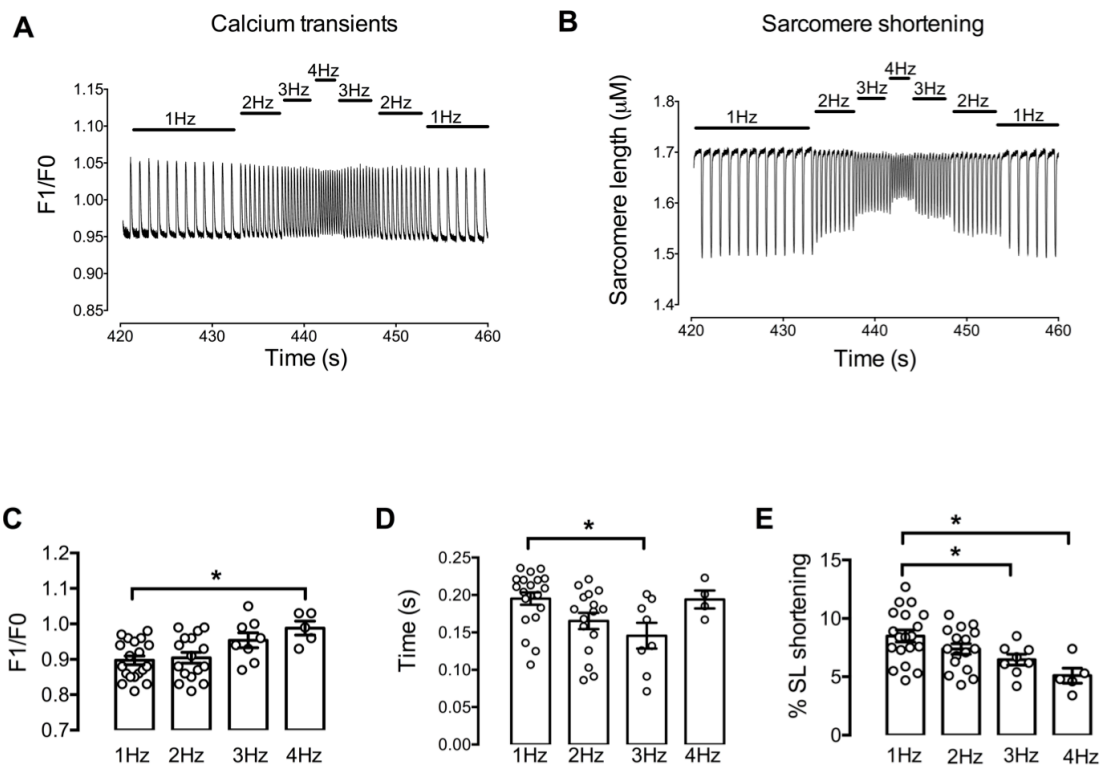


Figure 7.2. Frequency response of LV injection-isolated cells.

Ca²⁺ transients and SL were measured following pacing at varying frequencies (1-4Hz). A) Raw Ca²⁺ transients B) Raw SL. C) Diastolic Ca²⁺. D) Ca²⁺ transient decay (τ). E) % SL shortening. C-E (n \geq 9/3 cells/mice). Error bars indicate \pm S.E. significance taken as *P<0.05 with one-way ANOVA followed by Dunnett multiple comparisons test.

5.3.2. Adrenergic response of injection-isolated LV cardiomyocytes

Sian-Marie O'Brien isolated the cardiomyocytes and Dr Davor Pavlovic performed the calcium and cell/sarcomere length experiments. These experiments were conducted on C57/BL6 mice aged 8-12 weeks.

Adrenergic responses with the addition of +1 μ mol/l isoproterenol (ISO) were assessed in injection-isolated cardiomyocytes. Figure 7.3A shows representative raw traces from an injection-isolated LV cardiomyocyte. Addition

of +1 $\mu\text{mol/l}$ ISO amplified both Ca^{2+} transients (top) and SL shortening (bottom). Figure 7.3B shows a representative Ca^{2+} transient raw trace of electrically paced injection isolated LV cardiomyocyte, with control shown in black and +1 $\mu\text{mol/l}$ ISO in red. ISO clearly increased Ca^{2+} transient amplitude (left panel) and resulted in a faster Ca^{2+} transient decay (right panel) when normalised. The representative trace of a single beat SL shortening, with control shown in black and with +1 $\mu\text{mol/l}$ ISO in red (Figure 7.3C) demonstrates that SL length is clearly increased with the addition of ISO. Increasing doses of ISO increased Ca^{2+} transient amplitude (Figure 7.3D), decreased Ca^{2+} transient decay (τ) (Figure 7.3E) and increased SL shortening in a dose dependent-manner (Figure 7.3F). These findings are in accordance with previously published data (314-316).

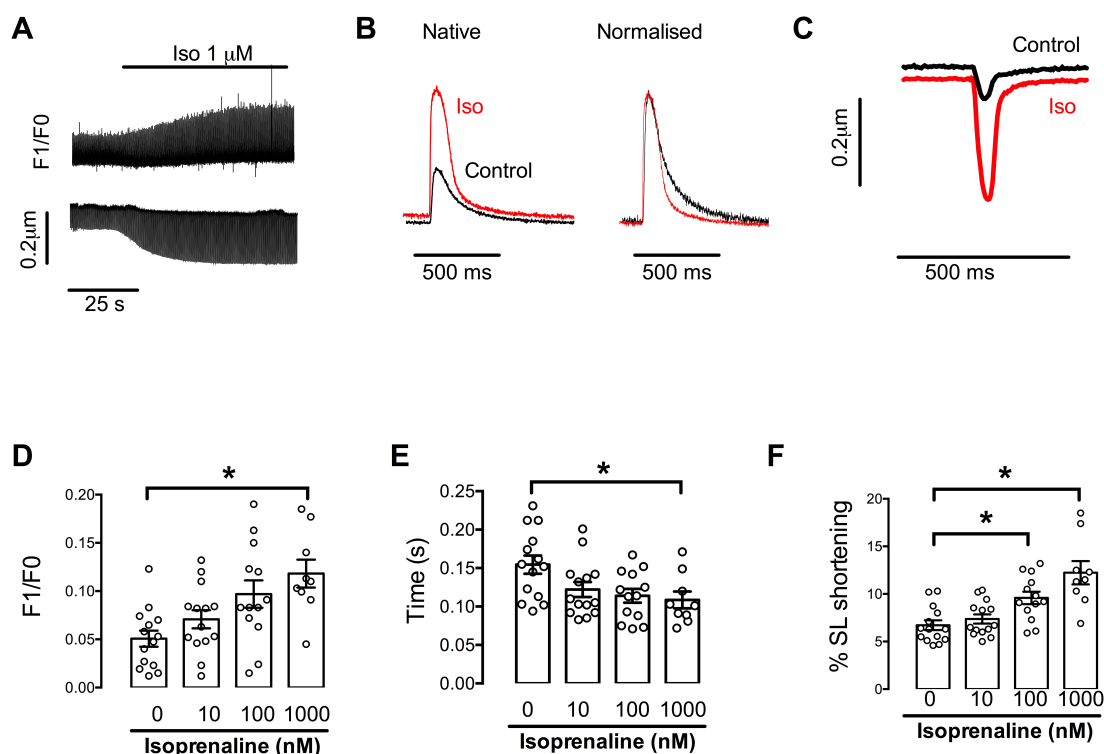


Figure 7.3. Adrenergic response of LV injection-isolated cells.

Adrenergic responses with the addition of (ISO). A) Representative raw traces of Ca^{2+} transient (top) and SL shortening (bottom). The period of $1 \mu\text{mol/l}$ ISO addition is marked in the figure. B) Representative raw calcium transient native (left) and normalised (right) trace of electrically paced injection isolated LV cardiomyocyte, with control shown in black and $+1 \mu\text{mol/l}$ ISO in red. C) Representative SL trace of injection isolated LV cardiomyocyte, with control shown in black and $+1 \mu\text{mol/l}$ ISO in red. D) Ca^{2+} transient amplitude E) Ca^{2+} transient decay (τ) and F) % SL shortening, with increasing dose of ISO ($n \geq 9/3$ cells/mice). Error bars indicate \pm S.E. significance taken as $*P < 0.05$ with one-way ANOVA followed by Dunnett multiple comparisons test.

5.3.3. Injection-isolated LV cardiomyocyte sodium channel IV and activation

Cardiomyocyte isolation and patch clamp experiments were conducted by Sian-Marie O'Brien and Dr Andrew Holmes. These experiments were conducted on C57/BL6 mice aged 8-12 weeks.

As described previously, activation of sodium channels drives the upstroke of the AP, determining the propagation of electrical impulses throughout the myocardium and is a target of AADs. Here it is assessed whether injection-isolated cardiomyocytes displayed typical I_{Na} compared to published data. Experiments were performed on Langendorff and injection isolated WT mouse LV cardiomyocytes to compare the sodium channel I/V relationship, using the relevant I/V patch clamp protocol described in the materials and methods (Table 1.5). This protocol enabled assessment of the voltage/current relationship and sodium channel activation.

Figure 7.4A shows a typical raw representative trace of the I_{Na} I/V curve from a single injection-isolated LV cardiomyocyte with the patch clamp protocol shown inset. The mean current-voltage relationship of I_{Na} density in injection-isolated LV cardiomyocytes ($n=8/3$ cells/mice) (Figure 7.4B) confirms that the peak I_{Na} is achieved at -30mV, as widely published by others (4, 46, 57, 317). Figure 7.4C shows a raw representative trace of the I_{Na} voltage-dependent steady-state inactivation of a single injection isolated LV cardiomyocyte, with the patch clamp protocol shown inset. The injection-isolated mouse LV cardiomyocytes sodium channels have comparable inactivation kinetics (Figure 7.4D) to published data using Langendorff isolated cardiomyocytes ($n=8/3$ cells/mice) (4, 46, 57, 317).

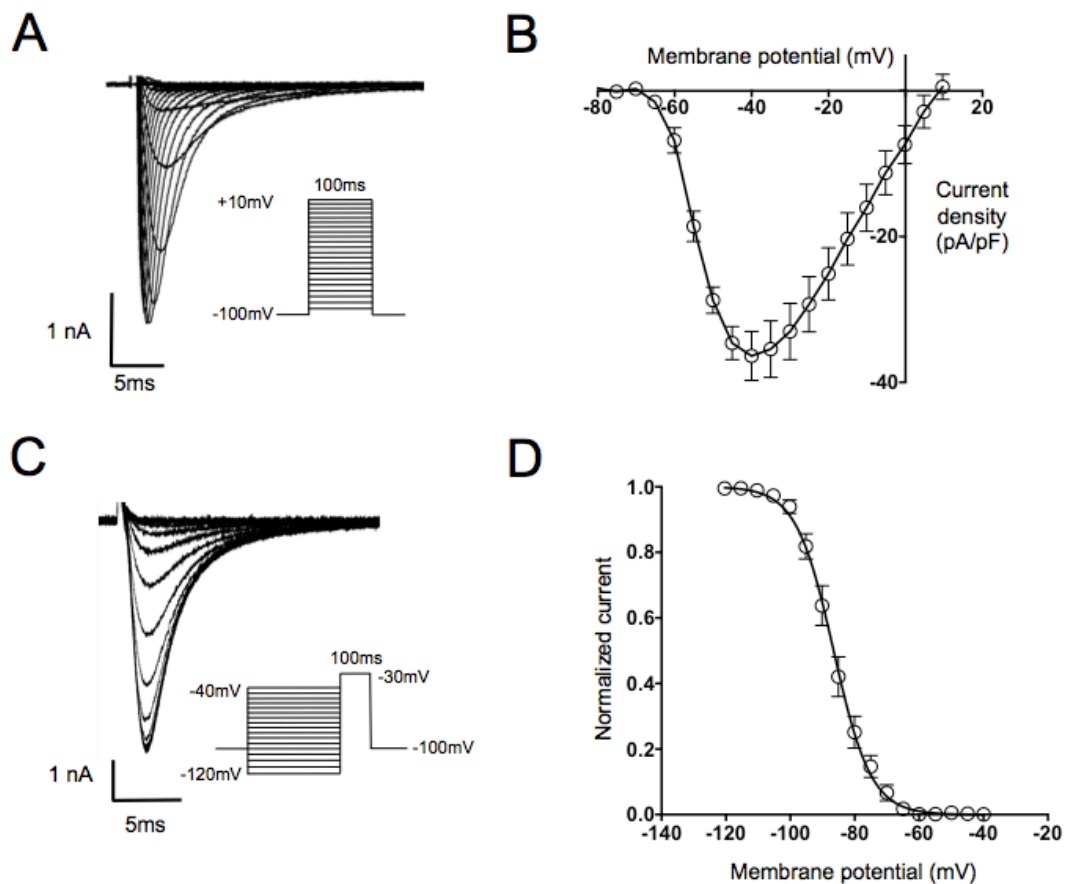


Figure 7.4. Injection isolated LV cardiomyocyte I/V relationship and sodium channel inactivation.

I_{Na} I/V curve and channel inactivation in injection-isolated LV cardiomyocytes from WT mouse hearts. A) Representative raw trace of the I_{Na} patch clamp protocol on the right. B) Current-voltage relationship of I_{Na} density of injection-isolated LV cardiomyocytes ($n=8/3$ cells/mice). C) Representative trace of the I_{Na} voltage-dependent steady-state inactivation, patch clamp protocol shown inset. D) Curve of normalised I_{Na} inactivation (I/I_{max}) fitted to the Boltzmann function ($n=8/3$ cells/mice).

5.4. Comparison of function and signalling characteristic between injection-based and Langendorff-based isolation techniques

Analysis of contractile response, Ca^{2+} handling, I_{Na} properties and stress markers between cardiomyocytes isolated with injection-isolation and

Langendorff-isolation is essential to directly compare the functionality of cardiomyocytes using the novel method.

5.4.1. Comparison of injection and Langendorff isolated LV cardiomyocyte cell and sarcomere length

Sian-Marie O'Brien isolated the cardiomyocytes and Dr Davor Pavlovic performed the calcium and cell/sarcomere length experiments.

Resting morphology was compared between injection-isolated cardiomyocytes and Langendorff isolated cardiomyocytes. There was no difference in resting cell length between Langendorff (n=19/3 cells/mice) and injection (n=19/3 cells/mice) isolated LV cardiomyocytes (Figure 7.5A). However, the resting SL of Langendorff isolated LV cardiomyocytes (n=19/3 cells/mice) was significantly less than in injection isolated LV cardiomyocytes (n=19/3 cells/mice) (Figure 7.5B).

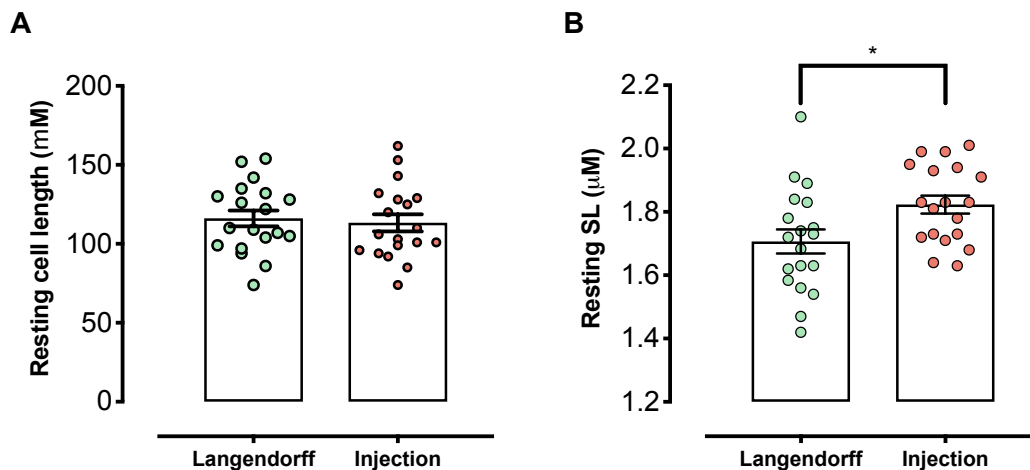


Figure 7.5. Diastolic cell length and sarcomere length of Langendorff and injection isolated cells.

Diastolic cell length and SL was measured were measured in Langendorff and injection isolated cardiomyocytes. A) Resting cell length of isolated LV cardiomyocytes (Langendorff= 116.1 ± 5.055 mM; $n=19/3$ cells/mice; injection= 113.3 ± 5.4 mM; $n=19/3$ cells/mice). B) Resting sarcomere length of isolated LV cardiomyocytes (Langendorff= 1.707 ± 0.03801 µM; $n=19/3$ cells/mice; injection= 1.823 ± 0.02828 µM; $n=19/3$ cells/mice) * $p < 0.05$. Error bars indicate \pm S.E.M. significance taken as * $P < 0.05$ with unpaired Student t-test.

5.4.2. Pacing effect on injection and Langendorff isolated LV cardiomyocytes

Sian-Marie O'Brien isolated the cardiomyocytes and Dr Davor Pavlovic performed the calcium and cell/sarcomere length experiments.

Preservation of diastolic Ca^{2+} and tight control of Ca^{2+} release and uptake is fundamental to coordinated myocardium contraction. Therefore, calcium-handling properties and SL at different pacing frequencies (1-3Hz) were compared between injection-isolated cardiomyocytes and Langendorff- isolated cardiomyocytes. There was no difference in diastolic Ca^{2+} between the

Langendorff and injection isolated cardiomyocytes at 1Hz, 2Hz or 3Hz (Langendorff n=16/3 cells/mice; injection n=16/3 cells/mice) (Figure 7.6A). There was no difference in Ca^{2+} transient amplitude between the Langendorff and injection isolated cardiomyocytes at 1Hz, 2Hz or 3Hz (Langendorff n=16/3 cells/mice; injection n=16/3 cells/mice) (Figure 7.6B). There was also no difference in Ca^{2+} decay constant (τ) between the Langendorff and injection isolated cardiomyocytes at 1Hz, 2Hz or 3Hz (Langendorff n=16/3 cells/mice; injection n=16/3 cells/mice) (Figure 7.6C). Additionally, there was no difference in % of SL shortening in the Langendorff and injection isolated cardiomyocytes at 1Hz, 2Hz or 3Hz (Langendorff n=16/3 cells/mice; injection n=16/3 cells/mice) (Figure 7.6D).

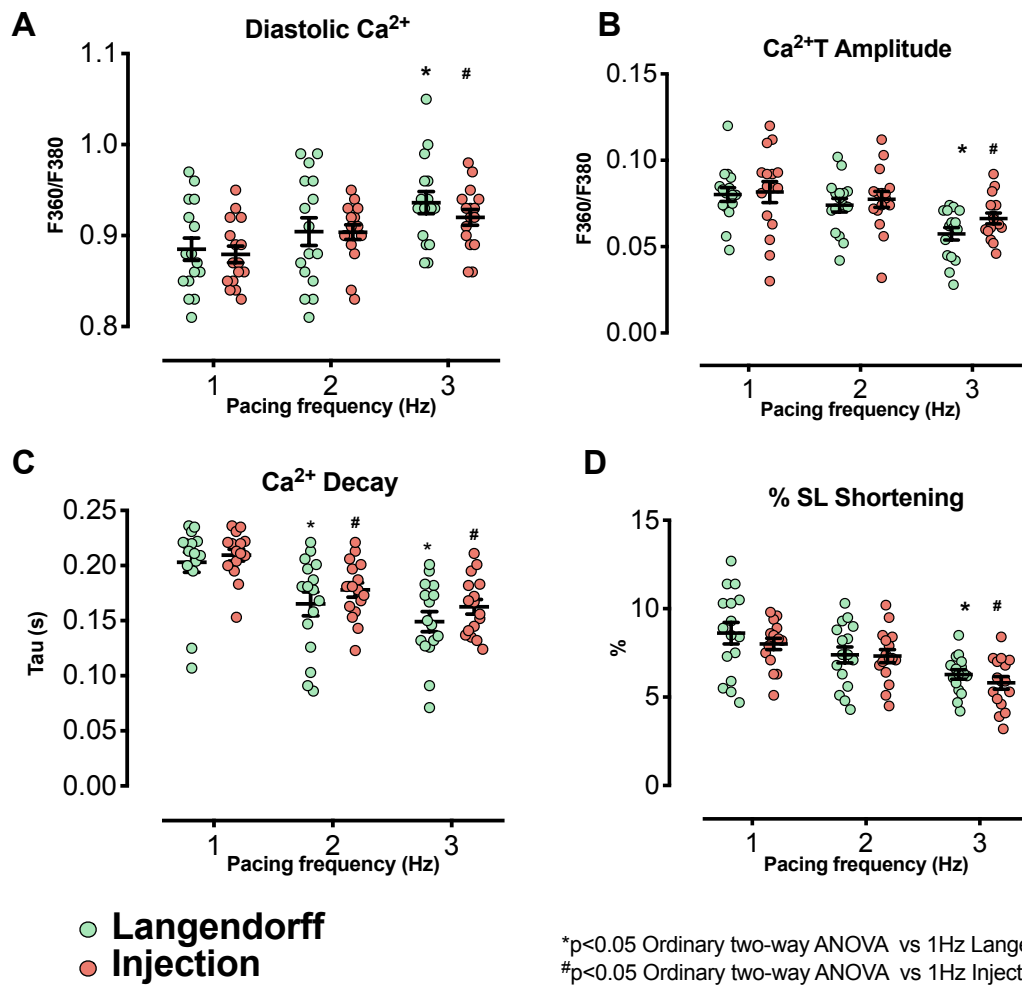


Figure 7.6. Pacing effect on Langendorff and injection isolated cells.

Ca²⁺ transients and sarcomere length were measured following pacing at varying frequencies (1-3Hz) in Langendorff and injection isolated cardiomyocytes. A) Diastolic Ca²⁺ in LV isolated cardiomyocytes at 1Hz (Langendorff=0.885 ± 0.01232 F1/F0; n=16/3 cells/mice; injection=0.8794 ± 0.009059 F1/F0; n=16/3 cells/mice), at 2Hz (Langendorff=0.9044 ± 0.01525 F1/F0; n=16/3 cells/mice; injection=0.9038 ± 0.008107 F1/F0; n=16/3 cells/mice), at 3Hz (Langendorff=0.9363 ± 0.01217 F1/F0; n=16/3 cells/mice; injection=0.92 ± 0.008563 F1/F0; n=16/3 cells/mice). B) Ca²⁺ transient amplitude in LV isolated cardiomyocytes at 1Hz (Langendorff=0.08019 ± 0.004004 F1/F0; n=16/3 cells/mice; injection=0.08163 ± 0.006124 F1/F0; n=16/3 cells/mice), at 2Hz (Langendorff=0.07400 ± 0.003949 F1/F0; n=16/3 cells/mice; injection=0.07744 ± 0.004603 F1/F0; n=16/3 cells/mice) and at 3Hz (Langendorff=0.05744 ± 0.003623 F1/F0; n=16/3 cells/mice; injection=0.06632 ± 0.003106 F1/F0; n=16/3 cells/mice). C) Ca²⁺ decay constant (τ) in LV isolated cardiomyocytes at 1Hz (Langendorff=0.202 ± 0.009071s; n=16/3 cells/mice; injection=0.2095 ± 0.005273s; n=16/3 cells/mice), at 2Hz (Langendorff=0.1653

± 0.01081 s; n=16/3 cells/mice; injection= 0.1779 ± 0.006605 s; n=16/3 cells/mice) and at 3Hz (Langendorff= 0.1491 ± 0.009074 s; n=16/3 cells/mice; injection= 0.1626 ± 0.006637 s; n=16/3 cells/mice). D) % of SL shortening in LV isolated cardiomyocytes at 1Hz (Langendorff= $8.619 \pm 0.6069\%$; n=16/3 cells/mice; injection= $8.006 \pm 0.3211\%$; n=16/3 cells/mice), at 2Hz (Langendorff= 7.388 ± 0.4517 ; n=16/3 cells/mice; injection= 7.319 ± 0.3737 ; n=16/3 cells/mice) and at 3Hz (Langendorff= 6.281 ± 0.2687 ; n=16/3 cells/mice; injection= 5.806 ± 0.359 ; n=16/3 cells/mice). Error bars indicate \pm S.E.M. significance taken as $*P < 0.05$ with two-way ANOVA followed by post-hoc multiple comparisons (Bonferroni) test.

5.4.3. Adrenergic response of injection and Langendorff isolated LV cardiomyocytes

Sian-Marie O'Brien isolated the cardiomyocytes and Dr Davor Pavlovic performed the calcium and SL experiments.

Adrenergic responses with the addition of $1 \mu\text{mol/l}$ ISO were compared between injection and Langendorff isolated cardiomyocytes by assessing the calcium-handling properties and SL. There was no difference in the percentage of SL shortening with the addition of $1 \mu\text{mol/l}$ ISO between Langendorff and injection isolated cardiomyocytes (Figure 7.7A) (Langendorff n=16/3 cells/mice; injection n=16/3 cells/mice). In both Langendorff and injection isolated cardiomyocytes Ca^{2+} decay constant (τ) was comparably significantly decreased by the addition of $1 \mu\text{mol/l}$ ISO (Figure 7.7B). This again demonstrates that injection-isolated cardiomyocytes display standard adrenergic responses and are suitable for biochemical signaling experiments.

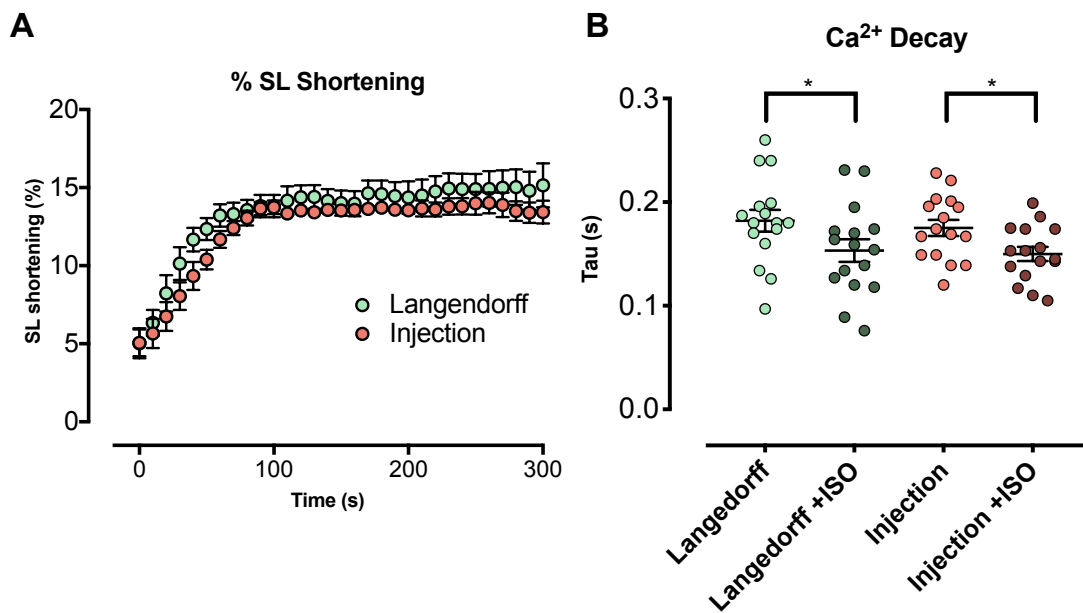


Figure 7.7. Adrenergic responses of Langendorff and injection isolated cells.

Adrenergic responses with the addition of +1 $\mu\text{mol/l}$ ISO in Langendorff and injection isolated cardiomyocytes. A) percentage of SL shortening with the addition of +1 $\mu\text{mol/l}$ ISO (Langendorff $n=16/3$ cells/mice; injection $n=16/3$ cells/mice). B) Ca^{2+} decay constant (τ) (control Langendorff= $0.182 \pm 0.01056\text{s}$; $n=16/3$ cells/mice; 1 $\mu\text{mol/l}$ ISO Langendorff= $0.1533 \pm 0.01092\text{s}$; $n=16/3$ cells/mice; control injection= $0.1751 \pm 0.007762\text{s}$; $n=16/3$ cells/mice; 1 $\mu\text{mol/l}$ ISO injection= $0.15 \pm 0.006755\text{s}$; $n=16/3$ cells/mice). Error bars indicate \pm S.E.M. significance taken as $*P<0.05$ with two-way ANOVA followed by post-hoc multiple comparisons (Bonferroni) test.

5.4.4. Injection and Langendorff isolated LV cardiomyocyte I_{Na} IV and activation

Experiments were performed on Langendorff and injection isolated WT mouse LV cardiomyocytes to compare the sodium channel I/V relationship, using the relevant I/V patch clamp protocol described in the materials and methods (Table 1.5). The currents were measured from a holding potential of -100mV up to $+10\text{mV}$ in 5mV increments and normalised to cell capacitance. This protocol

enabled assessment of the voltage/current relationship and sodium channel activation.

Figure 7.8A shows raw representative traces of the I_{Na} from injection isolated LV cardiomyocytes with the patch clamp protocol shown inset. The current-voltage relationship of the sodium channels of Langendorff isolated LV cardiomyocytes (n=8/4 cells/mice) and injection isolated LV cardiomyocyte (n=5/3 cells/mice) is shown in Figure 7.8B. Sodium channels have a peak current potential of -30mV, at which I_{Na} amplitude was comparable in LV cardiomyocytes isolated with both methods, Langendorff (Figure 7.8C).

The I/V curve data was fitted to a Boltzmann function to obtain the voltage dependence of the conductance activation of sodium channels using the initial downward slope of the curve (as described in the material and methods). This allows comparison of the voltage potential at which half of the sodium channels were activated (V_{50}) in the Langendorff and injection LV isolated cardiomyocytes (Figure 7.8D). The V_{50} of LV cardiomyocytes isolated with both methods was comparable.

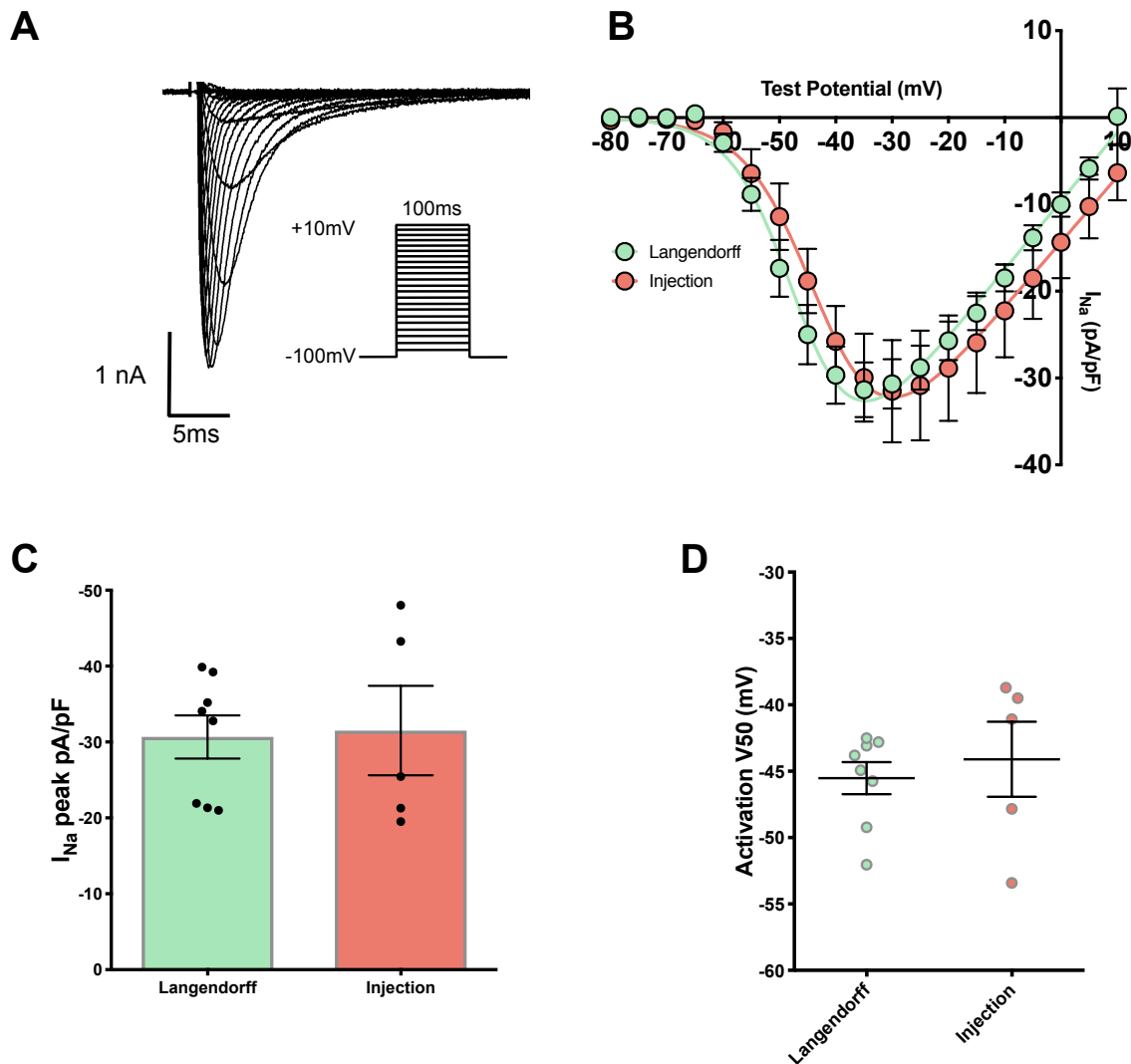


Figure 7.8. Langendorff and injection isolated LV cardiomyocyte I/V relationship and sodium channel activation.

I_{Na} I/V curve and channel activation in Langendorff and injection LV cardiomyocytes from WT mouse hearts. A) Representative raw trace of the I_{Na} from injection isolated LV cardiomyocytes with the patch clamp protocol on the right. B) Current-voltage relationship of I_{Na} density, Langendorff (n=8/4 cells/mice) and injection (n=5/3 cells/mice) isolated LV cardiomyocytes. C) I_{Na} peak density at a step from -100mV to -30mV in Langendorff (-30.67 ± 2.841 pA/pF; n=8/4 cells/mice) and injection (-31.51 ± 5.899 pA/pF; n=5/3 cells/mice) isolated LV cardiomyocytes. D) V50 of activation fitted to the Boltzmann distribution in Langendorff (-45.52 ± 1.209 mV; n=8/4 cells/mice) and injection (-44.1 ± 2.829 mV; n=5/3 cells/mice) isolated LV cardiomyocytes. Error bars indicate \pm S.E.M. significance taken as *P<0.05 with unpaired Student t-test.

5.4.5. Injection and Langendorff isolated LV cardiomyocyte sodium channel inactivation

Experiments were performed on Langendorff and injection isolated WT mouse LV cardiomyocytes to compare the potential at which the sodium channels inactivate (are no longer available), using the relevant steady-state inactivation patch clamp protocol described in the materials and methods chapter (Table 1.5). The voltage dependence of steady-state inactivation (channel availability, I/I_{max}) was determined from this protocol, as shown in Figure 7.9A and fitted to the Boltzmann function.

The Langendorff and injection isolated WT mouse LV cardiomyocytes sodium channels have comparable inactivation kinetics, as shown in Figure 7.9A; Langendorff isolated LV cardiomyocytes ($n=8/4$ cells/mice) and injection isolated LV cardiomyocyte ($n=5/3$ cells/mice). This is confirmed in Figure 7.9B V_{50} for inactivation.

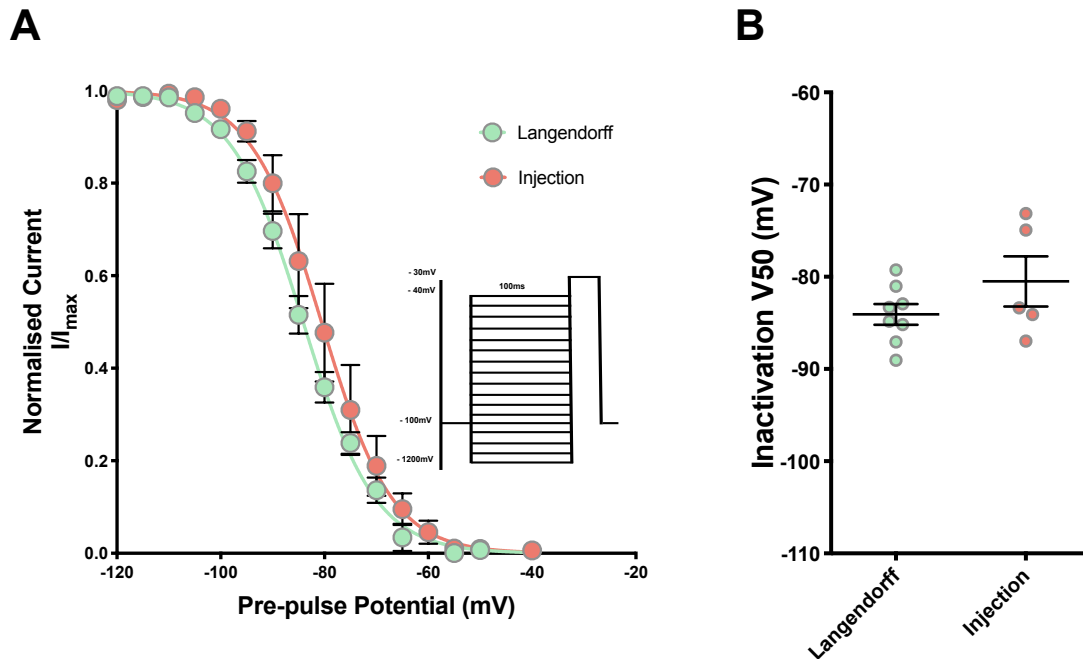


Figure 7.9. Langendorff and injection isolated LV cardiomyocyte sodium channel inactivation.

Channel steady-state inactivation in Langendorff and injection LV cardiomyocytes from WT mouse hearts. A) Curve of normalised I_{Na} inactivation (I/I_{max}) fitted to the Boltzmann function in Langendorff ($n=8/4$ cells/mice) and injection ($5/3$ cells/mice). B) V_{50} of inactivation fitted to the Boltzmann distribution in Langendorff ($-84.08 \pm 1.116\text{mV}$; $n=8/4$ cells/mice) and injection ($-80.5 \pm 2.721\text{mV}$; $n=5/3$ cells/mice). Error bars indicate \pm S.E.M. significance taken as $*P<0.05$ with unpaired Student t-test.

5.4.6. Injection and Langendorff isolated LV cardiomyocyte signalling

cascades

Sian-Marie O'Brien isolated the cardiomyocytes and Dr Davor Pavlovic performed the signalling experiments.

Biomechanical stress and calcium overload during cardiomyocyte isolation can result in activation of hypertrophic signaling cascades (318) and detrimental PKC- α activation (319). To assess the effect of Ca²⁺ and stress-dependent hypertrophic signaling cascades between the Langendorff-based and injection-based isolation methods, the protein expression and localisation of protein kinase C alpha (PKC- α), phosphorylation of extracellular signal-regulated kinase (ERK)1/2 and phosphorylation of PLM at PKC residues, was measured and compared in cardiomyocytes isolated from both methods. There was no difference detected in PKC- α , with cytosolic (inactivate) and membrane (active) fractions evenly distributed in the cardiomyocytes (Langendorff cyt n=8; Langendorff mem n=8; injection cyt n=8; injection mem n=8) (Figure 7.10A). Likewise, ERK1/2 phosphorylation was no different in cardiomyocytes isolated with both methods (Langendorff n=13; injection n=13) (Figure 7.10B). Additionally, there was no change detected in the expression or Ser63 phosphorylation of the cardiac stress protein PLM (Langendorff n=9; injection n=9) (Figure 7.10C), a downstream target of PKC- α . Experiments performed here clearly demonstrate that the injection-isolation method does not negatively affect cardiac intracellular signalling.

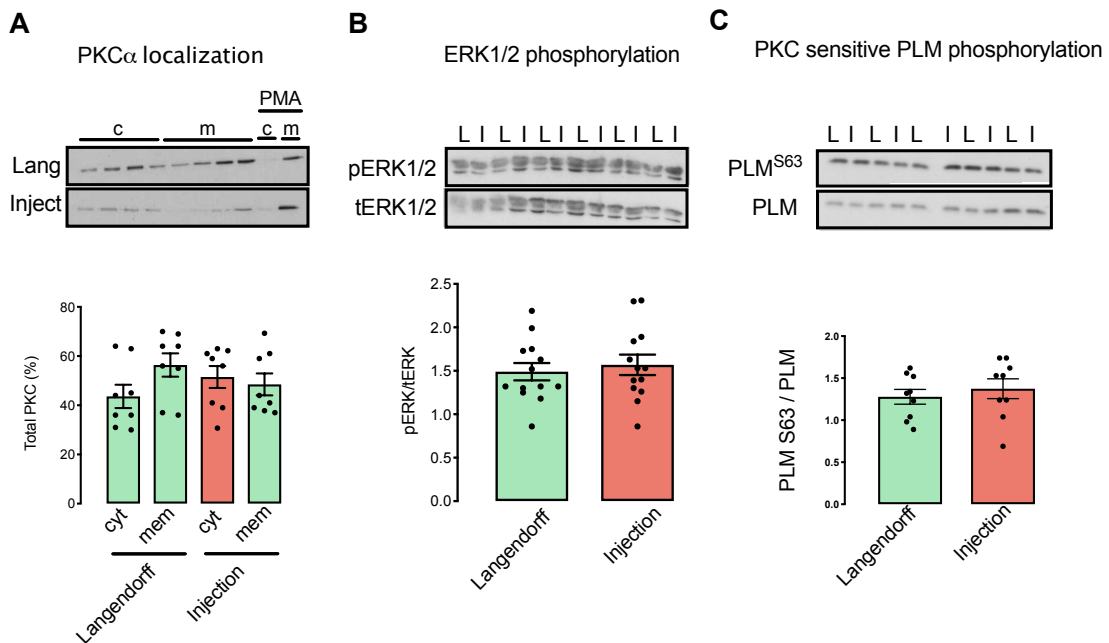


Figure 7.10. Stress signalling cascade associated protein expression in Langendorff and injection isolated LV cardiomyocytes.

Expression of PKC- α , ERK1/2, PLM and PLM phosphorylation at ser63 in cardiomyocytes isolated using Langendorff (L) or injection (I) protocols. A) PKC- α expression and cytosolic (cyt) / plasma membrane (mem) localisation, with PMA administration as positive control (Langendorff cyt=43.63 \pm 4.732AU; n=8; Langendorff mem=56.38 \pm 4.732AU; n=8; injection cyt=51.49 \pm 4.457AU; n=8; injection mem=48.51 \pm 4.457AU; n=8). B) ERK1/2 expression and phosphorylation (pERK) (Langendorff=1.489 \pm 0.09997AU; n=13; injection=1.568 \pm 0.118AU; n=13). C) PLM expression and phosphorylation at ser63 (Langendorff=1.278 \pm 0.08811AU; n=9; injection=1.374 \pm 0.1174AU; n=9). Error bars indicate \pm S.E.M. significance taken as *P<0.05 with one-way ANOVA (A) and unpaired Student t-test (B-C).

5.5. Chapter synopsis and discussion

5.5.1. Overview of main findings

The key findings of the chapter are described as follows:

- Injection-isolated LV cardiomyocytes display characteristic changes in Ca^{2+} transients, Ca^{2+} decay and SL shortening in response to changes in pacing frequency and addition of isoproterenol. No differences were observed when directly compared to Langendorff isolated LV cardiomyocytes.
- Injection-isolated LV cardiomyocytes have greater resting SL but the same levels of diastolic Ca^{2+} as those isolated using the Langendorff method.
- Injection-isolated LV cardiomyocytes exhibited the standard I_{Na} voltage relationship and kinetics and directly compared to those of Langendorff isolated LV cardiomyocytes.
- Langendorff and injection isolation protocols similarly affect stress-signalling cascades.

5.5.2. Protocol optimisation

Isolated mouse cardiomyocytes are essential for investigation into cardiac physiology and pathobiology. Nevertheless, the progress of research relying upon isolated cardiomyocytes is hindered by technical and logistical complications associated with the Langendorff-based isolation method. The novel injection-isolation approach described here is a convenient method to

isolate high yields of viable, Ca^{2+} tolerant cardiomyocytes from the adult mouse heart (183).

Langendorff-based cardiomyocyte isolation usually requires pre-injection of animals with an anticoagulant, such as heparin. However, heparin has proven to be detrimental to downstream PCR based analysis (283, 284). EDTA was examined as a substitute for heparinisation, and as a means of rapidly reducing calcium and thereby reducing calcium overload and calcium overload induced apoptosis. There are however concerns that high concentration of EDTA may be damaging to cardiomyocytes as lack of Ca^{2+} results in separation of membrane superficial laminae (303, 304). However, initial perfusion of the heart with Ca^{2+} free solution is usually imperative for effective cardiomyocyte isolation (320). Therefore, use of low concentrations of EDTA, or the higher Ca^{2+} affinity analogue EGTA, is widely reported in cardiomyocyte isolations (228, 321-323). The initial chelation of divalent cations with EDTA appears to have several benefits, aside of the release of intracellular connections, including anticoagulation and cessation of cardiomyocyte contraction (274, 302). The efficacy of EDTA for isolation of viable cardiomyocytes is evident in Figure 7.1B, as the high pre-clearing 5 mmol/L EDTA concentration produces the greatest yields of rod-shaped cardiomyocytes. The higher 25 mmol/L concentration may have presented with a slightly lower yield of cardiomyocytes possibly due to disruption of the cell membranes, effecting cardiomyocytes viability (303).

Generally, cardiomyocyte isolation protocols rely on dissociation buffers within a physiological pH range (7.0-7.4) (273, 280, 306, 324, 325). However, little evidence has been provided as to whether that pH range produces the highest yield of viable rod-shaped cardiomyocytes. In this study a pH of 7.8 proves optimal for the described injection-isolation protocol (Figure 7.1A). It is possible that more alkaline pH increases the affinity of EDTA for divalent cations, offsets acidification via the potential production of lactate in the myocardium (326), or improves glucose utilisation due to increased phosphofructokinase activity (327).

5.5.3. Comparable contractile and calcium handling properties of injection and Langendorff isolated LV cardiomyocytes

In order to establish whether cardiomyocytes isolated via the injection method are suitable for research calcium-handling properties must be comparable with published findings from Langendorff isolated cardiomyocytes. Therefore, experiments were performed to analyse the Ca^{2+} handling properties and adrenergic responses of the injection-isolated cardiomyocytes.

Post injection isolation and calcium reintroduction, LV cardiomyocytes remained quiescent and adhered to laminin-coated culture surfaces, with the typical angular morphology and expected organised sarcomeric patterns of LV cells isolated using the Langendorff technique (183). Injection isolation did not alter

resting cell length compared to Langendorff isolated cardiomyocytes (Figure 7.5A). This assures that with the injection method the ventricles did not undergo any additional ischemic damage than those of the Langendorff perfused heart during isolation, as change in cell length can be associated with cardiac tissue ischemia (328).

However, the resting SL was significantly greater in the injection-isolated cardiomyocytes (Figure 7.5B). SL is a significant determinant and indicator of cardiac mechanics as it is a function of Ca^{2+} binding. Diastolic Ca^{2+} is an indicator of cell stress and the greater the diastolic Ca^{2+} , the lower SL (329). Therefore, SL has been described as shortened under ischemic conditions (330) and the greater SL in injection-isolated cardiomyocytes suggests they could be healthier than the Langendorff isolated cardiomyocytes. Nevertheless, these differences were not sustained during field stimulation of the cardiomyocytes. When electrically paced the cardiomyocytes exhibited characteristic frequency-dependent changes in Ca^{2+} handling and SL shortening (Figure 7.2) (307-311) and did not differ from the cardiomyocytes isolated by the standard Langendorff method (Figure 7.6).

Furthermore, injection-isolated cardiomyocytes responded to adrenergic stimulation in a dose-dependent manner in accordance with other studies (314-316) (Figure 7.3) and showed no difference in % SL shortening or Ca^{2+} decay in direct comparison with Langendorff isolated cardiomyocytes (Figure 7.7).

Overall, based on these findings it can be assured that injection-isolated cardiomyocytes display standard Ca^{2+} handling properties, contractile characteristics and adrenergic responses.

5.5.4. Comparable I_{Na} of injection and Langendorff isolated LV cardiomyocytes

In order to establish the suitability of LV cardiomyocytes isolated by the injection method for patch clamp studies and assess functionality, sodium channel kinetics and current density were measured and compared with Langendorff isolated cardiomyocyte counterparts.

Injection-isolated cardiomyocytes displayed characteristic I_{Na} I/V relationship (Figure 7.4B) and inactivation kinetics (Figure 7.4D) compared to previously published LV cardiomyocyte data (4, 46, 54, 57, 317). Likewise, there was no difference in peak I_{Na} (Figure 7.8C), activation kinetics (Figure 7.8D) or inactivation kinetics (Figure 7.8B), in direct comparisons between Langendorff and injection isolated LV cardiomyocytes. Therefore, it can be concluded that the I_{Na} density, activation and inactivation kinetics of the injection-isolated cardiomyocytes are as expected and this data supports that these cells can be used for patch clamping experiments.

5.5.5. Comparable signalling cascade effects of injection and Langendorff isolated LV cardiomyocytes

In order to assess signalling cascades in injection and Langendorff isolated cardiomyocytes, the expression of biochemical stress and Ca²⁺ overload protein indicators were analysed.

Despite some differences in resting SL between Langendorff and injection isolated cardiomyocytes (Figure 7.5B), PKC- α , ERK1/2 and PLM expression was equal in cardiomyocytes isolated from both methods (Figure 7.10). Therefore, data presented here establishes that the injection-isolation method does not negatively affect cardiac intracellular signalling any more than the Langendorff isolation method.

Furthermore, as the injection method negates the need for Langendorff perfusion apparatus, it enables simpler and cheaper isolation with the ability to maintain a sterile environment if isolated cells are required for culturing. Additionally, the injection method does not require the precise identification and difficult cannulation of the small mouse aorta, so the likelihood of errors occurring from incorrect mounting of the heart, introduction of air, blood coagulation and ischemia are reduced. Overall, the novel Langendorff-free isolation protocol has proven to be a valuable method for obtaining mouse cardiomyocytes that are comparable in physiological health and responsiveness

to published findings and those that have been isolated with the Langendorff method. Therefore, injection isolation offers a novel and convenient method for obtaining mouse cardiomyocytes and data presented here can provide reassurance to current or perspective users of this method.

5.5.6. Potential injection-isolation method limitations

Although injection-isolation produces high yields of viable cardiomyocytes with comparable functionality to Langendorff isolated cardiomyocytes, there may be some limitations to the method. Firstly, in the injection-isolation method, reduction in resistance to injection pressure and loss of heart rigidity serve as benchmarks for assessing digestion completion. However, experience of the technique may be required in order to recognise these benchmarks and researchers may find it difficult to establish when digestion is complete and halt the experiment with over or under digested tissue. However, complete digestion is also difficult to definitively determine with the Langendorff-isolation method, as acceleration of perfusion rate under constant pressure does not always serve as an accurate benchmark and likewise requires method experience (331).

Another possible limitation of the injection method is that it may not be useful for research in infarcted hearts. Infarcted hearts have areas of thin scar tissue that can be ruptured (332), suggesting that the injection-isolation method may be too harsh for such tissue. Therefore, practical assessment of the injection-

isolation method on infarcted mouse hearts is imperative in order to establish the methods suitability under those circumstances.

6. Overall discussion

6.1. General outcomes

The primary aim of this thesis was to assess sodium channel biophysical properties in the atria compared to the ventricles, interpreting the physiological significance of chamber electrophysiological distinctions. These investigations were performed using isolated LA and LV cardiomyocytes and also examined the inhibition efficacy of flecainide as a sodium channel blocking AAD between the different chambers.

The main outcomes of this thesis are summarised below:

- Mouse LA I_{Na} density was smaller than LV I_{Na} density at physiological RMP, due to chamber distinctions in channel voltage dependence of inactivation. The mechanism causative of the distinctions in gating kinetics has been suggested to be due to chamber differences in expression of $Na_v\beta_2$ and $Na_v\beta_4$ (4, 5, 142, 185, 186) and these differences are also observed between mouse LA and LV within this study. However, human diseased LA and LV presented opposing $Na_v\beta_2$ expression distinctions.
- Flecainide demonstrated more potent inhibition of LA sodium channels than LV sodium channels likely due to distinctions in channel gating

kinetics. Additionally, the difference in inhibition efficacy would be expected to be even greater *in vivo* due to distinctions in physiological RMP between the chambers.

- There was no physiological difference between mouse Plako^{+/-} LA and LV I_{Na} density. This is likely due to the chamber distinctions in channel gating kinetics being evident but reduced between Plako^{+/-} LA and LV, compared to WT counterparts. Additionally, there was enhanced flecainide I_{Na} inhibition in the Plako^{+/-} LV compared to WT LV, with no difference in flecainide efficacy between the Plako^{+/-} chambers.
- The novel injection-based isolation method described in this thesis provided cardiomyocytes that were comparable to those isolated using the Langendorff-based method. This established a convenient mouse cardiomyocyte isolation method.

6.2. Physiological relevance of I_{Na} distinctions between the LA and LV

A key finding in this study is that mouse LA I_{Na} density is smaller than LV I_{Na} density at physiological holding potentials, due to differences in the inactivation gating kinetics between the chambers that has also been described by others (4, 5, 142, 185, 186). The relationship between channel inactivation kinetics and effect on current density at physiological holding potentials has not previously

been acknowledged when comparing I_{Na} between mammalian LA and LV. Former studies have described LA I_{Na} density as greater than that of the LV (4, 5, 142, 185, 186), without recognising that experiments which rely on hyperpolarised potentials do not provide *in vivo* representation.

Therefore, patch clamp experiments measuring I_{Na} at hyperpolarised potentials offer physiologically irrelevant information in terms of I_{Na} density, as holding potential greatly alters channel gating kinetics and absolute currents. This also dispels the lack of correlation with V_{max} findings; supporting the established understanding that V_{max} is greater in the mammalian LV than LA (31-34, 193, 194). Greater understanding of physiological LA I_{Na} is vital in order to improve pharmacological AF therapy and highlights the importance of consideration of physiological conditions.

6.3. Importance of LA I_{Na} distinctions as potential atrial-specific drug target

AF is the most common sustained cardiac arrhythmia in clinical practice (99), suggesting that the atria are more susceptible to arrhythmia than the ventricles. In depth understanding of atrial sodium channel distinctions could prove key to understanding the atria's increased susceptibility to arrhythmia. This thesis highlights several atrial sodium channel kinetic distinctions that may enhance arrhythmia occurrence within the atria.

Physiologically smaller LA I_{Na} may lead to reduced CV, which as previously described, can be proarrhythmic (1). Secondly, the negatively shifted inactivation of LA sodium channels suggests that depolarisation of the RMP as a result of medication, ischemia or hypoxia (212), would have a greater impact on reducing atrial peak I_{Na} . This again could lead to reduction in CV, potentially leading to arrhythmia generation (213). Additionally, the negatively shifted sodium channel activation of the atria compared to the ventricles, could indicate that the atrial sodium channels are more sensitive to untimely depolarisation of membrane potential. Therefore, atrial sodium channels may be more susceptible to premature activation and subsequent arrhythmias (216). Finally, the slower recovery time of the sodium channels may also be considered proarrhythmic, also due to potentially slower CV (98). Therefore, pharmacological alteration of atrial sodium channel kinetics could reduce the likelihood of arrhythmia generation/propagation. Consequently, identifying the molecular determinants driving distinctive atrial sodium channel activation, inactivation and recovery, may reveal novel drug targets for treatment and/or prevention of AF.

As described within this thesis, LA sodium channels may be less likely to reactivate prematurely as hyperpolarisation is required for sodium channels to convert from the inactivated state and be available for reactivation. Additionally, slower sodium channel recovery would hinder channel reopening during

repolarisation. Therefore, atria may display negligible or smaller $I_{Na,late}$ compared to the ventricles and this may be considered as cardioprotective. However, this is contradicted by previous studies that have demonstrated ranolazine, an $I_{Na,late}$ blocker, as an effective AF treatment (204-207). Consequently, further investigation is required in order to assess $I_{Na,late}$ in the atrial and ventricular chambers.

Due to the negative shift in LA sodium channel inactivation a greater proportion of the channels remain in the inactivated (closed) state compared to those of the LV. It is this property that perhaps makes LA sodium channels more sensitive to flecainide inhibition, as inactivated channels are more susceptible to blockade (7).

Greater understanding of the VGSC gating kinetics could highlight a target for the development of atrial specific AADs that only inhibit sodium channels that display atrial specific kinetic properties. As it was determined in this study and by others (4, 5, 142, 185, 186), atrial sodium channels are distinctive in terms of kinetics so it is feasible that they could be specifically targeted. Existing studies with several AADs have found that sodium channels in atrial cardiomyocytes/tissue are more sensitive to blockade than ventricular sodium channels (4, 5, 142, 185), as with flecainide in this study. However, none of those studies were able to identify a drug that had no inhibitory effect on the LV sodium channels. Therefore, the properties that render the atrial sodium

channels more susceptible to blockade could be more specifically targeted, avoiding any inhibition of ventricular sodium channels.

Furthermore, in this study it was confirmed that $\text{Na}_v\beta 2$ and $\text{Na}_v\beta 4$ expression is lower in the mouse LA than LV. This was supported by lower SCN4B mRNA expression and trend for lower SCN2B mRNA expression in the healthy human LA compared to the LV. This is comparable to protein expression findings reported by others in rat myocardial tissue and in healthy human tissue (4). Chen et al., presented data supporting a hypothesis that lower expression of $\text{Na}_v\beta 2$ and $\text{Na}_v\beta 4$ subunits in atrial cardiomyocytes may be responsible for the negative shift in activation, negative shift in inactivation and slower recovery of the LA sodium channels (4). Therefore, $\text{Na}_v\beta 2$ and $\text{Na}_v\beta 4$ may be the molecular determinants driving distinctive atrial sodium channel gating kinetics and could potentially provide novel drug targets for treatment of AF in patients.

However, it has been well documented that the co-expression of the other $\text{Na}_v\beta$ -subunits alongside $\text{Na}_v\beta 2$ and $\text{Na}_v\beta 4$ can cause further changes in channel gating kinetics (236, 238, 240, 241). Therefore, the effects of the other β -subunits on sodium channel function, and how all of the β -subunits interact with each other should be considered. Additionally, there is a lot of inconsistency in published data on the role of the $\text{Na}_v\beta 2$ and $\text{Na}_v\beta 4$, with opposing information on whether/how the subunits affect sodium channel gating kinetics (4, 64, 232-238). Consequently, more research is essential to form a definitive conclusion

on whether the lower expression of $\text{Na}_v\beta 2$ and $\text{Na}_v\beta 4$ in the LA is causative of kinetic distinctions and whether they are subsequently suitable atrial specific drug targets for AF treatment. Therefore, electrophysiological experiments examining the $\text{Na}_v 1.5$ current kinetics with and without the $\text{Na}_v\beta 2$ and $\text{Na}_v\beta 4$ individually and in combination are imperative in order to make definitive conclusions on the regulation of sodium channels by the β -subunits.

6.4. Significance of greater $\text{Na}_v\beta 2$ expression in diseased human LA

This thesis reveals increased $\text{Na}_v\beta 2$ in diseased human LA compared to healthy human LA. According to the hypothesis that lower expression of $\text{Na}_v\beta 2$ in the LA results in distinctive sodium channel gating kinetics compared to the LV (4), the diseased human LA may present with a more ventricular sodium channel phenotype.

Consequently, diseased atrial sodium channels may activate and inactivate at more positive potentials and have faster recovery. More positive activation could result in a reduction in the excitability of diseased LA cardiomyocytes and could be cardioprotective against premature initiation of sodium channels with minor depolarisation, inhibiting arrhythmia generation (216). However, a positive shift in activation could also lead to reduced I_{Na} as the threshold potential for activation is increased, with the proarrhythmic reduction in CV (1). Nevertheless, there may also be a positive shift in inactivation if the diseased LA present with a more LV phenotype. This could result in an increased I_{Na}

density *in vivo*, increasing CV and reducing the likelihood of arrhythmia generation (1). Proarrhythmic $I_{Na,late}$ may also be increased or decreased in diseased atria compared to healthy atria, if increased $Na_v\beta 2$ expression does alter gating kinetics. Overall, due to the many electrophysiological possibilities, further research is fundamental in order to directly compare the sodium channel gating kinetics between healthy and diseased LA.

6.5. Importance of no difference in I_{Na} density between Plako^{+/-} LA and LV

The observed smaller peak I_{Na} in WT LA compared to WT LV at a physiological holding potential is not apparent between the Plako^{+/-} LA and LV. Plako^{+/-} LA I_{Na} initiated from -75mV is no different to that of the Plako^{+/-} LV, also no differences were observed at any other holding potential. The slight positive shift in Plako^{+/-} LA sodium channel inactivation compared to that of the WT LA, could account for the lack of difference seen in the I_{Na} density between the Plako^{+/-} LA and LV. Therefore, amplified I_{Na} could be a causal factor of the increased atrial arrhythmia generation in endurance-trained mice with plakoglobin deficiency (259, 260). A slight increase of I_{Na} in the Plako^{+/-} LA could result in enhanced $I_{Na,late}$ which, combined with exercise and resulting increased cyclic adenosine monophosphate levels, could lead to intracellular Ca^{+} overload (262, 263). This could potentially predict increased AF vulnerability due to stress-induced triggered activity in plakoglobin deficient athletes.

Furthermore, no peak I_{Na} difference was observed between WT and Plako^{+/-} LV. This opposes the theory that ARVC patients with plakoglobin deficiency and associated reduction in LV Na_v1.5 expression (179, 180) would experience a proarrhythmic reduction of I_{Na} . Consequently, it must also be assessed whether the reduction in LV and RV Na_v1.5 expression, observed in ARVC plakoglobin deficient patients, is conserved in the mouse model. Alternatively, upregulation of other sodium channel isoforms may contribute to the I_{Na} in plakoglobin deficient hearts, as current density is not altered. Therefore, if Na_v1.5 expression is reduced in mouse Plako^{+/-} ventricles compared to WT ventricles, the expression of other sodium channel isoforms must also be assessed, in both the Plako^{+/-} mouse and plakoglobin deficient ARVC patients.

6.6. Flecainide has no differential inhibition between Plako^{+/-} LA and

LV

Unlike between WT LA and LV, there is no difference in % inhibition of I_{Na} between Plako^{+/-} LA and LV. This is due to 10.21% greater inhibition of Plako^{+/-} LV sodium channels compared to WT LV sodium channels. This is likely primarily due the reduced differences in channel gating kinetics between the Plako^{+/-} LA and LV, compared to between WT counterparts. Whether, altered expression of beta subunits plays a role in flecainide sensitivity is unclear and should be examined in future studies. Although ARVC patients can present with increased AF risk (258), ventricular arrhythmias are the primary clinical observation. Therefore, ARVC patients with plakoglobin deficiency would

benefit from the greater inhibition of LV I_{Na} with flecainide, as both ventricular and atrial arrhythmias could be suppressed simultaneously to the same degree.

6.7. Impact of a simplified Langendorff-free isolation method that produces high yields of viable mouse cardiomyocytes

The injection method enables simpler and cheaper cell isolation, with the ability to maintain a sterile environment, where isolated cells are required for culturing. Additionally, as the Langendorff apparatus is not utilised in this method, the likelihood of errors resulting from incorrect cannulation and/or mounting of the heart, introduction of air, blood coagulation and ischemia are also reduced (183).

An important conclusion of this study is the capability of the injection-isolation method to supply high yields of viable cardiomyocytes. The novel Langendorff-free isolation protocol has proven to be a valuable method for obtaining mouse cardiomyocytes that are comparable in physiological health and responsiveness. Crucially, the injection-isolated cardiomyocytes displayed; typical Ca^{+} handling properties, responses to electrical stimulation, amenability to patch clamping and stress-dependent hypertrophic signalling cascades, compared to published data and in direct comparison with Langendorff isolated cardiomyocytes. Therefore, the data presented within this study can provide reassurance to current or perspective users of this isolation method. Overall,

the injection-isolation method removes technical and logistical obstacles to cardiac studies, potentially expanding and accelerating innovative research within this field. Whether the methodology can be applied for isolation of cells from the post-infarcted hearts with large scars, thin myocardium that is susceptible to rupture due to high pressure needs to be examined.

6.8. Study limitations

6.8.1. General limitations

All experiments described within this thesis were performed *in vitro*, in isolated cardiomyocytes or cardiac tissue following surgical isolation of the intact heart from the mouse. Therefore, the heart could have been exposed to short periods of ischemia, hypoxia, acidosis and protein degradation, potentially affecting experimental outcomes (333-336). In order to limit the likelihood of tissue/cell impairment, isolation was carried out as rapidly as possible.

Additionally, the majority of the data within this thesis was obtained using a mouse model. The mouse cardiac electrophysiology (i.e. heart rate, absence of I_{Kr} and I_{Ks} and contractility force frequency) differs to that of the human heart. Therefore, translational aspects must be interpreted with caution. However, human heart tissue availability is very limited and exhibits great variability (337) and the mouse model does offer many benefits described within this study.

6.8.2. Patch clamp limitations

Attention to temperature and patch clamp protocol conditions is important when designing experiments, in order to determine accurate I_{Na} properties. It is beneficial to measure sodium channel properties using hyperpolarised potentials in patch clamp protocols as current is amplified and distinctions are easier to observe/analyse. This is shown in Figure 3.2 of this thesis, where I_{Na} density decreases as the holding potential becomes depolarised. However, as also demonstrated within this thesis, holding potential of cardiomyocytes has a great effect on the current kinetics observed. Therefore, it would be beneficial to measure peak I_{Na} , inactivation, activation and recovery kinetics of the channels, with patch clamp protocols that are more representative of *in vivo* electrophysiological conditions. For example, when assessing the I/V relationship, the holding potential of the cardiomyocytes could be paired to physiological holding potential *in vivo*, -80 to -90mV for LV and -60 to -80mV for LA cardiomyocytes (19, 20). This would provide physiologically relevant voltage dependence of activation data.

Similarly, when quantifying the voltage dependence of inactivation and recovery time, the potential that is used to stimulate peak I_{Na} could originate from a holding potential that is representative of cardiomyocytes *in vivo* RMP. Therefore, it would be advantageous to this study and all I_{Na} patch clamp studies, that physiologically relevant protocols were also completed. However, this would serve as a great logistical obstacle as it would require experiments to

be much longer and it is difficult to ensure cardiomyocytes remain healthy over prolonged electrophysiological experimentation. This would likely require more experiments to be run in order to achieve a substantial data set, proving a logistical and financial burden to this study.

Likewise, it has been demonstrated that temperature has an effect on the gating kinetics of VGSCs (338-340), potentially inducing differing effects on VGSCs between the LA and LV chambers. Consequently, it would be preferable for experiments to be completed at physiological temperature (36.5–37.5°C), requiring water baths to heat patch clamp solutions. However, patch clamp experiments within this thesis were carried out at room temperature and this must be considered a limitation of this study.

6.8.3. Western blot limitations

There was limited choice of Na_v1.5 antibodies, with the only antibody that worked (Alomone, ASC-005) consistently displaying multiple bands on the blots. Similarly, no measurement of Na_vβ1 or Na_vβ3 expression was made, as antibodies consistently did not yield any data.

Additionally, due to time constraints and difficulty with method optimisation, neither Na_v1.5 or Na_vβ4 expression was measured in diseased human LA and LV. Likewise, limited human healthy LV tissue means that it was not possible to

compare $\text{Na}_v1.5$ or β -subunits between diseased LV and healthy LV or healthy LA.

6.9. Future experiments

6.9.1. Electrophysiology experiments

In view of the results from this thesis a key investigation would be to perform additional patch clamp experiments measuring I_{Na} and flecainide inhibition in mouse LA and LV cardiomyocytes under more physiological conditions. This would include ensuring patch clamp solutions were kept at 36.5–37.5°C and chamber specific *in vivo* RMP was considered when designing all protocols (as described above). This would provide more physiologically relevant data.

It would also be interesting to measure the I_{Na} in the LA and LV from a diseased mouse model. This would assess whether the increased expression of $\text{Na}_v\beta2$ observed in diseased human LA affects channel gating kinetics as suggested. Additionally, examining flecainide inhibition would be beneficial in order to assess whether increase in LA $\text{Na}_v\beta2$ would reduce drug efficacy, if channels do exhibit LV gating kinetics. Firstly, additional Western blot experiments would be required in order to determine whether $\text{Na}_v\beta2$ expression is increased in the diseased mouse LA compared to WT LA in accordance with human data.

Patch clamp experiments measuring $I_{Na,late}$ in WT LA and LV cardiomyocytes would also offer insight into whether differences in channel gating kinetics result in differential $I_{Na,late}$, as hypothesised above. If sizeable $I_{Na,late}$ was measured in both chambers, the addition of a $I_{Na,late}$ inhibitor, such as ranolazine, would also reveal whether differences in gating kinetics affect drug efficacy.

Experiments measuring I_{Na} in HEK293 cells expressing $Na_v1.5$ with different combinations of the $Na_v\beta$ -subunits and then each $Na_v\beta$ -subunit individually, would provide definitive information of the effect of each of the subunits on gating kinetics and also consider interactions between the subunits. This would aim to determine whether differential expression of $Na_v\beta2$ and $Na_v\beta4$ between the LA and LV does regulate differences in channel gating kinetics.

6.9.2. Molecular experiments

Measurement of $Na_v\beta1$ and $Nav\beta3$ in WT LA and LV would offer a more conclusive study on the comparisons of the β -subunits. Likewise, expression of $Na_v\beta1$ and $Na_v\beta3$ between human diseased LA and LV would also make the study more comprehensive. Additionally, it is essential that $Na_v\beta1$, $Na_v\beta3$ and most notably $Na_v\beta4$ expression be compared between the healthy human LA and diseased LA, preferably also compared in diseased and healthy human LV samples, in order to complete the data set.

As described above, Western blot experiments would be required in order to determine whether $\text{Na}_v\beta 2$ expression is increased in the diseased mouse LA compared to WT LA in accordance with the human data.

Measurement of the expression of $\text{Na}_v 1.5$ in $\text{Plako}^{+/-}$ ventricles compared to WT ventricles would establish whether the observed reduction in ventricular $\text{Na}_v 1.5$ expression in plakoglobin deficient ARVC patients is conserved in the mouse model (179, 180). If expression of $\text{Na}_v 1.5$ is reduced in the $\text{Plako}^{+/-}$ mouse model, measurement of other sodium channel isoforms could aim to understand the lack of difference in I_{Na} between WT and $\text{Plako}^{+/-}$ LV.

References

1. Luo CH, Rudy Y. A dynamic model of the cardiac ventricular action potential. I. Simulations of ionic currents and concentration changes. *Circ Res.* 1994;74(6):1071-96.
2. Bers DM, Barry WH, Despa S. Intracellular Na⁺ regulation in cardiac myocytes. *Cardiovasc Res.* 2003;57(4):897-912.
3. Coppini R, Ferrantini C, Mazzoni L, Sartiani L, Olivotto I, Poggesi C, et al. Regulation of intracellular Na⁽⁺⁾ in health and disease: pathophysiological mechanisms and implications for treatment. *Glob Cardiol Sci Pract.* 2013;2013(3):222-42.
4. Chen KH, Xu XH, Sun HY, Du XL, Liu H, Yang L, et al. Distinctive property and pharmacology of voltage-gated sodium current in rat atrial vs ventricular myocytes. *Heart Rhythm.* 2016;13(3):762-70.
5. Caves RE, Cheng H, Choisy SC, Gadeberg HC, Bryant SM, Hancox JC, et al. Atrial-ventricular differences in rabbit cardiac voltage-gated Na⁽⁺⁾ currents: Basis for atrial-selective block by ranolazine. *Heart Rhythm.* 2017;14(11):1657-64.
6. Goodrow RJ, Jr., Desai S, Treat JA, Panama BK, Desai M, Nesterenko VV, et al. Biophysical comparison of sodium currents in native cardiac myocytes and human induced pluripotent stem cell-derived cardiomyocytes. *J Pharmacol Toxicol Methods.* 2018;90:19-30.
7. Zimetbaum P. Antiarrhythmic drug therapy for atrial fibrillation. *Circulation.* 2012;125(2):381-9.
8. Laizzo PA. Part II. Anatomy of the Human Heart. 3rd ed: Springer International Publishing; 2015.
9. Walker BR, Colledge NR, Ralston S, Penman ID, Britton R. Davidson's principles and practice of medicine 2014.
10. Guyton ACH, J.E. Textbook of Medical Physiology. 10th ed. Saunders, editor 2000.
11. Laks MM, Nisenson MJ, Swan HJ. Myocardial cell and sarcomere lengths in the normal dog heart. *Circ Res.* 1967;21(5):671-8.
12. Garrod D, Chidgey M. Desmosome structure, composition and function. *Biochim Biophys Acta.* 2008;1778(3):572-87.
13. Dibb KM, Clarke JD, Horn MA, Richards MA, Graham HK, Eisner DA, et al. Characterization of an extensive transverse tubular network in sheep atrial myocytes and its depletion in heart failure. *Circ Heart Fail.* 2009;2(5):482-9.
14. Severs NJ. The cardiac muscle cell. *Bioessays.* 2000;22(2):188-99.
15. Bird SD, Doevendans PA, van Rooijen MA, Brutel de la Riviere A, Hassink RJ, Passier R, et al. The human adult cardiomyocyte phenotype. *Cardiovasc Res.* 2003;58(2):423-34.
16. Davies MJ, Anderson RH, Becker AE. The conduction system of the heart 1983.
17. Feher J. Quantitative Human Physiology. 2nd ed: Academic Press; 2012.

18. Grandi E, Sanguinetti MC, Bartos DC, Bers DM, Chen-Izu Y, Chiamvimonvat N, et al. Potassium channels in the heart: structure, function and regulation. *J Physiol*. 2017;595(7):2209-28.
19. Gelband H, Bush HL, Rosen MR, Myerburg RJ, Hoffman BF. Electrophysiologic properties of isolated preparations of human atrial myocardium. *Circ Res*. 1972;30(3):293-300.
20. Shibata EF, Drury T, Refsum H, Aldrete V, Giles W. Contributions of a transient outward current to repolarization in human atrium. *Am J Physiol*. 1989;257(6 Pt 2):H1773-81.
21. Nerbonne JM, Kass RS. Molecular physiology of cardiac repolarization. *Physiol Rev*. 2005;85(4):1205-53.
22. Joung B, Chen PS, Lin SF. The role of the calcium and the voltage clocks in sinoatrial node dysfunction. *Yonsei Med J*. 2011;52(2):211-9.
23. Klabunde RE. *Cardiovascular physiology concepts* 2012.
24. Gaborit N, Le Bouter S, Szuts V, Varro A, Escande D, Nattel S, et al. Regional and tissue specific transcript signatures of ion channel genes in the non-diseased human heart. *J Physiol*. 2007;582(Pt 2):675-93.
25. Patel SP, Campbell DL. Transient outward potassium current, 'I_{to}', phenotypes in the mammalian left ventricle: underlying molecular, cellular and biophysical mechanisms. *J Physiol*. 2005;569(Pt 1):7-39.
26. Grant AO. Cardiac ion channels. *Circ Arrhythm Electrophysiol*. 2009;2(2):185-94.
27. Bartos DC, Grandi E, Ripplinger CM. Ion Channels in the Heart. *Compr Physiol*. 2015;5(3):1423-64.
28. Oudit GYB, P.H. *Cardiac Electrophysiology*. 7th ed 2018.
29. Salama G, London B. Mouse models of long QT syndrome. *J Physiol*. 2007;578(Pt 1):43-53.
30. Nerbonne JM. Studying cardiac arrhythmias in the mouse--a reasonable model for probing mechanisms? *Trends Cardiovasc Med*. 2004;14(3):83-93.
31. Amos GJ, Wettwer E, Metzger F, Li Q, Himmel HM, Ravens U. Differences between outward currents of human atrial and subepicardial ventricular myocytes. *J Physiol*. 1996;491 (Pt 1):31-50.
32. Wang Y, Xu H, Kumar R, Tipparaju SM, Wagner MB, Joyner RW. Differences in transient outward current properties between neonatal and adult human atrial myocytes. *J Mol Cell Cardiol*. 2003;35(9):1083-92.
33. Grandi E, Pasqualini FS, Bers DM. A novel computational model of the human ventricular action potential and Ca transient. *J Mol Cell Cardiol*. 2010;48(1):112-21.
34. O'Hara T, Virag L, Varro A, Rudy Y. Simulation of the undiseased human cardiac ventricular action potential: model formulation and experimental validation. *PLoS Comput Biol*. 2011;7(5):e1002061.
35. Wettwer E, Hala O, Christ T, Heubach JF, Dobrev D, Knaut M, et al. Role of I_{Kur} in controlling action potential shape and contractility in the human atrium: influence of chronic atrial fibrillation. *Circulation*. 2004;110(16):2299-306.
36. Bers DM. *Cardiac Electrophysiology: Excitation-Contraction Coupling*. 6th ed 2014.

37. Bers DM. Excitation-Contraction Coupling and Cardiac Contractile Force 2001.
38. Scheuer J, Bhan AK. Cardiac contractile proteins. Adenosine triphosphatase activity and physiological function. *Circ Res.* 1979;45(1):1-12.
39. Eisner DA, Caldwell JL, Kistamás K, Trafford AW. Calcium and Excitation-Contraction Coupling in the Heart 2017.
40. Bers DM. Cardiac excitation-contraction coupling. *Nature.* 2002;415(6868):198-205.
41. Wu ML, Vaughan-Jones RD. Interaction between Na⁺ and H⁺ ions on Na-H exchange in sheep cardiac Purkinje fibers. *J Mol Cell Cardiol.* 1997;29(4):1131-40.
42. Palty R, Silverman WF, Hershfinkel M, Caporale T, Sensi SL, Parnis J, et al. NCLX is an essential component of mitochondrial Na⁺/Ca²⁺ exchange. *Proc Natl Acad Sci U S A.* 2010;107(1):436-41.
43. Numata M, Petrecca K, Lake N, Orlowski J. Identification of a mitochondrial Na⁺/H⁺ exchanger. *J Biol Chem.* 1998;273(12):6951-9.
44. Dhar Malhotra J, Chen C, Rivolta I, Abriel H, Malhotra R, Mattei LN, et al. Characterization of sodium channel alpha- and beta-subunits in rat and mouse cardiac myocytes. *Circulation.* 2001;103(9):1303-10.
45. Wang Q, Li Z, Shen J, Keating MT. Genomic organization of the human SCN5A gene encoding the cardiac sodium channel. *Genomics.* 1996;34(1):9-16.
46. Balser JR. The cardiac sodium channel: gating function and molecular pharmacology. *J Mol Cell Cardiol.* 2001;33(4):599-613.
47. Catterall WA, Goldin AL, Waxman SG. International Union of Pharmacology. XLVII. Nomenclature and structure-function relationships of voltage-gated sodium channels. *Pharmacol Rev.* 2005;57(4):397-409.
48. Mishra S, Reznikov V, Maltsev VA, Undrovinas NA, Sabbah HN, Undrovinas A. Contribution of sodium channel neuronal isoform Nav1.1 to late sodium current in ventricular myocytes from failing hearts. *J Physiol.* 2015;593(6):1409-27.
49. Zimmer T, Haufe V, Blechschmidt S. Voltage-gated sodium channels in the mammalian heart. *Glob Cardiol Sci Pract.* 2014;2014(4):449-63.
50. Maier SK, Westenbroek RE, McCormick KA, Curtis R, Scheuer T, Catterall WA. Distinct subcellular localization of different sodium channel alpha and beta subunits in single ventricular myocytes from mouse heart. *Circulation.* 2004;109(11):1421-7.
51. Maier SK, Westenbroek RE, Schenkman KA, Feigl EO, Scheuer T, Catterall WA. An unexpected role for brain-type sodium channels in coupling of cell surface depolarization to contraction in the heart. *Proc Natl Acad Sci U S A.* 2002;99(6):4073-8.
52. Anyukhovskiy EP, Sosunov EA, Kryukova YN, Prestia K, Ozgen N, Rivaud M, et al. Expression of skeletal muscle sodium channel (Nav1.4) or connexin32 prevents reperfusion arrhythmias in murine heart. *Cardiovasc Res.* 2011;89(1):41-50.
53. Brackenbury WJ, Isom LL. Na Channel beta Subunits: Overachievers of the Ion Channel Family. *Front Pharmacol.* 2011;2:53.

54. Remme CA, Bezzina CR. Sodium channel (dys)function and cardiac arrhythmias. *Cardiovasc Ther.* 2010;28(5):287-94.
55. Ruan Y, Liu N, Priori SG. Sodium channel mutations and arrhythmias. *Nat Rev Cardiol.* 2009;6(5):337-48.
56. Oelstrom K, Goldschen-Ohm MP, Holmgren M, Chanda B. Evolutionarily conserved intracellular gate of voltage-dependent sodium channels. *Nat Commun.* 2014;5:3420.
57. Catterall WA. Structure and function of voltage-gated sodium channels at atomic resolution. *Exp Physiol.* 2014;99(1):35-51.
58. Motoike HK, Liu H, Glaaser IW, Yang AS, Tateyama M, Kass RS. The Na⁺ channel inactivation gate is a molecular complex: a novel role of the COOH-terminal domain. *J Gen Physiol.* 2004;123(2):155-65.
59. George AL, Jr. Inherited disorders of voltage-gated sodium channels. *J Clin Invest.* 2005;115(8):1990-9.
60. Rook MB, Evers MM, Vos MA, Bierhuizen MF. Biology of cardiac sodium channel Nav1.5 expression. *Cardiovasc Res.* 2012;93(1):12-23.
61. Isom LL, De Jongh KS, Patton DE, Reber BF, Offord J, Charbonneau H, et al. Primary structure and functional expression of the beta 1 subunit of the rat brain sodium channel. *Science.* 1992;256(5058):839-42.
62. Morgan K, Stevens EB, Shah B, Cox PJ, Dixon AK, Lee K, et al. beta 3: an additional auxiliary subunit of the voltage-sensitive sodium channel that modulates channel gating with distinct kinetics. *Proc Natl Acad Sci U S A.* 2000;97(5):2308-13.
63. Isom LL, Ragsdale DS, De Jongh KS, Westenbroek RE, Reber BF, Scheuer T, et al. Structure and function of the beta 2 subunit of brain sodium channels, a transmembrane glycoprotein with a CAM motif. *Cell.* 1995;83(3):433-42.
64. Yu FH, Westenbroek RE, Silos-Santiago I, McCormick KA, Lawson D, Ge P, et al. Sodium channel beta4, a new disulfide-linked auxiliary subunit with similarity to beta2. *J Neurosci.* 2003;23(20):7577-85.
65. Isom LL. Sodium channel beta subunits: anything but auxiliary. *Neuroscientist.* 2001;7(1):42-54.
66. Nuss HB, Chiamvimonvat N, Perez-Garcia MT, Tomaselli GF, Marban E. Functional association of the beta 1 subunit with human cardiac (hH1) and rat skeletal muscle (mu 1) sodium channel alpha subunits expressed in *Xenopus* oocytes. *J Gen Physiol.* 1995;106(6):1171-91.
67. Tan BH, Pundi KN, Van Norstrand DW, Valdivia CR, Tester DJ, Medeiros-Domingo A, et al. Sudden infant death syndrome-associated mutations in the sodium channel beta subunits. *Heart Rhythm.* 2010;7(6):771-8.
68. Olesen MS, Jespersen T, Nielsen JB, Liang B, Moller DV, Hedley P, et al. Mutations in sodium channel beta-subunit SCN3B are associated with early-onset lone atrial fibrillation. *Cardiovasc Res.* 2011;89(4):786-93.
69. Hakim P, Brice N, Thresher R, Lawrence J, Zhang Y, Jackson AP, et al. Scn3b knockout mice exhibit abnormal sino-atrial and cardiac conduction properties. *Acta Physiol (Oxf).* 2010;198(1):47-59.
70. Valdivia CR, Medeiros-Domingo A, Ye B, Shen WK, Algiers TJ, Ackerman MJ, et al. Loss-of-function mutation of the SCN3B-encoded sodium

channel β_3 subunit associated with a case of idiopathic ventricular fibrillation. *Cardiovasc Res*. 2010;86(3):392-400.

71. Medeiros-Domingo A, Kaku T, Tester DJ, Iturralde-Torres P, Itty A, Ye B, et al. SCN4B-encoded sodium channel β_4 subunit in congenital long-QT syndrome. *Circulation*. 2007;116(2):134-42.

72. Valdivia CR, Nagatomo T, Makielski JC. Late Na currents affected by α subunit isoform and β_1 subunit co-expression in HEK293 cells. *J Mol Cell Cardiol*. 2002;34(8):1029-39.

73. Bezzina CR, Rook MB, Groenewegen WA, Herfst LJ, van der Wal AC, Lam J, et al. Compound heterozygosity for mutations (W156X and R225W) in SCN5A associated with severe cardiac conduction disturbances and degenerative changes in the conduction system. *Circ Res*. 2003;92(2):159-68.

74. Lopez-Santiago LF, Meadows LS, Ernst SJ, Chen C, Malhotra JD, McEwen DP, et al. Sodium channel Scn1b null mice exhibit prolonged QT and RR intervals. *J Mol Cell Cardiol*. 2007;43(5):636-47.

75. Mishra S, Undrovinas NA, Maltsev VA, Reznikov V, Sabbah HN, Undrovinas A. Post-transcriptional silencing of SCN1B and SCN2B genes modulates late sodium current in cardiac myocytes from normal dogs and dogs with chronic heart failure. *Am J Physiol Heart Circ Physiol*. 2011;301(4):H1596-605.

76. Maltsev VA, Undrovinas AI. A multi-modal composition of the late Na⁺ current in human ventricular cardiomyocytes. *Cardiovasc Res*. 2006;69(1):116-27.

77. Undrovinas A, Maltsev VA. Late sodium current is a new therapeutic target to improve contractility and rhythm in failing heart. *Cardiovasc Hematol Agents Med Chem*. 2008;6(4):348-59.

78. Nicoll DA, Quednau BD, Qui Z, Xia YR, Lusk AJ, Philipson KD. Cloning of a third mammalian Na⁺-Ca²⁺ exchanger, NCX3. *J Biol Chem*. 1996;271(40):24914-21.

79. Quednau BD, Nicoll DA, Philipson KD. Tissue specificity and alternative splicing of the Na⁺/Ca²⁺ exchanger isoforms NCX1, NCX2, and NCX3 in rat. *Am J Physiol*. 1997;272(4 Pt 1):C1250-61.

80. Frank JS, Mottino G, Reid D, Molday RS, Philipson KD. Distribution of the Na⁽⁺⁾-Ca²⁺ exchange protein in mammalian cardiac myocytes: an immunofluorescence and immunocolloidal gold-labeling study. *J Cell Biol*. 1992;117(2):337-45.

81. Sipido KR, Acsai K, Antoons G, Bito V, Macquaide N. T-tubule remodelling and ryanodine receptor organization modulate sodium-calcium exchange. *Adv Exp Med Biol*. 2013;961:375-83.

82. Ottolia M, Torres N, Bridge JH, Philipson KD, Goldhaber JL. Na/Ca exchange and contraction of the heart. *J Mol Cell Cardiol*. 2013;61:28-33.

83. Ren X, Philipson KD. The topology of the cardiac Na⁽⁺⁾/Ca⁽²⁺⁾ exchanger, NCX1. *J Mol Cell Cardiol*. 2013;57:68-71.

84. Bridge JH, Smolley JR, Spitzer KW. The relationship between charge movements associated with I_{Ca} and I_{Na-Ca} in cardiac myocytes. *Science*. 1990;248(4953):376-8.

85. Reeves JP, Hale CC. The stoichiometry of the cardiac sodium-calcium exchange system. *J Biol Chem*. 1984;259(12):7733-9.

86. Hancox JC, Levi AJ. Na-Ca exchange tail current indicates voltage dependence of the Cai transient in rabbit ventricular myocytes. *J Cardiovasc Electrophysiol*. 1995;6(6):455-70.
87. Sipido KR, Volders PG, de Groot SH, Verdonck F, Van de Werf F, Wellens HJ, et al. Enhanced Ca(2+) release and Na/Ca exchange activity in hypertrophied canine ventricular myocytes: potential link between contractile adaptation and arrhythmogenesis. *Circulation*. 2000;102(17):2137-44.
88. Blanco G, Mercer RW. Isozymes of the Na-K-ATPase: heterogeneity in structure, diversity in function. *Am J Physiol*. 1998;275(5):F633-50.
89. Despa S, Bers DM. Na(+) transport in the normal and failing heart - remember the balance. *J Mol Cell Cardiol*. 2013;61:2-10.
90. Noguchi S, Mutoh Y, Kawamura M. The functional roles of disulfide bonds in the beta-subunit of (Na,K)ATPase as studied by site-directed mutagenesis. *FEBS Lett*. 1994;341(2-3):233-8.
91. Wang J, Schwinger RH, Frank K, Muller-Ehmsen J, Martin-Vasallo P, Pressley TA, et al. Regional expression of sodium pump subunits isoforms and Na⁺-Ca⁺⁺ exchanger in the human heart. *J Clin Invest*. 1996;98(7):1650-8.
92. McDonough AA, Velotta JB, Schwinger RH, Philipson KD, Farley RA. The cardiac sodium pump: structure and function. *Basic Res Cardiol*. 2002;97 Suppl 1:119-24.
93. Pavlovic D, Fuller W, Shattock MJ. The intracellular region of FXYD1 is sufficient to regulate cardiac Na/K ATPase. *FASEB J*. 2007;21(7):1539-46.
94. Han F, Bossuyt J, Despa S, Tucker AL, Bers DM. Phospholemman phosphorylation mediates the protein kinase C-dependent effects on Na⁺/K⁺ pump function in cardiac myocytes. *Circ Res*. 2006;99(12):1376-83.
95. Karmazyn M, Gan XT, Humphreys RA, Yoshida H, Kusumoto K. The myocardial Na(+) - H(+) exchange: structure, regulation, and its role in heart disease. *Circ Res*. 1999;85(9):777-86.
96. Orłowski J, Grinstein S. Na⁺/H⁺ exchangers of mammalian cells. *J Biol Chem*. 1997;272(36):22373-6.
97. Slepko E, Fliegel L. Structure and function of the NHE1 isoform of the Na⁺/H⁺ exchanger. *Biochem Cell Biol*. 2002;80(5):499-508.
98. Antzelevitch C, Burashnikov A. Overview of Basic Mechanisms of Cardiac Arrhythmia. *Card Electrophysiol Clin*. 2011;3(1):23-45.
99. Barra S, Fynn S. Untreated atrial fibrillation in the United Kingdom: Understanding the barriers and treatment options. *J Saudi Heart Assoc*. 2015;27(1):31-43.
100. Friberg J, Buch P, Scharling H, Gadsbøll N, Jensen GB. Rising rates of hospital admissions for atrial fibrillation. *Epidemiology*. 2003;14(6):666-72.
101. Mines G. On dynamic equilibrium of the heart. *J Physiol*. 1913;46:349-383.
102. Mines G. On circulating excitations in heart muscle and their possible relation to tachycardia and fibrillation. *Trans Roy Soc Can*. 1914;8:43-52.
103. Fenton FH, Cherry EM, Kornreich BG. Termination of equine atrial fibrillation by quinidine: an optical mapping study. *J Vet Cardiol*. 2008;10(2):87-103.
104. Einthoven W. Ueber die galvanometrische Registrierung des menschlichen Elektrokardiogramms, zugleich eine Beurtheilung der

- Anwendung des Capillar-Elektrometers in der Physiologie. Pflug Arch. 1903;99:472-80.
105. Camm AJ, Kirchhof P, Lip GY, Schotten U, Savelieva I, Ernst S, et al. Guidelines for the management of atrial fibrillation: the Task Force for the Management of Atrial Fibrillation of the European Society of Cardiology (ESC). *Europace*. 2010;12(10):1360-420.
106. Marijon E, Le Heuzey JY, Connolly S, Yang S, Pogue J, Brueckmann M, et al. Causes of Death and Influencing Factors in Patients with Atrial Fibrillation: A Competing Risk Analysis from the Randomized Evaluation of Long-Term Anticoagulant Therapy Study. *Circulation*. 2013;128(20):2192-201.
107. Kirchhof P, Breithardt G, Camm AJ, Crijns HJ, Kuck KH, Vardas P, et al. Improving outcomes in patients with atrial fibrillation: rationale and design of the Early treatment of Atrial fibrillation for Stroke prevention Trial. *Am Heart J*. 2013;166(3):442-8.
108. Nattel S, Hadjis T, Talajic M. The treatment of atrial fibrillation. An evaluation of drug therapy, electrical modalities and therapeutic considerations. *Drugs*. 1994;48(3):345-71.
109. Jahangir A, Lee V, Friedman PA, Trusty JM, Hodge DO, Kopecky SL, et al. Long-term progression and outcomes with aging in patients with lone atrial fibrillation: a 30-year follow-up study. *Circulation*. 2007;115(24):3050-6.
110. Wijffels MC, Kirchhof CJ, Dorland R, Allessie MA. Atrial fibrillation begets atrial fibrillation. A study in awake chronically instrumented goats. *Circulation*. 1995;92(7):1954-68.
111. Wyndham CR. Atrial fibrillation: the most common arrhythmia. *Tex Heart Inst J*. 2000;27(3):257-67.
112. Fabritz L, Guasch E, Antoniades C, Bardinet I, Benninger G, Betts TR, et al. Expert consensus document: Defining the major health modifiers causing atrial fibrillation: a roadmap to underpin personalized prevention and treatment. *Nat Rev Cardiol*. 2016;13(4):230-7.
113. DiFrancesco D. The role of the funny current in pacemaker activity. *Circ Res*. 2010;106(3):434-46.
114. Weiss JN, Garfinkel A, Karagueuzian HS, Chen PS, Qu Z. Early afterdepolarizations and cardiac arrhythmias. *Heart Rhythm*. 2010;7(12):1891-9.
115. Fink M, Noble PJ, Noble D. Ca(2+)-induced delayed afterdepolarizations are triggered by dyadic subspace Ca2(2+) affirming that increasing SERCA reduces aftercontractions. *Am J Physiol Heart Circ Physiol*. 2011;301(3):H921-35.
116. Comtois P, Kneller J, Nattel S. Of circles and spirals: bridging the gap between the leading circle and spiral wave concepts of cardiac reentry. *Europace*. 2005;7 Suppl 2:10-20.
117. Waks JW, Josephson ME. Mechanisms of Atrial Fibrillation - Reentry, Rotors and Reality. *Arrhythm Electrophysiol Rev*. 2014;3(2):90-100.
118. Iwasaki YK, Nishida K, Kato T, Nattel S. Atrial fibrillation pathophysiology: implications for management. *Circulation*. 2011;124(20):2264-74.

119. Wakili R, Voigt N, Kaab S, Dobrev D, Nattel S. Recent advances in the molecular pathophysiology of atrial fibrillation. *J Clin Invest*. 2011;121(8):2955-68.
120. Dobrev D, Nattel S. New antiarrhythmic drugs for treatment of atrial fibrillation. *Lancet*. 2010;375(9721):1212-23.
121. Winfree AT. Spiral waves of chemical activity. *Science*. 1972;175(4022):634-6.
122. Thomas D, Christ T, Fabritz L, Goette A, Hammwohner M, Heijman J, et al. German Cardiac Society Working Group on Cellular Electrophysiology state-of-the-art paper: impact of molecular mechanisms on clinical arrhythmia management. *Clin Res Cardiol*. 2019;108(6):577-99.
123. Zhang X, Ai X, Nakayama H, Chen B, Harris DM, Tang M, et al. Persistent increases in Ca(2+) influx through Cav1.2 shortens action potential and causes Ca(2+) overload-induced afterdepolarizations and arrhythmias. *Basic Res Cardiol*. 2016;111(1):4.
124. Zhang H, Garratt CJ, Zhu J, Holden AV. Role of up-regulation of IK1 in action potential shortening associated with atrial fibrillation in humans. *Cardiovasc Res*. 2005;66(3):493-502.
125. Darbar D, Kannankeril PJ, Donahue BS, Kucera G, Stubblefield T, Haines JL, et al. Cardiac sodium channel (SCN5A) variants associated with atrial fibrillation. *Circulation*. 2008;117(15):1927-35.
126. Moreno JD, Clancy CE. Pathophysiology of the cardiac late Na current and its potential as a drug target. *J Mol Cell Cardiol*. 2012;52(3):608-19.
127. Studenik CR, Zhou Z, January CT. Differences in action potential and early afterdepolarization properties in LQT2 and LQT3 models of long QT syndrome. *Br J Pharmacol*. 2001;132(1):85-92.
128. Woods CE, Olgin J. Atrial fibrillation therapy now and in the future: drugs, biologicals, and ablation. *Circ Res*. 2014;114(9):1532-46.
129. Davis EM, Packard KA, Knezevich JT, Campbell JA. New and emerging anticoagulant therapy for atrial fibrillation and acute coronary syndrome. *Pharmacotherapy*. 2011;31(10):975-1016.
130. Gage BF, van Walraven C, Pearce L, Hart RG, Koudstaal PJ, Boode BS, et al. Selecting patients with atrial fibrillation for anticoagulation: stroke risk stratification in patients taking aspirin. *Circulation*. 2004;110(16):2287-92.
131. Savelieva I, Kakouros N, Kourliouros A, Camm AJ. Upstream therapies for management of atrial fibrillation: review of clinical evidence and implications for European Society of Cardiology guidelines. Part II: secondary prevention. *Europace*. 2011;13(5):610-25.
132. Umana E, Solares CA, Alpert MA. Tachycardia-induced cardiomyopathy. *Am J Med*. 2003;114(1):51-5.
133. Camm AJ, Savelieva I, Lip GY, Guideline Development Group for the Ncgftmoaf. Rate control in the medical management of atrial fibrillation. *Heart*. 2007;93(1):35-8.
134. Anderson JL, Halperin JL, Albert NM, Bozkurt B, Brindis RG, Curtis LH, et al. Management of patients with atrial fibrillation (compilation of 2006 ACCF/AHA/ESC and 2011 ACCF/AHA/HRS recommendations): a report of the American College of Cardiology/American Heart Association Task Force on Practice Guidelines. *J Am Coll Cardiol*. 2013;61(18):1935-44.

135. Lei M, Wu L, Terrar DA, Huang CL. Modernized Classification of Cardiac Antiarrhythmic Drugs. *Circulation*. 2018;138(17):1879-96.
136. Pellman J, Sheikh F. Atrial fibrillation: mechanisms, therapeutics, and future directions. *Compr Physiol*. 2015;5(2):649-65.
137. Lip GY, Hee FL. Paroxysmal atrial fibrillation. *QJM*. 2001;94(12):665-78.
138. Pellman J, Sheikh F. A new mechanism links preamyloid oligomer formation in the myocyte stress response associated with atrial fibrillation. *J Mol Cell Cardiol*. 2015;80:110-3.
139. Ravens U, Wettwer E. Ultra-rapid delayed rectifier channels: molecular basis and therapeutic implications. *Cardiovasc Res*. 2011;89(4):776-85.
140. Machida T, Hashimoto N, Kuwahara I, Ogino Y, Matsuura J, Yamamoto W, et al. Effects of a highly selective acetylcholine-activated K⁺ channel blocker on experimental atrial fibrillation. *Circ Arrhythm Electrophysiol*. 2011;4(1):94-102.
141. Comtois P, Sakabe M, Vigmond EJ, Munoz M, Texier A, Shiroshita-Takeshita A, et al. Mechanisms of atrial fibrillation termination by rapidly unbinding Na⁺ channel blockers: insights from mathematical models and experimental correlates. *Am J Physiol Heart Circ Physiol*. 2008;295(4):H1489-504.
142. Burashnikov A, Di Diego JM, Zygmunt AC, Belardinelli L, Antzelevitch C. Atrium-selective sodium channel block as a strategy for suppression of atrial fibrillation: differences in sodium channel inactivation between atria and ventricles and the role of ranolazine. *Circulation*. 2007;116(13):1449-57.
143. Carlsson J, Miketic S, Windeler J, Cuneo A, Haun S, Micus S, et al. Randomized trial of rate-control versus rhythm-control in persistent atrial fibrillation: the Strategies of Treatment of Atrial Fibrillation (STAF) study. *J Am Coll Cardiol*. 2003;41(10):1690-6.
144. Hohnloser SH, Kuck KH, Lilienthal J. Rhythm or rate control in atrial fibrillation--Pharmacological Intervention in Atrial Fibrillation (PIAF): a randomised trial. *Lancet*. 2000;356(9244):1789-94.
145. Roy D, Talajic M, Nattel S, Wyse DG, Dorian P, Lee KL, et al. Rhythm control versus rate control for atrial fibrillation and heart failure. *N Engl J Med*. 2008;358(25):2667-77.
146. Wyse DG, Waldo AL, DiMarco JP, Domanski MJ, Rosenberg Y, Schron EB, et al. A comparison of rate control and rhythm control in patients with atrial fibrillation. *N Engl J Med*. 2002;347(23):1825-33.
147. Campbell TJ. Subclassification of class I antiarrhythmic drugs: enhanced relevance after CAST. *Cardiovasc Drugs Ther*. 1992;6(5):519-28.
148. de Lera Ruiz M, Kraus RL. Voltage-Gated Sodium Channels: Structure, Function, Pharmacology, and Clinical Indications. *J Med Chem*. 2015;58(18):7093-118.
149. Apostolakis S, Oeff M, Tebbe U, Fabritz L, Breithardt G, Kirchhof P. Flecainide acetate for the treatment of atrial and ventricular arrhythmias. *Expert Opin Pharmacother*. 2013;14(3):347-57.
150. Alboni P, Botto GL, Baldi N, Luzi M, Russo V, Gianfranchi L, et al. Outpatient treatment of recent-onset atrial fibrillation with the "pill-in-the-pocket" approach. *N Engl J Med*. 2004;351(23):2384-91.

151. Hudak JM, Banitt EH, Schmid JR. Discovery and development of flecainide. *Am J Cardiol.* 1984;53(5):17B-20B.
152. Somani P. Antiarrhythmic effects of flecainide. *Clin Pharmacol Ther.* 1980;27(4):464-70.
153. Borgeat A, Goy JJ, Maendly R, Kaufmann U, Grbic M, Sigwart U. Flecainide versus quinidine for conversion of atrial fibrillation to sinus rhythm. *Am J Cardiol.* 1986;58(6):496-8.
154. Crijns HJ, van Wijk LM, van Gilst WH, Kingma JH, van Gelder IC, Lie KI. Acute conversion of atrial fibrillation to sinus rhythm: clinical efficacy of flecainide acetate. Comparison of two regimens. *Eur Heart J.* 1988;9(6):634-8.
155. Holmes B, Heel RC. Flecainide. A preliminary review of its pharmacodynamic properties and therapeutic efficacy. *Drugs.* 1985;29(1):1-33.
156. Andrikopoulos GK, Pastromas S, Tzeis S. Flecainide: Current status and perspectives in arrhythmia management. *World J Cardiol.* 2015;7(2):76-85.
157. Iwai T, Tanonaka K, Inoue R, Kasahara S, Motegi K, Nagaya S, et al. Sodium accumulation during ischemia induces mitochondrial damage in perfused rat hearts. *Cardiovasc Res.* 2002;55(1):141-9.
158. Morganroth J, Anderson JL, Gentzkow GD. Classification by type of ventricular arrhythmia predicts frequency of adverse cardiac events from flecainide. *J Am Coll Cardiol.* 1986;8(3):607-15.
159. Echt DS, Liebson PR, Mitchell LB, Peters RW, Obias-Manno D, Barker AH, et al. Mortality and morbidity in patients receiving encainide, flecainide, or placebo. The Cardiac Arrhythmia Suppression Trial. *N Engl J Med.* 1991;324(12):781-8.
160. Anderson JL, Gilbert EM, Alpert BL, Henthorn RW, Waldo AL, Bhandari AK, et al. Prevention of symptomatic recurrences of paroxysmal atrial fibrillation in patients initially tolerating antiarrhythmic therapy. A multicenter, double-blind, crossover study of flecainide and placebo with transtelephonic monitoring. Flecainide Supraventricular Tachycardia Study Group. *Circulation.* 1989;80(6):1557-70.
161. Kirchhof P, Andresen D, Bosch R, Borggrefe M, Meinertz T, Parade U, et al. Short-term versus long-term antiarrhythmic drug treatment after cardioversion of atrial fibrillation (Flec-SL): a prospective, randomised, open-label, blinded endpoint assessment trial. *Lancet.* 2012;380(9838):238-46.
162. Tamargo J, Caballero R, Gomez R, Valenzuela C, Delpon E. Pharmacology of cardiac potassium channels. *Cardiovasc Res.* 2004;62(1):9-33.
163. Kvam DC, Banitt EH, Schmid JR. Antiarrhythmic and electrophysiologic actions of flecainide in animal models. *Am J Cardiol.* 1984;53(5):22B-5B.
164. Liu N, Denegri M, Ruan Y, Avelino-Cruz JE, Perissi A, Negri S, et al. Short communication: flecainide exerts an antiarrhythmic effect in a mouse model of catecholaminergic polymorphic ventricular tachycardia by increasing the threshold for triggered activity. *Circ Res.* 2011;109(3):291-5.
165. Nabar A, Rodriguez LM, Timmermans C, Smeets JL, Wellens HJ. Radiofrequency ablation of "class IC atrial flutter" in patients with resistant atrial fibrillation. *Am J Cardiol.* 1999;83(5):785-7, A10.

166. Donovan KD, Power BM, Hockings BE, Dobb GJ, Lee KY. Intravenous flecainide versus amiodarone for recent-onset atrial fibrillation. *Am J Cardiol.* 1995;75(10):693-7.
167. Martinez-Marcos FJ, Garcia-Garmendia JL, Ortega-Carpio A, Fernandez-Gomez JM, Santos JM, Camacho C. Comparison of intravenous flecainide, propafenone, and amiodarone for conversion of acute atrial fibrillation to sinus rhythm. *Am J Cardiol.* 2000;86(9):950-3.
168. Boriani G, Biffi M, Capucci A, Botto G, Broffoni T, Ongari M, et al. Conversion of recent-onset atrial fibrillation to sinus rhythm: effects of different drug protocols. *Pacing Clin Electrophysiol.* 1998;21(11 Pt 2):2470-4.
169. Carunchio A, Fera MS, Mazza A, Burattini M, Greco G, Galati A, et al. [A comparison between flecainide and sotalol in the prevention of recurrences of paroxysmal atrial fibrillation]. *G Ital Cardiol.* 1995;25(1):51-68.
170. Chimienti M, Cullen MT, Jr., Casadei G. Safety of flecainide versus propafenone for the long-term management of symptomatic paroxysmal supraventricular tachyarrhythmias. Report from the Flecainide and Propafenone Italian Study (FAPIS) Group. *Eur Heart J.* 1995;16(12):1943-51.
171. Aliot E, Denjoy I. Comparison of the safety and efficacy of flecainide versus propafenone in hospital out-patients with symptomatic paroxysmal atrial fibrillation/flutter. The Flecainide AF French Study Group. *Am J Cardiol.* 1996;77(3):66A-71A.
172. Naccarelli GV, Dorian P, Hohnloser SH, Coumel P. Prospective comparison of flecainide versus quinidine for the treatment of paroxysmal atrial fibrillation/flutter. The Flecainide Multicenter Atrial Fibrillation Study Group. *Am J Cardiol.* 1996;77(3):53A-9A.
173. Hohnloser SH, Zabel M. Short- and long-term efficacy and safety of flecainide acetate for supraventricular arrhythmias. *Am J Cardiol.* 1992;70(5):3A-9A; discussion A-10A.
174. Aliot E, Capucci A, Crijns HJ, Goette A, Tamargo J. Twenty-five years in the making: flecainide is safe and effective for the management of atrial fibrillation. *Europace.* 2011;13(2):161-73.
175. Rampazzo A, Nava A, Malacrida S, Beffagna G, Bauce B, Rossi V, et al. Mutation in human desmoplakin domain binding to plakoglobin causes a dominant form of arrhythmogenic right ventricular cardiomyopathy. *Am J Hum Genet.* 2002;71(5):1200-6.
176. Gerull B, Heuser A, Wichter T, Paul M, Basson CT, McDermott DA, et al. Mutations in the desmosomal protein plakophilin-2 are common in arrhythmogenic right ventricular cardiomyopathy. *Nat Genet.* 2004;36(11):1162-4.
177. McKoy G, Protonotarios N, Crosby A, Tsatsopoulou A, Anastasakis A, Coonar A, et al. Identification of a deletion in plakoglobin in arrhythmogenic right ventricular cardiomyopathy with palmoplantar keratoderma and woolly hair (Naxos disease). *Lancet.* 2000;355(9221):2119-24.
178. Sato PY, Musa H, Coombs W, Guerrero-Serna G, Patino GA, Taffet SM, et al. Loss of plakophilin-2 expression leads to decreased sodium current and slower conduction velocity in cultured cardiac myocytes. *Circ Res.* 2009;105(6):523-6.

179. Noorman M, Hakim S, Kessler E, Groeneweg JA, Cox MG, Asimaki A, et al. Remodeling of the cardiac sodium channel, connexin43, and plakoglobin at the intercalated disk in patients with arrhythmogenic cardiomyopathy. *Heart Rhythm*. 2013;10(3):412-9.
180. Shaw RM. Reduced sodium channels in human ARVC. *Heart Rhythm*. 2013;10(3):420-1.
181. Kirchhof P, Fabritz L, Zwiener M, Witt H, Schafers M, Zellerhoff S, et al. Age- and training-dependent development of arrhythmogenic right ventricular cardiomyopathy in heterozygous plakoglobin-deficient mice. *Circulation*. 2006;114(17):1799-806.
182. Yu TY. *Optical Imaging of Cardiac Atrial Activation and Repolarisation in Genetically Altered Models: The University of Birmingham*; 2015.
183. Ackers-Johnson M, Li PY, Holmes AP, O'Brien SM, Pavlovic D, Foo RS. A Simplified, Langendorff-Free Method for Concomitant Isolation of Viable Cardiac Myocytes and Nonmyocytes From the Adult Mouse Heart. *Circ Res*. 2016;119(8):909-20.
184. Burashnikov A, Antzelevitch C. Atrial-selective sodium channel block for the treatment of atrial fibrillation. *Expert Opin Emerg Drugs*. 2009;14(2):233-49.
185. Burashnikov A, Di Diego JM, Sicouri S, Ferreiro M, Carlsson L, Antzelevitch C. Atrial-selective effects of chronic amiodarone in the management of atrial fibrillation. *Heart Rhythm*. 2008;5(12):1735-42.
186. Li GR, Lau CP, Shrier A. Heterogeneity of sodium current in atrial vs epicardial ventricular myocytes of adult guinea pig hearts. *J Mol Cell Cardiol*. 2002;34(9):1185-94.
187. Taylor AL. What we talk about when we talk about capacitance measured with the voltage-clamp step method. *J Comput Neurosci*. 2012;32(1):167-75.
188. Kaufmann SG, Westenbroek RE, Maass AH, Lange V, Renner A, Wischmeyer E, et al. Distribution and function of sodium channel subtypes in human atrial myocardium. *J Mol Cell Cardiol*. 2013;61:133-41.
189. Watanabe H, Yang T, Stroud DM, Lowe JS, Harris L, Atack TC, et al. Striking In vivo phenotype of a disease-associated human SCN5A mutation producing minimal changes in vitro. *Circulation*. 2011;124(9):1001-11.
190. Xu Q, Patel D, Zhang X, Veenstra RD. Changes in cardiac Nav1.5 expression, function, and acetylation by pan-histone deacetylase inhibitors. *Am J Physiol Heart Circ Physiol*. 2016;311(5):H1139-H49.
191. Wang N, Huo R, Cai B, Lu Y, Ye B, Li X, et al. Activation of Wnt/beta-catenin signaling by hydrogen peroxide transcriptionally inhibits Nav1.5 expression. *Free Radic Biol Med*. 2016;96:34-44.
192. labs A. Anti-Nav1.5 (SCN5A) (493-511) Antibody [updated 5 Feb 2019. Antibody data sheet]. Available from: <https://www.alomone.com/p/anti-nav1-5/ASC-005>.
193. Golod DA, Kumar R, Joyner RW. Determinants of action potential initiation in isolated rabbit atrial and ventricular myocytes. *Am J Physiol*. 1998;274(6):H1902-13.
194. Berecki G, Wilders R, de Jonge B, van Ginneken AC, Verkerk AO. Re-evaluation of the action potential upstroke velocity as a measure of the Na⁺

- current in cardiac myocytes at physiological conditions. *PLoS One*. 2010;5(12):e15772.
195. Armstrong CM, Bezanilla F. Inactivation of the sodium channel. II. Gating current experiments. *J Gen Physiol*. 1977;70(5):567-90.
196. Yellen G. The moving parts of voltage-gated ion channels. *Q Rev Biophys*. 1998;31(3):239-95.
197. Kleber AG, Rudy Y. Basic mechanisms of cardiac impulse propagation and associated arrhythmias. *Physiol Rev*. 2004;84(2):431-88.
198. DeMarco KR, Clancy CE. Cardiac Na Channels: Structure to Function. *Curr Top Membr*. 2016;78:287-311.
199. Horn R, Patlak J, Stevens CF. Sodium channels need not open before they inactivate. *Nature*. 1981;291(5814):426-7.
200. Barman M. Proarrhythmic Effects Of Antiarrhythmic Drugs: Case Study Of Flecainide Induced Ventricular Arrhythmias During Treatment Of Atrial Fibrillation. *J Atr Fibrillation*. 2015;8(4):1091.
201. Hund TJ, Rudy Y. Rate dependence and regulation of action potential and calcium transient in a canine cardiac ventricular cell model. *Circulation*. 2004;110(20):3168-74.
202. Dumaine R, Wang Q, Keating MT, Hartmann HA, Schwartz PJ, Brown AM, et al. Multiple mechanisms of Na⁺ channel--linked long-QT syndrome. *Circ Res*. 1996;78(5):916-24.
203. Luo A, Ma J, Song Y, Qian C, Wu Y, Zhang P, et al. Larger late sodium current density as well as greater sensitivities to ATX II and ranolazine in rabbit left atrial than left ventricular myocytes. *Am J Physiol Heart Circ Physiol*. 2014;306(3):H455-61.
204. Guerra F, Romandini A, Barbarossa A, Belardinelli L, Capucci A. Ranolazine for rhythm control in atrial fibrillation: A systematic review and meta-analysis. *Int J Cardiol*. 2017;227:284-91.
205. De Ferrari GM, Maier LS, Mont L, Schwartz PJ, Simonis G, Leschke M, et al. Ranolazine in the treatment of atrial fibrillation: Results of the dose-ranging RAFFAELLO (Ranolazine in Atrial Fibrillation Following An Electrical Cardioversion) study. *Heart Rhythm*. 2015;12(5):872-8.
206. Burashnikov A, Di Diego JM, Barajas-Martinez H, Hu D, Cordeiro JM, Moise NS, et al. Ranolazine effectively suppresses atrial fibrillation in the setting of heart failure. *Circ Heart Fail*. 2014;7(4):627-33.
207. Bhimani AA, Yasuda T, Sadrpour SA, Khrestian CM, Lee S, Zeng D, et al. Ranolazine terminates atrial flutter and fibrillation in a canine model. *Heart Rhythm*. 2014;11(9):1592-9.
208. Schram G, Zhang L, Derakhchan K, Ehrlich JR, Belardinelli L, Nattel S. Ranolazine: ion-channel-blocking actions and in vivo electrophysiological effects. *Br J Pharmacol*. 2004;142(8):1300-8.
209. Du C, Zhang Y, El Harchi A, Dempsey CE, Hancox JC. Ranolazine inhibition of hERG potassium channels: drug-pore interactions and reduced potency against inactivation mutants. *J Mol Cell Cardiol*. 2014;74:220-30.
210. Persson F, Andersson B, Duker G, Jacobson I, Carlsson L. Functional effects of the late sodium current inhibition by AZD7009 and lidocaine in rabbit isolated atrial and ventricular tissue and Purkinje fibre. *Eur J Pharmacol*. 2007;558(1-3):133-43.

211. Poulet C, Wettwer E, Grunnet M, Jespersen T, Fabritz L, Matschke K, et al. Late Sodium Current in Human Atrial Cardiomyocytes from Patients in Sinus Rhythm and Atrial Fibrillation. *PLoS One*. 2015;10(6):e0131432.
212. King JH, Huang CL, Fraser JA. Determinants of myocardial conduction velocity: implications for arrhythmogenesis. *Front Physiol*. 2013;4:154.
213. Moe GK, Rheinboldt WC, Abildskov JA. A Computer Model of Atrial Fibrillation. *Am Heart J*. 1964;67:200-20.
214. Kagiya Y, Hill JL, Gettes LS. Interaction of acidosis and increased extracellular potassium on action potential characteristics and conduction in guinea pig ventricular muscle. *Circ Res*. 1982;51(5):614-23.
215. Cheng J, Makielski JC, Yuan P, Shi N, Zhou F, Ye B, et al. Sudden unexplained nocturnal death syndrome in Southern China: an epidemiological survey and SCN5A gene screening. *Am J Forensic Med Pathol*. 2011;32(4):359-63.
216. Rook MB, Bezzina Alshinawi C, Groenewegen WA, van Gelder IC, van Ginneken AC, Jongsma HJ, et al. Human SCN5A gene mutations alter cardiac sodium channel kinetics and are associated with the Brugada syndrome. *Cardiovasc Res*. 1999;44(3):507-17.
217. Catterall WA. Molecular properties of voltage-sensitive sodium channels. *Annu Rev Biochem*. 1986;55:953-85.
218. Catterall WA. Ion channel voltage sensors: structure, function, and pathophysiology. *Neuron*. 2010;67(6):915-28.
219. Aldrich RW, Corey DP, Stevens CF. A reinterpretation of mammalian sodium channel gating based on single channel recording. *Nature*. 1983;306(5942):436-41.
220. Tang L, Chehab N, Wieland SJ, Kallen RG. Glutamine substitution at alanine1649 in the S4-S5 cytoplasmic loop of domain 4 removes the voltage sensitivity of fast inactivation in the human heart sodium channel. *J Gen Physiol*. 1998;111(5):639-52.
221. Jaye DAX, Y.F; Sigg, D.C. *Basice Cardiac Electrophysiology: Excitable Membranes*. 1 ed. Boston: Spring; 2010.
222. Bezanilla F, Armstrong CM. Inactivation of the sodium channel. I. Sodium current experiments. *J Gen Physiol*. 1977;70(5):549-66.
223. Clancy CE, Tateyama M, Liu H, Wehrens XH, Kass RS. Non-equilibrium gating in cardiac Na⁺ channels: an original mechanism of arrhythmia. *Circulation*. 2003;107(17):2233-7.
224. Flaim SN, Giles WR, McCulloch AD. Arrhythmogenic consequences of Na⁺ channel mutations in the transmurally heterogeneous mammalian left ventricle: analysis of the I1768V SCN5A mutation. *Heart Rhythm*. 2007;4(6):768-78.
225. Roden DM, Woosley RL. Drug therapy. Flecainide. *N Engl J Med*. 1986;315(1):36-41.
226. Camm AJ, Lip GY, De Caterina R, Savelieva I, Atar D, Hohnloser SH, et al. 2012 focused update of the ESC Guidelines for the management of atrial fibrillation: an update of the 2010 ESC Guidelines for the management of atrial fibrillation--developed with the special contribution of the European Heart Rhythm Association. *Europace*. 2012;14(10):1385-413.

227. Hondeghem LM, Katzung BG. Time- and voltage-dependent interactions of antiarrhythmic drugs with cardiac sodium channels. *Biochim Biophys Acta*. 1977;472(3-4):373-98.
228. Syeda F, Holmes AP, Yu TY, Tull S, Kuhlmann SM, Pavlovic D, et al. PITX2 Modulates Atrial Membrane Potential and the Antiarrhythmic Effects of Sodium-Channel Blockers. *J Am Coll Cardiol*. 2016;68(17):1881-94.
229. Chaitman BR. Ranolazine for the treatment of chronic angina and potential use in other cardiovascular conditions. *Circulation*. 2006;113(20):2462-72.
230. Gautier P, Guillemare E, Marion A, Bertrand JP, Tourneur Y, Nisato D. Electrophysiologic characterization of dronedarone in guinea pig ventricular cells. *J Cardiovasc Pharmacol*. 2003;41(2):191-202.
231. Wang Z, Fermini B, Nattel S. Mechanism of flecainide's rate-dependent actions on action potential duration in canine atrial tissue. *J Pharmacol Exp Ther*. 1993;267(2):575-81.
232. Qu Y, Curtis R, Lawson D, Gilbride K, Ge P, DiStefano PS, et al. Differential modulation of sodium channel gating and persistent sodium currents by the beta1, beta2, and beta3 subunits. *Mol Cell Neurosci*. 2001;18(5):570-80.
233. Vijayaragavan K, Powell AJ, Kinghorn IJ, Chahine M. Role of auxiliary beta1-, beta2-, and beta3-subunits and their interaction with Na(v)1.8 voltage-gated sodium channel. *Biochem Biophys Res Commun*. 2004;319(2):531-40.
234. Chen C, Bharucha V, Chen Y, Westenbroek RE, Brown A, Malhotra JD, et al. Reduced sodium channel density, altered voltage dependence of inactivation, and increased susceptibility to seizures in mice lacking sodium channel beta 2-subunits. *Proc Natl Acad Sci U S A*. 2002;99(26):17072-7.
235. Meadows LS, Chen YH, Powell AJ, Clare JJ, Ragsdale DS. Functional modulation of human brain Nav1.3 sodium channels, expressed in mammalian cells, by auxiliary beta 1, beta 2 and beta 3 subunits. *Neuroscience*. 2002;114(3):745-53.
236. Aman TK, Grieco-Calub TM, Chen C, Rusconi R, Slat EA, Isom LL, et al. Regulation of persistent Na current by interactions between beta subunits of voltage-gated Na channels. *J Neurosci*. 2009;29(7):2027-42.
237. George AL, Jr. Genetic modulation of impaired cardiac conduction: sodium channel beta4 subunit missing in action. *Circ Res*. 2009;104(11):1238-9.
238. Watanabe H, Darbar D, Kaiser DW, Jiramongkolchai K, Chopra S, Donahue BS, et al. Mutations in sodium channel beta1- and beta2-subunits associated with atrial fibrillation. *Circ Arrhythm Electrophysiol*. 2009;2(3):268-75.
239. Nattel S. New ideas about atrial fibrillation 50 years on. *Nature*. 2002;415(6868):219-26.
240. Fahmi AI, Patel M, Stevens EB, Fowden AL, John JE, 3rd, Lee K, et al. The sodium channel beta-subunit SCN3b modulates the kinetics of SCN5a and is expressed heterogeneously in sheep heart. *J Physiol*. 2001;537(Pt 3):693-700.
241. Bezzina CR, Rook MB, Wilde AA. Cardiac sodium channel and inherited arrhythmia syndromes. *Cardiovasc Res*. 2001;49(2):257-71.

242. Undrovinas AI, Maltsev VA, Sabbah HN. Repolarization abnormalities in cardiomyocytes of dogs with chronic heart failure: role of sustained inward current. *Cell Mol Life Sci.* 1999;55(3):494-505.
243. Huang B, El-Sherif T, Gidh-Jain M, Qin D, El-Sherif N. Alterations of sodium channel kinetics and gene expression in the postinfarction remodeled myocardium. *J Cardiovasc Electrophysiol.* 2001;12(2):218-25.
244. Antzelevitch C, Belardinelli L, Wu L, Fraser H, Zygmunt AC, Burashnikov A, et al. Electrophysiologic properties and antiarrhythmic actions of a novel antianginal agent. *J Cardiovasc Pharmacol Ther.* 2004;9 Suppl 1:S65-83.
245. Wu L, Shryock JC, Song Y, Li Y, Antzelevitch C, Belardinelli L. Antiarrhythmic effects of ranolazine in a guinea pig in vitro model of long-QT syndrome. *J Pharmacol Exp Ther.* 2004;310(2):599-605.
246. Corrado D, Basso C, Pavei A, Michieli P, Schiavon M, Thiene G. Trends in sudden cardiovascular death in young competitive athletes after implementation of a preparticipation screening program. *JAMA.* 2006;296(13):1593-601.
247. Gemayel C, Pelliccia A, Thompson PD. Arrhythmogenic right ventricular cardiomyopathy. *J Am Coll Cardiol.* 2001;38(7):1773-81.
248. Thiene G, Nava A, Corrado D, Rossi L, Pennelli N. Right ventricular cardiomyopathy and sudden death in young people. *N Engl J Med.* 1988;318(3):129-33.
249. Brebilla-Perrot B, Jacquemin L, Houplon P, Houriez P, Beurrier D, Berder V, et al. Increased atrial vulnerability in arrhythmogenic right ventricular disease. *Am Heart J.* 1998;135(5 Pt 1):748-54.
250. Fontaine G, Umemura J, Di Donna P, Tsezana R, Cannat JJ, Frank R. [Duration of QRS complexes in arrhythmogenic right ventricular dysplasia. A new non-invasive diagnostic marker]. *Ann Cardiol Angeiol (Paris).* 1993;42(8):399-405.
251. Tabib A, Loire R, Chalabreysse L, Meyronnet D, Miras A, Malicier D, et al. Circumstances of death and gross and microscopic observations in a series of 200 cases of sudden death associated with arrhythmogenic right ventricular cardiomyopathy and/or dysplasia. *Circulation.* 2003;108(24):3000-5.
252. Heidbuchel H, Hoogsteen J, Fagard R, Vanhees L, Ector H, Willems R, et al. High prevalence of right ventricular involvement in endurance athletes with ventricular arrhythmias. Role of an electrophysiologic study in risk stratification. *Eur Heart J.* 2003;24(16):1473-80.
253. Corrado D, Wichter T, Link MS, Hauer RN, Marchlinski FE, Anastasakis A, et al. Treatment of Arrhythmogenic Right Ventricular Cardiomyopathy/Dysplasia: An International Task Force Consensus Statement. *Circulation.* 2015;132(5):441-53.
254. Wichter T, Borggrefe M, Haverkamp W, Chen X, Breithardt G. Efficacy of antiarrhythmic drugs in patients with arrhythmogenic right ventricular disease. Results in patients with inducible and noninducible ventricular tachycardia. *Circulation.* 1992;86(1):29-37.
255. Asimaki A, Tandri H, Huang H, Halushka MK, Gautam S, Basso C, et al. A new diagnostic test for arrhythmogenic right ventricular cardiomyopathy. *N Engl J Med.* 2009;360(11):1075-84.

256. Yin T, Getsios S, Caldelari R, Godsel LM, Kowalczyk AP, Muller EJ, et al. Mechanisms of plakoglobin-dependent adhesion: desmosome-specific functions in assembly and regulation by epidermal growth factor receptor. *J Biol Chem.* 2005;280(48):40355-63.
257. Troyanovsky SM, Eshkind LG, Troyanovsky RB, Leube RE, Franke WW. Contributions of cytoplasmic domains of desmosomal cadherins to desmosome assembly and intermediate filament anchorage. *Cell.* 1993;72(4):561-74.
258. Turagam MK, Flaker GC, Velagapudi P, Vadali S, Alpert MA. Atrial Fibrillation In Athletes: Pathophysiology, Clinical Presentation, Evaluation and Management. *J Atr Fibrillation.* 2015;8(4):1309.
259. Hepburn CS, F; Yu, T; Holmes, AP; Roth, VC; Wright, T; Kabir, SN; Menon, P; Wells, S; Vloumidi, E; Apicella, C; Luts, S; Fortmueller, L; Isaacs, A; Stoll, M; Gkoutos, G; Pavlovic, D; Kirchhof, P; Fabritz, L. Desmosomal instability increases atrial arrhythmia susceptibility after endurance training. 2018.
260. Syeda FK, M.; Vloumidi, E.; Holmes, A.P.; Osborne, B.; Hopkins, S.; Yu, T.; Riley, G.; Kirchhof, P.; Fabritz, L. Atrial Arrhythmia Susceptibility in Arrhythmogenic Right Ventricular Cardiomyopathy. 2014.
261. Li Q, Huang H, Liu G, Lam K, Rutberg J, Green MS, et al. Gain-of-function mutation of Nav1.5 in atrial fibrillation enhances cellular excitability and lowers the threshold for action potential firing. *Biochem Biophys Res Commun.* 2009;380(1):132-7.
262. Antzelevitch C, Nesterenko V, Shryock JC, Rajamani S, Song Y, Belardinelli L. The role of late I_{Na} in development of cardiac arrhythmias. *Handb Exp Pharmacol.* 2014;221:137-68.
263. Whyte GP, Stephens N, Senior R, Peters N, O'Hanlon R, Sharma S. Differentiation of RVOT-VT and ARVC in an elite athlete. *Med Sci Sports Exerc.* 2008;40(8):1357-61.
264. Syeda F, Holmes AP, Yu TY, Tull S, Kuhlmann SM, Pavlovic D, et al. PITX2 modulates atrial membrane potential and reduced PITX2 potentiates the antiarrhythmic effects of sodium-channel blockers. *JACC.* 2016;68:59-72; doi: 10.1016/j.jacc.2016.07.766.
265. Bouvier FM, C.; Roche, N.C.; Fiorina, L.; Poindron, D.; Moini, C.; Gandjbakhch, E. Effectiveness and safety of flecainide in arrhythmogenic right ventricular cardiomyopathy. *Archives of Cardiovascular Diseases Supplements.* 2018;10(1):98-9.
266. Ermakov S, Gerstenfeld EP, Svetlichnaya Y, Scheinman MM. Use of flecainide in combination antiarrhythmic therapy in patients with arrhythmogenic right ventricular cardiomyopathy. *Heart Rhythm.* 2017;14(4):564-9.
267. Ermakov S, Scheinman M. Arrhythmogenic Right Ventricular Cardiomyopathy - Antiarrhythmic Therapy. *Arrhythm Electrophysiol Rev.* 2015;4(2):86-9.
268. Vandamme TF. Rodent models for human diseases. *Eur J Pharmacol.* 2015;759:84-9.
269. Milani-Nejad N, Janssen PM. Small and large animal models in cardiac contraction research: advantages and disadvantages. *Pharmacol Ther.* 2014;141(3):235-49.
270. Guenet JL. The mouse genome. *Genome Res.* 2005;15(12):1729-40.

271. Recchia FA, Lionetti V. Animal models of dilated cardiomyopathy for translational research. *Vet Res Commun*. 2007;31 Suppl 1:35-41.
272. Hasenfuss G. Animal models of human cardiovascular disease, heart failure and hypertrophy. *Cardiovasc Res*. 1998;39(1):60-76.
273. Louch WE, Sheehan KA, Wolska BM. Methods in cardiomyocyte isolation, culture, and gene transfer. *J Mol Cell Cardiol*. 2011;51(3):288-98.
274. Berry MN, Friend DS, Scheuer J. Morphology and metabolism of intact muscle cells isolated from adult rat heart. *Circ Res*. 1970;26(6):679-87.
275. Bloom S. Phylogenetic differences in spontaneous contractility of isolated heart muscle cells. *Comp Biochem Physiol*. 1970;37(1):127-9.
276. Bloom S. Spontaneous rhythmic contraction of separated heart muscle cells. *Science*. 1970;167(3926):1727-9.
277. Dobrev D, Wettwer E, Himmel HM, Kortner A, Kuhlisch E, Schuler S, et al. G-Protein beta(3)-subunit 825T allele is associated with enhanced human atrial inward rectifier potassium currents. *Circulation*. 2000;102(6):692-7.
278. Vahouny GV, Wei R, Starkweather R, Davis C. Preparation of beating heart cells from adult rats. *Science*. 1970;167(3925):1616-8.
279. Langendorff O, Foster MS. Untersuchungen am überlebenden Säugethierherzen : 3. Abhandlung. Vorübergehende Unregelmässigkeiten des Herzschlages und ihre Ausgleichung 1898.
280. Bell RM, Mocanu MM, Yellon DM. Retrograde heart perfusion: the Langendorff technique of isolated heart perfusion. *J Mol Cell Cardiol*. 2011;50(6):940-50.
281. O'Connell TD, Rodrigo MC, Simpson PC. Isolation and culture of adult mouse cardiac myocytes. *Methods Mol Biol*. 2007;357:271-96.
282. MacDougall DA, Calaghan S. A novel approach to the Langendorff technique: preparation of isolated cardiomyocytes and myocardial samples from the same rat heart. *Exp Physiol*. 2013;98(8):1295-300.
283. Bai X, Fischer S, Keshavjee S, Liu M. Heparin interference with reverse transcriptase polymerase chain reaction of RNA extracted from lungs after ischemia-reperfusion. *Transpl Int*. 2000;13(2):146-50.
284. Garcia ME, Blanco JL, Caballero J, Gargallo-Viola D. Anticoagulants interfere with PCR used to diagnose invasive aspergillosis. *J Clin Microbiol*. 2002;40(4):1567-8.
285. Hadipour-Lakmehsari S, Driouchi A, Lee SH, Kuzmanov U, Callaghan NI, Heximer SP, et al. Nanoscale reorganization of sarcoplasmic reticulum in pressure-overload cardiac hypertrophy visualized by dSTORM. *Sci Rep*. 2019;9(1):7867.
286. Dorn LE, Lasman L, Chen J, Xu X, Hund TJ, Medvedovic M, et al. The N(6)-Methyladenosine mRNA Methylase METTL3 Controls Cardiac Homeostasis and Hypertrophy. *Circulation*. 2019;139(4):533-45.
287. Koyani CN, Trummer C, Shrestha N, Scheruebel S, Bourgeois B, Plastira I, et al. Saxagliptin but Not Sitagliptin Inhibits CaMKII and PKC via DPP9 Inhibition in Cardiomyocytes. *Front Physiol*. 2018;9:1622.
288. Zacchigna S, Martinelli V, Moimas S, Colliva A, Anzini M, Nordio A, et al. Paracrine effect of regulatory T cells promotes cardiomyocyte proliferation during pregnancy and after myocardial infarction. *Nat Commun*. 2018;9(1):2432.

289. Kimura A, Ishida Y, Furuta M, Nosaka M, Kuninaka Y, Taruya A, et al. Protective Roles of Interferon-gamma in Cardiac Hypertrophy Induced by Sustained Pressure Overload. *J Am Heart Assoc.* 2018;7(6).
290. Jam FA, Kadota Y, Mendsaikhan A, Tooyama I, Mori M. Identification of juvenility-associated genes in the mouse hepatocytes and cardiomyocytes. *Sci Rep.* 2018;8(1):3132.
291. Russo L, Muturi HT, Ghadieh HE, Wisniewski AM, Morgan EE, Quadri SS, et al. Liver-specific rescuing of CEACAM1 reverses endothelial and cardiovascular abnormalities in male mice with null deletion of Ceacam1 gene. *Mol Metab.* 2018;9:98-113.
292. Edwards KS, Ashraf S, Lomax TM, Wiseman JM, Hall ME, Gava FN, et al. Uncoupling protein 3 deficiency impairs myocardial fatty acid oxidation and contractile recovery following ischemia/reperfusion. *Basic Res Cardiol.* 2018;113(6):47.
293. Lee SH, Hadipour-Lakmehsari S, Miyake T, Gramolini AO. Three-dimensional imaging reveals endo(sarco)plasmic reticulum-containing invaginations within the nucleoplasm of muscle. *Am J Physiol Cell Physiol.* 2018;314(3):C257-C67.
294. Zhang M, Mongue-Din H, Martin D, Catibog N, Smyrnias I, Zhang X, et al. Both cardiomyocyte and endothelial cell Nox4 mediate protection against hemodynamic overload-induced remodelling. *Cardiovasc Res.* 2018;114(3):401-8.
295. Tan WL, Lim BT, Anene-Nzeliu CG, Ackers-Johnson M, Dashi A, See K, et al. A landscape of circular RNA expression in the human heart. *Cardiovasc Res.* 2017;113(3):298-309.
296. See K, Tan WLW, Lim EH, Tiang Z, Lee LT, Li PYQ, et al. Single cardiomyocyte nuclear transcriptomes reveal a lincRNA-regulated de-differentiation and cell cycle stress-response in vivo. *Nat Commun.* 2017;8(1):225.
297. Zhao RR, Ackers-Johnson M, Stenzig J, Chen C, Ding T, Zhou Y, et al. Targeting Chondroitin Sulfate Glycosaminoglycans to Treat Cardiac Fibrosis in Pathological Remodeling. *Circulation.* 2018;137(23):2497-513.
298. Lu XL, Zhao CH, Zhang H, Yao XL. iRhom2 is involved in lipopolysaccharide-induced cardiac injury in vivo and in vitro through regulating inflammation response. *Biomed Pharmacother.* 2017;86:645-53.
299. Zhou DC, Su YH, Jiang FQ, Xia JB, Wu HY, Chang ZS, et al. CpG oligodeoxynucleotide preconditioning improves cardiac function after myocardial infarction via modulation of energy metabolism and angiogenesis. *J Cell Physiol.* 2018;233(5):4245-57.
300. Verjans R, Peters T, Beaumont FJ, van Leeuwen R, van Herwaarden T, Verhesen W, et al. MicroRNA-221/222 Family Counteracts Myocardial Fibrosis in Pressure Overload-Induced Heart Failure. *Hypertension.* 2018;71(2):280-8.
301. Liao RaP, D. Techniques and Best Practices for Cardiomyocyte Isolation: Inside Scientific; 2018 [Available from: <https://insidescientific.com/webinar/cardiomyocyte-isolation-techniques-ionoptix>.
302. Nair P, Nair RR. Selective use of calcium chelators enhances the yield of calcium-tolerant myocytes from adult heart. *Indian J Exp Biol.* 1997;35(5):451-6.

303. Crevey BJ, Langer GA, Frank JS. Role of Ca²⁺ in maintenance of rabbit myocardial cell membrane structural and functional integrity. *J Mol Cell Cardiol.* 1978;10(12):1081-100.
304. Egorova MV, Afanas'ev SA, Popov SV. A simple method for isolation of cardiomyocytes from adult rat heart. *Bull Exp Biol Med.* 2005;140(3):370-3.
305. Zhou YY, Wang SQ, Zhu WZ, Chruscinski A, Kobilka BK, Ziman B, et al. Culture and adenoviral infection of adult mouse cardiac myocytes: methods for cellular genetic physiology. *Am J Physiol Heart Circ Physiol.* 2000;279(1):H429-36.
306. Graham EL, Balla C, Franchino H, Melman Y, del Monte F, Das S. Isolation, culture, and functional characterization of adult mouse cardiomyocytes. *J Vis Exp.* 2013(79):e50289.
307. Stuyvers BD, McCulloch AD, Guo J, Duff HJ, ter Keurs HE. Effect of stimulation rate, sarcomere length and Ca(2+) on force generation by mouse cardiac muscle. *J Physiol.* 2002;544(3):817-30.
308. Serizawa T, Terui T, Kagemoto T, Mizuno A, Shimosawa T, Kobirumaki F, et al. Real-time measurement of the length of a single sarcomere in rat ventricular myocytes: a novel analysis with quantum dots. *Am J Physiol Cell Physiol.* 2011;301(5):C1116-27.
309. Shintani SA, Oyama K, Kobirumaki-Shimosawa F, Ohki T, Ishiwata S, Fukuda N. Sarcomere length nanometry in rat neonatal cardiomyocytes expressed with alpha-actinin-AcGFP in Z discs. *J Gen Physiol.* 2014;143(4):513-24.
310. Bolck B, Munch G, Mackenstein P, Hellmich M, Hirsch I, Reuter H, et al. Na⁺/Ca²⁺ exchanger overexpression impairs frequency- and ouabain-dependent cell shortening in adult rat cardiomyocytes. *Am J Physiol Heart Circ Physiol.* 2004;287(4):H1435-45.
311. Katanosaka Y, Iwasaki K, Ujihara Y, Takatsu S, Nishitsuji K, Kanagawa M, et al. TRPV2 is critical for the maintenance of cardiac structure and function in mice. *Nat Commun.* 2014;5:3932.
312. Antoons G, Mubagwa K, Nevelsteen I, Sipido KR. Mechanisms underlying the frequency dependence of contraction and [Ca(2+)]_i transients in mouse ventricular myocytes. *J Physiol.* 2002;543(Pt 3):889-98.
313. Stemmer P, Akera T. Concealed positive force-frequency relationships in rat and mouse cardiac muscle revealed by ryanodine. *Am J Physiol.* 1986;251(6 Pt 2):H1106-10.
314. Molina CE, Johnson DM, Mehel H, Spatjens RL, Mika D, Algalarrondo V, et al. Interventricular differences in beta-adrenergic responses in the canine heart: role of phosphodiesterases. *J Am Heart Assoc.* 2014;3(3):e000858.
315. Dobson JG, Jr., Shea LG, Fenton RA. Adenosine A_{2A} and beta-adrenergic calcium transient and contractile responses in rat ventricular myocytes. *Am J Physiol Heart Circ Physiol.* 2008;295(6):H2364-72.
316. Harding SE, Vescovo G, Kirby M, Jones SM, Gurden J, Poole-Wilson PA. Contractile responses of isolated adult rat and rabbit cardiac myocytes to isoproterenol and calcium. *J Mol Cell Cardiol.* 1988;20(7):635-47.
317. Burashnikov A, Belardinelli L, Antzelevitch C. Atrial-selective sodium channel block strategy to suppress atrial fibrillation: ranolazine versus propafenone. *J Pharmacol Exp Ther.* 2012;340(1):161-8.

318. Heineke J, Molkenin JD. Regulation of cardiac hypertrophy by intracellular signalling pathways. *Nat Rev Mol Cell Biol.* 2006;7(8):589-600.
319. Braz JC, Gregory K, Pathak A, Zhao W, Sahin B, Klevitsky R, et al. PKC-alpha regulates cardiac contractility and propensity toward heart failure. *Nat Med.* 2004;10(3):248-54.
320. Wittenberg BA, White RL, Ginzberg RD, Spray DC. Effect of calcium on the dissociation of the mature rat heart into individual and paired myocytes: electrical properties of cell pairs. *Circ Res.* 1986;59(2):143-50.
321. Holmes AP, Yu TY, Tull S, Syeda F, Kuhlmann SM, O'Brien SM, et al. A Regional Reduction in Ito and IKACH in the Murine Posterior Left Atrial Myocardium Is Associated with Action Potential Prolongation and Increased Ectopic Activity. *PLoS One.* 2016;11(5):e0154077.
322. Mitcheson JS, Hancox JC, Levi AJ. Cultured adult cardiac myocytes: future applications, culture methods, morphological and electrophysiological properties. *Cardiovasc Res.* 1998;39(2):280-300.
323. Kaestner L, Scholz A, Hammer K, Vecerdea A, Ruppenthal S, Lipp P. Isolation and genetic manipulation of adult cardiac myocytes for confocal imaging. *J Vis Exp.* 2009(31).
324. Guo GR, Chen L, Rao M, Chen K, Song JP, Hu SS. A modified method for isolation of human cardiomyocytes to model cardiac diseases. *J Transl Med.* 2018;16(1):288.
325. Killeen MJ, Thomas G, Gurung IS, Goddard CA, Fraser JA, Mahaut-Smith MP, et al. Arrhythmogenic mechanisms in the isolated perfused hypokalaemic murine heart. *Acta Physiol (Oxf).* 2007;189(1):33-46.
326. Eisner DA, Smith GL, O'Neill SC. The effects of lactic acid production on contraction and intracellular pH during hypoxia in cardiac muscle. *Basic Res Cardiol.* 1993;88(5):421-9.
327. Scheuer J, Berry MN. Effect of alkalosis on glycolysis in the isolated rat heart. *Am J Physiol.* 1967;213(5):1143-8.
328. Lew WY, Nishikawa Y, Su H. Cardiac myocyte function and left ventricular strains after brief ischemia and reperfusion in rabbits. *Circulation.* 1994;90(4):1942-50.
329. Kourie JI. Interaction of reactive oxygen species with ion transport mechanisms. *Am J Physiol.* 1998;275(1):C1-24.
330. Anderson PG, Bishop SP, Digerness SB. Transmural progression of morphologic changes during ischemic contracture and reperfusion in the normal and hypertrophied rat heart. *Am J Pathol.* 1987;129(1):152-67.
331. Liao R, Podesser BK, Lim CC. The continuing evolution of the Langendorff and ejecting murine heart: new advances in cardiac phenotyping. *Am J Physiol Heart Circ Physiol.* 2012;303(2):H156-67.
332. Richardson WJ, Clarke SA, Quinn TA, Holmes JW. Physiological Implications of Myocardial Scar Structure. *Compr Physiol.* 2015;5(4):1877-909.
333. Motayagheni N. Modified Langendorff technique for mouse heart cannulation: Improved heart quality and decreased risk of ischemia. *MethodsX.* 2017;4:508-12.
334. Jian Z, Chen YJ, Shimkunas R, Jian Y, Jaradeh M, Chavez K, et al. In Vivo Cannulation Methods for Cardiomyocytes Isolation from Heart Disease Models. *PLoS One.* 2016;11(8):e0160605.

335. Curtis MJ. Characterisation, utilisation and clinical relevance of isolated perfused heart models of ischaemia-induced ventricular fibrillation. *Cardiovasc Res.* 1998;39(1):194-215.
336. Mahmood T, Yang PC. Western blot: technique, theory, and trouble shooting. *N Am J Med Sci.* 2012;4(9):429-34.
337. Camacho P, Fan H, Liu Z, He JQ. Small mammalian animal models of heart disease. *Am J Cardiovasc Dis.* 2016;6(3):70-80.
338. Ruff RL. Effects of temperature on slow and fast inactivation of rat skeletal muscle Na(+) channels. *Am J Physiol.* 1999;277(5):C937-47.
339. Milburn T, Saint DA, Chung SH. The temperature dependence of conductance of the sodium channel: implications for mechanisms of ion permeation. *Receptors Channels.* 1995;3(3):201-11.
340. Collins CA, Rojas E. Temperature dependence of the sodium channel gating kinetics in the node of Ranvier. *Q J Exp Physiol.* 1982;67(1):41-55.